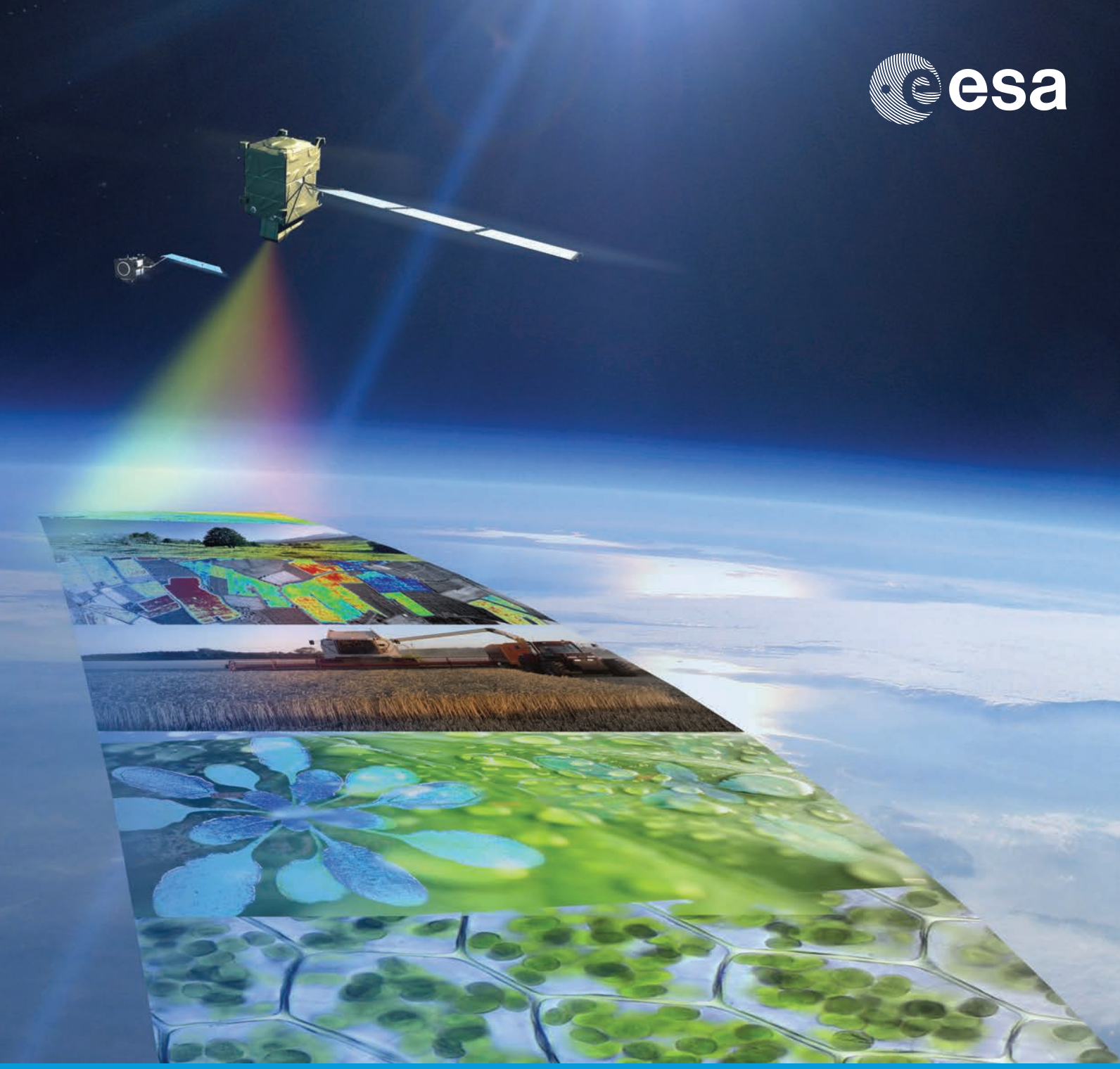

carbonsat **flex**

→REPORT FOR MISSION SELECTION

An Earth Explorer to observe vegetation fluorescence

www.esa.int

European Space Agency

SP-1330/2
June 2015

carbonsat flex

→ REPORT FOR MISSION SELECTION

An Earth Explorer to observe vegetation fluorescence

European Space Agency

Acknowledgements

This report is based on contributions from the FLEX Mission Advisory Group (MAG):

Jose Moreno – MAG Chairman (University of Valencia, ES)
Yves Goulas (Laboratoire de Meteorologie Dynamique du CNRS, Palaiseau, FR)
Andreas Huth (Helmholtz Centre of Environmental Research, Leipzig, DE)
Elizabeth Middleton (NASA GSFC, US)
Franco Miglietta (IBIMET-CNR, Florence, IT)
Gina Mohammed (P & M Technologies, Sault Ste. Marie, Ontario, CA)
Ladislav Nedbal (Research Centre Jülich, DE)
Uwe Rascher (Research Centre Jülich, DE)
Wout Verhoef (University of Twente, Enschede, NL)

Scientific content of the report was compiled by Matthias Drusch (ESA) with additional contributions, in particular, from Roberto Colombo and Micol Rossini (both from Università degli Studi di Milano-Bicocca, IT), Dirk Schüttemeyer and Remo Bianchi (both from ESA).

Technical content of the report was compiled by Umberto Del Bello and Antonio Gabriele, with contributions from Stefan Kraft, Jean-Loup Bezy, Pedro Jurado and Raffaella Franco, (all from ESA), based on inputs derived from the industrial Phase-A/B1 system and technical activities.

Recommended citation: ESA (2015). *Report for Mission Selection*: *FLEX*, ESA SP-1330/2 (2 volume series), European Space Agency, Noordwijk, The Netherlands.

Cover image design: ESA/ATG medialab
Cover photo credits: K. Peters (chloroplasts)
U. Rascher–Forschungszentrum Jülich (plant fluorescence)
L. Plougmann (field harvest)
U. Rascher–Forschungszentrum Jülich (field fluorescence)
Zoolook (hills)

An ESA Communications Production

Publication *Report for Mission Selection: FLEX* (ESA SP-1330/2, June 2015)

Production Editor K. Fletcher

Editing H. Rider (EJR-Quartz)

Layout I. Kenny (HE Space)

Publisher ESA Communications
ESTEC, PO Box 299, 2200 AG Noordwijk, the Netherlands
Tel: +31 71 565 3408 www.esa.int

ISBN 978-92-9221-428-9 (2 volumes)

ISSN 0379-6566

Contents

→ EXECUTIVE SUMMARY

Executive Summary

This report forms the basis for the selection of the eighth Earth Explorer mission within ESA's Earth Observation Programme. Two candidates, CarbonSat and FLEX, have undergone extensive feasibility studies. FLEX aims to quantify photosynthetic activity and plant stress by mapping vegetation fluorescence. CarbonSat aims to quantify sources and sinks of carbon dioxide and methane by measuring their distribution in the atmosphere. This report covers the FLEX mission.

The global population is growing rapidly. Projections indicate that there is a 95% probability that by 2050 Earth's population will be between nine and 11 billion. The World Bank estimates that we will need to produce 50–100% more food than we do today. This, together with improved standards of living, will stimulate increasing demands, which, in turn, will exert stresses on terrestrial and aquatic ecosystems that can threaten their inherent productivity and resilience. We are confronted by four main challenges that are highly interlinked:

— provide enough food, fibre, and water for an expanding global population
— ensure availability and access to energy for all
— protect and sustain natural resources and the environment
— ensure human well-being and health at a global scale

Food and feed, energy, natural resources, and human health form the foundation of a bioeconomy where the issue of growth sustainability is addressed in a holistic manner. International agencies consider the growth of the bioeconomy to be a high priority with its roots in the sustainable use of primary production potentials of our planet. In this context, photosynthesis constitutes the main biological process that, ultimately, enables life on Earth. To date, it has not been possible to directly observe the photosynthetic efficiency of the terrestrial vegetation layer from space.

Photosynthesis takes place in plant leaves, where atmospheric carbon dioxide is fixed and converted into energy-rich carbohydrates. Solar energy drives this biophysical/biochemical process. The conversion of solar energy into biochemically-usable energy happens in the light reaction of photosynthesis, which is a complex and highly regulated cascade of light absorption to electron transfer to biosynthesis. When chlorophyll molecules in a leaf absorb photons, electrons are energised to an excited state, with the fate of these 'excitons' dependent on the physiological status of the plant. For example, under optimal conditions, approximately 82% of the absorbed light is used for carbon assimilation while the remaining part is lost as heat and dissipated as emissions of chlorophyll fluorescence. Fluorescence, the radiant flux emitted, is therefore the most direct measurable reporter of photosynthetic efficiency.

The emission of the light referred to as chlorophyll fluorescence emanates from two photosystems working in sequence and harvesting incoming light. Chlorophyll fluorescence produced from the initial reactions in one photosystem occurs at wavelengths between 650–780 nm with a peak at ~685 nm. In the other photosystem, fluorescence occurs almost exclusively in the far-red/near-infrared spectrum (>700 nm, with a peak at ~740 nm). The full chlorophyll emission spectrum covers a wavelength range in the visible to near-infrared spectrum of ~640–800 nm. The two photosystems operate in a reaction chain and are commonly measured as a two-peak signal. Stress factors affect photosynthetic reactions and trigger dynamic regulation of the two photosystems. To advance our understanding of the functioning of the photosynthetic machinery, and the actual health and performance of terrestrial vegetation, quantification of the fluorescence emitted by the two photosystems

is needed together with information on the canopy structure, its composition, and temperature.

The FLEX mission will provide global maps of vegetation fluorescence emission spectra as primary measurements. It will focus on the relevant characteristics of fluorescence emission, namely:

— fluorescence emitted in the range of the oxygen absorption bands O_2-A and O_2-B, i.e. at 687 and 760 nm, with an unprecedented accuracy of 0.2 mW m^{-2} sr^{-1} nm^{-1}

— maximum fluorescence emission of the two peaks of the spectrum including the wavelength position of the peaks

— total fluorescence emission integrated over the full emission spectrum

— fluorescence emission from the two photosystems

For the quantification of photosynthesis it is necessary to simultaneously measure dynamic photochemical reflectance changes associated with energy dissipation mechanisms. These will be quantified by exploiting subtle accompanying changes in the green spectral region. Only the combined measurements from the entire spectral range covering 500–780 nm, together with information on vegetation temperature provided within the framework of the mission concept, will allow interpretation of the full fluorescence spectrum for the subsequent estimation of vegetation health status and carbon fixation.

The FLEX mission concept foresees a small satellite flying in tandem with Sentinel-3 to make optimal use of existing observation capabilities, providing a suite of measurements timed to be close enough together to minimise the effects of moving clouds. To meet the programmatic constraints with respect to the Call for Proposals for Earth Explorer 8, the space segment is based on recurring elements either already in orbit or about to fly, with optional configurations allowing a shared launch scenario. The FLEX satellite will carry the Fluorescence Imaging Spectrometer (FLORIS), which covers the 500–780 nm spectral range with varying spectral sampling and resolutions of 0.1 nm and 0.3 nm, respectively, in the oxygen absorption bands. The spatial resolution on the ground will be 300×300 m^2, capturing the scale of individual agricultural and forestry management units.

As a consequence of the FLEX Phase-A/B1 activities and preceding activities on fluorescence missions, the technical and scientific maturity has reached level 5 for all critical components. Critical technologies include the manufacturing and testing of a representative breadboard of the FLORIS high-resolution channel. In terms of scientific readiness, the mission and research objectives have remained stable with respect to the original proposal. In addition, end-to-end system performance simulations indicate that the mission objectives can be met. Using the HyPlant airborne demonstrator, the fluorescence retrieval has been consolidated and the targeted requirements for accuracy fulfilled. Vegetation stress has been successfully observed for a variety of environmental conditions and the validity of the mission concept has been confirmed. The proposed tandem concept has reached the expected readiness levels and is ready for selection and implementation.

The combination of FLORIS and Sentinel-3's optical and thermal sensors allows for an integrated package of measurements providing all the necessary auxiliary information to interpret the data and drive photosynthesis productivity models. The FLEX mission will provide measurements that have not been available before and will support a large number of applications, such as quantifying vegetation productivity, probing ecosystem drivers, land-use planning, and characterising limiting factors like stress. It is envisaged that the

FLORIS measurements will also support aerosol retrieval and applications over coastal zones and inland waters.

More than ever, advanced Earth observation capabilities are needed to understand and assess the impacts of global change on the health and productivity of Earth's vegetation resources including the carbon cycle, and the sustainability of the planet's capacity to provide necessary goods and ecosystem services. The availability of a space-based, rapidly accessible and reliable indicator of plant photosynthesis and related stress effects will help to address this need and support agricultural and resource management.

By quantifying vegetation fluorescence, the photochemical reflectance index, and surface temperature, the FLEX mission concept provides the most innovative and unique set of measurements to increase our understanding of actual photosynthetic efficiency, and the status of vegetation health and plant performance, while addressing related societal challenges previously identified. ESA considers that FLEX is sufficiently mature for implementation as Earth Explorer 8, with a small satellite that can be launched by 2022.

→ INTRODUCTION

1. Introduction

Events marking the current chapter in Earth's natural history provide vivid reminders of our vulnerability and underline the urgency with which we must achieve a sustainable existence on our home planet.

Understanding changes in the Earth system and the impact that humanity is having on its delicate balance is paramount. The ability to acquire new insight into Earth-system processes poses significant scientific and technical challenges. However, it also provides the stimulus and opportunity to develop new measurement capabilities, exploiting the unique vantage point of space to study the ebb and flow of natural processes and the impact human activity is having at local, regional and global scales.

As part of its Earth Observation Programme, the European Space Agency's series of 'Earth Explorer' satellite missions are the epitome of Europe's technical endeavour in realising new Earth-observing capabilities. These missions offer a stream of innovative measurement techniques to explore and understand different aspects of the Earth system. They embody the purpose of the Programme: to address scientific and technical challenges beyond the reach of individual Member States.

Priorities identified by the scientific community are used to guide the development of the Earth Explorer missions. Each has been selected to address and fulfil the strategic objectives of ESA's Living Planet Programme as well as contribute critical new elements to the global Earth-observing system infrastructure.

The guiding principle of defining, developing and operating Earth Explorer missions in close cooperation with the scientific community provides a tool to address the most critical Earth-science questions in as comprehensive and effective a manner as possible. The capability to develop and launch state-of-the-art technologies enables the European science community to achieve substantial scientific advances. It is already evident the extent to which the first Earth Explorers contribute to establishing new frontiers in our scientific knowledge of how the Earth system works, and how humankind influences natural processes.

Since the science and research elements of the Living Planet Programme were established in the mid-1990s, this user-driven strategy has resulted in the selection of seven Earth Explorer missions. Together, they cover a broad range of scientific topics. Importantly, their complementarity further stimulates the development of new applications of their data.

Earth Explorer missions are split into two categories: 'Core' and 'Opportunity'. Core Explorers address complex issues of scientific interest and typically employ substantial elements of new technology. By contrast, Opportunity missions are smaller and more affordable and have more focused scientific goals that can be achieved by novel uses of existing, lower-risk technologies. Through a process of peer review and selection, both types are implemented in separate cycles to ensure a steady flow of missions to address emerging key Earth-science questions.

The first cycle for Core missions resulted in the Gravity field and steady-state Ocean Circulation Explorer, GOCE, which was launched in March 2009, and the Atmospheric Dynamics Mission ADM-Aeolus, scheduled for launch in 2016. The second cycle, initiated in 2000, resulted in the Earth Clouds Aerosols and Radiation Explorer, EarthCARE, due for launch in 2018. The first cycle for Opportunity missions resulted in the ice mission CryoSat, which was rebuilt and launched in April 2010 following a launch failure in 2005, and the Soil Moisture and Ocean Salinity mission, SMOS, also launched in 2009. The second cycle resulted in the magnetic field mission, Swarm, which was launched in November 2013. A third cycle of Core missions, initiated by a Call for Ideas in

2005, led to the selection of the Biomass mission in 2013, since confirmed for full implementation in 2015.

In 2009, a third cycle of Opportunity missions was initiated with a call for mission proposals for the eighth Explorer. In November 2010, two candidates were selected for feasibility study (Phase-A/B1): CarbonSat and FLEX (Fluorescence Explorer).

— CarbonSat aims to quantify sources and sinks of carbon dioxide and methane by measuring their distribution in the atmosphere.

— FLEX aims to quantify photosynthetic activity and plant stress by mapping vegetation fluorescence.

The Reports for Mission Selection capture the status of the respective mission concept at the end of Phase-A/B1 activities. The two volumes will be provided to the Earth-observation community as a basis for the User Consultation Meeting to be held in September 2015, and for the subsequent recommendation for selection of a single Earth Explorer 8 mission.

Each Report for Mission Selection follows a common format and logic. Each identifies the scientific questions and related key societal issues motivating the mission and its research objectives. After establishing the scientific basis and rationale, specific mission objectives are outlined and traced to a set of requirements used for system concept definition. Consolidated descriptions of two competing technical concepts are provided for each candidate mission, the designs of which are optimised to respond to the mission requirements. Based on each design concept, the end-to-end performance is simulated and the maturity of the geophysical data processing is outlined. The results are used to establish the feasibility and maturity of the concept as well as to evaluate the capability to fulfil the mission requirements and scientific objectives.

Each report comprises this introductory first chapter and eight subsequent chapters as follows:

Chapter 2 – identifies the background and scientific issues to be addressed by the mission, considering the contribution of past and present activities in the field. It provides justification for the mission set in the post-2020 timeframe and includes a review of the current scientific understanding of the issue in question while identifying the potential advances in knowledge that the mission could provide.

Chapter 3 – draws on arguments presented in Chapter 2, and summarises specific research objectives and related mission objectives.

Chapter 4 – outlines the mission requirements, including required Level-2 geophysical data products and observational parameters, the need for these observations to be made from space, and aspects of timeliness and timing of the mission.

Chapter 5 – provides an overview of the system elements, including the space and ground segments, operations, calibration and the data processing up to Level-1b.

Chapter 6 – details the scientific data processing and validation concept, including processing and calibration/validation as well as the data processing techniques that need to be implemented to meet the data product requirements.

Chapter 7 – makes a comparison of the expected versus the required performance and ability to fulfil the research/observational objectives based on the documented system concept.

Chapter 8 – documents the readiness of the scientific user community in respect to planned use of the anticipated scientific products, the global context in terms of complementary missions as well as the operational or applications potential of the data products.

Chapter 9 – outlines a programme of implementation. It also addresses the scientific and technical maturity, the development status of key technologies, risks, logistics and schedules.

This Report for Selection covers the FLEX mission.

→ BACKGROUND AND SCIENTIFIC JUSTIFICATION

2. Background and Scientific Justification

Current changes in Earth's ecological systems and forecasts for the future are unprecedented in human history. Key thresholds have been breached as a result of climate change, biodiversity loss, artificially increased nitrogen (N) inputs and inadequate phosphorus (P) supply. The global scale of these changes means that all ecosystems are, and will continue to be, affected. This is leading to the modification of multiple and critical ecosystem services such as food production, posing rapidly increasing threats to sustainability worldwide.

Yet, the United Nations Food & Agriculture Organization (FAO) recently stated that the volume of traded agricultural products is rising faster than global production of biomass in agriculture and forestry. This is undoubtedly having an impact on global patterns of land use and land-use intensity (Kastner et al., 2014), resulting in a growing geographic disconnect between the places of production and the places where these products are being consumed. The preservation of both financial and environmental assets in a given region is increasingly leading to a displacement of agricultural production to other regions.

These primarily anthropogenic drivers are causing shifts in land use and land management, and potentially leading to detectable changes in the surface properties of Earth. Crops are rapidly expanding in areas where plants can be grown more intensively, while some old intensive-agricultural lands are being abandoned and are returning to nature. Human-driven geographical changes are occurring at rates that are much faster than any natural shift in vegetation, while desertification and changes in precipitation patterns are affecting plant phenology, and the recent rise in global temperature is modifying the geographical distribution of terrestrial vegetation in both managed and unmanaged ecosystems.

A global change scenario seems inevitable, the consequences of which will largely depend on the future trajectory of primary productivity on Earth – that being a critical driver in setting the upper limits of the planet's carrying capacity. This concept is recognised in the Land Challenges identified by the science strategy within the ESA Earth Observation Living Planet Programme (ESA, 2015b). Earth observation is one of the most powerful tools available to assess the occurrence of a sustainable biospheric metabolism or, in other words, the match between the production of sufficient food via plant and animal productivity and the preservation of a delicate environment and its services.

Most functions and services provided by the biosphere are rooted in the physiology of plants and, in particular, in the most critical chemical reaction that sustains life on Earth: oxygenic photosynthesis.

Currently, it is not possible to observe the actual photosynthetic activity of the vegetation layer from satellites. The most direct technique that can be applied detects the chlorophyll fluorescence, a measurable signal originating from the core of the photosynthetic machinery in plants. Observations of fluorescence will provide a completely new avenue for assessing the dynamics of actual photosynthesis at spatial scales that approach the size of individual management units. The technique offers a great advance over current methods that can only detect potential photosynthesis by observing passive reflectance in the optical spectral range.

2.1 Vegetation Diagnostics for a Sustainable Planet

We have already entered an era where anthropogenic activity is leading to major global changes, the consequences of which are likely to affect how ecosystems interact with critical global biogeochemical cycles, such as that

of carbon and water. Furthermore, there may also be repercussions for the sustainability of human societies as far as energy, food, water, nutrients and health are concerned.

2.1.1 Biogeochemical Cycles

Earth's carbon budget relies on a delicate balance between CO_2 emission and uptake. The uptake of CO_2 through plant photosynthesis and its release by respiration and other processes are critical components of this balance. However, since the industrial revolution, Earth's atmosphere has experienced a rapid increase in CO_2 to its present concentration level of 400 ppm (National Oceanic and Atmospheric Administration, 2015 data). This is 42% more than in pre-industrial levels. Anthropogenic contributors to CO_2 emissions are mainly fossil-fuel combustion and land-use change such as deforestation, logging, and intensive cultivation of cropland soils (Le Quéré et al., 2009).

Terrestrial vegetation absorbs approximately 120 Gt of carbon annually through the physiological process of photosynthesis. A large fraction of the carbon fixed by plants is returned back to the atmosphere through respiration within short time periods. On multiyear timescales, dead plant material is broken down and respired by microorganisms. The remaining carbon in ecosystems is defined as a net sink of atmospheric CO_2, whose amplitude and fluctuation are inherently associated with climate, vegetation patterns and the availability of water and nutrients to plants.

There is currently great uncertainty about the human impact on the magnitude of these processes, and there is an urgent demand to assess the role terrestrial vegetation plays in the carbon cycle. The most recent signs of decline in natural carbon sinks, such as in equatorial forests (Brienen et al., 2015), are seen as a critical alarm. A long and sustained increase in the rate of trees dying in forests that are undisturbed by direct human impact, the surge of tree mortality rates and the stall in forest growth rates are already having a significant impact on the capacity of forests to take up atmospheric carbon.

The fixation of CO_2 through photosynthesis is the first key process that removes carbon from the atmosphere. The annual uptake of atmospheric carbon by terrestrial plants exceeds the amount of carbon from fossil-fuel emissions and, hence, even small alterations of the terrestrial carbon balance are likely to have a major impact on atmospheric CO_2 concentrations. Small changes in gross photosynthesis will unavoidably have major impacts on the whole carbon cycle, with unpredictable impacts on short-, mid- and long-term carbon storage. This explains why a reliable prediction of photosynthesis over land is a priority as well as one of the ultimate goals of Earth-system science, which is seeking universal, generic modelling approaches applicable across multiple biomes and a wide range of vegetation types. Recent studies indicate that cumulative photosynthesis of major Earth biomes and ecosystems can be reliably estimated by a simplified index involving plant phenological status and physiological properties or, in other terms, by the product of the duration of CO_2 uptake and the maximum seasonal photosynthetic rate (Xia et al., 2015). Such a robust index can be seen as an estimator of how photosynthesis fluctuates over space and time in response to climate extremes and during recovery after disturbance.

For each molecule of CO_2 that is fixed photosynthetically, several hundred molecules of water are transpired. Even if a universal relationship between photosynthesis and transpiration cannot be established, it is understood that the two processes are intimately linked and correlated at the scale of individual biomes. This implies that the assessment of photosynthetic rates of a specific ecosystem also provides information from which overall evapotranspiration losses associated with plant growth and ecosystem productivity can be inferred. This is also a critical factor regulating feedback mechanisms between vegetation, the atmosphere, the biosphere and the climate.

The role of plants in regional, continental and global cycles is an emerging topic for a wide range of science disciplines and for biogeochemistry.

2.1.2 Sustainable Bioeconomy

The human population is growing rapidly and this trend is expected to continue for decades to come (Gerland et al., 2014). Projections indicate that there is a 95% probability that by 2050 there will be between 9 and 11 billion people on Earth, with Asia accounting for more than 52% of the population, and Africa 27%, Europe 8%, Latin America (including the Caribbean) 8%, and North America 5%. This, together with improved standards of living, places increasing demand on resources such as food and water, which, in turn, exerts stress upon terrestrial and aquatic ecosystems that can threaten their inherent productivity and resilience. Consequently, we are now confronted with four main challenges:

— provide enough food, fibre, and water for a growing global population
— ensure availability and access to energy for everyone
— protect and sustain natural resources and the environment
— ensure human well-being and health on a worldwide scale

The World Bank estimates that 50–100% more food will need to be produced than today. The central question of food security is how this vast increase in supply can be achieved sustainably and within the environmental boundaries that the complex Earth system sets. Climate change could cut crop yield significantly, while the land, oceans, forests, biodiversity and other forms of natural capital could be depleted at unprecedented rates. Conflicts are likely to seriously threaten our ability to achieve ambitious development goals (IFPRI, 2015) such as eradicating hunger and malnutrition by 2025. Currently, 46% of the developing world's population lives in countries affected by civil conflict, and the number of countries affected by civil conflict and political instability is increasing. Future food production will be severely limited by water availability, particularly in the poorest areas of the world. More than one and a half billion people live in areas of water scarcity. The amount of water used today for agriculture (7130 km^3) is likely to double to feed 9 billion people by 2050 (IWMI, 2011). Access to clean water helps prevent infectious and waterborne disease; access to a nutritious and constant food supply allows adequate health standards to be reached. The public health issues of imbalanced nutrition, inadequate access to food security and misappropriation of resources at governmental and household levels, are seen globally and affect billions of people. The global demand for energy is also growing rapidly, with expectations that it will double or possibly triple during the course of the century. The necessity to halt the buildup of greenhouse gases in the atmosphere, such as CO_2 from fossil-fuel combustion, is boosting the use of biomass for energy production. However, the increasing demand for land for bioenergy is in competition with land for food production (IEA, 2015).

It is obvious that addressing any one of these major challenges cannot be considered as a stand-alone task because of their interconnectedness (Fig. 2.1). These concepts – natural resources, energy, food & animal feed and human health – form the foundation of a sustainable bioeconomy where challenges to sustainability are addressed in a holistic manner. The growth of the bioeconomy is considered by international agencies (e.g. FAO) to be a high priority and has its roots in the sustainable use of the primary production potential of our planet. The Earth system affords an array of renewable resources which, when effectively used, are able to provide diverse goods and services to society. But this requires a proper understanding of the mechanisms

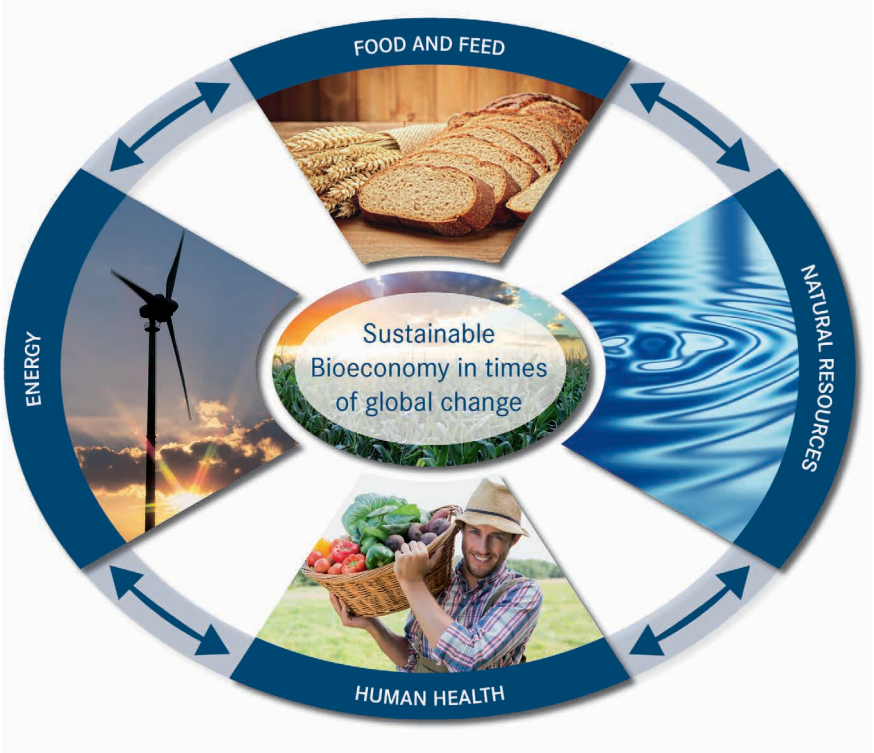

Figure 2.1. Societal challenges that science must address to ensure a proper balance with critical societal needs. The implementation of a sustainable bioeconomy lies at the core of the challenges. (Forschungszentrum Jülich)

through which terrestrial vegetation enables the acquisition of both resources and services via primary productivity.

Earth's primary productivity is under the threat of external forcing factors that have the potential to disrupt the complex equilibrium that sustains its success (Fig. 2.2). The magnitude and impact of some of those external pressures may be exacerbated by global changes that involve climate, population growth, and the current unsustainable management of some critical but limited and non-renewable resources.

Severe imbalances of soil nutrients (e.g. N and especially P) are expected to decrease primary productivity in the future. While N is unlikely to become a limiting factor for managed agricultural lands, and carbon uptake/capture potential might well increase as a result of increasing concentrations of atmospheric CO_2, P-limitations may become apparent since it is a scarce element. P comes from rocks and sediments, which are used to produce fertilisers, but P is being increasingly depleted. Changes in N:P ratios are likely to have serious consequences for ecosystems and crops (Penuelas et al., 2012). P is not only essential for plant growth, but it is required in large amounts. Plants need P throughout their life cycle, especially during early growth stages for cell division.

Water is already a scarce resource in many parts of the world and in some regions primary productivity is limited by drought (Sherwood and Fu, 2014). Changes in the climate may intensify the severity of droughts and worsen the competition for water between agricultural, industrial and civil uses, further aggravating potential shortages of this critical resource. Although cultivated plant varieties have been bred to achieve higher yields, recent studies show that an unanticipated side effect is greater susceptibility to water stress in these more productive varieties (Lobell et al., 2014).

Sustained heat waves are becoming more frequent. Their potential threat to primary productivity is well illustrated by the consequences of the 2003 heat wave in Europe (Ciais et al., 2005). The impact of extreme heat on terrestrial vegetation can be very different and have varying degrees of severity depending on other conditions occurring at the same time such as drought.

Herbivory and the spread of pests and disease are also seen as deepening threats. Global warming and intense farming may facilitate such spread, with

Figure 2.2. Environmental- and anthropogenically-driven changes threaten plant products and services globally. (Forschungszentrum Jülich)

obvious negative consequences on primary productivity and yields. Food commodities such as grains currently supply a large fraction of the calories required to sustain the global population, and up to 80% in several developing countries (Collar, 2014). However, the short life cycle of these crops, which are mainly annual crops, tends to increase susceptibility to parasites and pests.

The biosphere may be approaching a state shift similar to past events that led, for instance, to major extinctions of species (Barnosky et al., 2012). Long-term experiments support the view that such a shift is actually already happening, as pointed out in a meta-analysis of 73 studies made on different ecosystem types (Smith et al., 2015). Although it is difficult to predict the direction and magnitude of a shift, it is expected to significantly affect Earth's vegetation. In addition, shifts are likely to have consequences for a sustainable bioeconomy.

More than ever, effective methodologies are needed to assess the impact that these pressures are having on the health and productivity of Earth's vegetation, and to assess the planet's capacity to sustain the provision of necessary goods and ecosystem services. The availability of a space-based, rapidly accessible and reliable indicator of plant photosynthesis and related stress effects will help to address this need and support agricultural and resource management.

2.2 Photosynthesis – an Integrative Signature of Biosphere Dynamics

2.2.1 Principles of Photosynthesis

Photosynthesis is the process by which plants utilise sunlight, water, nutrients, and CO_2 to produce complex energy-rich biomolecules. It is the fundamental mechanism underlying plant growth and productivity, and, thus, energy and mass exchange. Overall, photosynthesis has an efficiency of just 3–6% in converting solar energy into biochemical energy (DeLucia et al., 2014). Nonetheless, it is the basic process that enables biomass accumulation

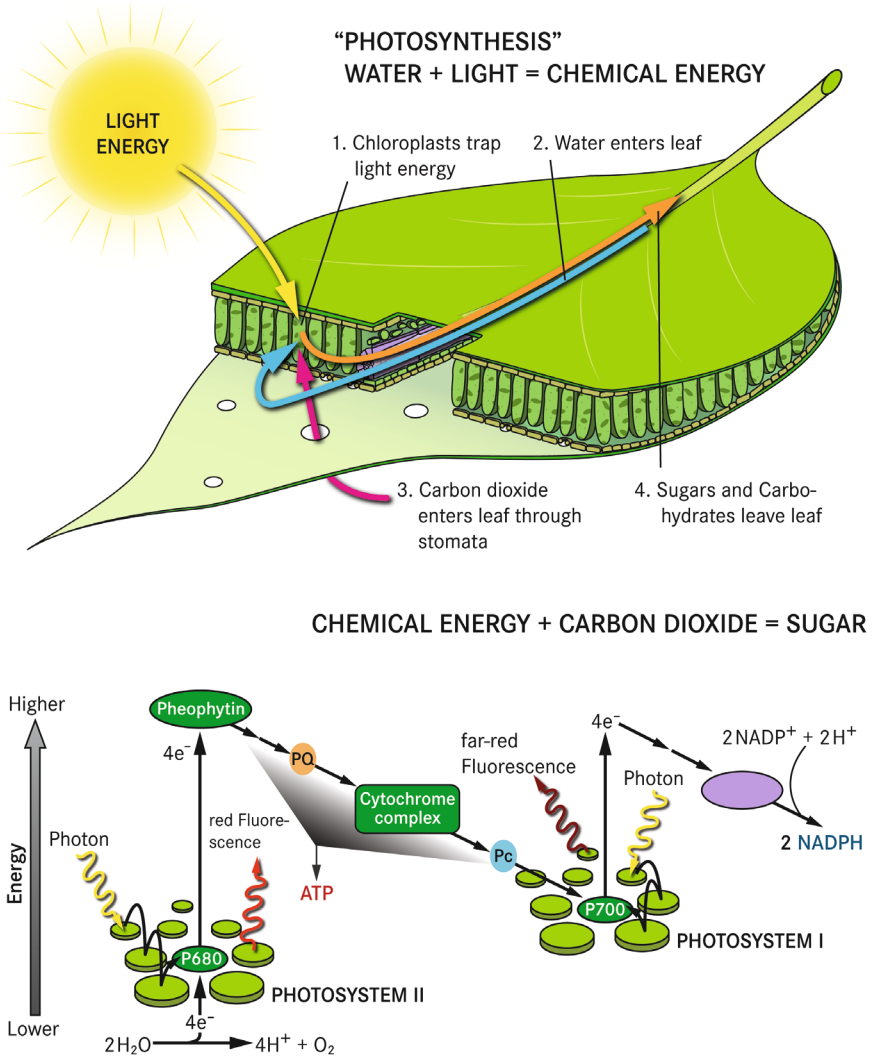

Figure 2.3. Photosynthesis: energy for life. This complex process takes place in plant leaves where atmospheric CO_2 is fixed and converted to energy-rich carbohydrates (top). The conversion of solar energy into to biochemically usable energy carriers (ATP and NADPH) occurs in the 'light reaction' of photosynthesis, which is a complex and highly regulated cascade of light absorption–electron transfer–biosynthesis (bottom). (Forschungszentrum Jülich)

in plants. Because plant growth and productivity require the availability of nutrients and water, in addition to adequate sunlight and warmth, variations in these conditions affect photosynthetic rates and, therefore, are reflected as changes in plant productivity. This is why photosynthesis can be considered to be an integrative indicator of biosphere dynamics. It is not by chance that photosynthesis has been, and continues to be, the subject of a vast body of research, for which ten chemistry Nobel prizes[1] have been awarded to researchers unravelling its complexity in the past decades.

Most green plants carry out the process of photosynthesis whereby atmospheric CO_2 is converted into energy-rich carbohydrates such as sugars and soluble carbohydrates, which then can be turned into the whole array of plant features ranging from the fragrance of a flower to the massive wooden trunks of trees. The process occurs mainly in leaves and needles. The sugars are transported out of the leaves and converted into the high diversity of plant products ranging from starch, oils, and proteins to secondary plant components, such as pigments, vitamins, and aromatic substances. The process uses energy from sunlight, which is absorbed by the plant's photosynthetic

[1] Paul D. Boyer and John E. Walker (1997), Rudolph Marcus (1992), Hartmut Michel, Robert Huber, and Johannes Deisenhofer (1988), Peter Mitchell (1978), Robert B. Woodward (1965), Melvin Calvin (1961), Richard Kuhn (1938), Paul Karrer (1937), Hans Fischer (1930), Richard M. Wilstatter (1915)

pigments, i.e. chlorophyll and carotenoids. Within the membranes of the chloroplasts, a complex cascade of biophysical and biochemical reactions are connected in series and are operated by two photosystems (Photosystems II and I, designated PS II and PS I), which, when combined, yield sufficient energy potential to drive the splitting of water molecules and linear electron transport. Ultimately, this 'light reaction' provides sufficient energy to produce two biochemical products, the biochemical reductant Nicotinamide Adenine Dinucleotide Phosphate (NADPH) and the biochemical energy carrier Adenosine Triphosphate (ATP) (Fig 2.3, bottom).

2.2.2 Regulation of Photosynthesis

Photosynthesis is a highly variable process, which plants optimise and regulate at different levels. Ecological, environmental and anthropogenic constraints influence plant adaptation. One way of looking at the efficiency of photosynthetic energy conversion is that it is regulated on three main levels (Fig. 2.4):

— canopy level: absorption of solar radiation depends on leaf exposure to light

— leaf level: light absorption depends on composition of photosynthetic pigments and internal leaf structure

— physiological level: the efficiency with which absorbed light energy is converted into biochemical energy and finally energy-rich carbohydrates depends on the functional status of the reactions described above

2.2.2.1 Canopy level

Sunlight is reflected, transmitted or absorbed by vegetation canopies. Light absorption results from a complex interplay between the amount and orientation of leaves and the 3D distribution of plants and plant organs. The plant kingdom exhibits a wide variety of canopy architectures for different ecological niches, each characterised by a complex pattern of spatial and temporal light availability. This depends on the structure of the canopy layer, the density of plant material and a canopy's reaction to environmental stress (e.g. leaf fall). Thus, the amount of light energy absorbed by a plant canopy varies considerably around the world.

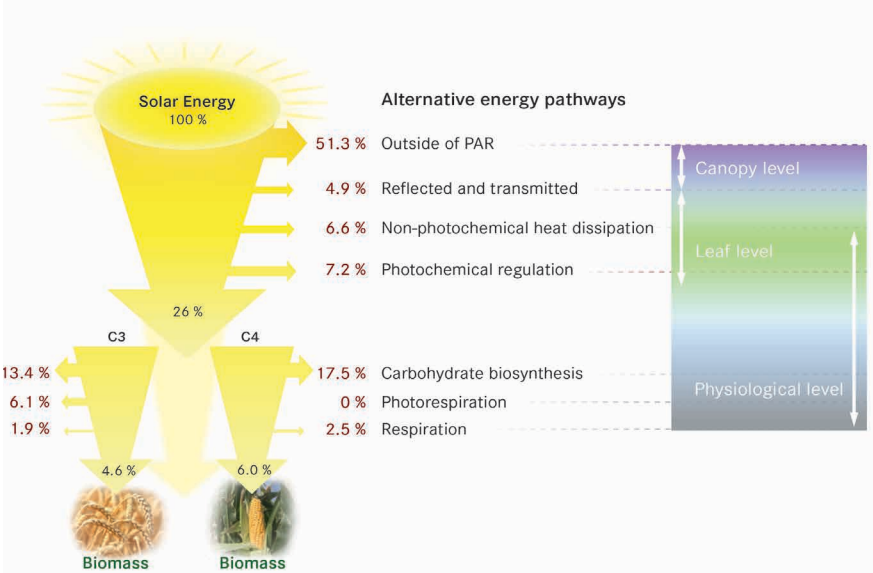

Figure 2.4. Energy flows from the primary energy of solar irradiance to the chemical energy in plant biomass. Various regulatory mechanisms greatly affect the efficiency on every level, resulting in a wide variety of conversion efficiency that spans different ecological strategies of plants (e.g. drought resistant cacti vs aquatic plants and 'C3' vs 'C4' plants). The numbers refer to modelling a 'standard' plant at 30°C. Actual numbers for a specific plant/canopy will show great variations, which illustrates the degree of regulation and variability. (Based on: Zhu et al., 2007 and 2010)

2.2.2.2 Leaf level

Some of the light absorbed by leaves is either not absorbed in the photosynthetic pigments or is not used for photosynthetic energy conversion. A substantial fraction of this energy is dissipated as heat through various regulated metabolic processes that increase under conditions unfavourable for photosynthesis (i.e. environmental stress). This heat dissipation, however, does not result in a measurable warming of the leaf, but travels through a series of metabolic pathways that dissipate excessive energy onto the photosynthetic apparatus.

2.2.2.3 Physiological level

The required energy potential difference between PS II and PS I is achieved by their different molecular organisation in the reaction centres. The activity involves charge transfer events, during which highly reactive molecules are generated and utilised. Imbalances in the electron transport reactions between the two photosystems can lead to an accumulation of noxious reactive molecules that can cause cell damage or death within the green parts of the plant. To prevent such damage, plants deploy a suite of regulatory mechanisms to balance the operation of the two photosystems in dynamic environmental conditions. Here, two main CO_2 fixation schemes operate: the C3 and C4 pathways. Although they differ in their efficiencies in converting biochemical energy to biomass, they have different advantages and disadvantages in different environmental conditions, with C4 plants tending to have an advantage in water-limited regions.

2.2.3 Environmental Stress and Photosynthesis

In many respects, the environments in which plants grow are dynamic. Light can fluctuate both in intensity and spectral qualities. Temperatures can plummet, which slows enzymatic reactions, and excessive heat can induce denaturation of enzymes and other proteins. Water deficits can trigger the closure of leaf pores (stomata), thus limiting the flow of CO_2 to the carbon fixing enzymes. Ozone and other toxic substances can directly and selectively impair components involved in photosynthetic reactions. These are but a few examples of abiotic stresses that can perturb the operation of the two photosystems.

Similarly, biotic stressors such as pathogens and herbivores impose even more complex strains on photosynthesis. With either stress category, the concerted operation of the two photosystems is dynamically regulated through a variety of protective physiological mechanisms that help to compensate for stress-induced limitations. The main protective mechanisms include limiting the flow of captured energy from antenna pigments to reaction centres, redistributing the absorbed energy between PS II and PS I and changing the flow of electrons between the linear and cyclic pathways. Additionally, various regulatory mechanisms are located directly within PS II that adjust the flow of energy in linear electron transport to dissipate excessive energy. These regulatory pathways can usually compensate for non-optimal environmental conditions. However, under sustained pressure, they may be exhausted, resulting in loss of plant vigour, productivity, and survival.

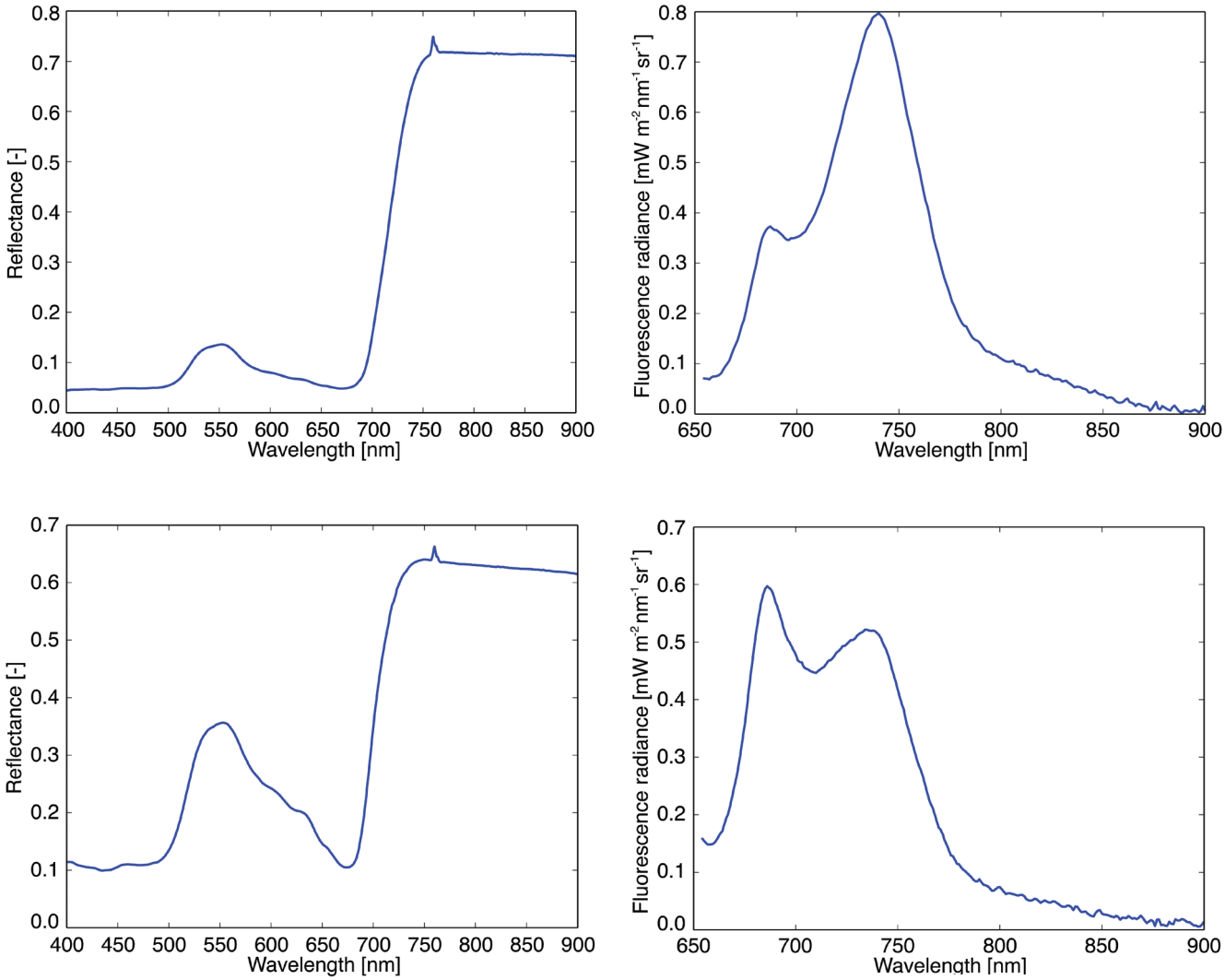

Figure 2.5. Measurements of reflectance (left) and fluorescence (right) spectra corresponding to two different species: (top) ivy (Hedera helix), (bottom) tobacco (Nicotiana tabaccum). The spectral signatures carry different information about structure and functioning of vegetation types. (University of Valencia)

2.3 Fluorescence – a Reporter for Photosynthetic Efficiency

When illuminated, green plants reflect, transmit and absorb light, but they also re-emit light in the form of fluorescence. When chlorophyll molecules in a leaf absorb photons, electrons are energised to an excited state. The fate of these 'excitons' depends on the physiological status of the plant. For example, under optimal conditions, approximately 82% of the absorbed light is used for carbon assimilation (photochemistry) while the remaining light is lost as heat and dissipated as chlorophyll fluorescence emissions. Fluorescence is, therefore, the most directly measurable reporter for photosynthetic efficiency.

2.3.1 Chlorophyll Fluorescence

So far, most information about terrestrial vegetation has been obtained from reflectance alone, but fluorescence provides additional critical information that becomes essential to accurately describe the photosynthesis process, which

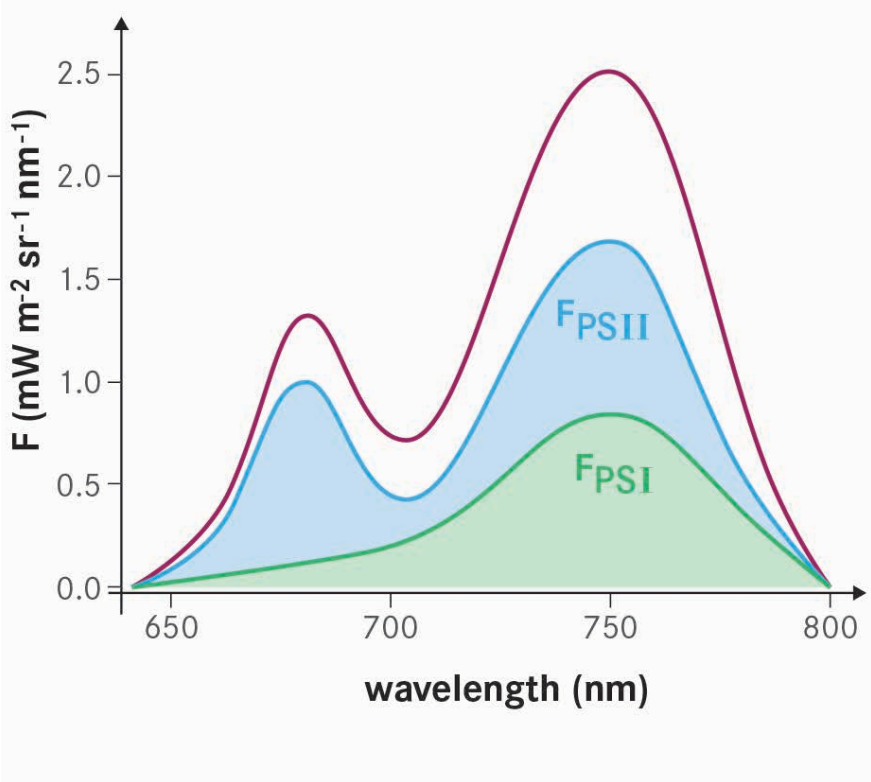

Figure 2.6 Total fluorescence emission spectrum based on the contributions from the two photosystems, PS II and PS I. Both photosystems operate in a reaction chain and are commonly measured as a two-peak signal, which are identified by their wavelength positions: F_{685} (originating mostly from PS II) and F_{740} (originating from both PS II and PS I). (Forschungszentrum Jülich)

is altered by the functional status of vegetation. The behaviour of vegetation with respect to reflected solar radiation (spectral reflectance) provides different 'signatures' of terrestrial vegetation that can be informative in identifying different vegetation types using the reflectance curve (Fig. 2.5, left panels). The emitted radiation (spectral fluorescence) can be used to identify the dynamical status of vegetation (Fig. 2.5, right panels).

In commonly occurring stress conditions, such as short-term drought, the background rate of fluorescence emission (correlated to the absorbed sunlight) has an additional emission contribution, assuming that the chlorophyll content remains stable. However, under extremely stressful conditions, very little energy goes to photochemistry, and hence energy dissipation via heat and fluorescence increases. These three processes (photochemistry, heat dissipation and fluorescence emission) are interlinked in a complex way, especially when vegetation stress occurs.

Considering fluorescence in more detail, the emission of the light referred to as chlorophyll fluorescence emanates from both PS II and PS I. Chlorophyll fluorescence produced from the initial reactions in PS II occurs at wavelengths between 650–780 nm with a peak at ~685 nm. In the case of PS I, fluorescence occurs almost exclusively in the far-red/near-infrared spectrum (>700 nm, with a peak at about 740 nm). The full chlorophyll emission spectrum covers a wavelength range in the visible- to near-infrared spectrum of ~640–800 nm. Both photosystems operate in a reaction chain and are commonly measured as a two-peak signal (Fig. 2.6). These two peaks (Lichtenthaler and Rinderle, 1988; Buschmann, 2007) are identified by their usual wavelength positions and, thus, are called F685 (originating mostly from PS II) and F740 (originating from both PS II and PS I). Abiotic as well as biotic stress factors affect photosynthetic reactions and trigger dynamic regulation of the two photosystems. PS II responses are particularly dynamic, as most regulatory mechanisms are operational there. Changes in the functional status of PS II are directly and mechanistically reflected in changes of the fluorescence emission signature.

Apart from light absorption to initiate photosynthesis, plants also need special mechanisms to protect them from light intensities in excess of that required for photochemistry in a given species or situation, otherwise there is a risk of photodamage to molecules and tissues. Various mechanisms serve

to minimise damage from excessive irradiation; these include conformational changes within the chlorophyll pigment bed, and chemical conversion between two forms of the carotenoid pigment xanthophyll (as violaxanthin and zeaxanthin). The latter mechanism is considered important in dissipation of excess light energy as heat – a key process of the phenomenon known as non-photochemical quenching (NPQ). The PRI spectral index has been shown to be responsive to the action of this xanthophyll cycle mechanism (Gamon et al., 1992). The PRI is measured in the spectral reflectance range between 500–600 nm, in particular around 531 nm, and normalised to a reference value taken at 570 nm.

2.3.2 Dynamic Response of Fluorescence to Variable Photosynthesis and Stress

When plants grow in optimal conditions, the heights of the two fluorescence peaks can be related directly to the efficiency of photosynthetic electron transport and, thus, provide an excellent proxy for actual photosynthetic light conversion. The relationship becomes undoubtedly more complicated when stress responses are involved, but this is indeed the most interesting aspect of using fluorescence to track vegetation stress. The three components of light energy usage (photochemistry, heat dissipation, and fluorescence emissions) behave differently when vegetation stress occurs (Fig. 2.7).

Plants have optimum ranges for photosynthesis within the resource milieu of light, moisture, and temperature, and the specifics of these optima are essentially characteristic for a given vegetation type. With sufficient resources and little to no stress, photosynthesis can proceed at or near maximum rates. In the presence of stress, however, adjustments in photobiology, photosynthesis and excess energy dissipation will transition through stages reflecting the increasing effects of strain. Since frost and drought are significant stressors in many crops, an associated decline in photosynthesis and increased protective measures, such as reduced light absorption and increased dissipation of absorbed light energy, occur, which tend to decrease the emission of fluorescence emission. With sustained or deepening stress, coping mechanisms can be exhausted quickly in non-hardy plants and damage to the photosynthetic molecular apparatus can produce an increase in fluorescence. This increase tends to be observed in non-hardy plants when there is frost present, owing to their greater susceptibility to molecular and tissue damage from the formation of internal ice crystals and the destruction of protein in the reaction centres of PS II (Fig. 2.3).

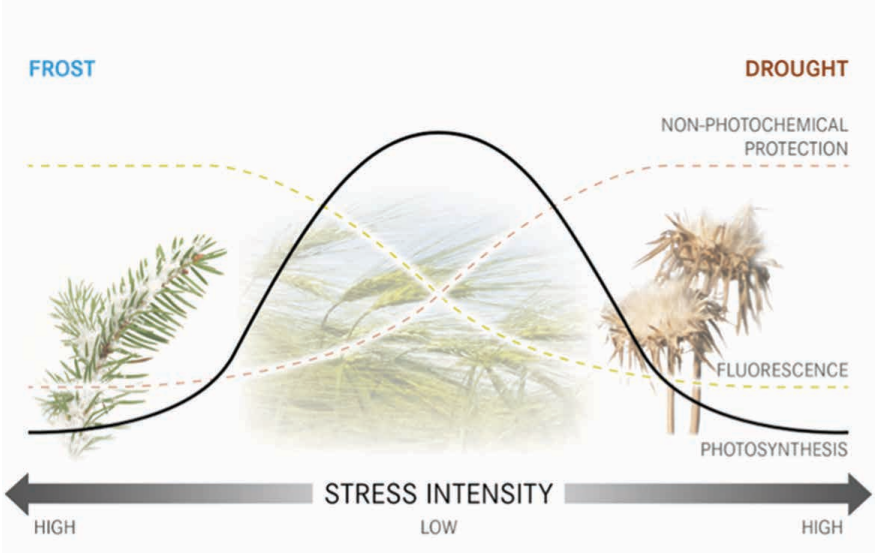

Figure 2.7. The three competing processes that affect photosynthesis for coupled but opposite stress intensity effects. (Forschungszentrum Jülich)

Going into more detail and considering drought stress in particular, a complex cascade of different regulatory events unfolds as follows:

— Dynamic response: reduced availability of water results in the closure of stomata, thereby reducing transpiration and also the rate of CO_2 uptake. This results in a dynamic adjustment of the energy flow within the photosynthetic apparatus, which can be detected by fluorescence changes, mainly in F685, that reflect responses at PS II. Such adjustments happen frequently in the course of a day. Healthy plants are usually able to accommodate such adjustments and normally no significant productivity loss occurs.

— Acute stress adaptation: if water remains limited, plants enter a state of functional stress response. As stomata stay closed, excessive absorbed light energy has to be dissipated and non-photochemical protection mechanisms become very important. In this phase, energy is redistributed between the two photosystems, producing changes in both F685 and F740. Such stress conditions may reduce yield or raise vulnerability to other stressors.

— Chronic stress conditions: if drought conditions get worse, molecular constituents and tissues can be damaged to such an extent that leaves die and shed, ultimately resulting in plant death and major yield losses. If there is substantial destruction to the chlorophyll pigments and PS II reaction proteins, there can be a phase of increased fluorescence. This is because there is reduced reabsorption of fluorescence and impaired electron transport. However, typically, chronic drought eventually results in a marked decrease in the overall fluorescence emission as well as changes in canopy reflectivity over the whole photosynthetically active radiation spectrum. Changes in fluorescence can be observed prior to the manifestation of irreversible vegetation damage and prior to associated reflectance changes.

Such complexity applies to any sort of stress, with differential balance between the three pathways of energy dissipation. The responses to temperature stress, nutrient deficiency, noxious chemicals, pests and diseases generate different cascades that can be modelled or anticipated based on current knowledge of plant photosynthetic mechanisms and ecophysiological responses. It is essential, therefore, that a complete representation of fluorescence emission peaks and emission profiles, as well as important ancillary reflectance features, biophysical information and environmental information, is available to allow these complexities to be properly understood and fluorescence changes accurately interpreted in a given situation.

To convert the biophysical processes of light absorption to the biochemical process of CO_2 uptake and transpiration, additional measurements are needed such as the actual canopy skin temperature and a dynamic spectral reflectance index (non-photochemical energy dissipation). In fact, energy balance and a significant component of the physiological behaviour of vegetation are driven by the canopy temperature. Chemical reactions driving photochemical energy conversions and carbon assimilation through photosynthesis are significantly affected by changes in temperature, as well as the partitioning of energy absorbed into photochemical processes. Thus, any interpretation of vegetation functioning must take into account the corresponding canopy temperature to properly understand the underlying phenomena responsible for the actual carbon assimilation through dynamic photosynthesis. The simultaneous global measurement of the full reflectance signature, dynamic spectral reflectance changes in the visible spectral range (e.g. PRI), two-peak fluorescence emission and surface temperature will for the first time allow the quantification of actual photosynthetic rates and the extent of gross primary productivity (GPP) across all ecosystems in the seasonal cycle. This capability represents an unprecedented leap in our capacity to evaluate carbon uptake rates and stress effects.

2.4 Readiness and Unique Contribution in the Global Context

Chlorophyll fluorescence has been used for decades in laboratory and field experiments as a tool to track vegetation photosynthetic responses, and as an indicator of photosynthetic stress effects and resilience. Applications of fluorescence methods have been extensive, spanning agriculture, forestry, horticulture and aquatic science. Fluorescence analysis is an ideal tool to track plant responses to environmental conditions, as it allows photosynthetic dynamics to be studied quickly in otherwise untouched vegetation, and repeatedly over time. Today, the ready availability of fluorescence laboratory and field instruments (Mohammed et al., 1995), together with a robust understanding of the underlying science, has made chlorophyll fluorescence analysis an established technique for basic and applied science.

The following subsection provides an overview of the science and knowledge related to fluorescence that has been established through experiments, observations and numerical modelling from the leaf level to the canopy scale.

2.4.1 Observing Fluorescence with Proximal Sensing

Considerable knowledge of the spatial and temporal dynamics of photosynthesis has come from fluorescence measurements made in the laboratory or under controlled environmental field conditions (temperature, light intensity, CO_2 concentration). Such studies have emphasised the use of active technologies, which use lasers or other artificial light sources for the excitation of fluorescence. However, a disadvantage of active techniques is that they cannot generally be used over great distances, owing to the power demands of the light sources. Therefore active methods have tended to be restricted to sensing leaves or small single canopies rather than imaging fluorescence over large areas. There has been a long-standing interest (Meroni et al., 2009) in advancing from active technologies to passive solar-induced methods suitable for use at larger spatial scales in natural ambient conditions.

The combination of active and passive techniques over the last few decades has resulted in a vast knowledge about photosynthesis dynamics and responses to different environmental and stress conditions. Such responses have been described and integrated into physiological models that are used

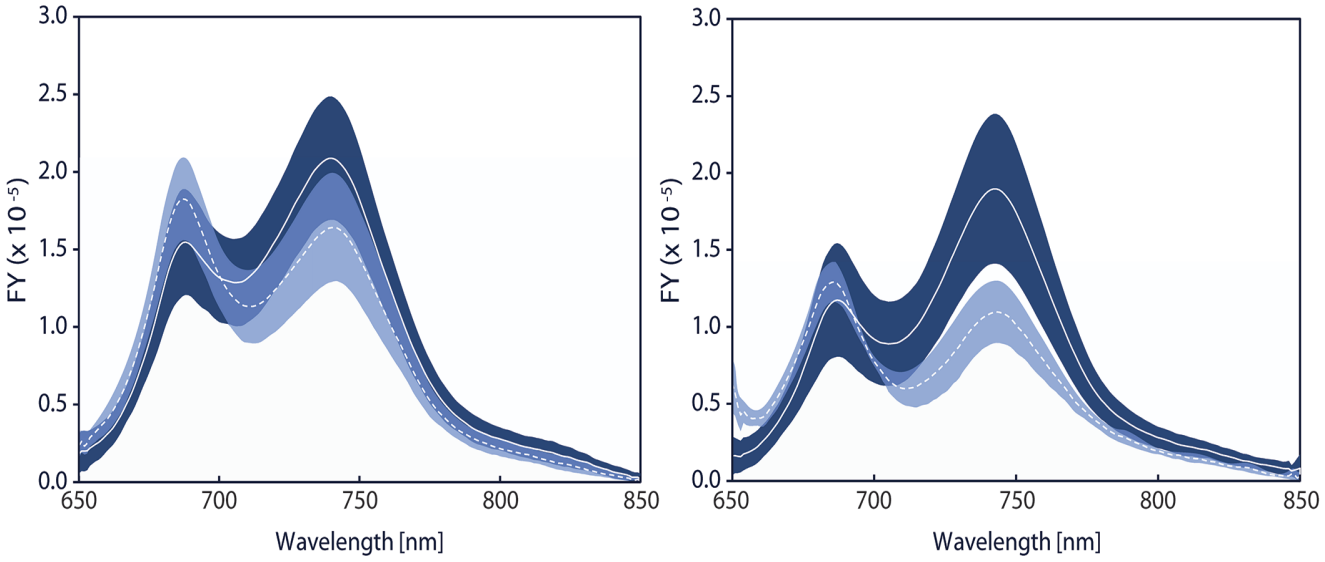

Figure 2.8. Fluorescence yield of P. x acerifolia (London planetree, left) and P. canariensis (Canary Island Date Palm, right) for low (solid lines) and high (dashed line) traffic emission exposure; bands indicate standard deviation. (Based on: Van Wittenberghe et al., 2013)

today and that are helpful for diagnosing and interpreting photosynthetic responses. From the many studies, it is evident that fluorescence measured with active and/or passive sensors is a valuable indicator of stress effects, vegetation health, and productivity. A recent meta-analysis examined effects of such ubiquitous stresses as water deficit, temperature extremes, and nutrient insufficiency (Ač et al., 2014).

Fluorescence information has proven to be very important in practical applications. For example, the 'Biomonitoring of urban habitat quality by airborne Hyperspectral measurements' (BIOHYPE) project used the shape of the fluorescence emission curve as an integrative indicator of pollution effects in the foliage of urban trees (Van Wittenberghe et al., 2013, 2014). The project's field experiments found that stress effects induced by traffic pollution were detectable by steady-state fluorescence yield indices assessed in tree leaves. The ratio of the red to far-red peaks, and the red peak (normalised by absorbed photosynthetic radiation) were the features most sensitive to the effects of traffic emissions, and these proved more sensitive to traffic pollution stress than did leaf pigment content (Fig. 2.8).

2.4.2 Observing Fluorescence with Airborne Sensors

A major challenge has been to prove that the vegetation fluorescence measurement techniques that were developed for laboratory and field conditions can, indeed, be transformed into remote-sensing systems operated from aircraft and satellites. Remote-sensing approaches enable the mapping of photosynthetic efficiencies over large geographical areas, and ultimately at the global scale using satellite measurements. Indeed, evidence is now available that such an advance is at hand.

In the course of the mission preparatory phases, an airborne fluorescence imager (HyPlant) was built. During 2012–14, this instrument was used in several field campaigns covering agricultural areas, grasslands, and various types of forest in Finland, Germany, France, Italy, Czech Republic, and the US (in cooperation with NASA).

Figure 2.9. The upper panel shows a reflectance image close to Klein Altendorf, Germany, and the lower panel provides a direct measure of canopy fluorescence emission as measured by the HyPlant airborne sensor. (Forschungszentrum Jülich)

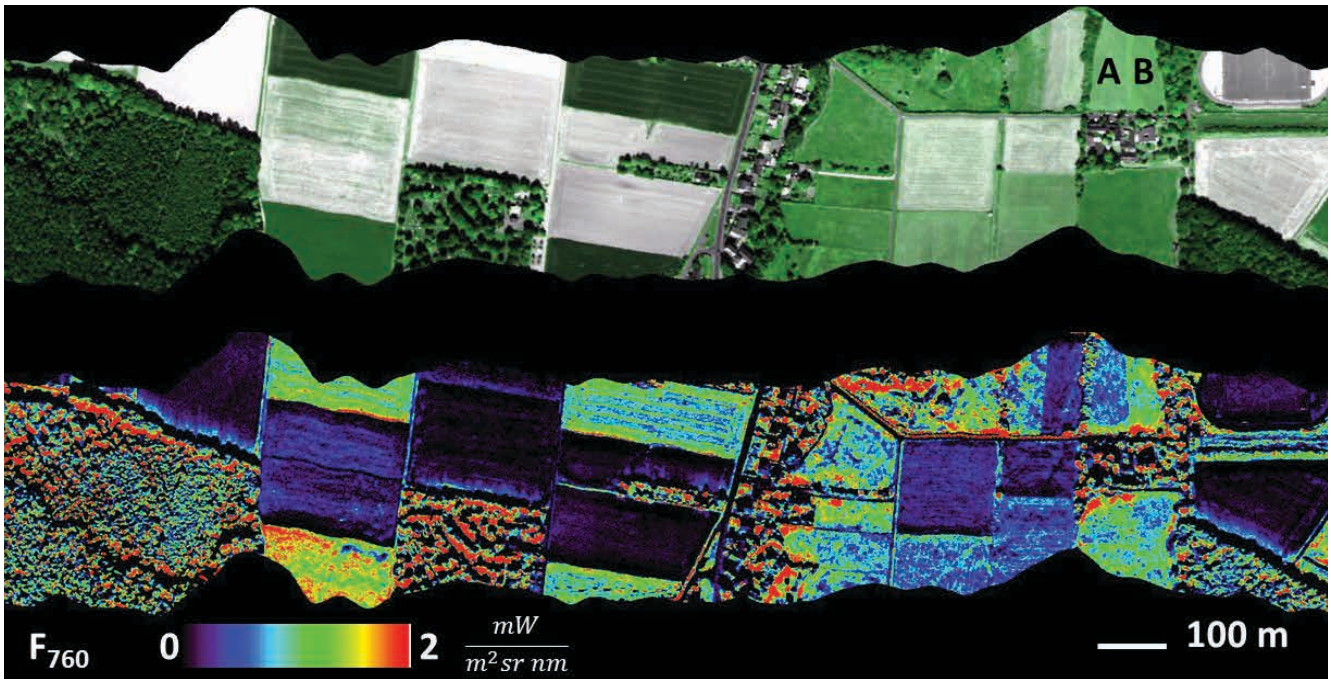

The fluorescence signal measured over various vegetation types shows totally novel and highly relevant spatial-temporal dynamics, which are not visible using traditional spectral reflectance. Taking the precision of the measurements and the natural biological variability into account, including the structural and functional properties of different vegetation types, the fluorescence patterns could be detected reliably in the airborne data.

As an example, reflectance and fluorescence maps obtained over an agricultural research site in Klein Altendorf, Germany, are shown (Fig. 2.9). This map shows large differences in fluorescence emission between different vegetation types (e.g. lower fluorescence in forests (left in lower panel) versus higher fluorescence in dense agricultural fields (middle and right in lower panel). In addition, the fluorescence emission clearly reveals information on vegetation status, which is not visible in the reflectance domain. For instance, the two fields denoted as A and B display almost identical reflectance (upper panel), while their fluorescence emission is very different (lower panel).

2.4.3 Attempts to Derive Fluorescence from Space

Preliminary space-based retrievals of fluorescence have been reported from a few missions, providing high spectral resolution measurements in the red to far-red range. These missions have been designed for atmospheric chemistry operating at coarse spatial resolution (≥30 km^2). They include GOSAT (TANSO-FTS sensor), MetOp (GOME-2), and Envisat (SCIAMACHY) (e.g. Frankenberg et al., 2011; Joiner et al., 2012). Newer missions that include NASA's recently launched OCO-2 mission allow discontinuous (~3 km^2) spatial samples for retrievals in the far-red (Frankenberg et al., 2014). In the future, Europe's Sentinel-5 Precursor (TROPOMI sensor) (Guanter et al., 2014) will also have the potential to measure fluorescence emission from space.

However, the relatively large pixel area of these measurements makes them unsuitable for addressing the information needs of many small agricultural and forestry land management units that provide important economic and ecosystem services. Moreover, the lack of simultaneous information about non-photochemical energy dissipation, canopy temperature and plant functional status, together with the fact that fluorescence is only retrieved in a very narrow spectral range, make the data from atmospheric chemistry missions of limited use for understanding land-surface processes and quantifying actual photosynthesis.

2.4.4 Modelling Fluorescence

Modelling of chlorophyll fluorescence emission has advanced considerably over the last decade, and various models now exist that quantify the link between fluorescence, other physiological parameters, and the functional status of plants at leaf level and beyond.

Leaf-level models of fluorescence emission were reviewed recently in the Fluorescence Explorer (FLEX) Sentinel-3 Tandem Mission Photosynthesis Study (Mohammed et al., 2014). The study identified process-based and semi-empirical formulations that could also be suitable for the incorporation of stress effects and used as upscaling models from leaf to canopy level (Magnani et al., 2009; Van der Tol et al., 2014). The most relevant physiological mechanisms have been incorporated in these models.

Modelling the transmission of incoming light and the fluorescence emission through the vegetation canopy is a complex process, which has been elucidated over the last decade also by means of an integrated leaf-canopy fluorescence model (FluorMOD, Miller et al. 2005). Current models are able to simulate the

effects of irradiance, vegetation structure and physiology on fluorescence and photosynthesis. More recently, models, such as SCOPE, have been refined and updated with novel components for improved representation of leaf physiology and radiative transfer (Verrelst et al., 2014).

Current simulators combining these leaf–canopy models and atmospheric-radiative transfer schemes are able to compute top-of-atmosphere (TOA) radiances at the relevant spectral resolution.

2.4.5 Use of Fluorescence Measurements in Vegetation Models

Statistical approaches to linking fluorescence emission to physiological attributes such as photosynthetic efficiency or stress status have used a range of strategies – from simple correlations and empirical associations to sophisticated process-based mechanistic modelling. These approaches may be considered at leaf, canopy, and global scales, along with modelling applications. Reducing uncertainty in modelling global patterns of GPP dynamics and responses would greatly advance the understanding of terrestrial carbon fluxes in Earth System Models.

At global and regional scales the incorporation of fluorescence emission measurements has the potential to improve modelling of GPP. For example, fluorescence variables might serve as a proxy for light-use efficiency (LUE) in models of GPP that use LUE, and absorbed photosynthetically active radiation (APAR) (Garbulsky et al., 2014).

Space-based fluorescence measurements may be important in constraining terrestrial dynamic global vegetation models (DGVMs). These models are valuable but complex tools to study processes and interactions between vegetation and atmosphere, and they may be used to integrate vegetation dynamics in global-climate simulations (Quillet et al., 2010). Initial efforts to assimilate satellite-derived far-red fluorescence with DGVMs indicate that uncertainty in predicted GPP might be reduced by 40–70 % in high productivity tropical and temperate regions of North America, Europe, and South America (Parazoo et al., 2014). These investigators concluded that satellite measurement of fluorescence presents a new opportunity to quantify GPP response to climate factors and potentially to constrain carbon-cycle predictions.

2.5 Scientific Challenges and Gaps

The societal challenges and needs related to the biogeochemical cycles and a sustainable bioeconomy translate into the following overarching scientific challenges:

— A better understanding of carbon and water fluxes between vegetation, the atmosphere, and the geosphere is needed at local to global scales

— The cause-effect relationships between environmental factors and vegetation stress need to be determined

— Anthropogenic influences on vegetation functioning need to be assessed

Understanding and quantifying the actual photosynthetic rate or, in other words, the plant performance, is the common element when addressing these challenges.

Until now, Earth observation missions addressing vegetation properties at the relevant spatial resolutions and scales primarily addressed land-cover type and change, structural parameters, and constituents. These parameters

can provide estimates of potential photosynthesis and – when combined with numerical models – the computations yield estimates of actual photosynthesis (as expressed through GPP). So far, the estimation of photosynthetic rate or GPP from remotely-sensed absorbed solar radiation have depended mainly on knowledge of the LUE, photosynthetic active radiation (PAR), and the fraction of APAR (Goetz and Prince, 1999), or the fraction of atmospheric carbon, which is assimilated by plant canopies per unit of light absorbed. Since it has been found that each of the parameters may not be very accurate and can have similar error structures introduced through uncertainties, for example, in the atmospheric correction or bidirectional surface reflection, the spatial and temporal variability cannot be captured accurately by current satellite-based GPP retrieval methods. In addition, early models assumed LUE to be constant, but it is now well understood that factors such as temperature and moisture stresses, among others, modulate LUE to a large extent.

This calls for more exact methods to retrieve photosynthesis at global scales in a remote-sensing framework. Solar-induced fluorescence, which is related directly to the efficiency of photosynthesis, is likely to bring in substantial innovation in Earth observation, thus fostering a real revolution in the way remote sensing can 'sense' photosynthesis from space.

As a particularly innovative mission, FLEX will enable, for the first time, terrestrial vegetation to be observed using an emitted rather than a reflected light signal. The key challenge is to observe photosynthesis from space using a novel approach: something capable of revolutionising Earth observation based on the approximation that photosynthesis is given by the product of the fraction of light absorbed by the vegetation and the light-conversion efficiency of canopies. The expectation is that the combined use of fluorescence, surface temperature and photochemical reflectance will finally reduce the uncertainty in the quantification of photosynthetic rates so that primary productivity of both managed and unmanaged ecosystems can be assessed. Europe has the opportunity to lead this revolution in the way space missions address this type of critical question. The capacity to measure photosynthesis from space is unprecedented and paves the way for a new generation of satellite missions designed to support science-based strategies for sustainable development.

The proposed FLEX mission will also address all five land challenges (L1 to L5) identified in ESA's Living Planet Programme: Scientific Achievements and Future Challenges (ESA, 2015b). FLEX will:

— satisfy L1 *(Natural processes and human activities and their interactions on the land surface)* by quantifying the spatio-temporal dynamics of photosynthesis – the most important natural biological process in vegetation – and by reporting on human impacts upon managed and natural ecosystems

— meet L2 *(Interactions and feedbacks between global change drivers and biogeochemical cycles, water cycles, including lakes and rivers, biodiversity, and productivity)* by describing the spatio-temporally variable rates of carbon uptake from the atmosphere within specific land areas/ecosystem types, and relating these to limiting factors such as drought, high temperature or nutrient deficiencies; and by deriving implications for associated water and energy cycles

— address L3 *(Structural and functional characteristics of land use systems to manage sustainably food, water and energy supplies)* by delineating and quantifying the conversion of solar energy into agricultural and fibre production for food and biomass

— address L4 *(Land resource utilisation and resource conflicts between urbanisation, food and energy production and ecosystem services)* by

discriminating various land cover types and their photosynthetic function within defined anthropogenic boundaries (e.g. counties, nations) and land-use patterns, to relate this information to food availability and energy use during production of core and derived plant products

— satisfy L5 *(How limiting factors (e.g. freshwater availability) affect processes on the land surface and how this can adequately be represented in prediction models)* by relating observed photosynthetic patterns in space and time to primary limiting factors such as drought, high temperature or nutrient deficiencies, and by integrating plant biological and biophysical parameters within the context of mechanistically based diagnostic and predictive models of physiology and radiative transfer in vegetation canopies

FLEX is oriented to bridge these challenges through an advanced scientific Earth observation capacity that will support innovative science, knowledge-based policy development, and strategic implementation, bringing a fresh and timely approach to addressing critical gaps in our understanding and for the management of the world's vegetation resources.

→ RESEARCH OBJECTIVES

3. Research Objectives

Observing vegetation on the global scale continues to be a key element in Earth observation programmes. Current and planned missions dedicated to global terrestrial vegetation monitoring, both directly (e.g. SPOT Vegetation and Proba-V) and indirectly (e.g. Sentinel-2 and Sentinel-3), provide measurements related to the amount, structure or constituents of vegetation such as leaf-area index, fractional cover, water content, chlorophyll content, or land-cover type and land change.

Combined with auxiliary information and/or numerical models, these observations have been used to estimate potential photosynthetic activity. To address the challenges and scientific questions outlined in the previous chapter, a deeper understanding of the functioning of plants at a global scale is required. Observations of the actual photosynthesis and vegetation health status provide relevant and essential information across a wide range of application areas, vegetation types and climate variability.

Scientific and management applications include food security, biodiversity, ecosystems and land-use changes, as well as other applications related to: the sustainable use of plant products in a bio-based economy, integrated water-management, global-carbon modelling and better prediction of the effects of global change. However, actual photosynthetic activity of terrestrial vegetation and early vegetation stress cannot be measured directly through current remote-sensing approaches.

It was outlined in Chapter 2 that for the assessment of photosynthetic activity, fluorescence measurements represent a unique and novel capability to be exploited; no other measurement protocol applicable to space measurements allows the retrieval of such an indicator of actual canopy photosynthesis. A particular advantage of fluorescence is its capacity to serve as a pre-visual indicator of stress effects before damage is irreversible and detectable through reflectance measurements. This feature makes it of substantial benefit in practical applications such as agronomic-crop improvement and forest-vegetation assessment under the pressures of a changing climate. Notably, the capacity of fluorescence to track photosynthetic strain and recovery could prove to be a significant indicator of the integrity of vegetative carbon sinks, possibly more so than gross primary production (GPP). Given the importance of anthropogenic impacts associated with land-use change and varying management practices, knowledge of the actual functioning of the photosynthetic machinery inside the plants will provide information that has not been made available through existing Earth observation capabilities.

The overarching research objective addressed through FLEX is an improved understanding of the actual functioning and photosynthetic efficiency of vegetation. It will be the first mission that facilitates the direct measurement of the cause–effect relationships between plant health, photosynthesis and vegetation functioning. These will be studied under changing environmental conditions and at a spatial scale supporting individual agricultural and forestry management units:

— To support the identification of optimal growing and management strategies for a performance appraisal of vegetation for stress resistance in the context of crop production and food security

— To provide an early pre-visual identification of stress effects to help track resilience and recovery of plant photosynthetic function, to delimit vegetation sites compromised by biotic and abiotic stresses, and to identify vegetation stands affected by insect or disease in order to schedule measures to salvage a harvest

— To better understand and describe processes related to the dynamics of plant photosynthesis that will result in more accurate estimates of GPP and foster the development and improvement of carbon assimilation in dynamic vegetation models

— To enhance our knowledge of the coupling of the carbon and water cycles and to improve the predictive capability of current model systems

3.1 Mission objectives

By quantifying information on the full fluorescence emission spectra, we can improve our understanding of how light is used by plants. This is the approach used by plant physiologists in laboratories and in the field. FLEX would provide such measurements from space and allow retrieval of the relevant parameters of fluorescence emission as the most direct indicator of photosynthesis and vegetation stress.

The core mission objective of FLEX is to provide measurements capturing the spatial and temporal dynamics of vegetation fluorescence emission. Observations will be performed globally over a range of environmental and vegetative situations at spatial resolutions that address the spatial scale of individual management units. This includes observing different plant species, C3 and C4 dynamics, different age structures, seasonal fluorescence patterns, and year-to-year differences in fluorescence behaviour.

The fluorescence signal originates from the core complexes of the photosynthetic machinery where energy conversion of absorbed photosynthetically active radiation occurs. Because the photosynthetic apparatus is a highly complex but organised structure, the emission spectrum of fluorescence that originates from the photosynthetic apparatus is well known. It occurs with two peaks that have broad bands with maxima around 685 nm and 740 nm. The height of the two peaks is variable, reflecting, among other processes, the efficiency of photosynthetic electron transport. Thus, fluorescence is a proxy for actual photosynthetic light conversion and the functioning of the plants. To address the research objectives outlined above, it is therefore mandatory to retrieve information on the full fluorescence spectrum covering the spectral range from 650 to 800 nm.

The FLEX mission will provide global maps of vegetation fluorescence emission as primary measurements. It will focus on the relevant characteristics of the fluorescence emission spectra (Fig. 3.1), which are:

— Fluorescence emitted in the range of the oxygen absorption bands O_2-A (F_{687}) and O_2-B (F_{760}), i.e. at 687 nm and 760 nm, with an accuracy of 0.2 mW m^{-2} sr^{-1} nm^{-1}.

— Maximum fluorescence emission of the two peaks ($maxF_{<685>}$ and $maxF_{<740>}$) including the wavelength position of the peaks with an accuracy of 0.2 mW m^{-2} sr^{-1} nm^{-1} and 5 nm, respectively.

— Total fluorescence emission integrated over the full emission spectrum. Using these anchor points the full two-peak emission spectrum of fluorescence (F_{tot}) will be retrieved with an accuracy of 10% for normal reference conditions.

— Fluorescence emission from PS II and PS I. While the data described above are direct outputs of the Level-2 processing algorithm as described in Chapter 6, the calculation of emissions related to the two photosystems involves auxiliary data and models. F_{PSI} and F_{PSII} will be the main data products for higher-level applications, including assessments of vegetation stress and vegetation modelling with an accuracy of 10%.

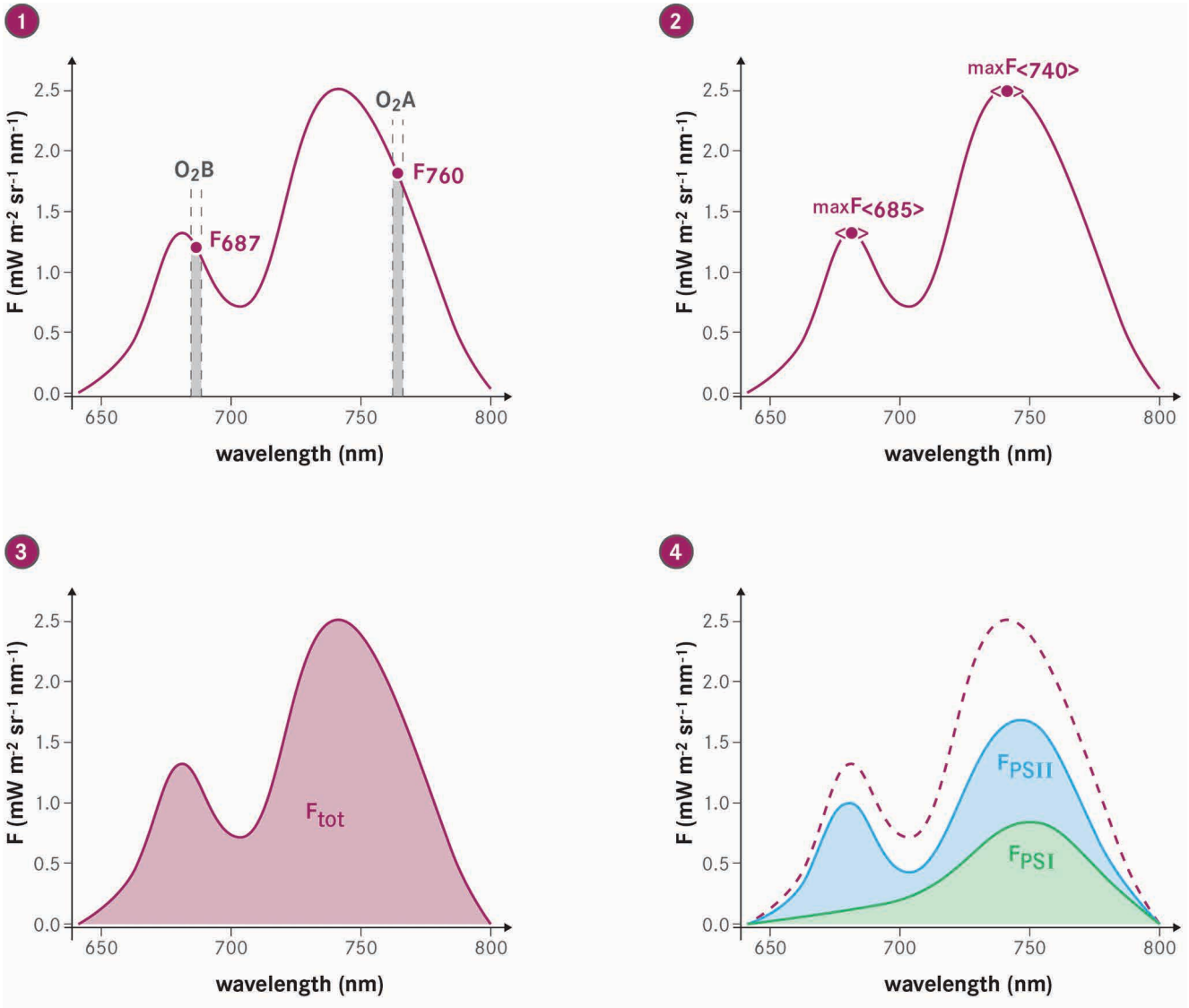

Figure 3.1. Fluorescence products from FLEX. (1) Fluorescence emission is retrieved in the range of the two oxygen absorption lines, i.e. at 687 nm and at 760 nm (F_{687} and F_{760}). (2) The maxima of fluorescence emission ($maxF_{\langle 685\rangle}$ and $maxF_{\langle 740\rangle}$) and the position of the peaks' maxima around 685 and 740 nm are also derived. (3) From these anchor points the full fluorescence emission spectrum (F_{tot}) is reconstructed (area under the curve). Finally, (4) The emissions originating from photosystems II and I are calculated (Forschungszentrum Jülich).

The novel measurements provided through FLEX will deliver the most direct estimates of photosynthetic efficiency and activation/deactivation status of the photosynthetic machinery, providing a more precise determination of the duration of the growing season in boreal ecosystems than current reflectance measurements from a satellite.

Another key mission objective is to simultaneously measure dynamic photochemical reflectance changes associated with energy dissipation mechanisms, which exploit the subtle changes in the green spectral region. This information has been used to estimate non-photochemical heat dissipation – a critical quantity to derive photosynthesis. Such changes take place in the 500–600 nm spectral range, and describe the adaptation of vegetation to an excess of light and stress. The spectral coverage provided through the FLEX mission will allow for a more precise analysis of the changes described by the Photochemical Reflectance Index (PRI). These dynamic reflectance changes do not only represent a necessary complement to fluorescence measurements, but also become essential to establish the relationship between fluorescence and photosynthesis.

In a first simplified approach, it can be assumed that the integrated fluorescence emission is proportional to photosynthesis rates, with the associated slope determined by the PRI. In a more sophisticated analysis using data assimilation techniques, the complementary information about fluorescence and photochemical-reflectance change constrains the retrieval of photosynthesis under variable stress conditions better than using fluorescence alone or spectral-reflectance changes separately.

In addition, canopy temperature estimated from thermal-infrared measurements is also necessary because photosynthesis itself is a function of temperature, and most factors relating environmental stress and energy balance are also linked to canopy temperature. Thus, a simultaneous observation of canopy temperature together with fluorescence measurements is mandatory for a proper understanding of the variability observed in fluorescence measurements and a proper link between fluorescence and actual photosynthesis.

3.2 Additional Related Vegetation Parameters

The FLEX mission will be able to provide estimates of surface reflectance in the visible range with high spectral resolution, to derive vegetation properties that enable the proper understanding of the background vegetation physiological and environmental conditions that determine the degree of vegetation stress, actual plant photosynthesis and GPP. The techniques to derive these parameters are well established:

— leaf chlorophyll content (LCC) and leaf area index (LAI) are derived through well-established model inversion techniques from the broadband reflectance signal between 400 and 800 nm, and provide information on canopy structure and composition

— fluorescence normalised by the light absorbed by chlorophyll quantifies fluorescence-yield: a parameter providing an estimate of fluorescence emissions that is independent of seasonal irradiance variability and linked more directly to canopy phenology

The FLEX measurements will be used to make unprecedented calculations of vegetation properties and state estimates. Such higher-level properties will fundamentally increase our scientific understanding of the spatial-temporal variability and the predictability of plant functioning. For example, actual rates of photosynthesis or GPP are derived by combining measurements of fluorescence, non-photochemical heat dissipation and surface temperature. The combination of these signals addresses the actual photochemical events of photosynthesis most directly, specifically those related to the efficiency of photosystems II and I.

→ OBSERVATIONAL REQUIREMENTS

4. Observational Requirements

This chapter provides the observational requirements for the FLEX mission concept. All the requirements relating directly to the mission objectives were outlined in Chapter 3. Here, the overall spatial and temporal sampling requirements are provided, as well as the information needed for the accurate retrieval and proper interpretation of vegetation fluorescence levels. To acquire all necessary measurements, and in order to make optimal use of existing observational capabilities within the Copernicus programme, the FLEX mission is proposed as a tandem concept with Sentinel-3.

Because it is a tandem mission concept, the spatial and temporal colocation requirements between FLEX and Sentinel-3 measurements are derived, as well as radiometric cross-calibration requirements. The specific observational requirements for the FLEX instrument are then stated. As the instrument is the core of the mission, optimised for vegetation fluorescence measurements, its spectral coverage, spectral resolution and sampling, signal-to-noise ratio (SNR), and radiometric calibration requirements are indicated. Lastly, the FLEX Level-1, Level-2 and higher-level products are defined.

4.1 Spatial and Temporal Sampling Requirements to Observe Global Vegetation Fluorescence

Because vegetation fluorescence is highly dynamic, appropriate spatial and temporal sampling is a key part of the mission. High spatial resolution is needed to identify changes at the level of land management units, but monthly observations at global scales are also needed to observe the seasonal dynamics of vegetation.

4.1.1 Spatial Coverage Requirements

The objective is to have a global land coverage mission that observes vegetation photosynthesis through the seasonal cycles and the activation/deactivation of the photosynthetic mechanisms. Global coverage should be achieved for all land surfaces between 56°S and 75°N including major islands (greater than 100 km^2). Because of the potential relevance of island biodiversity for carbon studies, a mask will be used to define the effective spatial coverage over specific coastal areas and islands of special interest. As a minimum requirement, coastal waters within 50 km of any land as well as ocean waters with a depth of less than 10 m will be covered.

4.1.2 Spatial Sampling Requirements

Observing physiological processes and the status of vegetation health usually requires very high spatial resolution in order to identify as many plant types as possible. However, land–atmosphere interactions are barely modelled in great detail for large areas and in most cases surface–atmosphere coupling is represented at reduced spatial resolution.

For the qualitative and quantitative assessment of the vegetation functioning and for downstream applications related to agricultural management and food security, the measurements should reflect the spatial scale of fields or management units. Most of these relevant units can be addressed with a spatial resolution of 300×300 m^2 (Table 4.1).

In the particular case of carbon exchange between the surface and the atmosphere, the combination of requirements results in an optimum spatial

Land type	Area [km^2]
Boreal forest stands: Canada (NW Alberta), class 1 of 2 (Stelfox and Wynes, 1999)	0.1
Farms: Europe (European Commission, 2013)	0.1
Forests: Europe, class 2 of 5 (Forest Europe, UN Economic Commission for Europe (UNECE), Food and Agriculture Organization (FAO), 2011)	0.1–1.0
Forests: Europe, class 3 of 5 (Forest Europe, UNECE, FAO, 2011)	1.0–5.0
Farms – Canada (Statistics Canada, 2011)	3.1
Forests – Europe, class 4 of 5 (Forest Europe, UNECE, FAO, 2011)	5.0–100

Table 4.1. Typical extent of different land types addressed by FLEX.

resolution in the range of 0.01–0.09 km^2. This is detailed enough to identify vegetated patches while resolving interactions at scales comparable to typical heights of the atmospheric boundary layer. In addition, many validation activities are based on *in situ* measurements from flux towers, which represent a certain homogeneous area around a station. Here the resolution of 0.01–0.09 km^2 would also be reasonable and in line with other data sources and modelling efforts.

In order to avoid aliasing, for the sampling distance of 300 m, the spatial resolution is assumed to be of 330–350 m.

4.1.3 Time of Observation

In low light or when the canopy is not affected by stress, the diurnal cycle of vegetation fluorescence tends to follow illumination levels, with a maximum around noon. However, on days with high illumination levels, steady-state chlorophyll fluorescence is usually highest in the early morning and typically starts to decrease at around 10:00 local time, reaching minimum values between noon and early afternoon. Because the clear-sky diurnal illumination levels always show a maximum at noon, the absolute fluorescence tends to be at a maximum around noon in most cases, although the fluorescence yield can become minimal. According to eco-physiological research, the best time for capturing the clearest signals would be around mid-morning, local time, in high illumination conditions, as illustrated in Fig. 4.1. As a balance between maximum fluorescence emission and maximum solar illumination, observation time should be around 9:30–10:00 local time.

Such optimal illumination conditions cannot be achieved everywhere along the orbital path, owing to changes in local time. Therefore, a compromise must be achieved. Selecting 10:00 as the time to cross the equator results in local

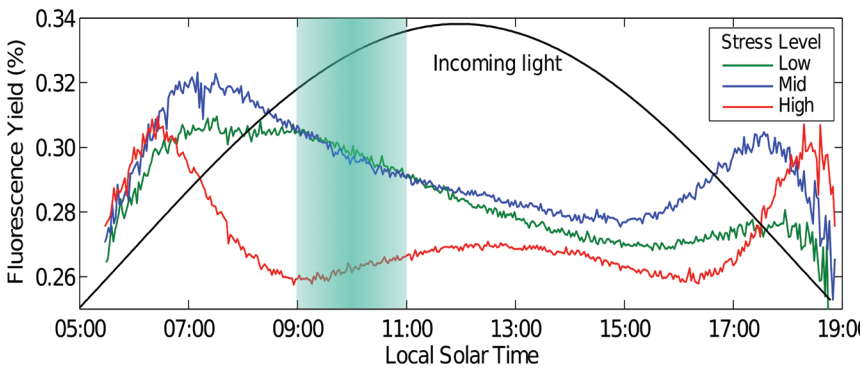

Figure 4.1. Typical fluorescence yield variations along a diurnal cycle in varying environmental conditions inducing variable vegetation-stress cases. (University of Valencia)

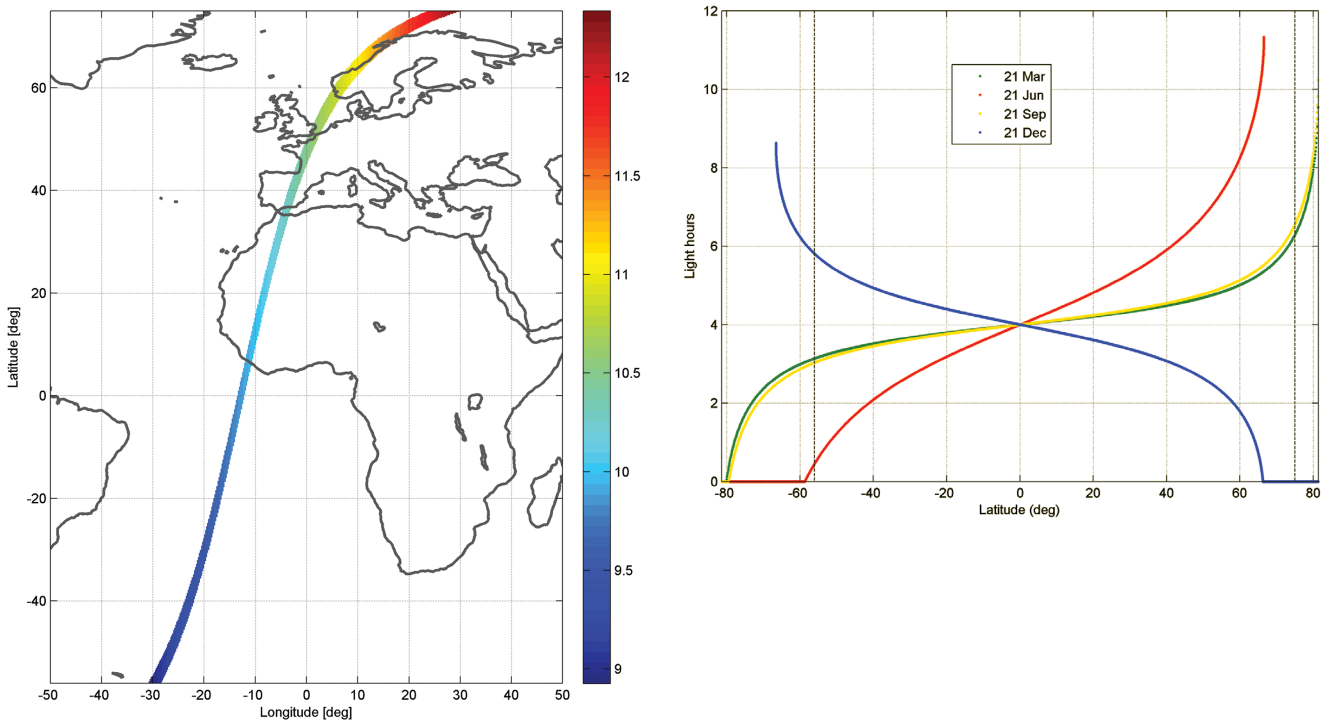

Figure 4.2. Left: instantaneous time of observation as a function of latitude for a 10:00 equatorial crossing. Right: number of illumination hours over each target at the time of satellite overpass as a function of latitude for different seasons. (Elecnor Deimos)

observation times between 09:00 in southern Argentina and 11:30 in northern Finland, which are the extreme cases for land observations (Fig. 4.2, left).

On the other hand, in order to use the measured fluorescence signal in models and applications, such measurements must be done when the plants are acclimatised to being illuminated, that is, plants that have already been exposed to sunlight for several hours when the satellite passes overhead. This varies with latitude along the orbit and also varies with the season. By choosing 10:00 as the equatorial crossing time, the resulting solar illumination hours as a function of latitude (Fig. 4.2, right) guarantee adequate measurements in most areas and for most times of the year and when plants are photosynthetically active.

Scaling from instantaneous measurements to daily-integrated estimates can be optimised using numerical models, additional meteorological observations and advanced data assimilation schemes.

4.1.4 Temporal Sampling Requirements

The objective of the mission is not to provide global coverage in a short period of time, but to observe the seasonal cycles and the activation/deactivation of the photosynthetic mechanisms where photochemistry is adjusted to a lesser or greater level of activity. A revisit time of about one month would be acceptable to observe the variability of vegetation activity at seasonal to annual scales (time-steps in models go from 15–30 minutes for meteorological dynamics to one month for seasonal vegetation dynamics). It must be emphasised that having one observation per month at the equator will imply more frequent acquisitions over high latitudes owing to orbital overlap, so that the temporal frequency will increase with latitude.

4.1.5 Mission Duration

The mission aims to observe solar-induced vegetation fluorescence to assess and monitor the actual photosynthetic activity of different biomes and their interannual changes related to climate variability. Three full vegetation cycles are needed to cover general trends and extreme events affecting plant ecosystems. Since these are needed both in the northern and the southern hemisphere, the total duration of the mission must be established at 3.5 years (taking into account potential shifts in launch dates and excluding the commissioning phase). A duration of five years would provide more statistical relevance to seasonal and interannual cycles and increase the probability of observing extreme events.

4.2 Information for Retrieval and Interpretation of Vegetation Fluorescence Dynamics

The overall set of measurements needed to accurately determine fluorescence from space and to derive useful plant indicators from such measurements are outlined in this section. Deriving canopy fluorescence from space requires knowledge about the properties of the atmosphere including its transmittance. To relate fluorescence to photosynthesis and plant stress conditions, additional information is needed about the amount of vegetation and its condition, exposure to illumination and canopy temperature.

4.2.1 Information Needed for the Retrieval of Fluorescence from Space

Estimating the fluorescence spectral quantities mentioned in Chapter 3 (i.e. F_{687}, F_{760}, the peak heights and peak wavelengths, spectrally-integrated fluorescence F_{tot} and the $F_{PS\ I}$ and $F_{PS\ II}$ contributions) requires the retrieval of the complete fluorescence spectrum at sufficient radiometric and spectral resolutions. The fluorescence signal cannot be measured directly, as it is always superimposed on a background signal of reflected light (Fig. 4.3). The ratio of the reflected plus emitted light and the incoming solar irradiance is described

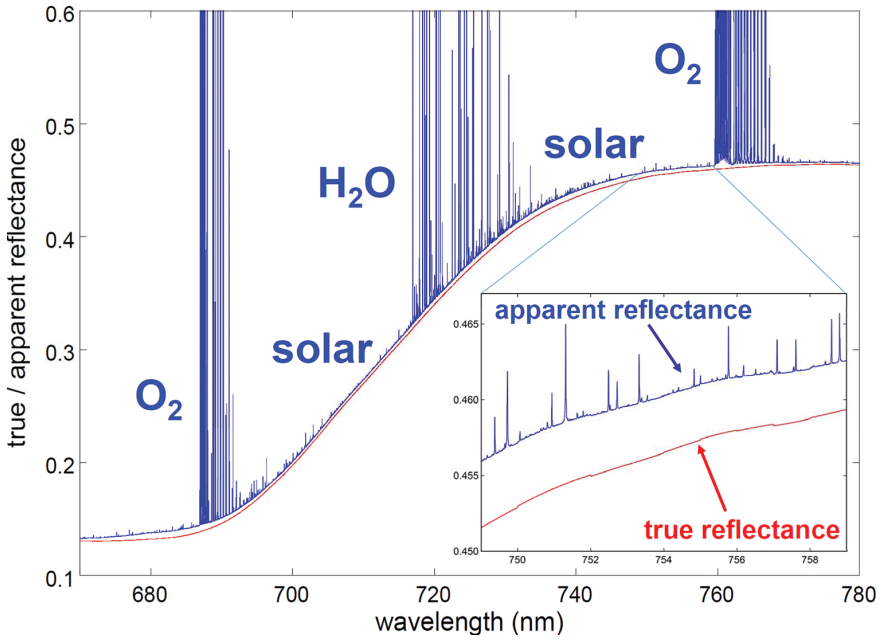

Figure 4.3. Apparent surface reflectance (blue) and actual surface reflectance (red) in the spectral range of fluorescence emission. The differences are dominated by the presence of absorption bands in solar irradiance arriving at the surface, either caused by solar Fraunhofer lines or terrestrial O_2 or water vapour absorptions. Inset: Zoom of a spectral region dominated by Fraunhofer lines, which produce much smaller effects than the strong terrestrial absorptions. (University of Valencia)

as the apparent reflectance. In laboratory conditions, one can decouple the two signals by selecting the illumination wavelengths, thus cancelling the reflected component in the spectral region of fluorescence emission. However, in natural sunlight, such separation is not possible and the two signals are always measured together. Since the amount of chlorophyll fluorescence emitted by a leaf represents a very small fraction of the reflected light in the visible part of the spectrum, there is no possibility of directly decoupling the fluorescence signal from the background reflectance.

However, retrieving fluorescence from spaceborne measurements is possible because the spectra of fluorescence and reflectance of vegetation are both smooth functions of wavelength, whereas surface solar irradiance becomes highly spectrally variable. Photons reaching the sensor that have been reflected by vegetation have followed different paths through the atmosphere than photons that have been emitted as fluorescence by the vegetation. In the former case, the photons followed the Sun–target–sensor route, and in the latter case only the target–sensor route. The former type of photon carries information about the spectrum of the Sun as reflected by the spectrally smooth surface and about the two-way transmission through the atmosphere, whereas the latter type of photon shows the signature of a smooth fluorescence spectrum that is only partly attenuated by the one-way transmission through the atmosphere.

Decoupling fluorescence emission and reflected radiance is possible in the spectral ranges where there is a strong spectral contrast in surface illumination, and absorption features in the solar irradiance arriving at the surface, e.g. gaseous absorption bands or Fraunhofer Lines.

Absorption features in solar irradiance arriving at Earth's surface are either due to absorptions already present in the solar irradiance arriving at the top of atmosphere (absorption lines caused by chemical processes in the Sun) or absorptions owing to the atmosphere (caused mainly by terrestrial gases such as water vapour and oxygen), provided that they are strong enough and spectrally narrow enough to expect the surface reflectance to be smooth within the absorption feature. Solar absorption bands are called Fraunhofer lines, and they tend to cause very small features in the apparent reflectance as they are relatively small absorptions. Fraunhofer lines do not vary as a result of changes in the atmosphere and retrievals are not affected by atmospheric disturbances. However, they do vary with solar activity and the distance between the Sun and Earth, and they are also affected by scattering effects (i.e. Raman scattering) and other disturbances. The main problem in using Fraunhofer lines is the fact that resolving the small fluorescence features (Fig. 4.3) requires very high spectral resolution and a very high SNR, which limits the applicability of this methodology to coarse spatial resolutions that are larger than management unit scales.

Water vapour absorption lines could be potential candidates for the fluorescence emission retrieval, but they are spatially and temporally highly variable. Water vapour also has a strong vertical variability in the atmosphere. In fact, spatial variability in water vapour can be even larger than that of fluorescence, therefore, water vapour absorption lines cannot be used for fluorescence retrievals.

Atmospheric oxygen, on the other hand, is quite constant in space and time and vertically homogeneous. The oxygen absorptions are well characterised and can be taken as stable. The dependence on surface pressure (surface altitude) and other contaminating effects is well known and can be corrected. As illustrated in Fig. 4.3, the oxygen absorptions are so strong that they produce sharp characterisation in the apparent reflectance of vegetation, which is the key element for fluorescence retrieval. The O_2 absorption features centred at 687 nm and 761 nm provide very strong oscillations of atmospheric transmittance and largely overlap with the chlorophyll-fluorescence emission spectrum of plants. They are strong enough and optimally located in the

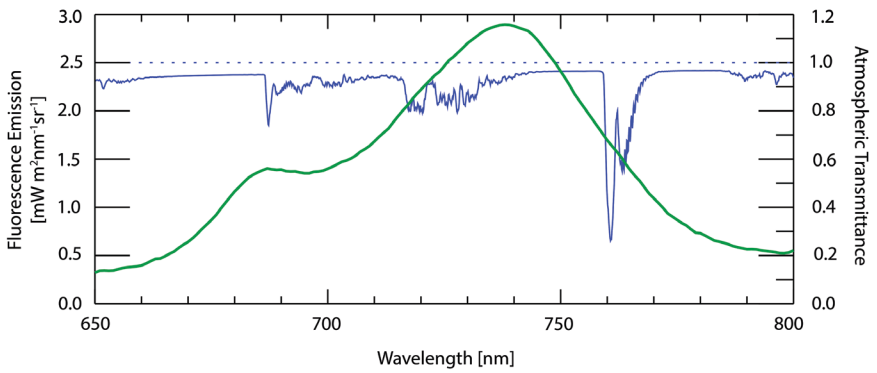

Figure 4.4. Spectral fluorescence emission (green) and atmospheric transmittance (blue), showing the absorption features present in the spectral range of fluorescence emission. (University of Valencia)

spectrum to serve for fluorescence retrievals, even at moderate spectral resolutions as illustrated in Fig. 4.4.

Although the total range of fluorescence emission is between 650 nm and 850 nm, the spectral region from 780 nm to 850 nm is strongly dominated by water vapour absorption, which is highly variable in space and time and therefore less suitable for the retrieval of fluorescence. Since the fluorescence level in this range is rather low, it is proposed to limit the spectral range for fluorescence retrievals to 650–780 nm. In this range the fluorescence levels are sufficiently high to generate a measurable response.

Fluorescence spectra have smooth shapes that can be described as the contributions from two main peaks. The first peak in the red spectral region at 685 nm is strongly related to the photosynthetic activity of PS II, whereas the second peak at 740 nm is more influenced by PS I, although the fluorescence spectra of both overlap substantially. The fluorescence from PS II is strongly related to the photosynthetic activity of the plant, whereas the fluorescence efficiency of PS I is more or less constant, mostly reflecting the amount of photosynthetically active radiation (PAR) absorbed by chlorophyll. Information from both peak regions is required to allow the decomposition of the measured fluorescence spectrum into the contributions that can be attributed to PS I and PS II.

Separation of reflected and emitted signals is performed in a two-step process. First, an atmospheric correction is carried out to estimate the apparent reflectance at top of canopy (TOC), which still includes the fluorescence signal, expressed as positive spikes in the reflectance spectrum at the wavelengths of absorption lines. Fluorescence is then decoupled from background reflectance by spectral fitting techniques. Details on the actual fluorescence retrieval are provided in Chapter 6.

Because of the need to compensate for atmospheric scattering and absorption effects in the measured top-of-atmosphere (TOA) radiances, additional inputs are needed for atmospheric correction, including aerosol characterisation and water vapour. Information on water vapour requires measurements in the atmospheric water vapour absorption bands, while aerosol characterisation requires measurements across the spectrum from the blue to the shortwave infrared, preferably including dual-angle observations of the same target through two different atmospheric paths.

4.2.2 Information Needed to Interpret Vegetation Fluorescence Dynamics

After the vegetation fluorescence-emission spectrum is retrieved, interpretation of the dynamics of these vegetation fluorescence values requires additional information to determine actual photosynthesis rates, vegetation health and stress conditions. For instance, fluorescence can be higher simply because the growth of vegetation results in a higher Leaf Area Index (LAI) or increased

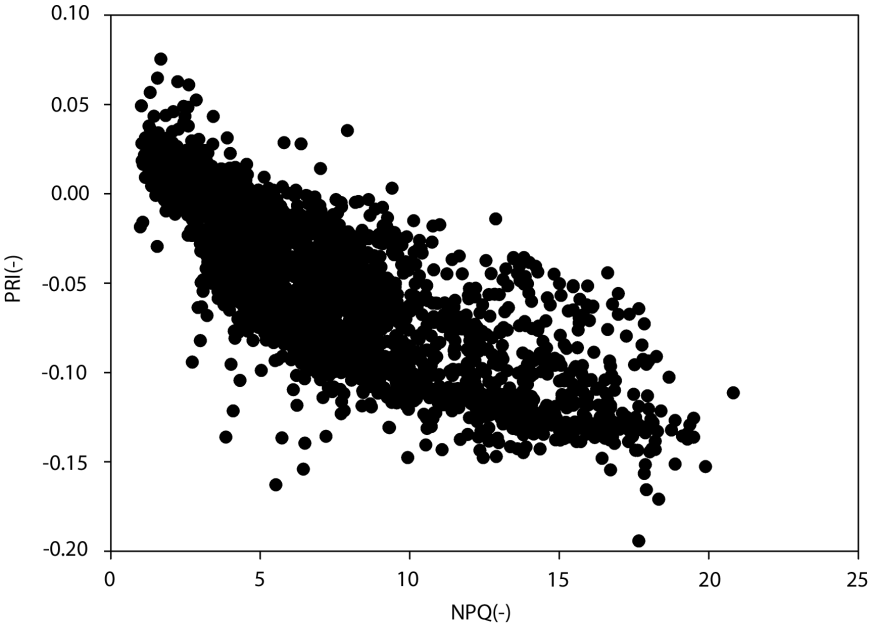

Figure 4.5. Experimental results showing the relationship between PRI and NPQ, measured over a forest from tower-based instruments and covering seasonal time scales. (F. Magnani–University of Bologna)

fractional cover of the soil, without implying differences in photosynthesis levels or plant stress conditions.

One element that is particularly important is the relationship between fluorescence and photosynthesis. For plants already adapted to solar illumination conditions (i.e. mid-morning), fluorescence becomes positively correlated with photosynthesis, but the slope of such linear relationship is a function of the regulated energy dissipation mechanisms that are activated. This means that the relative amount of fluorescence carries information about the sum of photosynthesis and regulated heat dissipation called non-photochemical quenching (NPQ). This NPQ is related to a self-protection mechanism that plants invoke when they are exposed to excessive light levels.

There is a clear and direct relationship between spectral reflectance changes around the range of 530 nm (as described through the Photochemical Reflectance Index, PRI) and regulated energy dissipation mechanisms expressed as NPQ (Fig. 4.5). Moreover, it is well understood that such relationships are mediated by the link between NPQ and maximum fluorescence emission under light-saturated conditions, which, in turn, is regulated by energy dissipation mechanisms associated to the xanthophyll cycle. The data shown in Fig. 4.5 are tower-based measurements taken over several months when vegetation was in a period of growth. NPQ and PRI were measured simultaneously, indicating the coupling between reflectance changes and non-photochemical energy dissipation over seasonal time scales relevant for the observations carried out by FLEX. The relationship between photochemical changes (as expressed through the PRI) and energy dissipation mechanisms (NPQ) is essential to establish a mathematical relationship between fluorescence and photosynthesis valid under all conditions.

Lastly, all biophysical and physiological processes are regulated by canopy temperature, so that the simultaneous measurement of canopy temperature is a prerequisite to properly interpret the observed dynamic changes in vegetation fluorescence.

In summary, for a proper interpretation of the observed fluorescence levels, the following additional information is required:

— non-photochemical energy dissipation, through dynamic reflectance changes

— total light absorbed by plant, which depends in particular on plant chlorophyll, LAI, and its fractional coverage (f_{Cover})

— canopy temperature

These parameters must be measured at the same time as fluorescence, while other useful information (for example, land-cover maps) does not require strict simultaneous observation.

4.3 Tandem Mission Concept with an Operational Mission

The measurements needed for the accurate retrieval of vegetation fluorescence emissions and interpretation of the observed values requires a number of instruments. To make optimal use of existing capabilities provided through operational satellites, a tandem mission concept is proposed, ensuring simultaneous measurements with a minimum impact of spatial and temporal co-location errors. The Copernicus programme offers the opportunity to develop and operate the tandem mission concept. This not only represents an innovative way of addressing a scientific problem by using available assets rather than duplicating existing systems, but also introduces a scientific and technological challenge in the implementation, which is appropriate for an Earth Explorer concept.

The FLEX satellite will need to fly in tandem with a mission that will be operational at the time FLEX is implemented. It cannot be another Earth Explorer or other mission with a limited life, but an operational mission guaranteed for a long time, to avoid programmatic constraints on the implementation of FLEX. Moreover, such an operational mission should provide all the required additional information through a dedicated ground segment already in place and with guaranteed data access. Since the FLEX satellite will fly in the same orbit as the tandem satellite, operations of both satellites will be guaranteed.

With this in mind, the best strategy would be to use a tandem satellite operated by ESA (for example a meteorological mission, or a satellite in Europe's Copernicus programme). FLEX would be the first ESA mission to be implemented as a tandem concept, adding more innovation to its original measurements of fluorescence.

Of the operational satellites that should definitely be available in 2020–30, and of those that have sensors offering the required spatial and temporal resolutions and provide the spectral information needed, the following missions could be suitable:

— Sentinel-2
— Sentinel-3
— MetOp

Satellites from space agencies other than ESA have been also considered, but no ideal solution has been found in terms of spatial/spectral requirements. This, along with potential programmatic constraints, has resulted in this option being discarded.

4.3.1 Optimum Tandem Satellite: Copernicus Sentinel-3

Disentangling the emitted and reflected light measured at the TOA is a complex task relying on information collected over a large spectral range. To make optimal use of existing capacities and to reduce the complexity of the mission

and associated implementation costs, a tandem mission concept is foreseen for FLEX. The most critical information required from the tandem partner satellite is related to the characterisation of the atmosphere (clouds, aerosols and water vapour) and land-surface characteristics (land-cover type, biophysical parameters and surface temperature). These variables can be provided as data products from external sources, or derived from external Level-1b/Level-1c data after integration with FLEX Level 1b/Level-1c data. The second option is preferred so that retrievals are fully consistent, particularly for those related to atmospheric information used for the atmospheric correction of FLEX data.

This information will be available on an operational routine basis from systems that are not constrained by the lifetime or the launch date of an Earth Explorer-type satellite. This is only possible if the partner satellite is an operational mission designed to provide data continuity for an extended period. In this context the Copernicus Sentinel missions are ideal candidates. Sentinel-3 can deliver the required auxiliary datasets and is, therefore, the baseline companion for FLEX. However, synergies and benefits could also be expected from data provided by the Sentinel-2 satellite, which provides part of the required supporting data at a higher spatial resolution than Sentinel-3, enabling a better description of the atmosphere and the heterogeneity of the land surface. However, the limitations identified with Sentinel-2 are the absence of observations in the thermal infrared, and limited spatial coverage. Thus, Sentinel-3 is presented as an optimum candidate. Moreover, the overpass time of Sentinel-3 is in agreement with the optimum requirements to measure fluorescence from space (10:00 at the Equator).

The FLEX mission concept therefore foresees flying in tandem with the Sentinel-3 mission, making optimal use of measurements from both systems. Sentinel-3 will provide information related to the atmospheric state needed for fluorescence retrieval algorithms. It also provides land-surface characterisation. The Ocean and Land Colour Instrument (OLCI) will deliver this auxiliary information in the visible spectrum, and the Sea and Land Surface Temperature Radiometer (SLSTR) offers dual-angle visible/infrared information as well as thermal infrared. The FLORIS (Fluorescence Imaging Spectrometer) instrument on the FLEX satellite will provide the key measurements for fluorescence retrieval and for characterisation of vegetation photosynthesis and stress conditions.

The observation requirements of FLEX related to the tandem concept are driven by two aspects: firstly, the temporal delay between FLORIS and OLCI measurements for a given point on Earth must be short, minimising the effects of moving clouds. Secondly, the observation angle of FLORIS should be as close as possible to nadir, limiting any variations that result from an oblique view through the atmosphere and surface bidirectional reflectance distribution function (BRDF) effects.

Since small observation zenith angles of up to about 5° are assumed to be tolerable, it is expected that the FLORIS imaging geometry will be optimised to coincide with the OLCI and SLSTR nadir views. It is noted that coregistration with OLCI, with its higher spatial resolution, is more important than coregistration with SLSTR, which has a lower spatial resolution. It is therefore suggested that the nominal view of FLORIS coincides with the OLCI nadir swath (camera 4).

4.3.2 Temporal Coregistration Requirements for FLEX and Sentinel-3

Analysis of the temporal coregistration requirements for Sentinel-3 and FLEX has revealed that cloud displacement is the most critical factor. For synergy products that are influenced by clouds (land-surface temperature, fraction of

absorbed photosynthetically active radiation (fAPAR), surface reflectance), and given the possibilities offered by the buffering of Sentinel 3 cloud masks, a time delay between FLEX and Sentinel-3 of 6–15 seconds is affordable. None of the other synergy products imposes additional constraints for the envisaged time delay.

Surface temperature is also relevant for translating fluorescence products to higher-level vegetation products. The SLSTR on Sentinel-3 will provide observations of surface temperature at almost the same time as observations of fluorescence, with a maximum time shift of 15 seconds.

4.3.3 Spatial Coregistration Requirements for FLEX and Sentinel-3

As the key mission data products at Level 2 are based on measurements from different instruments onboard two satellites, spatial coregistration is critical. Using an approach that was developed for the automatic orthorectification and coregistration of optical satellite images (Leprince et al., 2007), and given the expected time delay between FLEX and Sentinel-3 (6–15 seconds), a geometric misregistration accuracy between FLORIS and OLCI of about 0.2 pixels will be achieved. Concerning the geometric coregistration between FLORIS and SLSTR, since the temperature information provided by SLSTR is provided at a larger spatial sampling scale and since overall temperature effects may be modelled at larger scales, it is expected that the coregistration requirement with SLSTR can be relaxed by a factor of 3–5.

Since the key element in the FLEX data-processing strategy is the coregistration between FLEX data and Sentinel-3 data, the preferred option would be to assume a data-processing scheme where FLORIS and OLCI data are relatively geolocated, while OLCI and SLSTR are absolutely georeferenced by the Sentinel-3 geolocation algorithms.

4.3.4 Coverage and Swath Width

The repeat cycle of Sentinel-3 and the swath width of FLORIS drive the number of observations over a given location. Sentinel-3 will complete 385 orbital tracks in 27 days, which implies that at the equator a minimum swath width of 104 km is required to achieve complete global land coverage. However, a wider swath of 150 km is preferred to achieve a higher observation frequency at higher latitudes of once per four days, corresponding to the time interval between the acquisitions of two partly overlapping adjacent tracks. Observations corresponding to a swath of 150 km are, therefore, expected to be sufficient to demonstrate and observe the spatial and temporal variability of vegetation fluorescence with full global coverage.

4.4 Observational Requirements Related to FLORIS

The specific requirements for an optimised instrument dedicated to the measurements of vegetation fluorescence from space are defined in the following subsections.

4.4.1 Measurements of Vegetation Fluorescence

Spectral range is determined by the full range of fluorescence emissions, while spectral resolution and spectral sampling are determined with the objective of decoupling the fluorescence-emission signal from the background

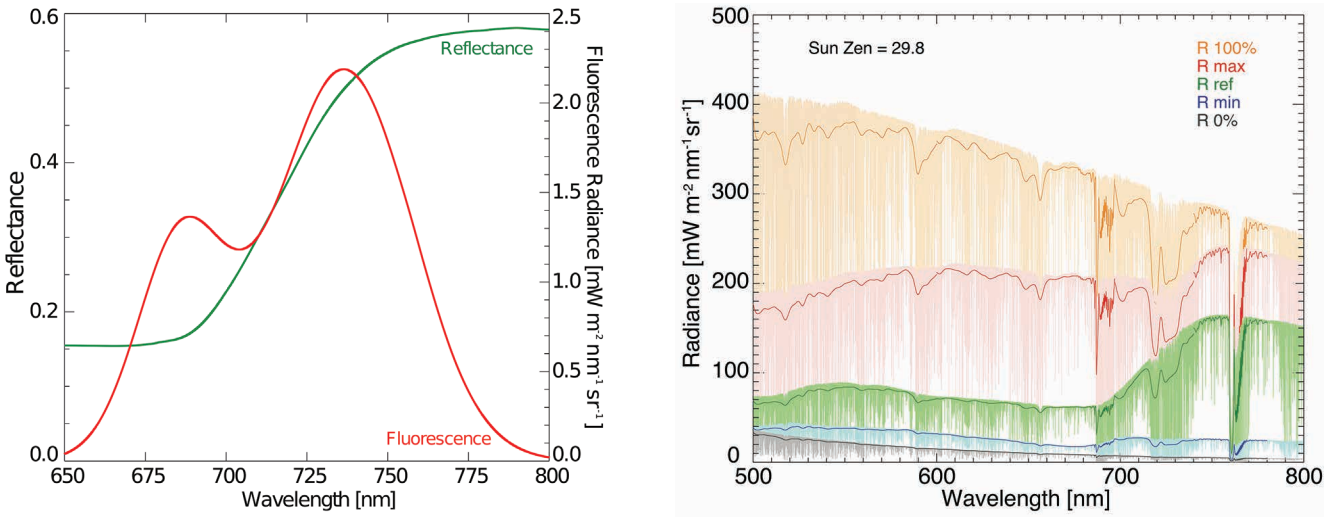

Figure 4.6. Left: Typical spectra of surface reflectance (green curve) and fluorescence (red curve). Right: Corresponding reference TOA radiance levels. Expected minimum and maximum values for the TOA radiance signal based on typical ranges of surface reflectance and fluorescence are also given. For reference, extreme ranges of 0% and 100% surface reflectance are indicated. (University of Valencia)

reflected signal. Finally, to meet the accuracy requirements for the vegetation fluorescence products, SNR requirements are established for consistent spectral resolution and spectral sampling settings.

4.4.1.1 Spectral resolution and sampling requirements

The shape of the fluorescence-emission spectrum, which covers 650–800 nm, directly dictates the spectral range requirements. In order to avoid the effects of water vapour absorption at the upper end of that spectral interval, the selected range is 650–780 nm.

For the given (reference) values of reflectance and fluorescence (Fig. 4.6, left), the TOA radiance signal levels are computed (Fig. 4.6, right). Typical, minimum and maximum values of TOA radiance signal levels are reported with the reference radiance levels for which the SNR will be defined. Extreme cases of 0% and 100% surface reflectance are also indicated.

Between 650 nm and 780 nm, the spectral resolution requirements are dictated by the ability to disentangle the fluorescence emission from the background reflected radiance. Absorption features in the incident solar irradiance determine this separability over the vegetation canopy reflectance. Figure 4.7 shows the ratio between the fluorescence signal and the reflected signal as a function of spectral resolution. It indicates the separability between fluorescence emission and background reflected signal, for both signals at the TOA. Optimal separability is achieved when such curves have a definite maximum, which is the case for most of the spectral bands. It can be seen that high spectral resolution is not always optimal. Above 0.6 nm, the fluorescence separability degrades monotonically with decreasing spectral resolution, but the separability also degrades for resolutions below 0.3 nm for many bands. Thus, there is an optimal spectral resolution around 0.3 nm where the best separability between fluorescence emission and background reflectance is achieved.

The case shown in Fig. 4.7 corresponds to the most critical spectral range, right inside the O_2 A absorption feature, which is the most demanding structure at the maximum of the absorption. The analysis has been performed over the full 650–780 nm spectral range, and similar results are obtained for both O_2-A

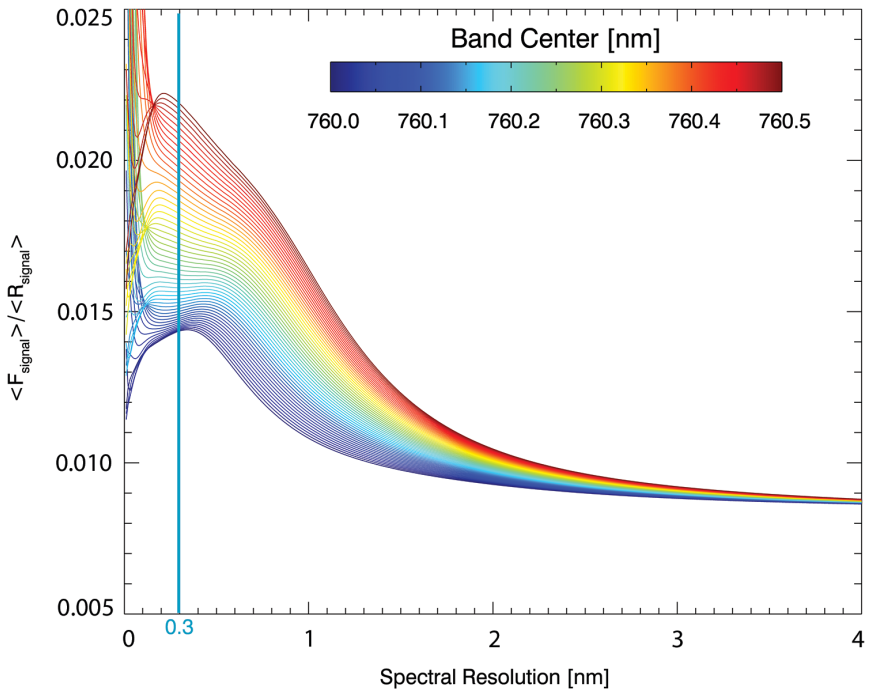

Figure 4.7. Optimal separability between the fluorescence signal (F) and the background reflected signal (R) as a function of spectral resolution, for the most critical spectral range inside the O_2-A absorption feature used for fluorescence retrievals. (University of Valencia)

and O_2-B absorption features about optimal spectral resolution for fluorescence retrieval.

Spectral sampling, given the required spectral resolution, is specified to avoid aliasing in the measured signal. To achieve this, and given the characteristic shape of spectral radiance curves in the spectral range covered by the instrument, requires a factor of three between sampling and resolution. That is, given a spectral resolution of 0.3 nm in the spectral ranges where maximum spectral resolution is required, a sampling of 0.1 nm in such spectral regions would be adequate.

This high spectral resolution is not needed everywhere in the spectral range covered by the instrument. There is no requirement for a constant spectral sampling interval (SSI) and spectral resolution across the covered spectral range. It can be optimised in each spectral region according to the spectral resolution needed to resolve the spectral features and to minimise the data rate given the large volume of data resulting from such spectral observations.

The criteria adopted requires keeping the maximum spectral sampling only at the critical absorption bands (O_2-A and O_2-B spectral ranges) while for other spectral intervals without critical absorption features the spectral sampling can be degraded from 0.1 nm up to 2 nm as a function of the spectral features present in each spectral interval.

4.4.1.2 Signal-to-noise requirements

The SNR requirements are dictated by the accuracy needed to derive vegetation fluorescence. The primary information to be used by models and applications is the total energy emitted as fluorescence by vegetation; that is, the total integral of fluorescence over the whole spectral range of the fluorescence emission.

The spectrally-integrated overall fluorescence emission is, according to many field experiments at leaf and canopy levels, typically around 80–150 mW m^{-2} sr^{-1}, with typical standard deviation of 15–25 mW m^{-2} sr^{-1}. Maximum values can go up to more than 200 mW m^{-2} sr^{-1} in extreme conditions.

These values should be measured with an accuracy of approximately 10% for a typical emission range, which is typically 8–15 mW m^{-2} sr^{-1}

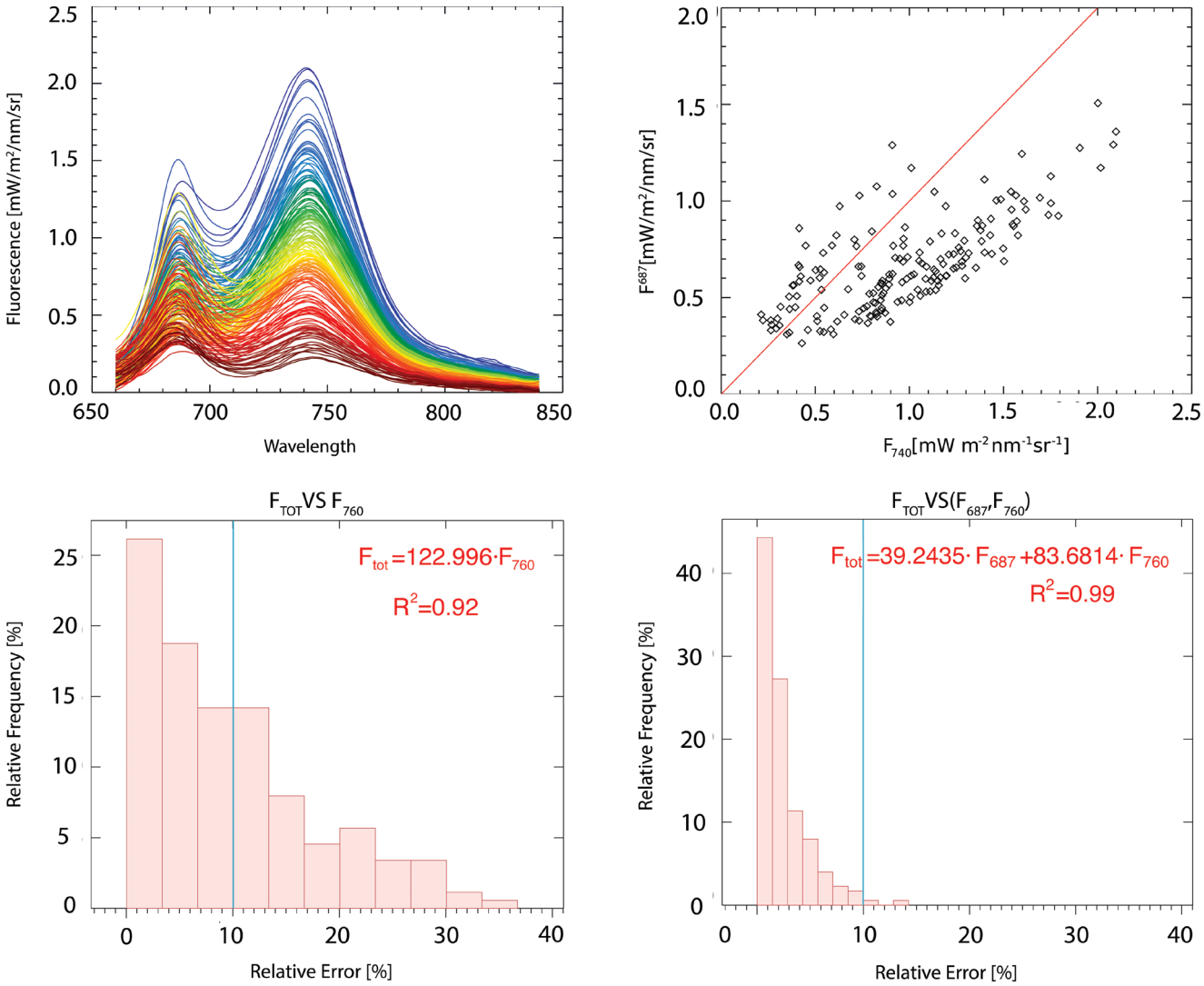

Figure 4.8. Top left: Measurements of actual fluorescence emission collected in dedicated field experiments over a large range of conditions. Top right: scattergram of the heights of the two emission peaks, showing the decorrelation between the heights of the two peaks. Bottom left: histogram of errors resulting in the reconstruction of the spectrally-integrated fluorescence by using only the second peak F_{761}, resulting in errors larger than the 10% requirement. Bottom right: histogram of errors resulting in the reconstruction of the spectrally-integrated fluorescence by using both fluorescence-emission peaks, resulting in a total error below the 10% requirement. (University of Valencia)

in absolute values. This accuracy will allow us to discriminate several different levels of photosynthesis from the minimum to the maximum expected values in typical conditions. Obviously, for very low signal levels the relative error will be larger, while for high fluorescence ranges the accuracy will be better than 10%. Moreover, the 10% accuracy in the retrieved fluorescence is within the expected natural variability of the signal at the canopy level caused by the different behaviour of individual leaves. Fluorescence measurements at the leaf level obtained during a series of field experiments reveal the large variability of the spectral signature (Fig. 4.8, top left). The information contained in the two peaks at 687 nm and 740 nm is different and exhibits large variability even in a dataset that includes measurements in unstressed conditions (Fig. 4.8, top right). In a second step, the integrated-fluorescence-emission values were computed from the measured spectra and compared with estimates based on the emissions in the two oxygen absorption bands at 687 nm and 761 nm. When only the emission at 761 nm is used to estimate the spectrally integrated total fluorescence, fewer than 60% of the reconstructed values meet the 10% accuracy requirement

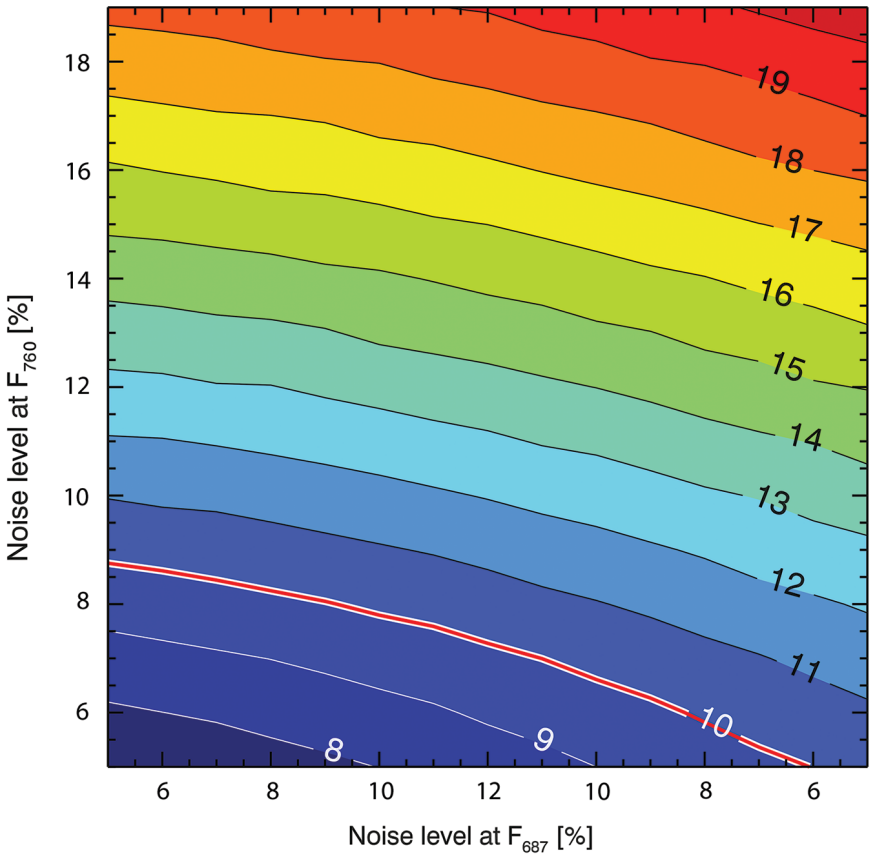

Figure 4.9. Relative error in the determination of the overall spectrally-integrated total fluorescence emission as a function of the error in the determination of the height of the two peaks by measuring F_{687} and F_{761}. (University of Valencia)

(Fig. 4.8, bottom left). When only the emission at 687 nm is used, this number drops to 31% (not shown). Only when both the emission peaks are used to derive the integrated value does the achieved accuracy fall within the required 10% range (Fig. 4.8, bottom right).

Since the two peaks do not contribute in the same way to the overall fluorescence emission, to obtain a total error of 10% in the integrated total fluorescence, the error in the measurements at each of the individual peaks should be limited to about 9% for F_{761} and about 17% for F_{687} (Fig. 4.9).

Given the TOA radiance signal expected for typical surface reflectance and fluorescence levels, an extensive study has been carried out to determine optimal SNR values that will allow the retrieval of fluorescence within the established errors for each of the two emission peaks, and thus for the overall integrated value. The result was that a 10% error in the fluorescence signal at the TOA level will drive the achievement of a 10% accuracy in the retrieval of the overall integrated-fluorescence emission by the 'spectral fitting' method used as the retrieval technique. Thus, varying the TOA reference radiance signal

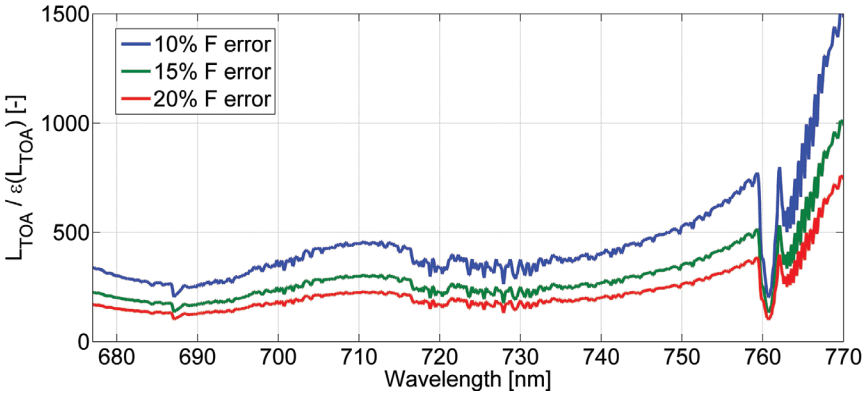

Figure 4.10. Ratio between total TOA radiance signal and the variations in the TOA signal caused by an error of 10, 15 and 20% in the contribution of fluorescence to the total signal. Such values are used to determine the required instrumental SNR to retrieve total canopy fluorescence with an error in the order of 10% in the spectrally-integrated value. (University of Valencia)

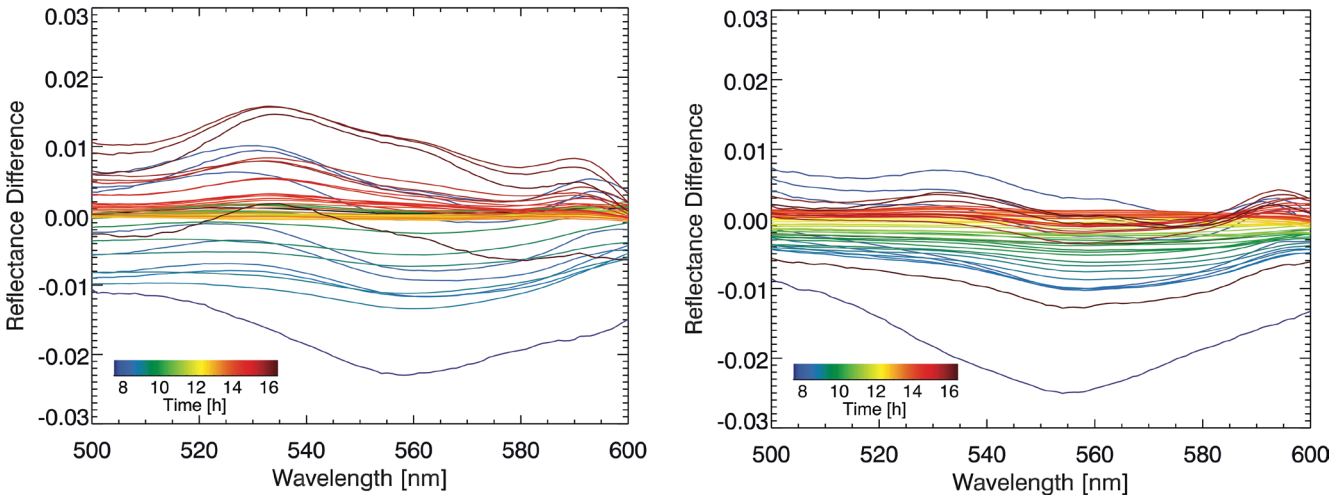

Figure 4.11. Reflectance changes over a daily cycle (with respect to the reflectance values measured at noon) for unstressed vegetation (left) and water stressed vegetation (right). Significant changes occur in the range 510–550 nm, but they affect the full 500–600 nm spectral range. (University of Valencia)

for 10%, 15% and 20% in the corresponding contribution of TOA fluorescence allows the derivation of the corresponding SNR requirements (Fig. 4.10).

Combining the varability in the TOA radiance signal as a function of fluorescence emission (Fig. 4.10), and the conditions imposed by the spectral fitting technique used as the retrieval algorithm, the SNR requirements for each spectral interval, for the corresponding spectral sampling, are finally set to the values reported in Table 4.2.

4.4.2 Requirements for Determining Pathways for Energy Dissipation

Radiation absorbed by chlorophyll is used for photosynthesis, dissipated as heat, or re-emitted as fluorescence. As stated earlier, NPQ can be related to a self-protection mechanism that plants invoke when they are exposed to excessive levels of light. It is also known that xanthophylls (a collection of carotenoids) change where violaxanthin is converted into zeaxanthin (Demmig-Adams and Adams 1996, 2000). This, in turn, results in subtle changes of the reflectance spectrum of green leaves in the spectral region around 530 nm (Gamon et al., 1992).

The PRI is defined as the ratio of the difference and the sum of the reflectance values at 531 nm and 570 nm, and can be used to identify the changes mentioned above. Consequently, PRI can provide information about the heat dissipation by NPQ and, in combination with fluorescence, actual photosynthetic activity or GPP (Gross Primary Production) can be derived (Rossini et al., 2010), and identify stress in vegetation.

However, the changes associated with NPQ energy dissipation mechanisms as a function of plant physiological status do not only influence the reflectance at 531 nm and 570 nm. When measuring at the canopy level, structural effects (e.g. variations in the inclination of the leaves) may cause other reflectance changes that can change variations directly associated with NPQ mechanisms. In order to overcome such potential limitations, it is necessary to measure the full 500–600 nm reflectance spectrum and then look at the dynamics of the overall spectral reflectance curve, rather than variations at 531 nm and 570 nm only (Fig. 4.11).

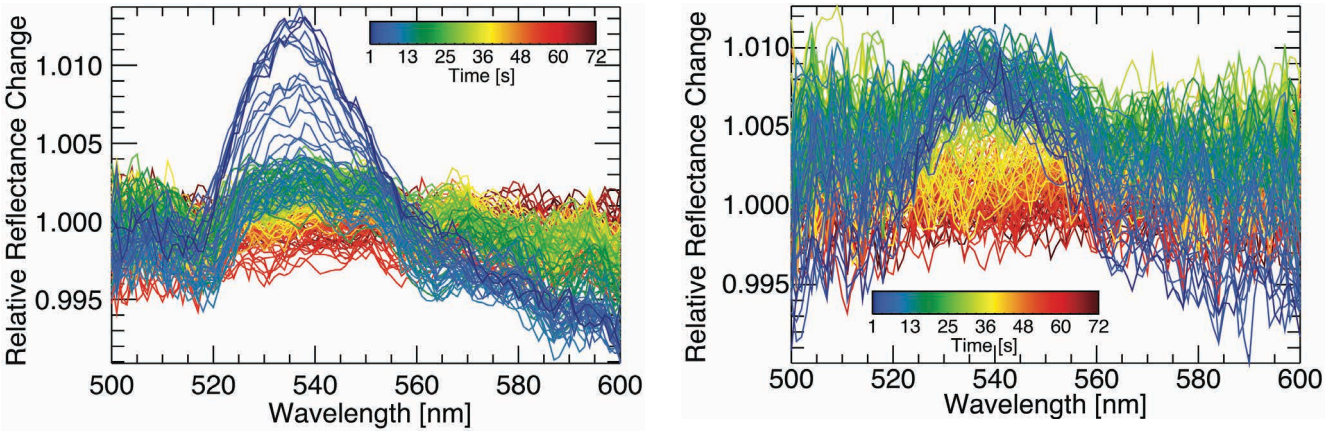

Figure 4.12. Experimental measurement of the variability in vegetation reflectance associated with photochemical changes in the 500–600 nm spectral range for two vegetation species (left: tobacco, right: hibiscus). Fast-induced illumination changes over a short period (72 seconds) were used to test the magnitude of the effects. (University of Valencia)

Thus, in order to properly relate the changes in fluorescence to respective changes in photosynthesis, a simultaneous measurement of the dynamics of reflectance changes in the 500–600 nm spectral region is an absolute must. There are some single wavelengths where the changes are more pronounced, but to decouple the different contributions the full wavelength range should be measured with enough spectral resolution to see the variability in the signal.

Since individual atmospheric absorption features are not to be resolved in the range 500–600 nm, spectral sampling and resolution requirements in this spectral region are optimised to observe vegetation reflectance changes linked to non-photochemical energy dissipation mechanisms. FLORIS will measure vegetation reflectance in the 500–600 nm range at medium spectral resolution (3 nm), with 2 nm sampling, to derive PRI with a strict geometric and temporal coregistration with fluorescence products. As both fluorescence and PRI have a high dynamic variability (Gamon et al., 1992), these synergetic observations present a unique opportunity to derive higher-level vegetation products related to environmental constraints on photosynthesis.

Using very fast changes in illumination over short periods (72 seconds), the magnitude of the effects has been measured for several vegetation species (Fig. 4.12). The values obtained have then been used to derive the requirements for spectral resolution and sampling required to observe such changes. A spectral resolution of 3 nm with a spectral sampling of 2 nm is adequate to resolve such photochemical reflectance changes associated with energy dissipation.

Using long time-series of field measurement at the canopy level (Fig. 4.13), the absolute changes in PRI have been determined (including both decrease and increase in surface photochemical reflectance) and show the typical

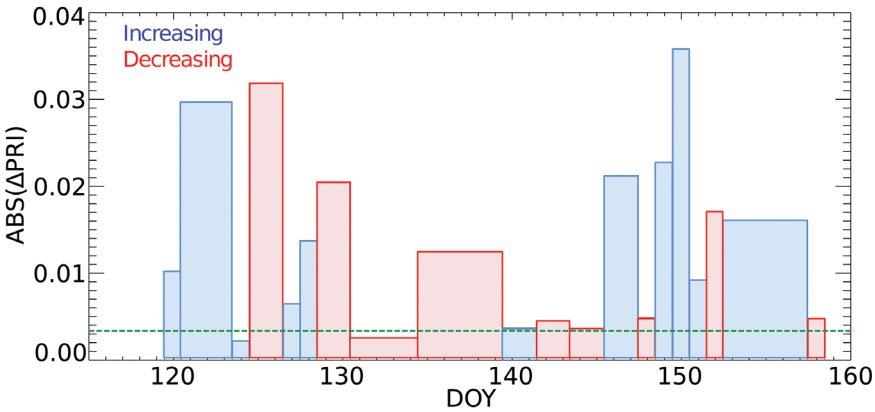

Figure 4.13. Observed changes in photochemical reflectance over a boreal forest in the 500–600 nm range as a function of time. The green dashed line indicates the SNR value of 245, which was selected as the requirement. Observable absolute changes are above the line; very small reflectance changes below the line will not be resolved. (University of Valencia)

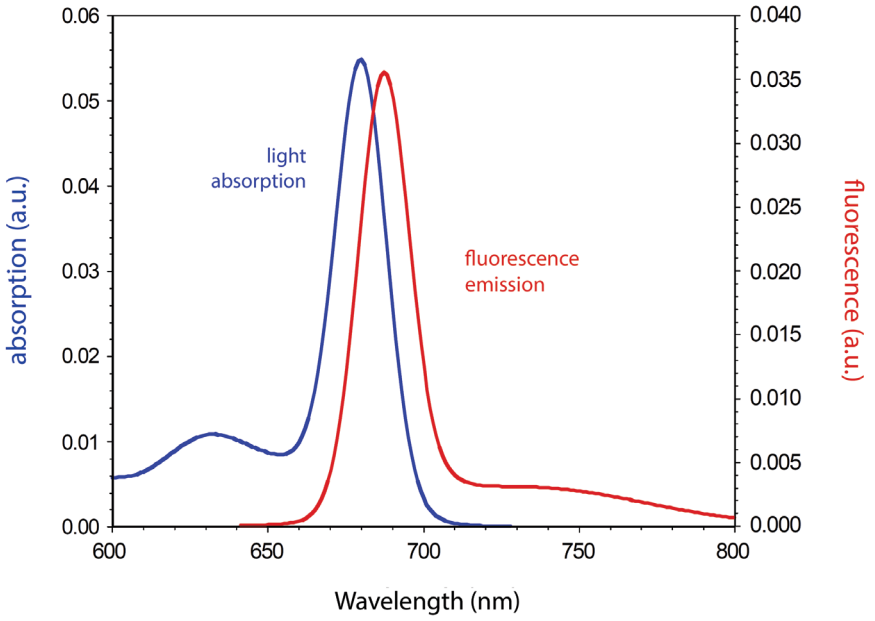

Figure 4.14. Light absorption by chlorophyll and corresponding chlorophyll fluorescence emission spectrum. (University of Valencia)

variability in such measurements over time. They have been used to derive the SNR requirements for spectral reflectance in the 500–600 nm range given the dynamic range of variability in the signal, as illustrated in Fig. 4.13.

Because some photochemical reflectance changes are extremely small, and in some places take place at timescales of minutes, such small changes will not be detectable. However, the spectral sampling and signal-to-noise requirements adopted for FLEX will allow most relevant changes at time scales of weeks to months to be measured (Fig. 4.13), which are relevant for the FLEX mission.

4.4.3 Requirements for Deriving Light Absorption by Vegetation

Since the radiance emitted as fluorescence also depends on the intensity of incident light, and in particular of the amount of light absorbed by vegetation chlorophyll, the determination of the amount of light absorbed by chlorophyll is essential for an adequate interpretation of the measured fluorescence levels.

As illustrated in Fig. 4.14, while fluorescence emission drives the radiometric requirements in the 650–800 nm range, chlorophyll absorption is the dominant feature in the 600–650 nm range.

Since chlorophyll content determines the amount of light that is absorbed by photosynthetic pigment, the fraction of light absorbed by chlorophyll, which is re-emitted as fluorescence, can then be computed if light absorption is also determined. The traditional method of using absorbed photosynthetically

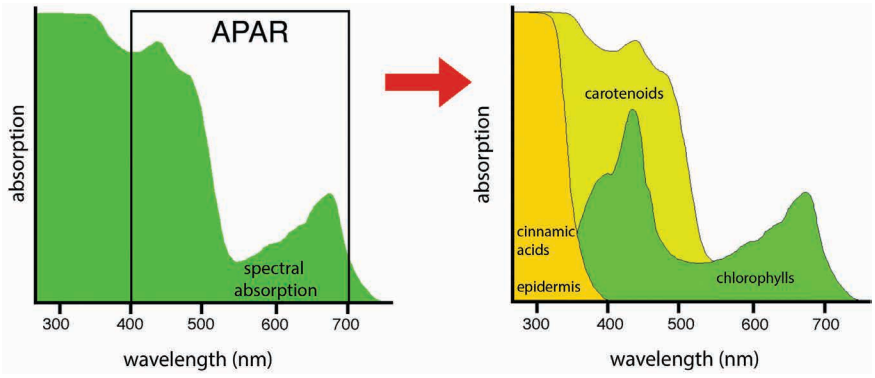

Figure 4.15. Decoupling light absorption by chlorophyll and light absorption by non-photochemical pigments (carotenoids) in the PAR range of 400–700 nm. (University of Valencia)

Band	PRI band	Chlorophyll absorption	O_2-B band		Red-edge		O_2-A band			
λ(nm)	500–600	600–677	677–686	686–697	697–740	740–755	755–759	759–762	762–769	769–780
Spectral Resolution (nm)	3	3	0.6	0.3	2	0.7	0.7	0.3	0.3	0.7
Spectral Sampling (nm)	2	2	0.5	0.1	0.65	0.5	0.5	0.1	0.1	0.5
SNR	245	245	340	175	425	Linear 510–1015	1015	115	Linear 115–455	1015

Table 4.2. Spectral resolution, SSI and SNR requirements for each spectral range at the threshold level for the reference radiance

active radiation (APAR) as a measurement of absorbed light is not fully appropriate when using fluorescence measurements, because, as indicated in Fig. 4.15, APAR contains all the light absorbed in the range 400–700 nm. This includes both photosynthetic (chlorophyll) and non-photosynthetic or accessory (carotenoids) elements. The amount of light absorbed by chlorophyll is of primary interest when computing the fraction of absorbed light re-emitted as fluorescence.

Decoupling between light absorption by chlorophyll and light absorption by other vegetation constituents becomes necessary. This requirement drives the spectral resolution and sampling needed in the spectral range 600–650 nm.

4.4.4 Overall Spectral Range, Resolution, Sampling and SNR Requirements

Table 4.2 summarises the requirements on spectral sampling, spectral resolution, and SNR for the different spectral regions. The SNR values are given for the specific SSI. The SNR values are assumed to be valid after binning.

Given the retrieval concept assumed to derive vegetation fluorescence by spectral fitting methods, making use of sharp spectral features in the solar irradiance spectrum, FLORIS covers the O_2-A and O_2-B absorption lines with a subnanometre resolution of 0.3 nm. It is recommended to apply an enhanced spectral sampling density of 0.1 nm in the O_2 sub regions 686–697 nm and 759–769 nm for an optimum spectral calibration in these regions. Outside these regions, spectral binning can be applied to increase the SNR and to accommodate data rate constraints.

4.4.5 Requirements for Absolute Signal Calibration and Stability

Since FLEX uses a retrieval concept that is based on a spectral fitting technique, the relative radiometric accuracy is dictated by the acceptable error in the ‘least-squares’ spectral fitting procedure that compares the measured values with the modelled values. Absolute radiometric accuracy required for all the instrument’s spectral bands should be within the 5% threshold limit. This limit must be understood as being the result of all the contributions that may result in absolute radiance errors: 3% absolute error over uniform vegetated scenes corresponding to nominal observations, 1% corresponding to remaining polarisation sensitivity and 1% corresponding to potential straylight effects. Radiometric recalibration owing to spectral shifts and relative biases are explicitly included in the data-processing scheme to compensate for systematic

spectral calibration errors. However, a stability of 0.5% is required along a single orbit to allow consistency in retrievals and to avoid the need for radiometric recalibration of each single scene.

For the absolute radiometric calibration it must be noted that, contrary to atmospheric observations where individual lines or micro-windows are used to establish quantitatively the composition of the atmosphere, the extraction of vegetation fluorescence is based on the use of the complete spectral information. In fact, the key issue is the systematic variation caused by radiometric calibration errors versus systematic variations in radiance caused by changes in Aerosol Optical Thickness (AOT), surface pressure, water vapour content and surface reflectance and fluorescence contributions (Fig. 4.16). Fortunately, when considering the large 650–780 nm spectral range instead of isolated small spectral absorption features, each systematic contribution has a different spectral pattern. In order to distinguish between the different effects from the variations illustrated in Fig. 4.16, it is necessary that absolute radiometric calibration allows the decoupling of the different effects. Those with strong spectral variations are easy to characterise by using the known shape of the spectral features, and the most difficult effects are those giving an overall spectrally smooth effect over the whole spectral range. Such smooth changes in the overall spectral shape will have a direct impact on the compensation of aerosol effects (AOT), so that systematic variations in absolute radiometric calibration will be interpreted as variations in the effective aerosol load and aerosol type in the absence of external references to constrain the aerosol retrievals.

The absolute accuracy is also driven by the absolute radiation levels required to extract fluorescence with the envisaged accuracy of 0.2 mW m^{-2} sr^{-1} nm^{-1}. However, it is more important for the mission to achieve relative accuracy to separate all the contributions to the measurement. Absolute accuracy is required mainly to establish long-term stability for the anticipated products.

Notice that the spectral resolution used in Fig. 4.16 is the same as requested for FLORIS in each spectral range, illustrating the capability to separate the different contributions in the TOA signal in the actual spectral resolution, which would be available in FLEX. On the other hand, water vapour is well characterised by using additional Sentinel-3 information and aerosols are also characterised by using OLCI and SLSTR spectral bands and SLSTR dual-angle capability. Variations in surface pressure (Fig. 4.16, green line) is well constrained from high-resolution digital elevation models (DEMs), so that the variability driven by fluorescence is decoupled from other spectral variations when using the full spectral range, even in the presence of relative errors in absolute radiometric calibration.

An important factor for fluorescence measurements is the specific requirement for radiometric performances in the instrument related to the in-filling of spectral absorption lines by instrument effects. This is particularly

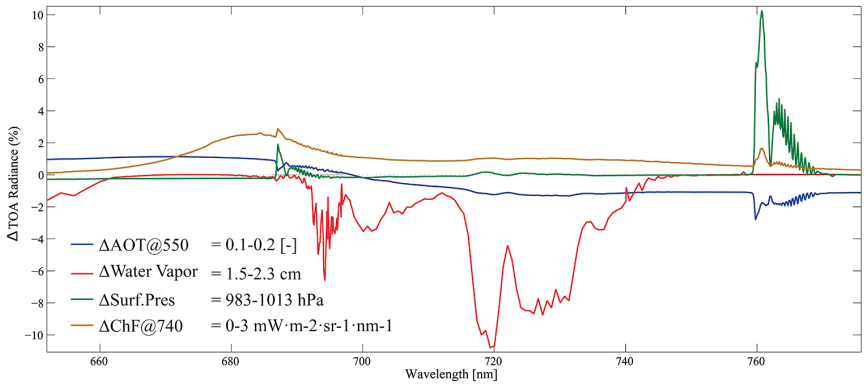

Figure 4.16. Relative impact on TOA radiance of AOT, surface pressure, water vapour and chlorophyll fluorescence, for surface conditions corresponding to typical green vegetation reflectance and fluorescence emission. (University of Valencia)

the case for potential spatial/spectral straylight effects. Since radiances outside the absorption feature are much higher than the radiances inside the spectral absorption, any contamination caused by straylight effects will result in inaccurate retrievals of fluorescence. In fact, the absolute radiance requirements for FLORIS given earlier are applicable to all potential contaminations (residual polarisation effects, straylight, radiometric calibration errors, etc.), but straylight deserves special attention. While straylight effects could be corrected by deconvolution, reference scene cases have been defined to check potential contamination problems under realistic scenarios with relevance for fluorescence measurements. The main source of inaccuracies resulting from straylight effects comes from the presence of small scattered clouds over a vegetation scene. For FLORIS, specific reference target scenes have been defined to test performances under straylight effects. Such scenes consist of vegetation with various levels of absolute reflectance (reference value, minimum and maximum typical cases), a scattering atmosphere with typical aerosol load, and realistic cloud field patterns representing cases where vegetation areas are surrounded by clouds and where clouds are only present at the edge of the image, thus resulting in a gradient of influence as a function of the distance of vegetation targets to the bright objects. Realistic synthetic scenes representing actual cloud types and characteristics and realistic surface reflectances are preferable for testing straylight effects in conditions similar to those that will be encountered by FLEX. More details about straylight effects tested for realistic cloudy scenes are discussed in Chapter 7.

On the other hand, since FLORIS data and OLCI/SLSTR data from Sentinel-3 are used together in the retrieval of vegetation fluorescence, and in particular in the atmospheric correction of the TOA radiances to derive surface apparent reflectance, radiometric coregistration between the FLORIS and Sentinel-3 spectral bands is required. This is particularly the case between FLORIS and OLCI data because they share a common spectral interval and the radiances measured by both sensors in the same spectral range must agree in order to guarantee full consistency in the data-processing scheme. Specific requirements are established for the correspondence between OLCI bands and the equivalent spectral range in FLORIS. Since FLORIS has much higher spectral resolution than OLCI, FLORIS spectral bands are convolved to simulate each of the OLCI bands in the overlapping spectral interval. Actual OLCI measurements and simulated OLCI bands from FLORIS are then cross-calibrated to be within 2% difference in absolute radiance calibration for all the spectral bands in the common spectral range.

4.5 FLEX Products

Potential users of FLEX data are international science organisations, national science institutions, regional/local science institutions, private science organisations, academic research groups/individuals, associations, cooperatives and federations. Each user has different levels of data usage, from global modelling of the carbon cycle to tracking vegetation disasters/recovery from stress in agricultural and forestry applications.

The different FLEX user profiles define the requirements in terms of data acquisition, data access, data archiving, data distribution, and timeliness for data access.

The FLEX mission is specifically oriented to provide scientific users with vegetation fluorescence maps, together with photosynthesis-related products and other biophysical products, which are also derived as part of the Level-2 data-processing algorithms.

The overall strategy of data exploitation assumes three levels of products and applications that go from local to regional to global studies. The three data levels correspond to:

Level-1 Products	Definition
FLORIS Level-1a	Level-0 data reformatted, calibrated, geolocated, time-referenced and annotated with ancillary information for FLORIS data. Data converted into physical units and corrected for instrumental effects.
FLORIS Level-1b	L-1b products contain quality-controlled, spectrally and geometrically characterised and radiometrically calibrated into TOA radiances in $mWm^{-2} sr^{-1} nm^{-1}$, keeping the nominal geometry of acquisition for each individual instrument.
FLORIS + OLCI/SLSTR Level-1c	Level-1c products contain FLORIS-1b product projected onto a reference geographical grid. Radiance values are resampled to match output grid pixels.

Table 4.3. Level-1 products.

— TOA radiances (which is mostly dedicated to calibration/validation users at local scales, but from which advanced users can develop some dedicated applications, mostly innovative new products at regional and global scales);

— Level-2 fluorescence products (from which a number of applications can be developed including studies of land dynamics and land-surface changes at regional and global scales)

— Photosynthesis products at higher levels (from which plant physiology models at local scales and carbon cycle models at global scale can be developed, together with data fusion at mesoscale levels with other models and products)

4.5.1 Level-1 Products

Standard Level-1a and Level-1b products are to be delivered (Table 4.3), while the Level-1c products will not only consist of FLORIS measurements, but are geolocated, cross-calibrated TOA radiance measurements from FLORIS, OLCI and SLSTR.

For this Level-1c product, data processing starts from Level-1b data for all FLORIS, OLCI and dual-view SLSTR measurements, and by means of a single algorithm a single Level-1c TOA radiance data product is generated, which merges all the FLORIS/OLCI/SLSTR data onto a common geographical grid. Because FLORIS and OLCI both have same spatial resolution and common spectral coverage, the strategy puts the OLCI data in the geometry of FLORIS measurements (to avoid, as far as possible, resampling FLORIS data). Then SLSTR data, which have lower spatial resolution and less spectral similarity with FLORIS, are also put into the FLORIS geometry using colocation between OLCI and SLSTR.

The Level-1c product, combining all the FLORIS, OLCI and SLSTR measurements are the starting point for further Level-2 and higher-level products.

In addition, FLEX Level-1c products incorporate OLCI and SLSTR products converted to the FLORIS geometry from original Sentinel-3 OLCI and SLSTR Level-1b products, using a consistent procedure for the three instruments and a single resampling step.

Table 4.4. Level-2 products.

Level-2 Products	Definition
O_2-A and O_2-B emission values (F_{761} and F_{687})	Accuracy requirement at 300 × 300 m^2 spatial resolution: 0.2 mW m^{-2} sr^{-1} nm^{-1}
Total fluorescence emission (spectrally-integrated value)	Accuracy requirement at 300 × 300 m^2 spatial resolution: 10% of the integrated value
Peak values ($\lambda_{\langle 680\rangle}$,$F_{\langle 680\rangle}$ and $\lambda_{\langle 740\rangle}$,$F_{\langle 740\rangle}$)	Accuracy requirement at 300 × 300 m^2 spatial resolution: 0.2 mW m^{-2} sr^{-1} nm^{-1}
Surface temperature	Accuracy: 1–2K, derived from Sentinel-3 SLSTR
Non-photochemical energy dissipation	Regulated energy dissipation, accounts for the fraction of light absorbed by non-photochemical pigments (carotenoids/chlorophyll ratio and violaxanthin/ zeaxanthin ratio, anthocyanin)

4.5.2 Level-2 and Potential Higher-Level Products

Higher-level products include the basic fluorescence products at Level-2, the photosynthesis and vegetation-stress products and additional products such as GPP and dynamic stress (Tables 4.4 and 4.5).

The Level-2 products include the main fluorescence products (total integral, height and position of the two emission peaks) and also the values of fluorescence at the two main absorption bands O_2-A and O_2-B. The reason for such products is that most field instruments to be used for validation purposes use such oxygen absorption features so it is quite useful to compare this with other data sources. Finally, the decomposition of fluorescence emission into PS I and PS II emissions is also provided as a product.

The non-photochemical energy dissipation is provided as a Level-2 product to later compute photosynthesis, as the relationship between fluorescence and photosynthesis also depends on the amount of non-photochemical energy dissipation.

Higher Level Products	Definition
PS I-PS II contributions	Derived from $F_{\langle 680\rangle}$ and $F_{\langle 740\rangle}$ to give the $F_{PS\ I}$, $F_{PS\ II}$ corresponding missions
Fluorescence quantum efficiency	Ratio between energy emitted as fluorescence versus actual chlorophyll specific absorbed energy (dimensionless)
Photosynthesis rate	Effective charge separation at PS II, interpreted as actual electron current resulting in photosynthetic reactions
Vegetation stress	Defined as 'actual photosynthesis/potential photosynthesis' using the ratio of the two emission peaks and estimate of non-photochemical energy dissipation
Spatial mosaics	Regional/continental/global maps
Temporal composites	Monthly/seasonal/annual composites
Activation/deactivation of photosynthetic machinery	Determines actual length of the growing season
Dynamic vegetation stress	Derived by data assimilation with dynamical vegetation model accounting for temporal changes
GPP	Derived by data assimilation with usage of external inputs (meteorological data, land-cover maps)

Table 4.5. Higher-level products.

Because total fluorescence emission depends on the amount of light absorbed by vegetation (illumination levels), the ratio between fluorescence emission and light absorbed by photochemical pigments is the relevant magnitude for many applications. This 'fluorescence quantum efficiency' ratio is also given as a Level-2 product in addition to the basic fluorescence products. Note that this product also based on measurements from the Sentinel-3 mission.

Another relevant product for the FLEX mission is the canopy temperature, provided by SLSTR thermal channels.

Apart from the given Level-2 products, a number of higher-level products have been identified for FLEX (Table 4.5) and will be delivered through dedicated science centres and other data-processing infrastructures.

4.5.3 Data Latency

Timeliness is the appropriate temporal span between data acquisition and product delivery. This, in general, is an essential requirement for operational services and is important for scientific users running computationally expensive models in data assimilation modes. For key FLEX objectives, a latency of 24 hours to generate Level-1 products is sufficient. However, FLEX observations disseminated in near-realtime (i.e. within three hours of sensing) could support vegetation-stress monitoring in operational environments and any emerging application related to Sentinel-3.

→ MISSION ELEMENTS

5. Mission Elements

This chapter provides the technical description of the FLEX mission, as derived from the preparatory activities at Phase-A/B1 level. It shows how this mission concept can respond to the scientific requirements defined in the previous chapters.

The system description is based mainly on the results of parallel Phase-A/B1 system studies by two industrial consortia (Airbus Defence and Space, 2011; Thales Alenia Space France, 2011). Where appropriate, both implementation concepts (Concept A and Concept B) are described, to present significantly different approaches capable of meeting the mission requirements described in Chapter 4.

Following an overview of the mission architecture and the proposed orbit (Sections 5.1 and 5.2), the space segment is described in detail (Section 5.3) followed by the launcher, ground segment and operations concepts (Sections 5.4, 5.5 and 5.6). The overall mission performance is summarised in Chapter 7.

5.1 Mission Architecture Overview

The main architectural elements are depicted in Fig. 5.1.

The space segment consists of a satellite carrying a single payload, the Fluorescence Imaging Spectrometer (FLORIS). The satellite flies in loose formation with either the Sentinel-3A or the Sentinel-3B satellite to achieve the required observation coregistration between FLORIS and both the Ocean and Land Colour Instrument (OLCI) and the Sea Land and Surface Temperature Radiometer (SLSTR) instruments carried on the Sentinel-3 satellites. The formation concept foresees that both satellites will fly in the same orbital plane, with FLEX flying ahead of Sentinel-3, preceding it by approximately 100 km. This configuration allows the temporal requirement for coregistration of observations to be met while ensuring that there is no risk of collision, by allocating sufficient reaction time in case of contingencies.

The baseline Vega launcher places the satellite into a phasing orbit, from which FLEX manoeuvres into its nominal orbit, i.e. that of Sentinel-3. There is an option for a dual-launch on Vega, by taking advantage of a small satellite platform. This is described in Section 5.3.6.

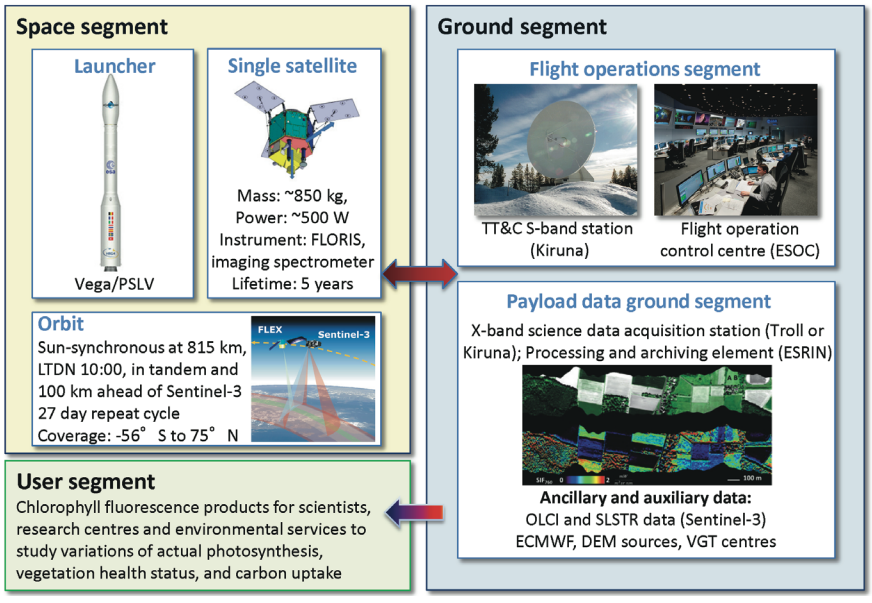

Figure 5.1. FLEX mission architecture. (ESA)

The mission performs nadir observations of the Top of Atmosphere (TOA) radiance in the 500–780 nm spectral band. The chlorophyll fluorescence signal emitted by vegetation is retrieved by means of spectral fitting methods. The FLORIS instrument comprises a high-resolution spectrometer, which allows fine spectral sampling of the O_2 absorption features: O_2-A and O_2-B centred at 760 nm and 687 nm, respectively, and a low-resolution spectrometer, which covers the full 500–780 nm spectral range at a lower resolution.

The ground segment uses the generic Earth Explorer ground segment infrastructure, comprising:

— the Flight Operations Segment (FOS), which includes the Telemetry, Tracking and Command (TT&C) ground station and the Flight Operations Control Centre (FOCC)

— the Payload Data Ground Segment (PDGS), which includes the Science Data Acquisition Station, the Processing and Archiving Element and the Mission Planning and Monitoring Element

The FLEX FOS obtains orbit and mission planning data from the Sentinel-3 FOS to ensure consistent formation-flying operations. The FLEX scientific data is delivered via an X-band downlink to a single high-latitude ground station in, for example, Kiruna in Sweden. Science data, processed up to Level-2 by the PDGS, are made available to users within 24 hours.

5.2 Mission Analysis

5.2.1 Orbit Selection

The selection of the orbit, formation control and orbit maintenance are driven by the temporal and spatial coregistration requirements between FLEX and Sentinel-3 measurements. The formation concept ensures that the temporal coregistration between the FLEX observations and the OLCI and SLSTR (nadir view) observations of the same target is always within the required 6–15 seconds. At the same time, the ground swath covered by FLEX observations is entirely contained within the ground swath of the nadir-looking OLCI camera, this being camera number 4.

FLEX fulfils the temporal and spatial coregistration requirements by flying in the same orbit as Sentinel-3, at an average altitude of 814.5 km and preceding it by a maximum of 15 seconds. The FLEX–Sentinel-3 formation is shown in Fig. 5.2.

The FLEX orbit has a repeat cycle of 27 days and the Local Time of the Descending Node (LTDN) is 10:00. The distance between FLEX and Sentinel-3 oscillates between 100 km and 115 km for Concept A and between 30 km and

Orbit Properties	
Repeat cycle	14+7/27
Repeat cycle length	27 days
Semi-major axis	7177.926 km
Inclination	98.645°
Orbits/cycle	385
LTDN	10:00
Min. distance FLEX–Sentinel-3	100 km (Concept A)/30 km (Concept B)
Max. distance FLEX–Sentinel-3	115 km (Concept A)/45 km (Concept B)

Table 5.1. FLEX orbit properties.

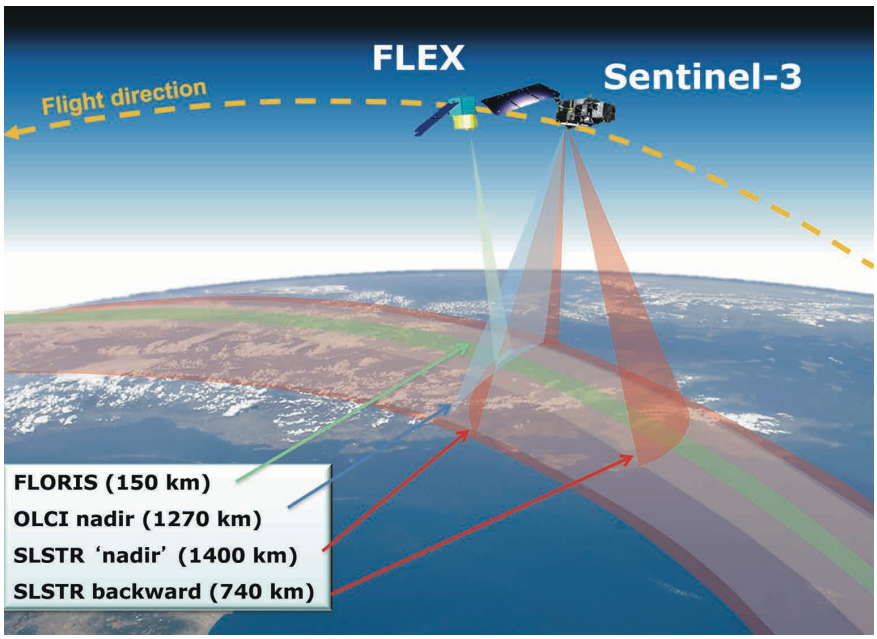

Figure 5.2. FLEX–Sentinel-3 formation with the different sensor swath widths. (ESA)

45 km for Concept B, depending on the relative orbit decay of the two satellites within an orbit control cycle. The orbit properties are summarised in Table 5.1.

For Concept A, the distance between the two satellites is driven by the need to avoid interference during simultaneous data download of Sentinel-3 to Svalbard and FLEX to Kiruna. For Concept B, the baseline ground station for data download is Troll in Antarctica, which does not present an interference issue. Analyses have shown that this formation is completely safe for both nominal operations and contingencies, as already demonstrated in far more challenging formations (e.g. TerraSAR-X/TanDEM-X) in which the distance between satellites is of the order of hundreds of metres.

5.2.2 Mission Profile

In order to achieve the required relative position with respect to Sentinel-3, FLEX is launched into an initial phasing orbit in the same orbital plane but at a different altitude, hence a different orbital period with respect to the reference Sentinel-3 orbit. The orbital period difference causes a slow relative drift between the positions of FLEX and Sentinel-3. Once the target relative position between the two satellites is reached, an in-plane manoeuvre is performed to modify the semi-major axis of the orbit and achieve the reference mission orbit altitude.

Full coverage of the areas of interest, comprising all land zones between 56°S and 75°N, including major islands and coastal zones, is achieved during the 27-day repeat cycle. For these areas, FLEX takes measurements whenever the Sun Zenith Angle (SZA) is lower than 75°. As a consequence of this constraint, the coverage is limited to areas south of 52°N during winter. The satellite attitude varies along the orbit to guarantee a nadir view of Earth's surface during observation arcs and to maximise the solar array illumination during the remaining orbit. For both concepts, this is achieved by maintaining the instrument pointing to nadir during observation arcs and by performing attitude slew manoeuvres over the poles when the satellite is not in eclipse. During eclipse arcs, the satellite is kept geocentric pointing. Sun-based radiometric calibration is performed at the South Pole, outside the observation arcs. During such events, which are planned to occur every four weeks, the satellite performs a yaw manoeuvre to orient the calibration port towards the Sun, allowing illumination of a diffuser.

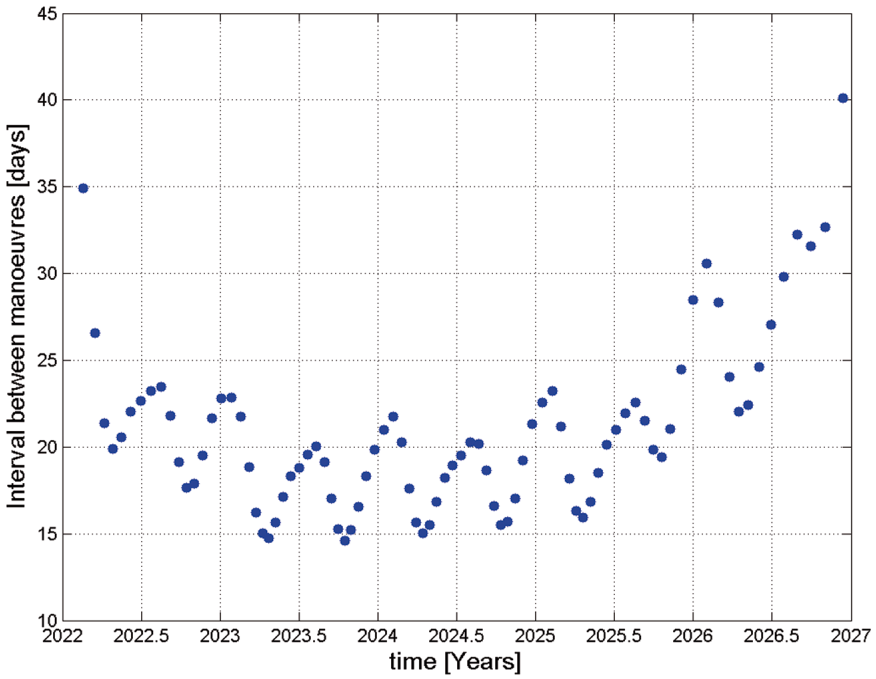

Figure 5.3. Interval between in-plane orbit control manoeuvres, assuming launch in 2022. (Airbus Defence and Space)

The threshold requirement is for a mission lifetime of 3.5 years, but with five years as the goal. To maintain loose formation, FLEX follows the same orbit correction strategy as Sentinel-3, with in-plane and out-of-plane manoeuvres being executed every time Sentinel-3 executes its manoeuvres. The frequency of the in-plane orbit control manoeuvres varies throughout the mission life depending on the fluctuations of atmospheric density, which, in turn, depends on solar activity and, consequently, on the launch date. For a launch in 2022, as shown in Fig. 5.3, in-plane manoeuvres are performed at a frequency varying between 15 and 40 days, while inclination manoeuvres are executed approximately every three months.

Figure 5.4 shows the evolution of the FLEX–Sentinel-3 temporal separation between acquisitions of the FLORIS and the OLCI and SLSTR nadir observations (blue and light blue, respectively). The red and green lines represent the

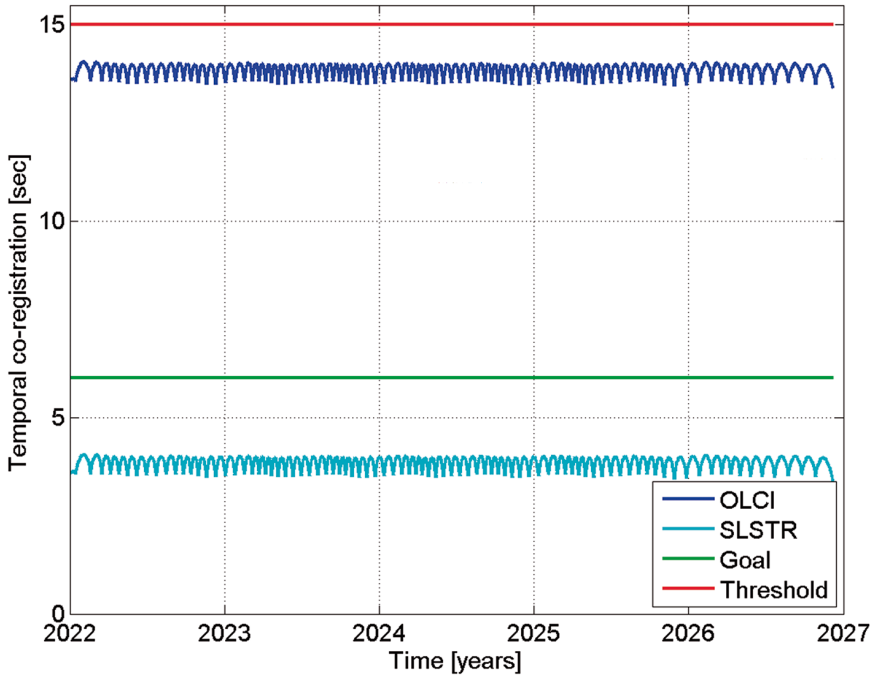

Figure 5.4. Evolution of temporal distance between FLEX and Sentinel-3. (Airbus Defence and Space)

required threshold/goal temporal coregistration requirement. Thanks to the similarity of the ballistic coefficients of the two satellites, the time by which FLEX would exceed the temporal coregistration requirement is longer than the interval between orbit maintenance manoeuvres (Fig. 5.3). Therefore, there is no need for dedicated formation control manoeuvres and FLEX maintains the formation with Sentinel-3 by simply performing its nominal orbit control manoeuvres.

The planned formation configuration, with FLEX flying ahead of Sentinel-3, is based on the fact that the ballistic coefficient of FLEX is slightly lower than that of Sentinel-3. Such configuration ensures that, in the event that control of the FLEX satellite is lost, the distance between the two satellites increases naturally. Scenarios where one or the other satellite goes into safe mode were investigated, confirming that there is no issue for formation controllability and safety.

The similarity of the ballistic coefficients of the two satellites, the coordination between the FOS of FLEX and that of Sentinel-3 (based at Eumetsat) for the execution of orbit maintenance manoeuvres, and the large initial distance altogether ensure that no collision risk will arise during the whole mission life in both nominal and contingency situations. The vast experience already available in operating far more challenging formations (e.g. TerraSAR-X/TanDEM-X, A-Train, PRISMA) will be exploited in both FOS development and operations.

5.3 Space Segment

The FLEX space segment consists of a single satellite carrying the FLORIS payload and flying in formation with Sentinel-3. Concepts A and B are both based on recurrent platforms, Sentinel-5 Precursor for Concept A and Proteus MKII NATO satellite for Concept B. This ensures that the required levels of performance are met with comfortable margins in terms of mass, power and consumables, and allows the satellite development to approach the industrial cost target of an Earth Explorer Opportunity mission while minimising development risks.

The physical satellite configuration is driven by the accommodation of the payload. Both concepts foresee the payload mounted on top of the platform, guaranteeing an unobstructed view of Earth. The main difference between the concepts is that in Concept A all the avionics are embedded inside the platform, while Concept B features a modular architecture with a generic service module and a mission-specific payload module accommodating the instrument, the Main Electronics (ME), and the Payload Data Handling and Transmission (PDHT).

The satellite configuration is described in Subsection 5.3.1, followed by the payload concept in Subsection 5.3.2, and complemented by the description of the overall satellite subsystems and budgets in Subsections 5.4.4 and 5.4.5, respectively.

5.3.1 Satellite Configuration

The FLEX satellite configuration design is based on the careful consideration of:

— accommodation of the FLORIS payload so that the instrument has an unobstructed nadir view of Earth

— pointing and coregistration requirements, which favour the isostatic mounting of the instrument on a specific payload support panel

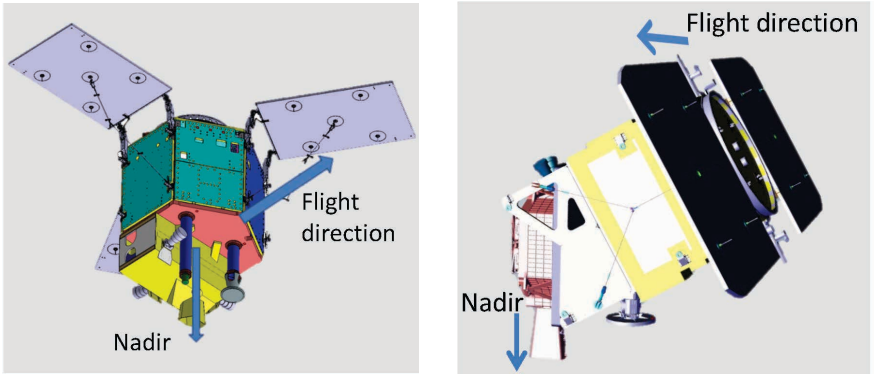

Figure 5.5. Satellite configuration for Concept A (left) and Concept B (right). (left: Airbus Defence and Space, right: Thales Alenia Space)

— Line of Sight (LOS) stability

— Vega launcher fairing envelope, which limits the size and shape of the instrument and the overall satellite, particularly in the case of a dual-launch

— Assembly, Integration and Testing (AIT) to ensure that the instrument integration and the platform integration are decoupled, for maximum schedule and cost efficiency

Although there are some differences, both baseline concepts developed by the industrial consortia allow the above requirements to be fulfilled.

Concept A is based on a compact hexagonal platform hosting all the avionics equipment, the propulsion module and a three-wing deployable solar-array assembly for power generation. The FLORIS instrument is thermally decoupled from the platform and mounted isostatically on a dedicated Payload Interface Panel (PIP). Three startrackers are placed on the PIP to ensure negligible thermoelastic distortions and so that there is no need for on-ground processing to compensate for distortions. The platform communicates with the payload for command and control purposes through an MIL-1553B interface, while the payload data link is provided by a SpaceWire link. The flight direction is defined by the instrument entrance slit and corresponds to the X-axis direction of the platform reference system. During observation arcs and eclipses, the satellite maintains a geocentric attitude and slew manoeuvres are executed over polar arcs to optimise illumination of the solar-array, and hence power generation.

For Concept B, the service module is based on a cubic platform that provides structural support for the payload module and contains all the platform subsystems required for operations and the survival of the satellite. To avoid the need for a pointing mirror in the instrument, Concept B foresees FLEX flying with a platform roll angle of 60° with respect to nadir, and performs yaw-steering manoeuvres during the polar arcs of the orbit to maximise the solar illumination of the two-wing solar array assembly. The FLORIS instrument is mounted isostatically on a dedicated Payload Interface Module (PIM) placed on top of the service module. The PIM houses the FLORIS instrument, the electronics, the PDHT equipment, three startrackers and four Sun sensors. To guarantee a clear nadir view of Earth, the PIM is inclined by 30° with respect to the service module. The PIM lateral panels support the solar array hold-down and release mechanisms, providing the necessary stiffness to support the solar arrays during launch.

For both concepts, four thrusters are located at the bottom of the satellite (launch vehicle interface) and, therefore, an attitude slew manoeuvre is needed to perform the orbit maintenance manoeuvres.

Additional satellite configurations, based on a small platform from the Myriade Evolution family and compatible with a dual-launch scenario, have been assessed by both Contractors and are described in Subsection 5.3.5.

5.3.2 Payload

The payload consists of a single instrument observing Earth in the nadir direction. The following subsections address the observation principles and the description of the instrument, starting with an overview of the instrument concepts, followed by a discussion of the impact of key requirements at Level-1b on the detailed definition of the instrument. The instrument concept is presented by describing the main subsystems and the calibration strategy.

5.3.2.1 Observation principle

FLORIS is a high-resolution imaging spectrometer acquiring data in the 500–780 nm spectral range, with a sampling of 0.1 nm in the oxygen bands (759–769 nm and 686–697 nm) and 0.5–2.0 nm in the red edge, chlorophyll absorption and Photochemical Reflectance Index (PRI) bands. Sentinel-3's OLCI and SLSTR instruments provide complementary information to retrieve the fluorescence signal from OCLI's camera 4 and the SLSTR nadir view respectively. The observations made by FLEX and Sentinel-3 instruments of the same target on the ground must be acquired within 6 seconds (goal) to 15 seconds (threshold) of each other.

FLORIS operates in pushbroom mode with a spatial sampling of about 300×300 m^2 and a swath width of 150 km, which is entirely contained within the Sentinel-3 OLCI camera-4 swath, the one closest to the nadir direction. The instrument calibration relies on both cross-calibration with the equivalent bands of OLCI and a dedicated onboard calibration device. The FLEX and Sentinel-3 images are coregistered by on-ground processing through correlation algorithms. An overview of the FLORIS bands and those of the Sentinel-3 OLCI and SLSTR instruments is given in Fig. 5.6.

5.3.2.2 FLORIS configuration

FLORIS is an imaging grating spectrometer, benefiting from the heritage of instruments such as MERIS on Envisat and OLCI on Sentinel-3, albeit with enhanced spectral resolution and throughput covering the spectral range between 500 nm and 780 nm. For the required spectral range and spectral resolution, the best solution was found to be to have two separate spectrometers, covering the low-resolution spectral range and the high-resolution spectral range. The two industrial consortia derived two concepts that are similar with respect to the band configuration, but different in their optical design (Fig. 5.7).

In both designs, a telescope images the ground onto a slit and then a spectrometer images the slit onto a focal plane, while dispersing the light in the Along Track (ALT) direction. In Concept A, two separate instruments, each with a telescope and a spectrometer, image the same ground area (i.e. the swath). In

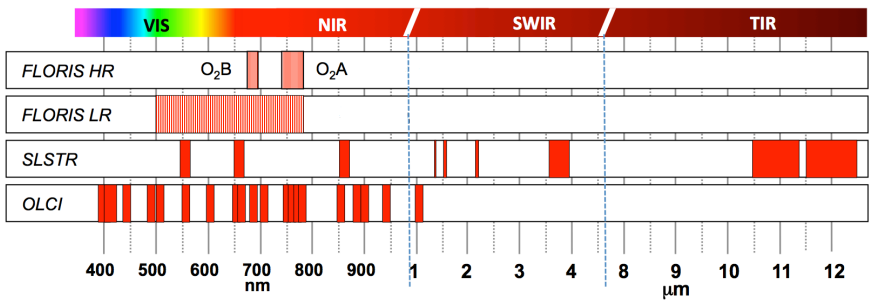

Figure 5.6. Comparison of FLORIS spectral ranges and Sentinel-3 instrument bands. (ESA)

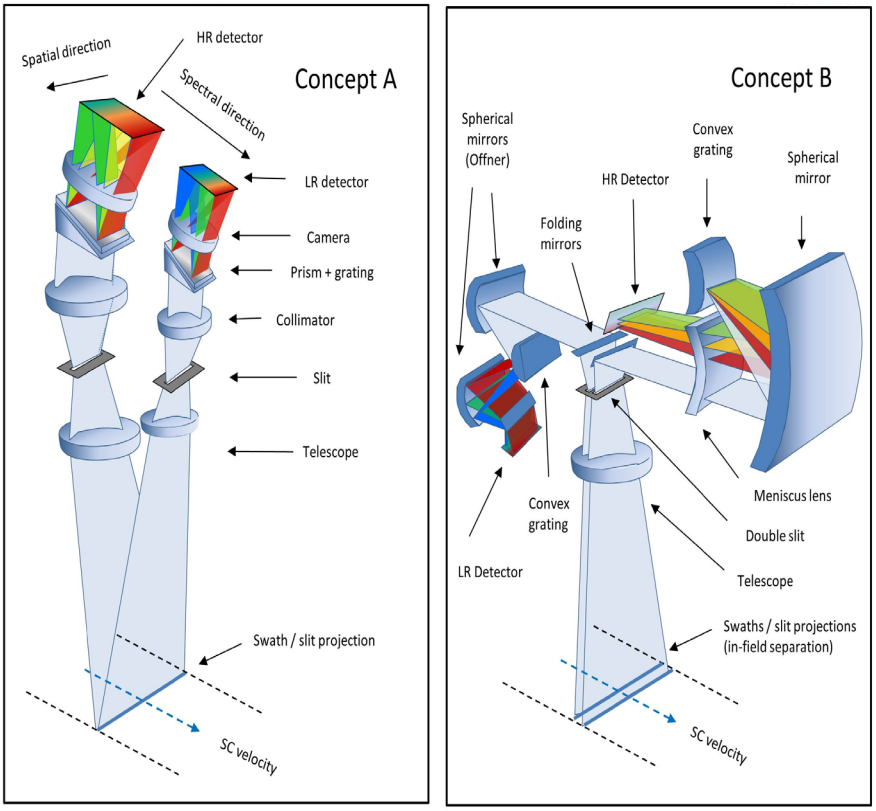

Figure 5.7. FLORIS instrument concepts. (ESA)

Concept B, an in-field separation is realised by introducing a double-slit, which allows the use of a common telescope. The swath of the two spectrometers is then imaged with a time difference of about two seconds.

FLORIS comprises:

— a wide-band spectrometer with low spectral resolution (FLORIS-LR), covering 500 nm to 780 nm in Concept A and up to 740 nm in Concept B

— a narrow-band spectrometer (FLORIS-HR), which covers the O_2-A and O_2-B bands at high spectral resolution

To fulfil the Signal-to-Noise Ratio (SNR) requirements, the FLORIS-HR has a pupil size of about 80 mm and the FLORIS-LR requires a pupil size of about 40 m. Since FLORIS will measure low light levels at the oxygen absorption lines, it is essential to maintain low straylight levels and to implement a calibration system that can achieve radiometric accuracies within 5%. FLORIS-HR has a spectral resolution of ~0.3 nm around the oxygen absorption bands and a Spectral Sampling Interval (SSI) of ~0.1 nm. FLORIS-LR provides a medium spectral resolution of about 2 nm with a SSI of ~0.65 nm.

To achieve the polarisation requirement, FLORIS-HR and FLORIS-LR in both concepts are equipped with a polarisation scrambler located in front of the telescope(s) and covering the full pupil. The HR spectrometer optics have been designed such that the spectral and spatial coregistration requirements are fulfilled at data Level-0.

5.3.2.3 Observation requirements

The key observational Level-1b requirements that drive the design of FLORIS are summarised in Table 5.2.

The following sections summarise the impact of the main Level-1b requirements on the instrument design.

Observational requirement	Specification	Comment
Pointing	Nadir	The swath will be within that of OLCI camera 4
Dynamic range	Covering L_{min} to L_{max}	Expected radiance levels for the application, dynamic range is extended to cloud radiance to support straylight correction
Swath width	150 km	Derived from coverage requirements
Spatial Sampling Distance (SSD)	300 m	Identical for all spectral channels within 5% Constant to better than 1% during in-orbit lifetime across-track (ACT) and along-track (ALT)
System Integrated Energy (SIE)	>70% over an area of 1.2 SSD	ALT and ACT
	>90% over an area of 1.6 SSD	ALT and ACT
Spectral band coverage	See Table 5.3	
Spectral Resolution and Sampling	See Table 5.3	
SNR	See Table 5.3	
Spectral stability	1 nm	Over mission lifetime
	0.1 Spectral Sample Interval (SSI)	During observational time of one orbit
	1 SSI max. variation	Between onground calibration and inflight operation
Knowledge of Instrument Spectral Response Function (ISRF)	Better than 1%	(TBC)
Spectral coregistration	<0.1 SSD	Spectrometer smile, detector misalignment
Spatial coregistration (intra/ interband)	<0.15/0.3 SSD	Spectrometer keystone, detector misalignment
FLEX interchannel temporal coregistration	<2 seconds	
Absolute radiometric accuracy	5%	Including polarisation and straylight sensitivity
Relative radiometric accuracy	1%	Spectral and spatial
Polarisation sensitivity	2%	FLORIS-LR
	1%	FLORIS-HR
Calibration	Sun-based	Using sunlit diffuser at calibration port

Table 5.2. Level-1b observational requirements that drive the FLORIS design.

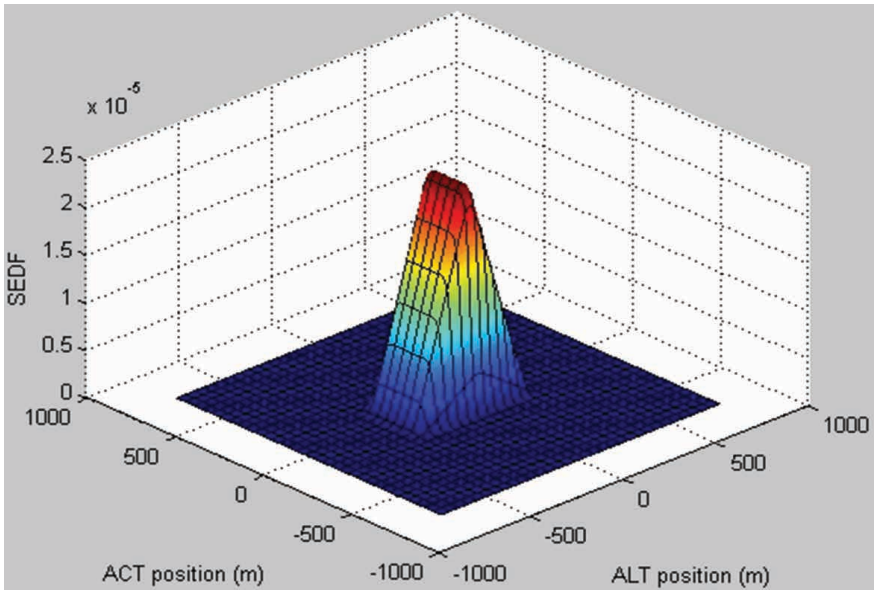

Figure 5.8. The FLORIS SEDF. The triangle in the ALT direction results from the smear generated by the satellite motion during the integration time. (ESA)

5.3.2.3.1 Geometric requirements

FLORIS will provide spectrally-resolved imagery with 300 m SSD over a swath width of 150 km. To determine the imaging quality, the System Integrated Energy (SIE) has been specified, which is determined by the spatial performance of the instrument, the platform pointing stability, the satellite velocity and projection onto the ground. It is obtained by integrating the System Energy Distribution Function (SEDF), over a specified surface area *A*. The SEDF describes the spatial distribution of the target radiance when measuring a spatial sample in any spectral channel. An SIE of 70% can be achieved at 1.2×1.1 SSD for both instrument concepts. A plot of the predicted SEDF for both designs is shown in Fig. 5.8.

5.3.2.3.2 Spectral requirements

The requirements on Spectral Resolution (SR), SSI and SNR are shown in Table 5.3.

The spectral requirements described in Table 5.3 could be fulfilled with a spectrometer design that samples the entire required wavelength range at the most demanding sampling of 0.1 nm. This would, however, entail the implementation of a detector with about 2800 lines, which will not be available in the near future. For this reason, both industrial consortia have chosen a design in which the high-resolution and low-resolution sampling functions are assigned to two separate spectrometers. Each spectrometer has a fixed spectral sampling that corresponds to the best value required for its respective ranges. Spectral binning is then performed on board for spectral regions that require less demanding spectral sampling. Figure 5.9 shows the predicted ISRF, obtained by the convolution of the slit function ($rect_{Slit}$), the detector pixel ($rect_{pix}$) function and the optical Line Spread Function (LSF) of the spectrometer at a specific wavelength λ i.e:

$$ISRF(\lambda) = rect_{Slit} * rect_{pix} * LSF(\lambda) \tag{5.1}$$

The SSI is a factor of three lower than the SR to avoid aliasing in areas where high resolution is required.

Because of its high resolution, FLORIS can be spectrally calibrated using narrow atmospheric features once per orbit. To ensure that the spectral scale does not vary between these calibrations, FLORIS requires a relatively high spectral stability (0.1 SSI), which needs the temperature of the instrument to be stabilised at ±1°C.

Table 5.3. FLORIS spectral and SNR requirements at Level-1b.

Band	Band I	O_2-B		Band II			O_2-A		
λ [nm]	500–677	677–686	686–697	697–740	740–755	755–759	759–762	762–769	769–780
SR Full Width at Half Maximum (FWHM)	3.0	0.7	0.3	2.0	0.7		0.3		0.7
SSI	2.0	0.5	0.1	1.0	0.5		0.1		0.5
SNR	245	340	175	425	Linear from 510 to 1015	1015	115	Linear from 115 to 455	1015

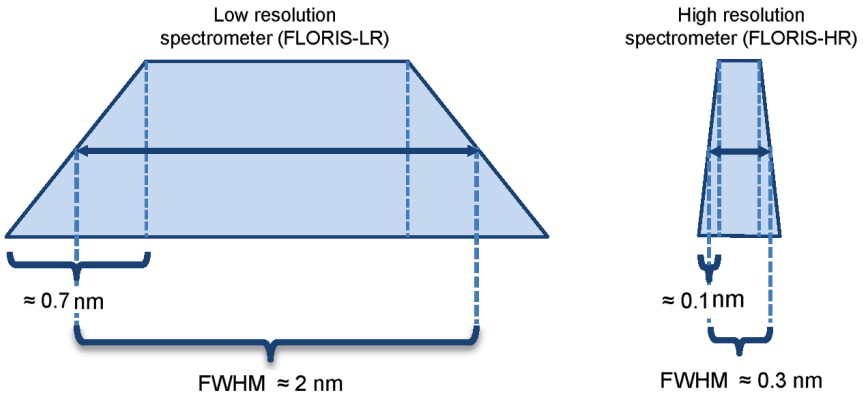

Figure 5.9. Geometrical ISRF of FLORIS-LR (left) and FLORIS-HR (right). (ESA)

5.3.2.3.3 Radiometric requirements

SNR

Remote sensing of vegetation chlorophyll fluorescence requires a relatively large dynamic range of the detected signal, owing to the low radiance at the absorption edge of the O_2-A-band, in particular at 761 nm. The requirement of SNR=115 at SSI of 0.1 nm between 759 nm and 762 nm drives the radiometric sizing. The grating is the most important element in the instrument because it can significantly vary the throughput depending on the diffraction efficiency. Activities have been performed to optimise this parameter.

For the investigated concepts it was found that pupil sizes of about 80 mm for FLORIS-HR and about 40 mm for FLORIS-LR are needed to fulfil the SNR requirements as given in Table 5.2. In addition, Charge Coupled Device (CCD) detectors have been selected because of their inherent advantages over Complementary Metal-Oxide Semiconductor (CMOS) devices in terms of readout noise and dynamic range.

Absolute radiometric accuracy

Absolute radiometric accuracy of 5% entails the use of an onboard diffuser, deployed into the instrument Field of View (FOV) when flying over the South Pole, outside the observation arc of the sunlit orbit. When the system is operated in solar calibration acquisition mode, the spectral radiance generated by the diffuser at the entrance of the instrument is calculated using a solar reference irradiance database, the bidirectional reflectance distribution function of the diffuser and the knowledge of the calibration mode geometry.

This calibration allows the absolute sensitivity of the instrument to be determined and the parameters of the radiometric model, as established by the on-ground measurements, to be updated. The satellite pointing during acquisition may evolve, generating a modification of the solar illumination on the diffuser. For more robust computations, this effect is also taken into account. The illumination conditions are determined thanks to the Attitude Orbit Control System (AOCS) measurements that provide the orientation of the satellite with respect to the Sun. The solar diffuser orientation inside the satellite is a parameter measured on the ground and provided in calibration files. The radiometric accuracy is also affected by the linearity of the system, since Earth radiance and Sun irradiance on the diffuser are measured at different levels. A linearity requirement of 1% is therefore set at Level-0, which demands on-ground calibration of the detector and the detection electronics over the full signal range.

As stated earlier, straylight is a major concern and an allocation of 1% (at the reference radiance level) has been made in the radiometric budget, which impacts both the instrument design and the on-ground characterisation. The latter is required to generate an accurate model for on-ground calibration to reduce the residual straylight contribution.

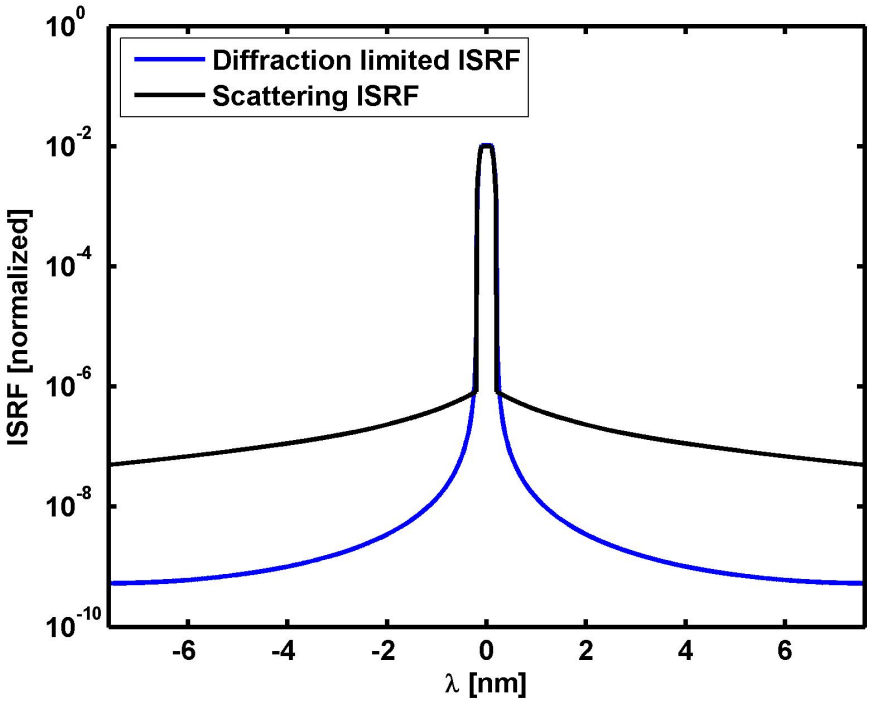

Figure 5.10. A typical ISRF on a logarithmic scale showing the diffraction-limited ISRF and scattering ISRF of FLORIS-HR. (ESA)

Scattering by the optical elements is the major contributor to straylight. It affects the wings of both spatial and spectral response functions and, therefore, determines the straylight sensitivity of any spectrometer. This is illustrated in Fig. 5.10, which shows the estimated ISRF of a point source in the focal plane of the high-resolution spectrometer. The X-axis indicates the spectral direction in the focal plane, where each 0.028 mm-long pixel corresponds to a wavelength step of 0.1 nm. It can be seen that the scattered light constitutes the major straylight driver, rather than the diffraction, and therefore has to be minimised.

In all spectrometers, straylight generates a measurement error in both the spatial and spectral domain. In order to achieve an instrument design fulfilling the straylight requirements, the two major contributors need to be carefully controlled, namely the cleanliness of the instrument because of contamination and the surface micro-roughness of the optics. A particular contributor is the grating, which, owing to the manufacturing process, may exhibit a surface roughness larger than conventional polished optics (mirrors and lenses). Focused work has been performed in the frame of the pre-development activities aimed at minimising scattering from the grating and the results are shown in Chapter 7.

Polarisation sensitivity

Light scattered by atmospheric molecules can be highly polarised depending on the spectral absorption depth. To desensitise the instrument to the polarisation state of incoming radiation, so that the radiometric accuracy is not degraded, a polarisation scrambler has been implemented in both concepts. The scrambler is placed at the input pupil, so that any polarisation-sensitive element, e.g. the fold-mirror, the grating and the antireflection coatings, will provide the same throughput independent of the polarisation state of the incoming radiation. As shown in Chapter 7, thanks to the scrambler the achieved polarisation sensitivity is as low as 1% in the O_2-A band, which is the most critical owing to high absorption in the atmosphere.

Coregistration requirements

Spatial coregistration between spectral channels can be separated into intraband and interband coregistration. The intraband coregistration addresses the difference of the spatial origin of any spectral channel within the band of a single spectrometer. The requirement is mainly related to the keystone of the instrument (the variation of the spatial position as a function of the wavelength in the focal plane) and the detector misalignment. The interband spatial coregistration relates the difference of the spatial position of the spectral channels between the two different spectrometers. For both proposed concepts, the intraband coregistration is very good since the optical distortion is very small. The requirement of 0.15 SSD can be met and is not considered as a design driver. The co-alignment to achieve coregistration between the spectrometers (interband) requires a good alignment of the optics and the detectors. The requirement of 0.3 SSD needs a careful alignment process and good inflight stability.

Spectral coregistration includes errors generated by the spectrometer smile and the detector misalignment. Errors have been minimised to avoid (a) processing artefacts from resampling on a common wavelength scale and (b) signal cross-coupling owing to charge collection inefficiencies within the detector during charge transfer.

5.3.2.4 Payload subsystems

This section describes the main subsystems of FLORIS.

5.3.2.4.1 Optical concepts

The Concept A optical design of FLORIS-HR is shown in Fig. 5.11. The system uses refracting lenses for the telescope, collimator and camera. The telescope has an external entrance pupil of ~80 mm diameter, and 228 mm focal length. It forms an Earth image on the spectrometer entrance slit, which is 42 mm long and 0.084 mm wide. It is preceded by a baffle to reduce out-of-field straylight, and a scrambler to reduce the instrument polarisation sensitivity.

Spectral filters are located immediately behind the entrance slit and in front of the two detectors. The filter placed behind the slit, which is tilted 7° to control unwanted reflections, cuts off wavelengths above 810 nm. The filters in front of the detectors cut off wavelengths below 620 nm for the detector assigned to the O_2-B band, and below 680 nm for the O_2-A band. This minimises out-of-band sensitivity and spectral straylight.

The beam from the slit is collimated. It passes through a prism and a flat transmitting diffraction grating and is then focused onto the detector by the camera lenses. The camera and collimator lenses are identical (each with a focal length of 154 mm) for manufacturing convenience, working together at unit magnification. The collimator forms a pupil image on the grating.

The grating has a spatial frequency of 1500 cycles per mm, and operates in Littrow condition, in the first order, for the mid-wavelength (728.5 nm) of the HR range. The prism is included to correct the smile distortion of the image (curvature of the image of the entrance slit) produced by the grating.

As indicated in the lower illustration in Fig. 5.11, the design includes a flat fold-mirror in front of the telescope. The fold-mirror allows the major axis of the optical system to lie in a plane orthogonal to the nadir (Earth-view) axis. The overall length of the HR optics, including the fold-mirror and image area, is 991 mm.

The Concept A LR optical design is shown in Fig. 5.12. The principle and general shape of the LR system is similar to that of the HR system, but it has a smaller (~40 mm) aperture and a much wider spectral range. As with the HR

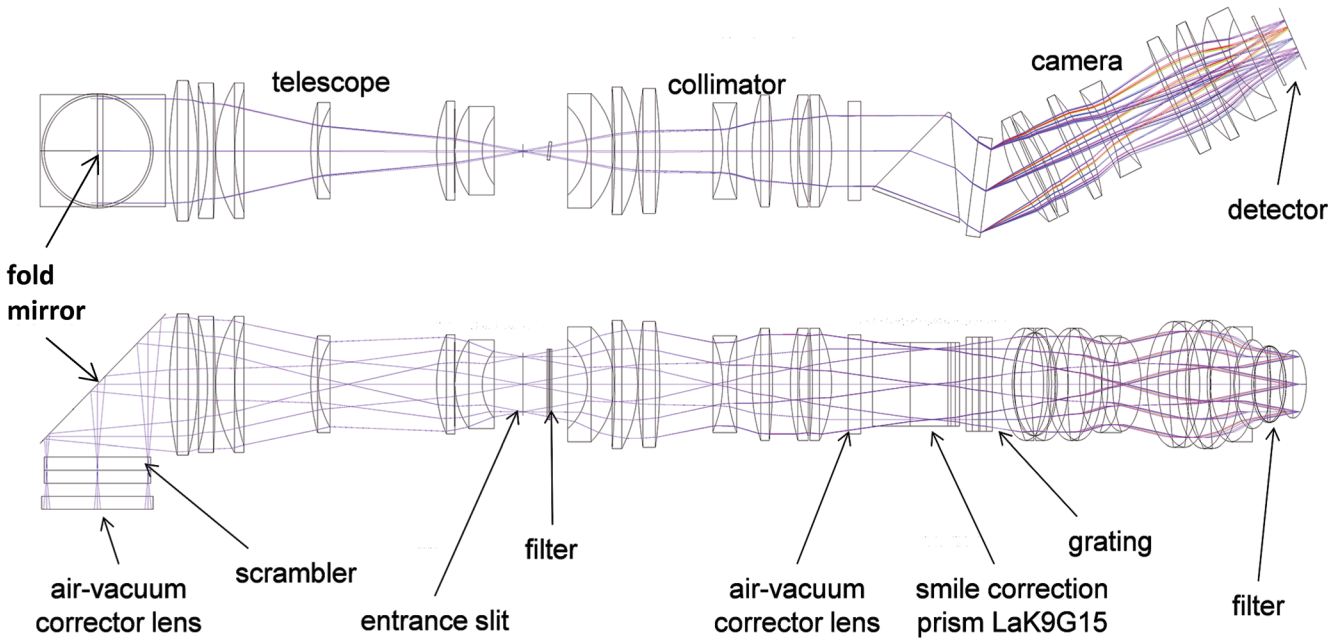

Figure 5.11. Concept A FLORIS-HR optical layout with nadir direction (top) and ACT direction (bottom). The air-vacuum corrector lenses are removed in the flight model configuration. (Airbus Defence and Space)

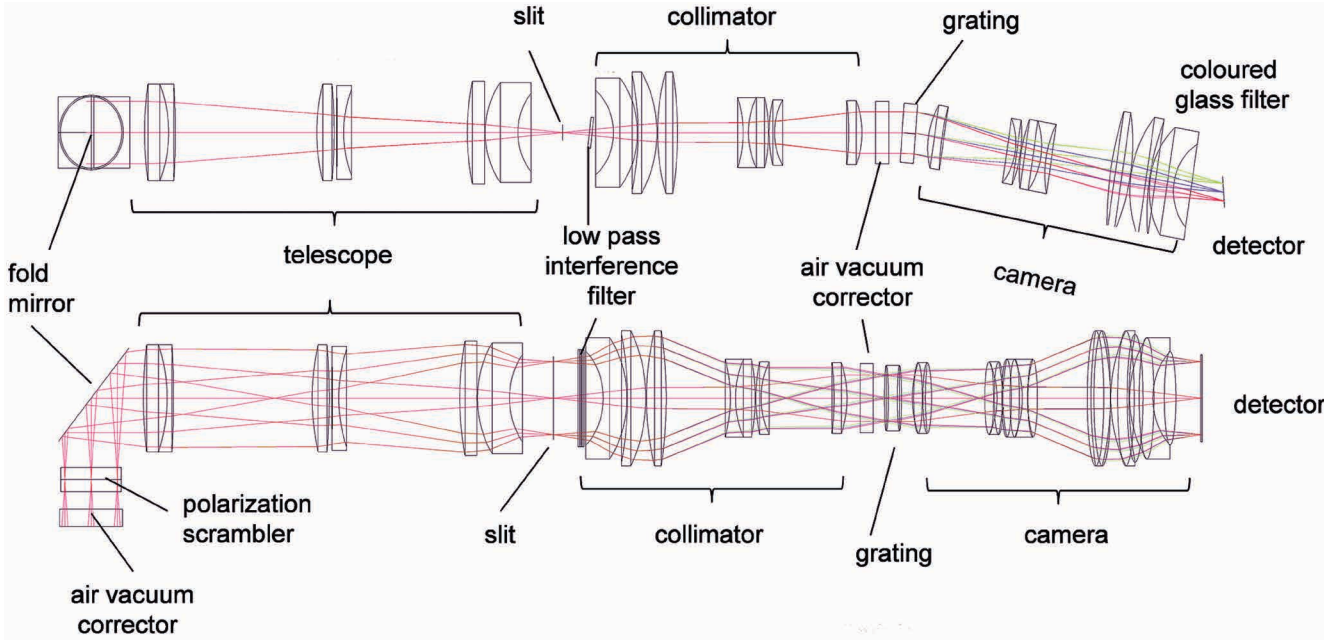

Figure 5.12. Concept A FLORIS-LR optical layout with nadir direction (top) and ACT direction (bottom). The air-vacuum corrector lenses are removed in the flight model configuration. (Airbus Defence and Space)

system, it includes a polarisation scrambler and a flat fold-mirror in front of the telescope. The tilted filter following the entrance slit cuts off below 450 nm. Like the HR optics, it carries the dielectric coating, cutting off at wavelengths larger than 810 nm. The diffraction grating has a spatial frequency of 254 cycles per mm, and operates in first order. The LR detector is tilted 13.7° for chromatic correction. The overall length of the LR optics, including the fold-mirror and image area, is 872 mm.

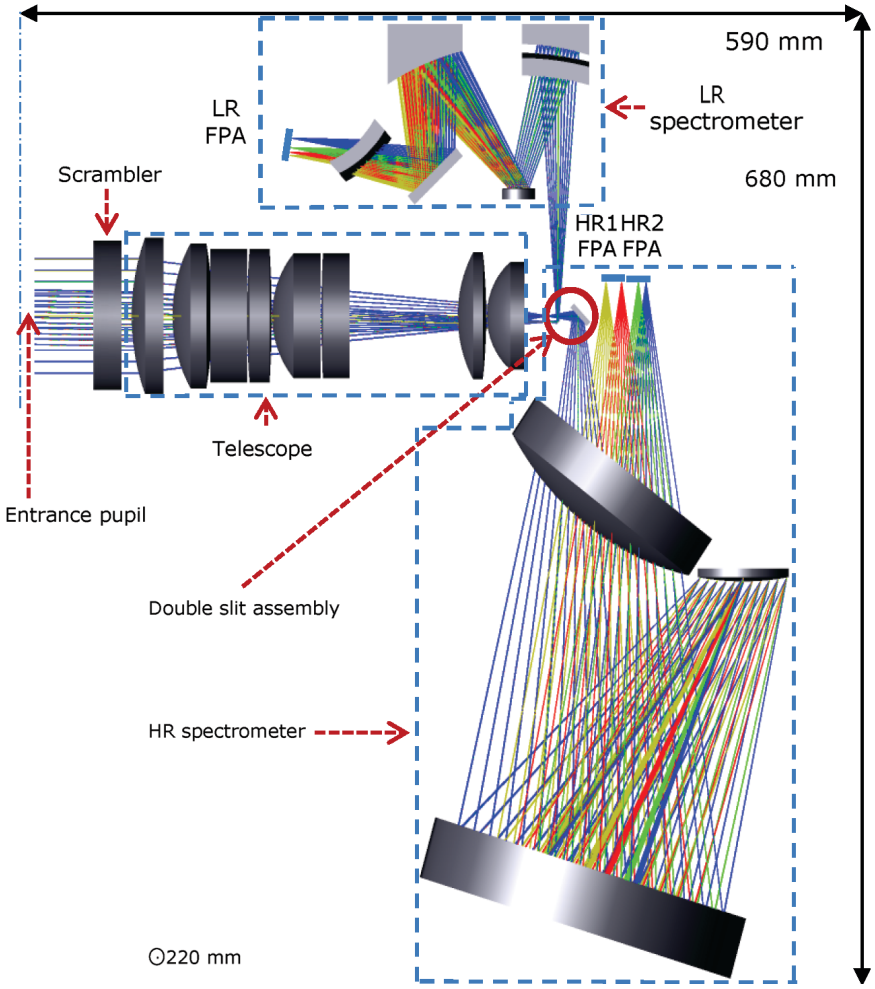

Figure 5.13. Optical concept of the FLORIS-HR and LR spectrometer for Concept B. (Thales Alenia Space)

The optical design of Concept B is shown in Fig. 5.13. It is based on a single telescope, with a focal length of 244.5 mm and an f-number of 3.1, which forms an Earth image onto two identical slits in the focal plane separated by 4 mm. This separation corresponds to 13.4 km on the ground and is equivalent to 2 seconds of temporal coregistration at the satellite altitude, in line with requirements.

Two flat fold-mirrors follow the double-slit assembly to direct the beams towards the HR and LR spectrometers. The telescope is preceded by a baffle, to reduce out-of-field straylight, and a scrambler to reduce the instrument polarisation sensitivity.

The LR dispersion is obtained by means of a standard three-mirror Offner spectrometer with a reflective convex grating of 500 grooves per mm, while the HR channel makes use of a Littrow Offner like spectrometer with a reflective convex grating of 1450 grooves per mm. Both spectrometers have unit magnification. The optical design of Concept B also foresees the use of filters to minimise out-of-band sensitivity and spectral straylight.

The overlapping spectral range (677–697 nm) has been introduced to simplify the spectral coregistration between the two spectrometers. Holographic gratings are used to reduce spectral straylight caused by grating imperfections (roughness, profile errors, etc.), which directly impact the fluorescence measurement accuracy within the O_2 absorption band.

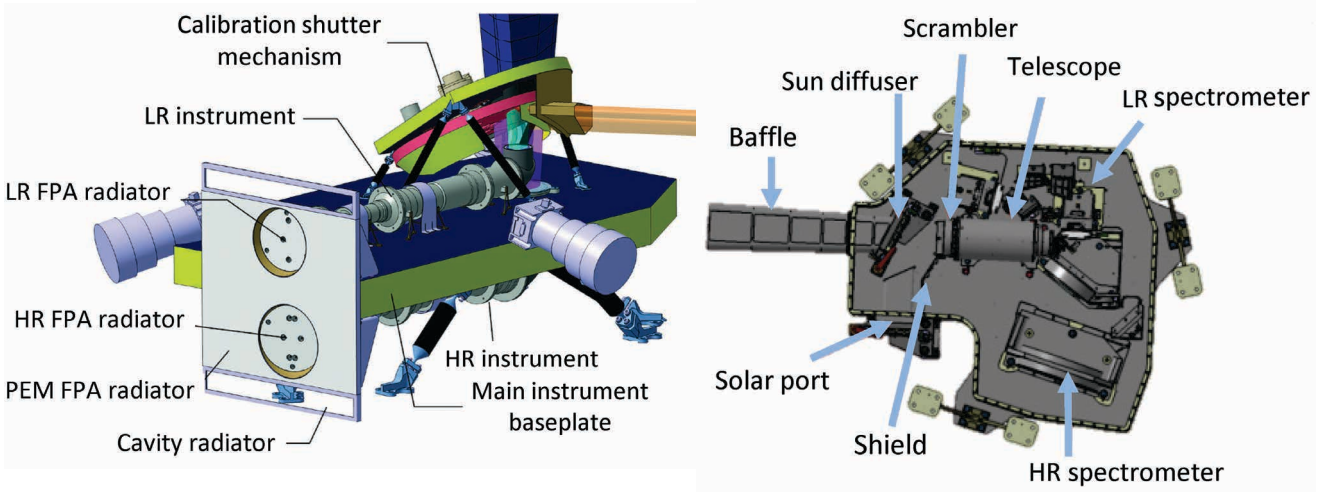

Figure 5.14. Internal instrument mechanical configuration of Concept A (left) and Concept B (right). (left: Airbus Defence and Space, right: Thales Alenia Space)

5.3.2.4.2 Mechanical and thermal architecture

The mechanical accommodation of the two concepts is shown in Fig. 5.14. Concept A uses a back-to-back configuration, where the two spectrometers are both located on one side of a Carbon Fibre Reinforced Plastic (CFRP) optical bench. Flat fold-mirrors provide the nadir view towards Earth, as well as the view to the Sun-illuminated diffusers mounted on a calibration assembly. In Concept B, the telescope and the two spectrometers are located on the same side of an aluminium optical bench. The nadir view towards Earth is realised by mounting the instrument on a PIM tilted by about 30° with respect to the platform.

Apart from the internal baffles and lens sealing, the FLORIS instrument is covered by Multi-Layer Insulation (MLI) in Concept A and aluminium housing in Concept B. The startrackers are mounted either on the instrument baseplate or on the PIM, as shown in Fig. 5.15. In both concepts the instrument is decoupled mechanically and thermally from the platform thanks to an isostatic mounting made of three low-conduction bipods, and it is mounted either on the platform top panel (Concept A) or on the PIM (Concept B) .

The instrument thermal architecture relies on a conventional concept, making use of a limited number of active thermal control loops. The accommodation of the dissipative sources and radiative surfaces ensures a stable and homogenous temperature of the optics to reach the stability required. Apart from the detectors, which must be stabilised at –20°C or below, all the other optical elements are maintained at about 20°C, which facilitates assembly, integration and verification activities.

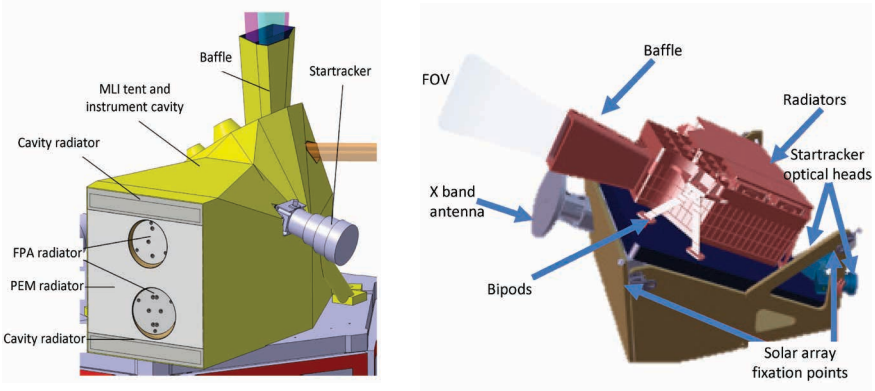

Figure 5.15. Instrument structures for Concept A (left) and Concept B (right). (Airbus Defence and Space (left), Thales Alenia Space (right)

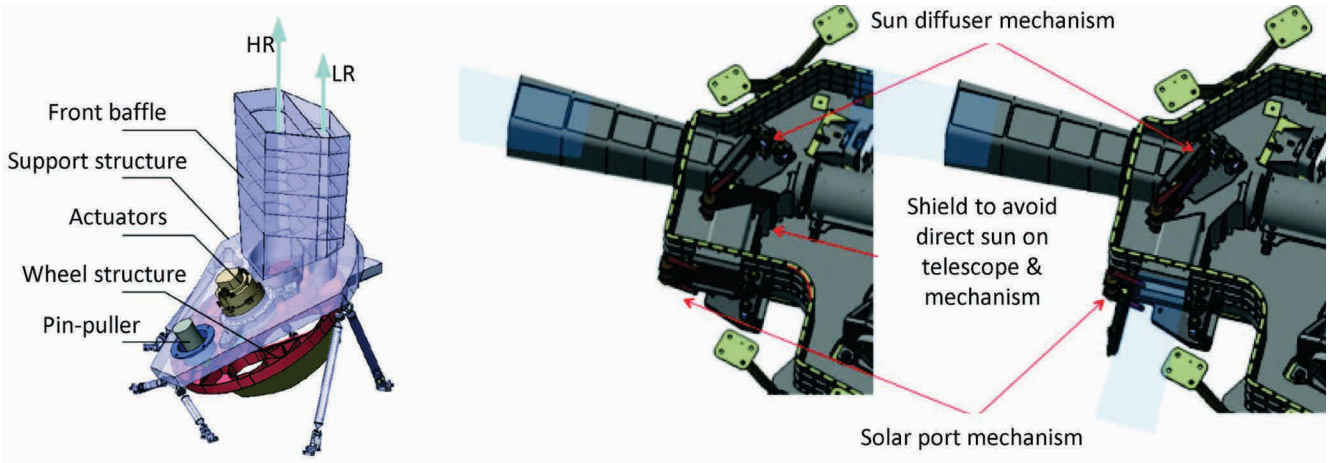

Figure 5.16. Diffuser and shutter mechanisms of Concept A (left) and the diffuser and shutter mechanisms (centre and right) of Concept B. They are not visible in Fig. 5.15 since they are embedded in the structure. (left: Airbus Defence and Space, right: Thales Alenia Space)

For thermal stability aspects and to limit the variation of the required heating power, all the radiators and dissipative elements (detectors, proximity electronics) are accommodated on the anti-Sun side (+Y face). The thermal models have been coupled with the optical analyses in dedicated software applications to verify the spectral stability of the instrument. The camera, collimator and telescope are independently thermally controlled with dedicated heating lines to ensure a temperature stability of about ±1°C. The focal plane and detectors are stabilised at a temperature of about –20°C with an accuracy of approximately ±0.1°C to limit the effect of dark current fluctuation on the signal. Radiators are accommodated close to the dissipative elements to optimise heat extraction.

5.3.2.4.3 Mechanisms

Concepts A and B both use mechanisms to deploy a diffuser for radiometric calibration and to protect the instrument from contamination during launch and on-ground activities, and from direct Sun illumination during the Launch and Early Orbit Phase (LEOP).

The calibration mechanism of Concept A consists of a wheel that is steerable in three positions corresponding to shutter, imaging and calibration functions. Switching among the positions is performed through a harmonic drive rotary actuator. The wheel is maintained in the shutter position during ground operations and launch phase, to prevent any contamination or Sun illumination on the optics.

Wheel rotation is prevented during the launch phase either by powering the rotary actuator or by a pin-puller mechanism. The rotary actuator with pin puller was used in the Copernicus Sentinel-2 Multispectral Instrument (MSI). The mechanism allows positions to be switched in less than 30 seconds. The mechanism and wheel are mounted on a dedicated structure that also incorporates the front baffle (Fig. 5.16, left).

The calibration of Concept B (Fig. 5.16, centre and right) relies on two separate mechanisms that operate a solar port and a Sun diffuser. The solar port is kept closed during nominal operations and opened by means of a stepper motor during calibration to allow illumination of the Sun diffuser.

The Sun diffuser rotation is managed by the torque provided by two preloaded torsional springs and it is controlled by a stepper motor acting as a brake. The mechanism closes the Earth baffle exit for calibration and keeps it open in nominal observation mode. For both concepts, radiometric calibration

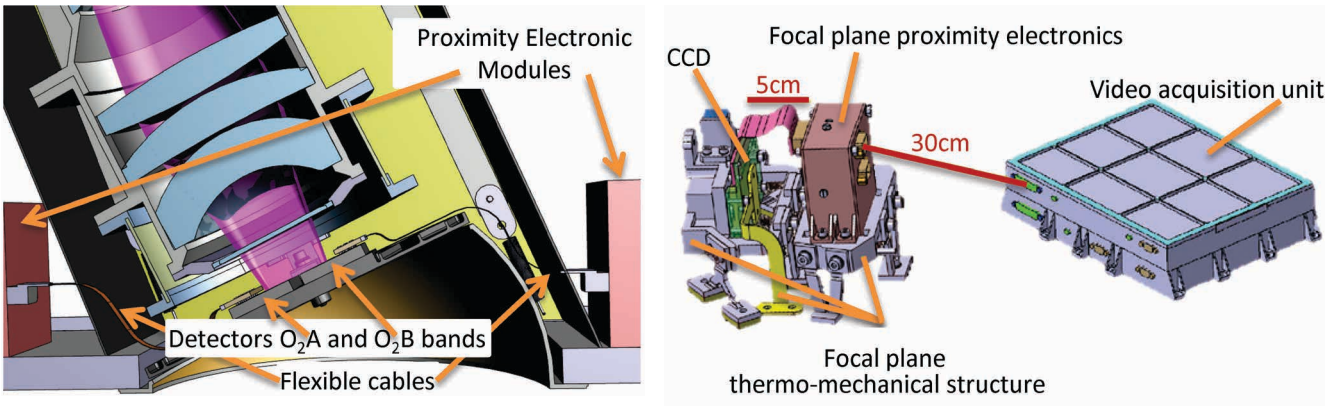

Figure 5.17. Focal plane configurations of Concept A (left) and Concept B (right). (Left: Airbus Defence and Space, right: Thales Alenia Space)

will be performed close to the South Pole, with an illumination angle of 65° on the diffuser, providing radiance levels close to the reference radiance.

5.3.2.4.4 Focal plane architecture

The mountings of the detectors differ for the two concepts. In Concept A the focal plane is directly mounted on the camera optic mounts with a low-conductivity titanium shell. In Concept B the detectors are mounted in a thermally isolated way on the optical bench of the instrument. In order to limit noise, the proximity electronics in both concepts will be mounted closely to the detectors and directly coupled to the radiators. Detectors will be kept operational during the whole orbit to avoid temperature stability issues.

5.3.2.4.5 Detectors

Both FLORIS instrument concepts are based on one detector type and format, used for FLORIS-LR and for the two bands of FLORIS-HR. Quantum efficiency close to 100% at 761 nm can be reached by means of a very low reflectivity

Figure 5.18. Schematics of the FLORIS detector layout. (Airbus Defence and Space)

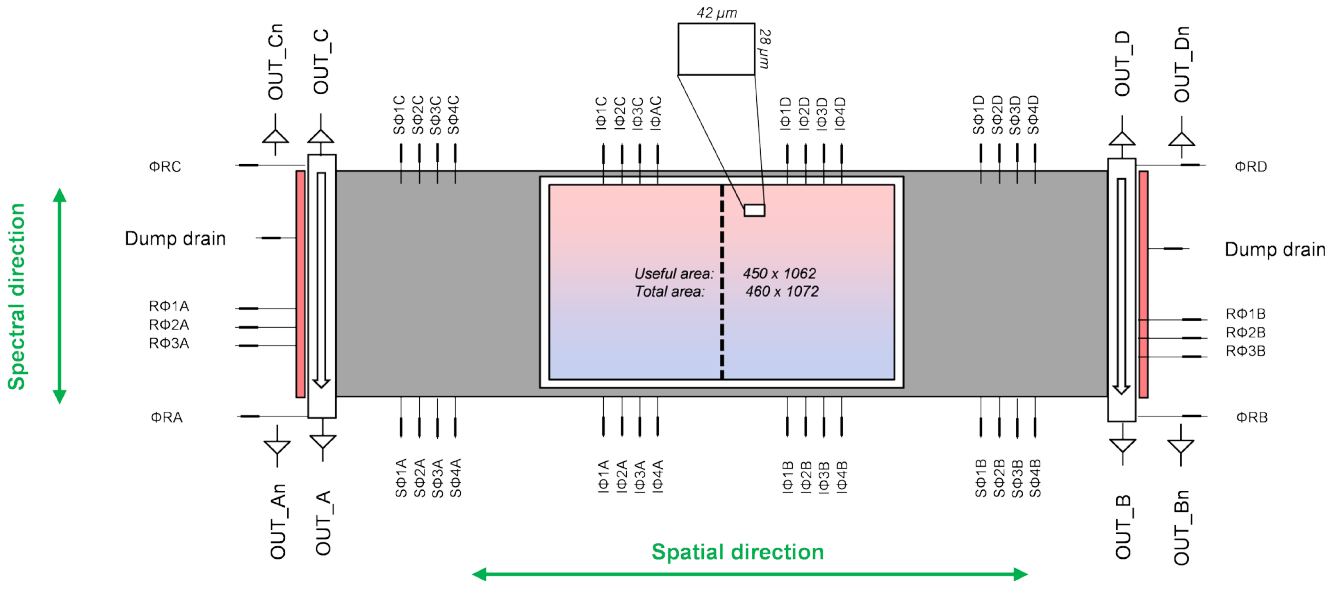

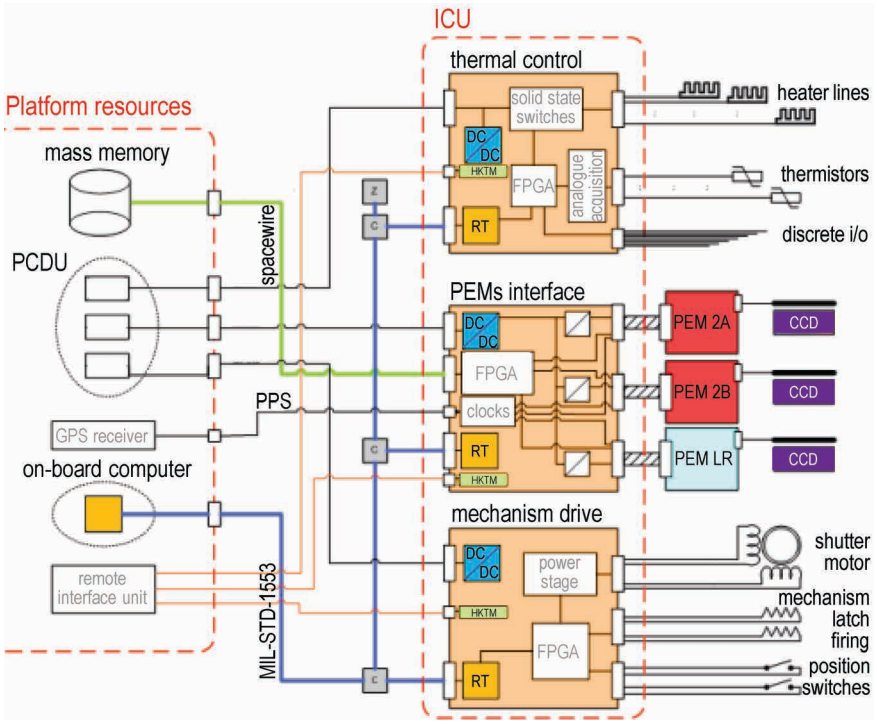

Figure 5.19. Electronics scheme for Concept A. (Airbus Defence and Space)

coating. The expected reduced sensitivity at lower wavelengths is compensated in the FLORIS-LR spectrometer by the sufficient throughput to match the SNR requirements.

The format of the detector is 1070×460 pixels and it is implemented as a frame transfer CCD in split frame configuration. The frame transfer is performed along the spatial direction. Two adjacent lines are binned in the serial register allowing the data to be read out at a resolution of 300 m.

The full-well capacity of a single pixel of 28×42 microns is almost 1.25 million electrons. The expected operating temperature is in the range 240–250K to minimise dark signal noise. Two video output ports will be operated at a frequency of 2.5 MHz. A pre-development activity has started with a leading manufacturer to mitigate future development risks and has reached the stage of Preliminary Design Review. This activity benefits from a similar configuration that is being developed for the Sentinel-4 and Sentinel-5 Precursor missions.

5.3.2.4.6 Payload electronics

In Concept A, the Instrument Control Unit (ICU) manages the interface between FLORIS and the platform, and is made of three independent boards, powered by dedicated power lines and driven by the Onboard Computer (OBC) via the MIL-STD-1553 bus and three command/control remote terminals (Fig. 5.19).

One board operates the calibration mechanism and controls the firing of latches that lock the mechanisms during launch. This board is powered independently and is only used during the calibration phases. The second board is dedicated to the thermal management of the instrument, acquiring thermal sensor readings and driving the heaters accordingly. The last board manages the three Proximity Electronics Modules (PEMs) as well as science data including acquisition, processing, packetisation and transmission to the mass memory unit via SpaceWire links. The three PEMs, one for each CCD, are mounted as close as possible to the detector to minimise noise on detector cables and perform detector operations via biasing, sequencing, clock level translation, video chain implementation, data conditioning and transmission to the ICU.

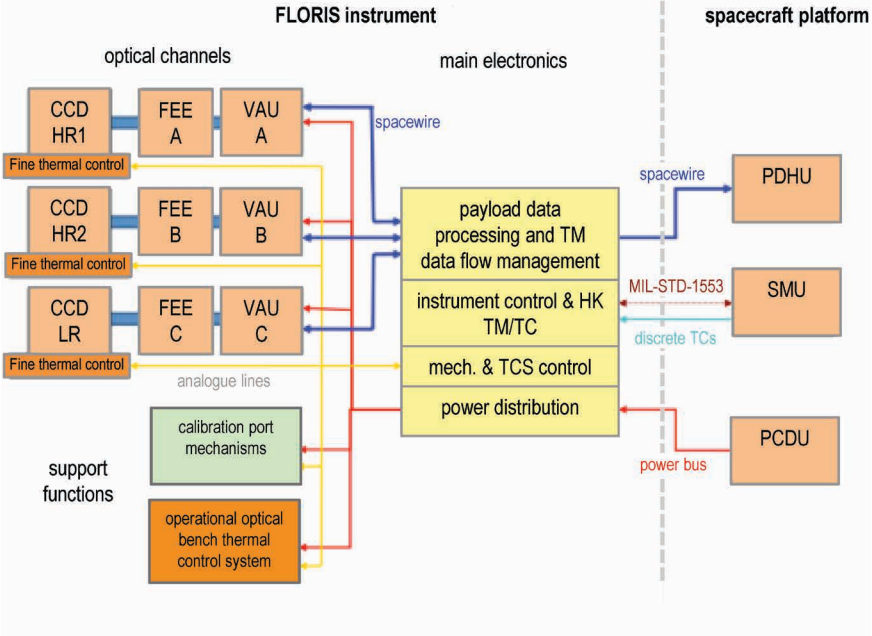

Figure 5.20. Electronics scheme for Concept B. (Thales Alenia Space)

In Concept A the redundancy scheme of the electronic functions is based on the implementation of a fully-redundant ICU. The SpaceWire links towards nominal and redundant mass memory are cross-strapped. In case of failure, switching to the redundant ICU and reconfiguring it are managed by the OBC. The PEM are not redundant, but have interfaces towards both nominal and redundant ICU. The Calibration and Shutter Mechanism motor has two sets of windings, connected to the ICU Nominal/Redundant. The thermal hardware is duplicated, thermal sensors are tripled and majority voting is applied.

In Concept B (Fig. 5.20), the FLORIS instrument is completely controlled by the ME, and interfaces the satellite management unit (SMU) via a MIL-STD-1553 bus, the Payload Data Handling Unit (PDHU) via SpaceWire links and the Power Conditioning and Distribution Unit (PCDU) via the power bus. It is composed of four separate boards.

One board is in charge of operating the two calibration mechanisms and of the thermal management of the instrument. The second board is in charge of the management of the three Front-End Electronics/Video Acquisition Units (FEE/VAUs), one for each detector, which are mounted as close as possible to the detector to minimise noise on detector cables. They are in charge of detector operations via biasing, sequencing, clock level translation, video-chain implementation, data conditioning and transmission.

The third board is devoted to instrument command and control and Housekeeping Telemetry (HKTM), while the fourth board, for power distribution, provides power to all instrument subsystems. The redundancy scheme is also based on a fully-redundant ME, with cross-strapped SpaceWire links to Nominal/Redundant Mass Memory Unit. FEE and VAU are not in a redundant configuration, but have a nominal and redundant interface towards the ME. Thermal lines and sensors, as well as calibration mechanisms, are fully redundant in this concept.

5.3.2.5 Payload on-ground characterisation and inflight calibration

5.3.2.5.1 Spectral and spatial response on-ground characterisation

For the purpose of modelling the instrument to ensure the proper establishment of the spectral scale and to estimate straylight in the instrument, it is required to measure the response of the instrument. Whereas the spatial and spectral response can be measured by knife-edge methods and scanning

of the wavelength, determination of the response at larger distances from the peak requires illumination with a monochromatic point source to establish the response at level of 8 to 9 orders of magnitude with respect to the peak. This exact characterisation is required to apply straylight correction methods, as done for other high-resolution spectrometers such as MERIS, OLCI and Tropomi.

5.3.2.5.2 Spectral inflight calibration

It is planned to derive the spectral calibration from the features of the atmosphere, i.e. by vicarious calibration, therefore there is no need for an absolute spectral calibration on the ground. However, to ensure the proper characterisation of the instrument on the ground, the spectral scale will be established with accuracy better than 1 nm. The use of lamps with known emission lines is sufficient for this purpose.

5.3.2.5.3 Radiometric inflight calibration

As mentioned, both concepts will make use of a diffuser deployed in front of the instrument aperture to perform radiometric calibration. The solar diffuser produces a radiance that is spatially uniform. Also the variation of its spectral shape varies very smoothly. It is known that diffusers can generate relatively high frequency variations, but these are very small and are expected also to average out during the acquisition of signals at different illumination angles. This will be re-confirmed by measurements in future phases. As a result, it is considered that the calibration measurement is close to a situation of a homogeneous scene and consequently the differential straylight is expected to be very low, so that it does not need to be taken into account for the solar-diffuser related calculations.

The pixel-to-pixel relative gains, which are related to the photo-response of the detector, are assumed stable in time. These gains are characterised on the ground before launch and are not part of the parameters to be undertaken using the solar diffuser calibration. This assumption will be confirmed during/after the detector radiation tests.

The spectral absolute instrument response is measured on the ground for each spectrometer and is assumed to have a low frequency evolution along wavelengths. It is considered that the differential temporal evolution along the spectrum is a linear function of the wavelength and will be measured by the use of the diffuser. The solar diffuser calibration, thus, aims to update the parameters of the spectral absolute calibration gain evolution.

5.3.2.5.4 Dark signal inflight calibration

Independently of the solar diffuser calibration, which aims to operate on the ‘gain’ part of the radiometric model, the inflight calibration concept includes re-estimation of the dark signal on a regular basis. The dark signal calibration does not make use of the solar diffuser, but it is necessary that up-to-date dark current data are acquired before going into calibration with the diffuser.

The calibration of the dark signal uses acquisitions realised either in an eclipse part of the orbit above dark scenes (oceans, for example), or with the shutter closed. In this way the radiance at instrument inputs can be considered negligible, so that the raw measurement is directly representative of the dark signal map at focal plane level, with a dark noise added. The determination of the dark signal, for a given sample, is then easily retrieved by averaging the raw measurements over a large number of lines. As a by-product, the

estimation of the standard deviation of the signal directly gives an assessment of the dark noise.

5.3.2.5.5 LOS determination

Geometric annotations will be provided with respect to the location of the image on Earth in terms of, for example, the four corners and the centre of the acquired image. Also, the average pointing conditions over the acquired scene are computed and appended. Restitution of the location on the ground of any pixel is based on the direct use of the geometric model.

For a given spatial sample acquired at a certain time, the computation uses the quaternions provided by startrackers to derive the transfer matrix from inertial frame to terrestrial frame and data from the Global Positioning System (GPS) receiver to derive the position of the satellite.

The remaining parameters involved in the computation are fixed calibration parameters, available in calibration files. The localisation of the image on Earth is then realised by computing the intersection of the line with the Earth ellipsoid (or optionally with a Digital Elevation Model (DEM). The processing is applied for each pixel of FLORIS along the considered product scene.

5.3.3 Platform

5.3.3.1 Overview

Both concepts rely on recurrent platforms and are based on flight-proven designs with extensive reuse of off-the-shelf components. This section describes each platform subsystem and provides the rationale for the architecture of the subsystems and the selection of components.

5.3.3.2 Structure

The mechanical design is driven by the need to accommodate the FLORIS instrument within the volume available under the Vega rocket fairing and ensure compatibility with the launcher mechanical environment. Figure 5.21 shows the two structural concepts proposed for FLEX. They are designed to sustain the launch loads by providing a direct load path to the launcher.

Concept A is based on an integrated solution supporting both the platform and the payload. The structure is a hexagonal prism 1.6 m high and 1.7 m across. A double cone structure provides the transition between the launch vehicle interface and the hexagonal body.

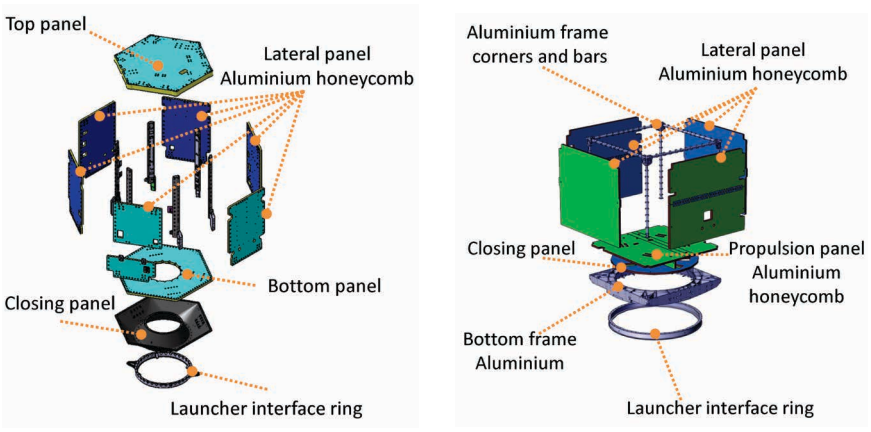

Figure 5.21. FLEX structural concepts. (left: Airbus Defence and Space, right: Thales Alenia Space)

The inner cone provides support to the propulsion module, while the reaction wheels, the solar array deployment mechanism as well as other small avionics elements are mounted on the bottom floor. Six aluminium-alloy machined frame beams connect the bottom floor to the top floor, which serves as the payload interface structure. The six lateral panels, made of aluminium honeycomb, act as thermal radiators and support the main avionics equipment units, which are mounted on the panel inner faces and can be accessed during AIT by folding the panels downwards.

Concept B is based on a modular architecture with separate service module (Fig. 5.21 right) and payload interface module. The service module interface is a square box of aluminium sandwich panels, assembled on a tubular frame to facilitate integration operations. The main load path is provided by the primary structure, which is made of four lateral panels and a top panel, a bottom frame and a bottom panel, and a launcher interface ring.

The alignment of the four lateral panels with the launcher interface ring optimises the load transfer from top to bottom and provides high stiffness without implementation of a more complex central tube solution. The PIM structural concept is based on a prismatic structure (Fig. 5.15 right) with aluminium sandwich panels, assembled on a tubular frame to facilitate integration operations.

For the instrument support panel, a CFRP sandwich is used to increase the stiffness and structural stability. Aluminium struts support the lateral panels and solar array holding points, while minimising constraints for the accommodation of startrackers and the instrument (radiator FOV). The Finite Element Model (FEM) analysis has enabled the elements of the payload module to be sized.

In both concepts, a standard 937-mm diameter adapter ring provides the interface to the Vega launcher.

The structure compatibility with the launcher environment has been assessed through dedicated mechanical analyses. The results of the dynamic analyses showed that the fundamental axial and longitudinal frequencies of both concepts are compliant with the Vega requirements. Static analyses to assess the response of the structure to quasi-static loads during launch have also been performed, confirming the adequacy of the proposed designs.

The results of the thermoelastic analyses show that thermoelastic deformations between the instrument LOS and the startracker optical heads stay within the allocated budget so that the overall instrument pointing performance can be met with good margins.

5.3.3.3 Mechanisms

Both concepts make use of release mechanisms to keep the solar array in the stowed position during launch and to release for deployment. Standard solutions, foreseeing the presence of hinges, a stiffener and a hold-and-release mechanism, are employed for the solar arrays. The only difference between the two concepts is in the location of the holding points, which are placed on the platform lateral panels in Concept A and on the payload module structure in Concept B.

5.3.3.4 Thermal control

Thermal requirements are not critical for the FLEX platform and can be fulfilled by well-proven passive thermal control design, including heater lines and thermistors, requiring minimum customisation for the FLEX mission. The platform heat rejection is achieved by using less than 50% of the available radiative surface available on the lateral panels. All internal units are painted

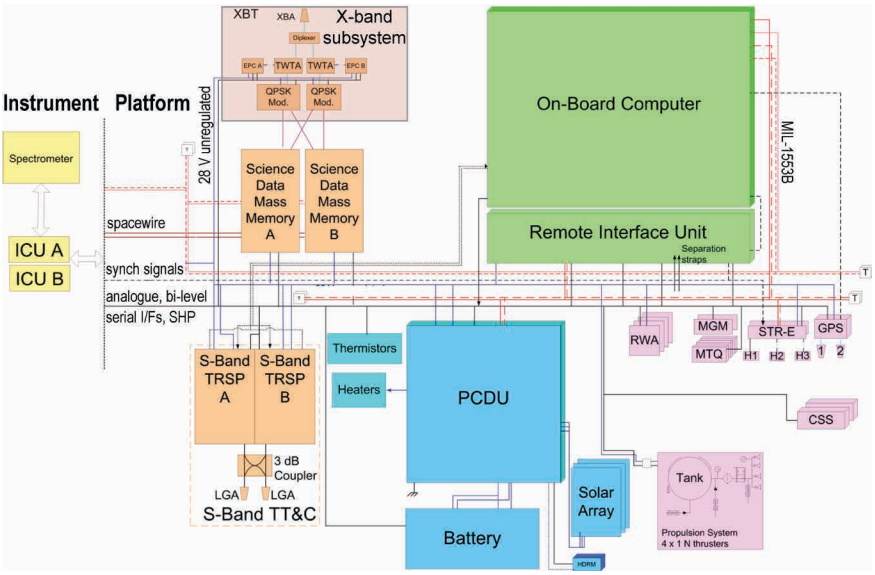

Figure 5.22. FLEX top-level electrical architecture for Concept A. (Airbus Defence and Space)

in black and mounted on the platform walls by means of interface fillers and thermal doublers to improve the conductive coupling with the radiators.

Internal sidewalls are also painted in black to make the temperature of the internal cavities uniform, while the non-radiative external surfaces of the platform are covered with MLI. Temperature sensors and heaters are placed in the units, payload bench and propellant tank to prevent excessive cooling during the cold phases (eclipses, LEOP and safe mode). Individual active thermal control is implemented for the batteries and the propulsion module, which are thermally decoupled from the platform by means of MLI wrapping. In both concepts, the payload is thermally decoupled from the platform by means of MLI placed on both sides of the PIP, as well as by low-conductivity mounting bipods. The PIP is controlled by means of heaters to maintain a very stable temperature and to minimise the thermoelastic distortions induced on the FLORIS instrument.

5.3.3.5 Electrical architecture

The electrical architecture is designed to integrate the relevant platform subsystems so as to ensure:

— command and control of the complete satellite in all relevant operating modes

— acquisition, storage and transmission to ground of payload data, auxiliary data and HKTM

— power generation, storage and distribution to the platform units and to the FLORIS payload

The two concepts make use of heritage solutions and equipment, and while presenting many similarities, they differ in some fundamental aspects.

The command and control functions are executed by the OBC, which communicates with the platform and payload units via two fully-redundant MIL-1553B buses. The science data communication link from the payload to the mass memory unit is accomplished by a cross-strapped cold-redundant SpaceWire interface for high data-rate transmission. The PCDU performs

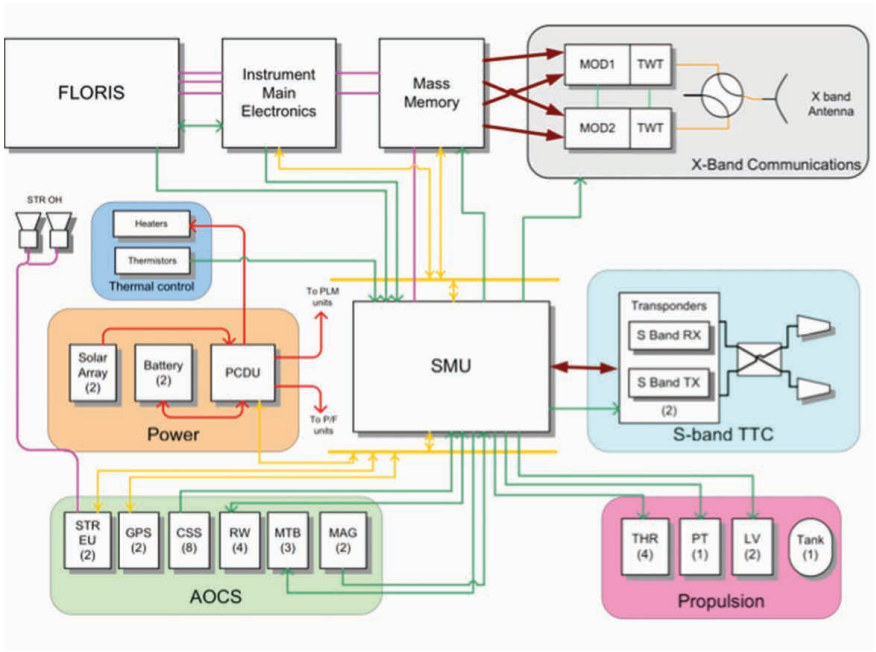

Figure 5.23. FLEX top-level electrial architecture for Concept B. (Thales Alenia Space)

the satellite power conditioning functions autonomously, and these are implemented without use of software to increase robustness.

The two concepts differ in the management of non-intelligent units, this being the task of a Remote Interface Unit (RIU) in Concept A, and implemented directly via the central SMU in Concept B.

Two different approaches have also been considered for the interface with the payload. The ICU of Concept A uses hard-wired logic (a field-programmable gate array (FPGA), for example) and is completely driven by the OBC. In Concept B, the ME has its own separate software and is directly in charge of FLORIS active thermal control, mode management and Failure Detection, Isolation and Recovery (FDIR). The payload data-handling unit directly manages the mass memory packet and drives the X-band transponder. During safe mode the OBC is in charge of the thermal control survival of the instrument.

5.3.3.6 Command and data handling

The Command and Data Handling subsystem provides the following functions:

— overall satellite command and control including AOCS algorithms

— running the onboard autonomy and FDIR

— provision and distribution of ground- and software-issued commands to the satellite

— collection and storage of satellite HKTM

— onboard time generation, synchronisation, maintenance and distribution

In both concepts, the data-handling architecture is based on a recurrent design with extensive heritage. However, while Concept A is based on two physical units, the OBC and the RIU, in Concept B a centralised SMU includes in a single mechanical unit all the functions as well as the circuitry and interfacing capability for acquisition and commanding of the whole satellite.

Command and control data are exchanged via three fully-redundant buses, two MIL-1553B buses to connect the OBC to the platform units and to the payload units, and one SpaceWire bus to link the payload science data to

the mass memory. Realtime HKTM is acquired by the central computer and transmitted to the ground using the S-band downlink. In both concepts, a dedicated interface enables stored HKTM to be downlinked via the X-band system, though in emergencies the downlink can be carried out via the S-band system.

The central computer maintains and distributes the onboard time reference, which is synchronised to UTC time provided by the GPS receiver part of the AOCS.

All the onboard processing of the science data is carried out by the FLORIS central electronics. The OBC is based on a Leon-3 microprocessor (SCOC3) in Concept A, and an ERC-32 microprocessor in Concept B. The OBC internal mass memory has a capacity of 3.8 Gb in concept A and of 8 Gb in Concept B, at End of Life (EOL).

The PDHT subsystem includes all equipment required to acquire, store and transmit the scientific data generated by the payload to the ground and consists of the Mass Memory Unit (MMU) and the X-band data downlink system.

The data flow starts from the instrument ICU/ME, which ensures the transfer of data to the MMU for storage until the next scheduled ground station pass. The MMU stores the payload data, auxiliary data required for payload data processing (e.g. position, velocity and attitude data) as well as the platform and payload HKTM. The X-band data downlink subsystem consists of two cold-redundant Travelling Wave Tube Amplifiers (TWTAs) and a single X-band antenna assembly. After amplification by the high-power amplifiers, the Radio Frequency (RF) signal is fed to the fixed isoflux X-band antenna through a waveguide redundancy switch.

The selected PDHT solutions are based on recent Copernicus Sentinel mission developments with minor modifications. Concept A is based on the Sentinel-5 Precursor solution, with minor upgrades to meet the FLEX requirements. The mass memory has storage capacity of 1 Tb at EOL and makes use of NOT+AND (NAND) flash technology boards. The mass memory sizing is based on the assumption that scientific data will be downlinked to the Kiruna ground station in Sweden.

The distance between Kiruna and Svalbard, which is the baseline ground station for the Sentinel-3 satellite, has been taken into account via a dedicated RF interference analysis demonstrating that the in-orbit separation between FLEX and Sentinel-3 is sufficient to avoid RF interference when the scientific data is downlinked. The X-band data downlink system is based on an off-the-shelf unit that transmits at a rate of 310 Mb s^{-1}. Quadrature Phase Shift Keying (QPSK) modulation and Reed-Solomon coding are applied to the signal before transmission to the ground.

Concept B is an upgrade of the Sentinel-3 solution. The mass memory consists of two Synchronous Dynamic Random Access Memory (SDRAM) memory modules of 256 Gb each for a total storage capacity of 512 Gb at EOL while the X-band data downlink transmits the stored data on ground at a rate of 260 Mb s^{-1}. Before transmission, Eight-Phase Shift Keying (8PSK) modulation is applied to the signal.

In Concept B, the scientific data are downlinked to the Troll ground station in Antarctica, which allows FLEX to fly closer to Sentinel-3 without any risk of RF interference during downlink. The proposed solution is also robust with respect to any future changes, e.g. a selection of the Kiruna ground station, as this will only imply an increase of the storage capacity needs, which can be easily achieved by using NAND flash modules instead of the current SDRAM selected modules.

5.3.3.7 Electrical power

The electrical power subsystem supports the following functions:

— generation of power
— energy storage
— power regulation and distribution to all equipment

The average power consumption is about 450 W in Concept A and 525 W in Concept B. Both concepts present classic electrical power architectures with classic design solutions.

An internally-redundant PCDU is responsible for distributing power from the solar array and the battery to the platform and payload equipment, providing power control and battery charge control. A direct-energy-transfer power conditioning scheme comprising a classic sequential-shunt-switching regulator has been selected as a baseline for both concepts. The PCDU distributes power via single power lines that are protected by folding and/or latching current limiters. Critical equipment, namely the OBC and the S-band transponder, is connected through resettable current limiters, which maintain power to the protected unit even after an anomaly. Both concepts use a non-regulated 28 V power bus that is compatible with the satellite power needs.

Power is generated by the solar array. In Concept A the solar array has three wings, each with an area of 1.8 m^2. In Concept B there are two wings each with an area of 3.69 m^2. In both cases the panels use triple-junction Gallium-Arsenide cells with efficiency of 28% at beginning of life. The maximum power generated at EOL is ~1300 W for Concept A and ~1500 W for Concept B.

The battery will be used in eclipse and during contingency operations and consists of two modules of lithium-ion stackable decks with the capacity of ~160 Ah, providing the required storage margin. Off-the-shelf units, with heritage from previous missions, have been selected for both concepts.

In order to comply with the ESA guidelines on space debris mitigation, a complete passivation of the power subsystem will be performed once the satellite has reached the end of its operational life. All the energy stored in the battery will be permanently depleted and the solar array will be prevented from recharging it.

In Concept A, electrical passivation is achieved in two steps. A modification of the central software is patched to the satellite to point the solar array away from the Sun. At the same time, the satellite thermal control set points are set to higher temperature to increase the satellite default consumption and fully discharge the battery.

The solution in Concept B foresees the presence of an electrical passivation unit made of simple shunts between the solar array positive and return lines and between the solar array and the PCDU. During electrical passivation operations, the relays are closed and all the solar array current is shunted, which leads to a battery full discharge. The electrical passivation unit has the strong advantage of requiring no modification to current spacecraft heritage, and shows no development risk because of its low complexity.

5.3.3.8 TT&C

The TT&C subsystem provides S-band communication capabilities between the satellite and the ground station. Two omnidirectional antennas ensure a communication link for all possible attitudes of the satellite in nominal and non-nominal conditions. The subsystem provides the following functions:

— command reception, for reception and demodulation of commands sent from the ground station

— telemetry, for modulation and transmission of realtime HK data to the ground

— ranging and Doppler tracking, providing range and range-rate information as a backup of the onboard GPS receiver data for orbit determination in the event of an emergency

The TT&C functions are implemented via a traditional architecture using a functional chain consisting of two S-band transponders connected to two S-band low-gain antennas via a 3 dB hybrid splitter/coupler. The receivers are used in hot redundancy while the transmitters are used in cold redundancy.

During nominal operations the subsystem only transmits realtime HKTM, but during emergency operations it also has the capability to downlink recorded telemetry. Telecommands are uplinked at a rate of 64 kb s^{-1} in Concept A and 28 kb s^{-1} in Concept B, while two operational modes are used to downlink the telemetry data. A low data-rate link transmitting at 128 kb s^{-1} and using a SP-L/PM modulation scheme supports downlink of telemetry in parallel with ranging and Doppler tracking operations.

A high data-rate downlink using an Offset Quadrature Phase Shift Keying (OQPSK) modulation scheme supports the downlink of recorded telemetry with no ranging capabilities. Data are transmitted at 1 Mb s^{-1} in Concept A and 1666 kb s^{-1} in Concept B.

5.3.3.9 AOCS

The AOCS concepts are based upon three distinct modes of operations. All modes are implemented in software and distinguished by the suite of hardware (sensors and actuators) used. The actuators consist of reaction wheels and magnetotorquers. The sensors comprise startrackers, magnetometers, coarse Sun sensors and a GPS receiver. A more detailed description of the main modes follows.

5.3.3.9.1 Initial acquisition and safe hold mode

This mode is active as of satellite separation from the launcher or triggered by the FDIR after detection of a critical failure. It aims to reduce the residual satellite angular momentum and acquire the attitude necessary for starting solar power generation. Starting from any arbitrary orientation and angular rate, the satellite is driven and maintained in a Sun-pointing attitude. In this mode, only vital satellite functions are maintained and the satellite is put into safe conditions where it is able to survive for a time only limited *a priori* by the consumables. Coarse Sun sensors and magnetometers provide the satellite attitude estimation while magnetotorquers and reaction wheels perform the necessary control functions.

5.3.3.9.2 Normal mode

This mode is in charge of attitude control during nominal operation, i.e. during scientific observations and instrument calibration. Both concepts use a gyro-less approach, providing the realtime attitude and angular rate estimate using startrackers and Kalman filters. Concept A uses a three-head startracker while Concept B uses a two-head startracker. Attitude control in normal mode is performed by the reaction wheels with momentum management via the magnetotorquers. A four-reaction-wheel pyramid configuration provides balanced capacity on every axis of the satellite and is tolerant to a single wheel failure.

While in normal mode, FLEX performs a sinusoidal yaw steering manoeuvre with amplitude of about 4° and a period of one orbit to compensate

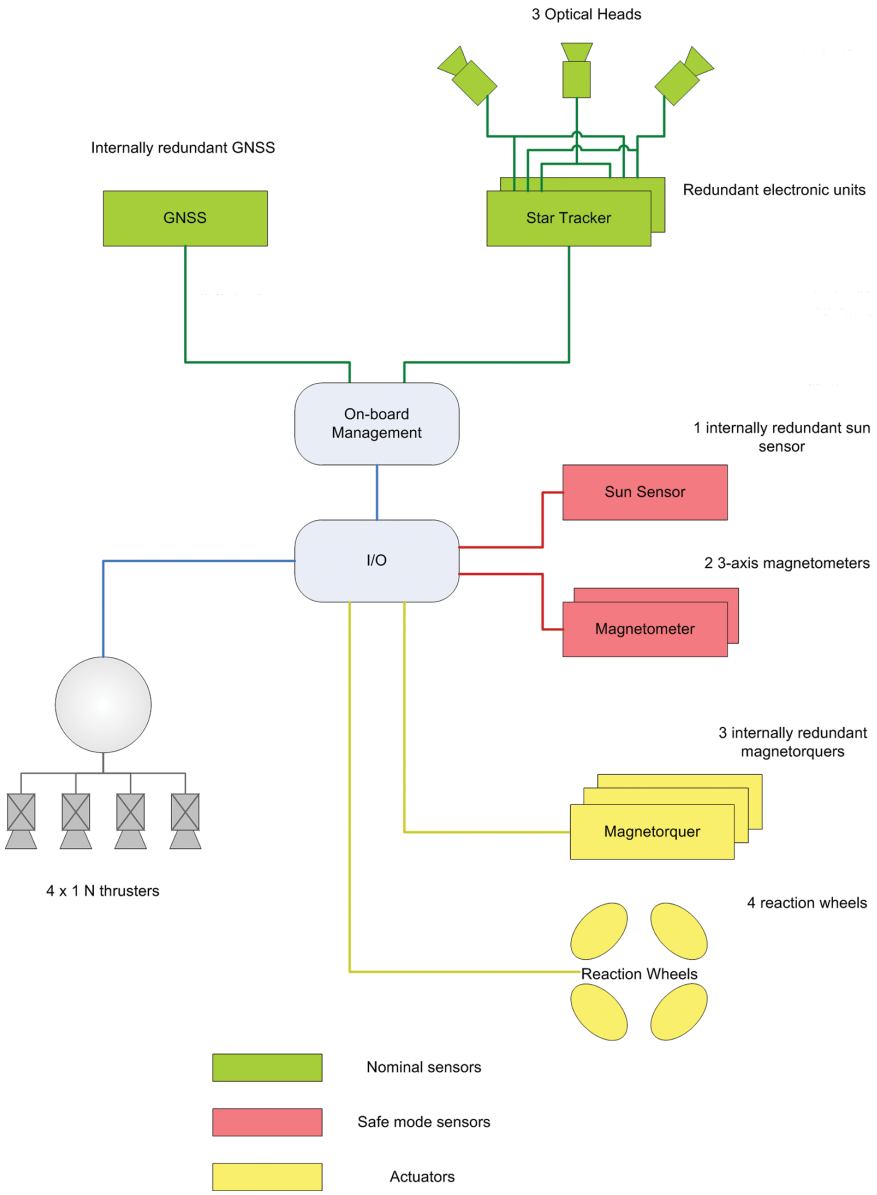

Figure 5.24. FLEX AOCS architecture. (Airbus Defence and Space)

for East–West movement of observed points caused by Earth's rotation. This also ensures that the relative velocity between the instrument and the observed target is aligned. Pitch and roll control laws are also implemented to point the instrument's LOS at the required altitude along the orbit.

The satellite attitude is maintained in geocentric pointing during observation arcs and eclipse, while specific control laws are implemented to maximise the power generation in the remaining part of the orbit. In Concept A, a Sun-pointing sub-mode with pitch steering guarantees optimal orientation of the solar arrays over the polar arcs. In Concept B, owing to a different satellite configuration, the same goal is achieved via a yaw steering law, which makes the satellite yaw angle match the Sun azimuth.

5.3.3.9.3 Orbit control mode

This mode is in charge of performing any in-plane and out-of-plane orbit manoeuvres during the commissioning, nominal and EOL phases. All the manoeuvres are performed using thrusters. Reaction wheels are used to perform a slew manoeuvre before and after the thrust to properly orient the

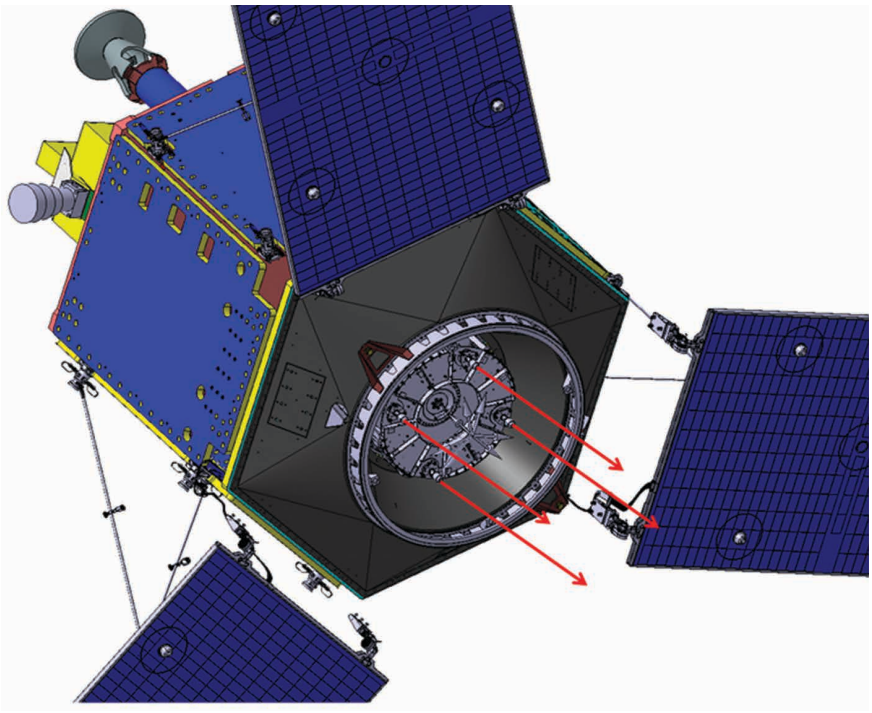

Figure 5.25. Example thruster configuration for Concept A. (Airbus Defence and Space)

satellite. Attitude control during the thrust phase is performed by pulse-off modulation in Concept B and via the reaction wheels in Concept A.

5.3.3.10 Propulsion

The FLEX propulsion subsystem provides the necessary thrust for correction of launcher injection errors, for orbit control manoeuvres and for the EOL deorbiting manoeuvre. Heritage equipment and standard solutions are used in both concepts. In addition, both concepts are based on a hydrazine system, pressurised with helium and operated in blow-down mode.

The propellant tank is mounted inside the central cone of the platform and an assembly of four 1 N thrusters operated in cold redundancy is located on the

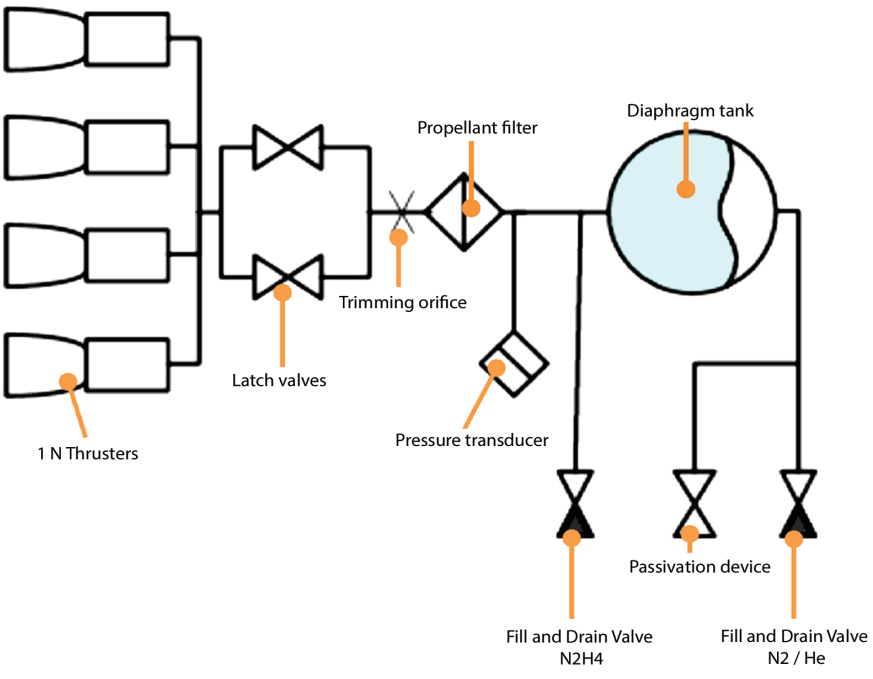

Figure 5.26. FLEX propulsion subsystem architecture for Concept B. (Thales Alenia Space)

base-plate interface with the launcher, as shown in Fig.5.25. Isolation of one failed thruster ensures that the remaining mission could still be satisfactorily performed using the second pair of thrusters.

In Concept A, the propellant tank is based on heritage design from Sentinel-5 Precursor, SPOT-6/7 and SEOSAT. With a loading capacity of 81 kg, it offers considerable margins with respect to the 54 kg allocated in the propellant budget. The tank in Concept B, which is based on a recurrent design from a NATO satellite, has a maximum propellant loading capacity of 70 kg, versus 57 kg of fuel allocated in the Concept B propellant budget.

In order to comply with the ESA requirements on debris mitigation, which impose the complete depletion of all the energy sources stored on board after the operational phase, the propellant tank will be completely emptied when the deorbiting manoeuvres have been completed. In Concept A, this passivation is achieved by performing nominal orbit control manoeuvres until the tank is completely empty. The Concept B solution, illustrated in Fig. 5.26, foresees a small modification of the propulsion subsystem, consisting of the addition of an EOL passivation pyrovalve, which when opened allows complete depletion of all the propellant residuals.

5.3.4 Budgets

5.3.4.1 Mass budget

Table 5.4 reports the mass budgets for the various cases studied, including the following margins:

— harness: 30%
— completely new developments: 20%
— new developments derived from existing hardware: 15%
— existing units requiring minor/medium modification: 10%
— existing units: 5%

An additional 15% margin at system level has been applied to protect against unpredictable mass evolutions and/or balancing needs. Differences in payload mass are a result of the different concepts.

The launch margin gives good confidence on the robustness of the concepts with respect to the mass. If FLEX is launched on Vega-C (Consolidated Vega decided by the ESA Council at Ministerial level in 2014), whose maiden flight is planned for 2018, the launch margin is much larger, increasing the programmatic attractiveness of a dual-launch configuration.

5.3.4.2 Power budgets

The power budgets for the different operating modes are detailed in Table 5.5.

5.3.4.3 Delta-V budget

The delta-V budgets are shown in Table 5.6. The main difference in the final delta-V budget comes from the different allocations for the EOL deorbit manoeuvre. While Concept B foresees a reentry within 25 years of mission completion, Concept A, owing to available margins in terms of propellant, foresees a ~23 $m\,s^{-1}$ higher delta-V allocation to the deorbiting manoeuvre, leading to a reentry within 15 years of mission completion.

Table 5.4. Mass budgets for Concepts A and B.

	Concept A (kg)	Concept B (kg)
Platform total	546.2	537.9
Payload total	116.0	133.4
Dry mass total	662.2	671.3
System margin	99.3	100.7
Dry mass (incl. margins)	761.5	772.0
Propellant	83.9	55.8
Wet mass	845.4	827.8
Launcher performance	1260.0	1260.0
Launcher adapter	76.5	76.5
Launch margin	338.1	355.7

Table 5.5. Power budgets for Concept A and B.

Operating Mode	Concept A [W]	Concept B [W]
Safe mode	383.3	420.0
Orbit control	458.5	417.7
Observation and downlinking	549.2	747.0
Nominal (orbit average)	442.9	525.7

Table 5.6 Delta-V budgets for Concepts A and B.

	Concept A [m s^{-1}]	Concept B [m s^{-1}]
Launcher injection corrections	30.5	29.9
Orbit control manoeuvres	32.0	31. 7
Collision avoidance	3.1	3.1
Deorbit manoeuvre	84.4	61.2
Total	150.0	125.9

Table 5.7. Propellant budgets for Concepts A and B.

Concept A	Concept A [kg]	Concept B [kg]
Launcher injection corrections	14.2	13.1
Orbit control manoeuvres	14.6	14.5
Collision avoidance	1.4	1.4
Deorbit manoeuvre	32.5	25.2
Residuals	1.4	1.6
Total	64.1	55.8
Tank capacity	81	70
Tank margin	16.9	14.2

Table 5.8. Mass memory sizing for Concepts A and B.

	Concept A	Concept B
Instrument data rate [Mb s^{-1}]	104	116
Downlink rate [Mb s^{-1}]	310	260
Average instrument duty cycle [%]	18.9	13
Mass memory requirement [Gb]	658	444
Mass memory size EOL [Gb]	1000	512

5.3.4.4 Propellant budget

The propellant budgets are shown in Table 5.7. Both concepts present comfortable margins with respect to the relevant tank capacity.

5.3.4.5 Date rate and volume

The data rate and volume budget is presented in Table 5.8. Concept A foresees a longer average instrument duty cycle and higher mass memory requirements than Concept B. The longer duty cycle is a consequence of an operational strategy foreseeing acquisition of data over water bodies when the duration of such acquisitions do not exceed a given value, currently set at 60 seconds. This reduces the amount of mass memory recording events and simplifies the mission timeline. The difference in terms of mass memory sizing is also a consequence of the ground station selection. Concept B uses Troll as baseline X-band ground station, which has longer visibility than Kiruna. Therefore mass memory needs for Concept B are lower than for Concept A.

5.3.5 Accommodation on a Myriade Evolution Platform

In the course of the FLEX Phase-A/B1 studies, CNES, in partnership with Airbus Defence and Space and Thales Alenia Space, initiated the Myriade Evolution programme, aimed at developing a highly recurrent platform product for scientific, defence and commercial applications to be available in 2015–25.

Such a platform, targeting Sun-synchronous orbits in the 500–800 km altitude range, can carry payloads of up to 150 kg and offer performances in line with FLEX requirements. The programmatic advantage of the Myriade Evolution is a shared launch capability, so the possibility to accommodate the FLORIS payload on this smaller platform was investigated for both concepts.

Given the common involvement of both Airbus Defence and Space and Thales Alenia Space in the programme, Concepts A and B present a high level of similarity. They mainly differ in the payload accommodation configuration and in the choice of some platform equipment. The platform is composed of a service module carrying all the avionic equipment and a payload module for the accommodation of the instrument.

The service module structure is a rectangular box made of aluminium alloy sandwich panels with two deployable solar array wings. A 937 mm ring located on the X-panel provides a standard interface with the Vega launcher. Both

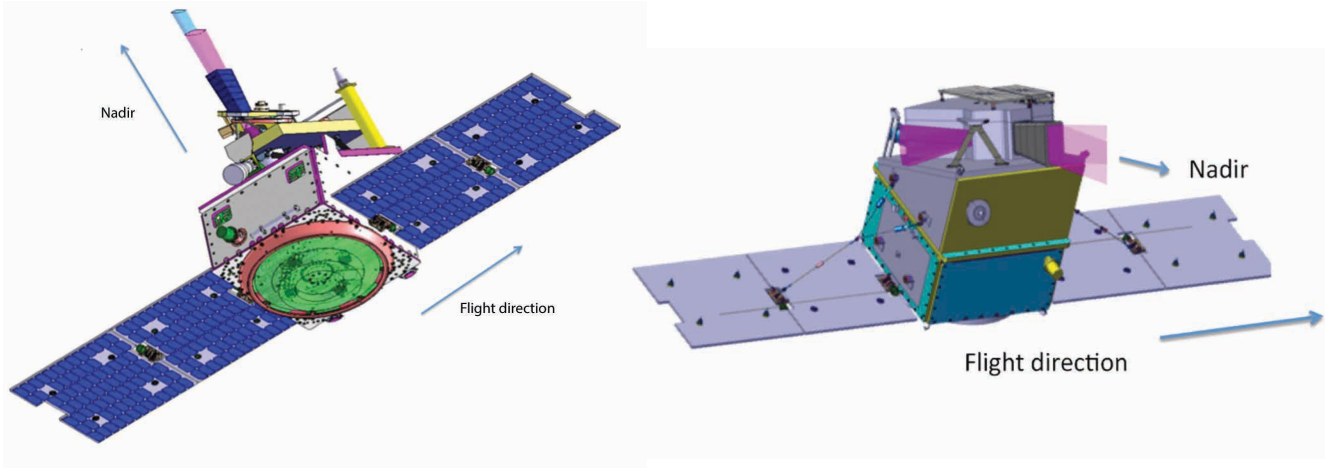

Figure 5.27. Satellite configuration for Concept A (left) and Concept B (right) on a Myriade Evolution platform. (Airbus Defence and Space (left), Thales Alenia Space (right)

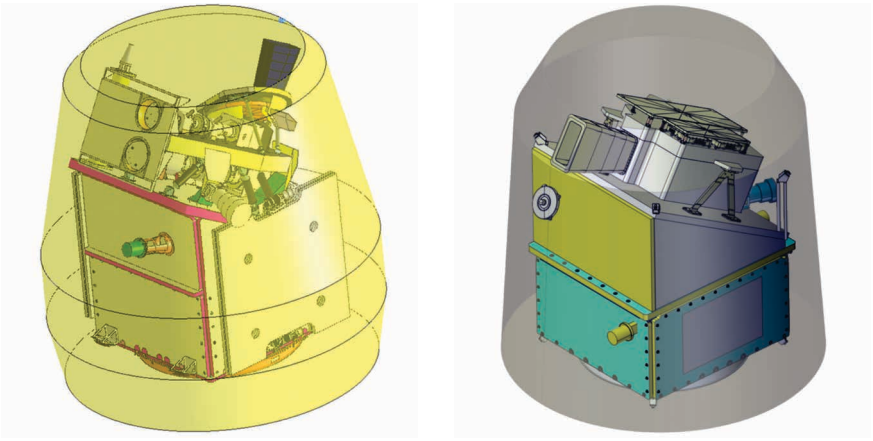

Figure 5.28. Myriade Evolution configuration, Concept A (right) and Concept B (left), in Vega's VESPA adapter. (left: Airbus Defence and Space, right: Thales Alenia Space)

concepts foresee the presence of a tilted payload support structure to optimise the illumination of the solar array while ensuring that the instrument is pointing to nadir. However, while in Concept A the angle between the platform X-axis and the direction of nadir is 30°, in Concept B the angle is 60°.

The two concepts share most of the platform avionics equipment and, although some proprietary solutions are employed (e.g. solar array, startracker units, propulsion module), the performance provided by both concepts fulfils FLEX needs with only minor customisation of the platform, namely the addition of a third battery module and the modification of the mass memory to enlarge the data storage from 512 Gb to 1024 Gb.

A major difference between the Myriade Evolution platform and the baseline concepts proposed during the FLEX Phase-A/B1 studies concerns the propulsion module. Because of the limited volume available inside the service module, the tank has a propellant capacity corresponding to 29 kg of hydrazine. This may be slightly insufficient to perform the final manoeuvre for reentry, which is the most demanding in terms of delta-V, if performed at the end of the five-year lifetime goal. However, this limitation can be overcome, either by reducing the mission lifetime to e.g. four years (still compliant with margins with the nominal lifetime of 3.5 years), or by employing a green propellant, which – as for other propulsion elements – is being qualified within the Myriade Evolutions and ESA programmes. Thanks to the higher specific impulse (~6%) and higher density (~24%) of such propellant with respect to hydrazine, the propellant mass increases to 45 kg, which fulfils the needs associated to the goal lifetime with comfortable margins.

The compact platform service module, which measures 980 mm along the Y-axis and 1020 along the Z-axis, makes the satellite concept suitable for accommodation within the VESPA adapter of the Vega launcher. This solution means that the launch cost could be shared with a co-passenger satellite, which is particularly attractive from a programmatic standpoint.

The accommodation exercise shows that both concepts present a minor interference with the fairing owing to the baffle of the FLORIS instrument. However, out-of-field straylight analyses conducted at payload level indicate that the baffle length could be reduced, therefore giving confidence on the overall accommodation inside the VESPA adapter.

The mass, power, delta-V and propellant budgets are presented in Tables 5.9, 5.10, 5.11 and 5.12, respectively.

	Concept A [kg]	Concept B [kg]
Platform total	267.8	277.6
Payload total	128.9	126.3
Dry mass total	396.6	403.9
System margin	59.4	60.6
Dry mass (incl. margins)	456.1	464.5
Propellant	29.0	28.0
Wet mass	484.1	492.5
Launcher performance (VESPA configuration)	600	600
Launcher adapter	76.5	76.5
Launch margin	37.4	31.0

Table 5.9. Mass budgets for Concepts A and B using a Myriade Evolution platform.

Operating Mode	Concept A [W]	Concept B [W]
Safe mode	193.4	233.0
Orbit control	370.8	429.0
Downlinking	416.2	438.0
Nominal (orbit average)	324.2	355.0

Table 5.10. Power budgets for Concept A and B using a Myriade Evolution platform (average values).

	Concept A [m s^{-1}]	Concept B [m s^{-1}]
Launcher injection corrections	24.5	20.3
Orbit control manoeuvres	24.6	23.7
Collision avoidance	2.5	2.5
Deorbit manoeuvre	70.8	67
Total	122.4	120.1

Table 5.11. Delta-V budgets for Concepts A and B using a Myriade evolution platform.

	Concept A [kg]	Concept B [kg]
Launcher injection corrections	6.2	5.3
Orbit control manoeuvres	6.3	6.1
Collision avoidance	0.6	0.6
Deorbit manoeuvre	15.4	14.7
Residuals	0.5	0.8
Total	29.0	27.5
Tank capacity	29.0	29.0
Tank margin	0	1.5

Table 5.12. Propellant budgets for Concept A and B using a Myriade Evolution platform for a four-year mission.

5.4 Launcher

The compatibility of the space segment concepts with both the baseline and backup launchers has been demonstrated.

The baseline launch vehicle for FLEX is Vega, launched from Kourou in French Guiana. As shown in Table 5.13 and Fig. 5.30, the satellite fits in Vega with significant margins in terms of mass and volume. The Vega performance shows reasonable margins on the injection performance.

Table 5.13. Launch vehicle performance and margins.

	Vega Performance [kg]	Wet mass + Launcher Adapter [kg]	Margin [kg]
Concept A	1260	921.9	338.1
Concept B	1260	904.3	355.7

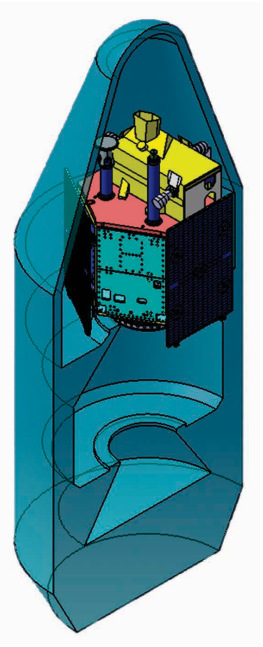

Figure 5.29. Accommodation of FLEX satellite in the PSLV fairing (Concept A). (Airbus Defence and Space)

Rockot from Eurockot Launch Services was initially selected as a backup launcher. However, in 2014 it was announced that Rockot will retire in 2016 so a preliminary assessment of possible alternative backup launchers has been carried out. This resulted in a good degree of confidence compatibility with the Polar Satellite Launch Vehicle (PSLV) from the Indian Space Research Organisation (ISRO), as shown in Fig. 5.29. Both concepts use the 937-mm launcher interface ring.

5.5 Ground Segment and Data Processing

5.5.1 Overview of Ground Segment Elements

The current generation of Earth Explorer ground segments uses generic components configured or adapted to each satellite. In line with this approach, the FLEX ground segment consists of two main components, the FOS and the PDGS as shown in Fig. 5.31. The FOS includes the TT&C ground station and the FOCC. The TT&C ground station provides the following main functions:

— HKTM acquisition
— telecommand uplink
— satellite tracking
— data connection to the FOCC

During LEOP, a dedicated ground station network supports the operations. This network uses Estrack core and enhanced stations where possible. The FOCC is based at ESOC and will provide the following main functions:

Figure 5.30. Accommodation of FLEX in the Vega fairing. Concept A left and Concept B right. (left: Airbus Defence and Space, right: Thales Alenia Space)

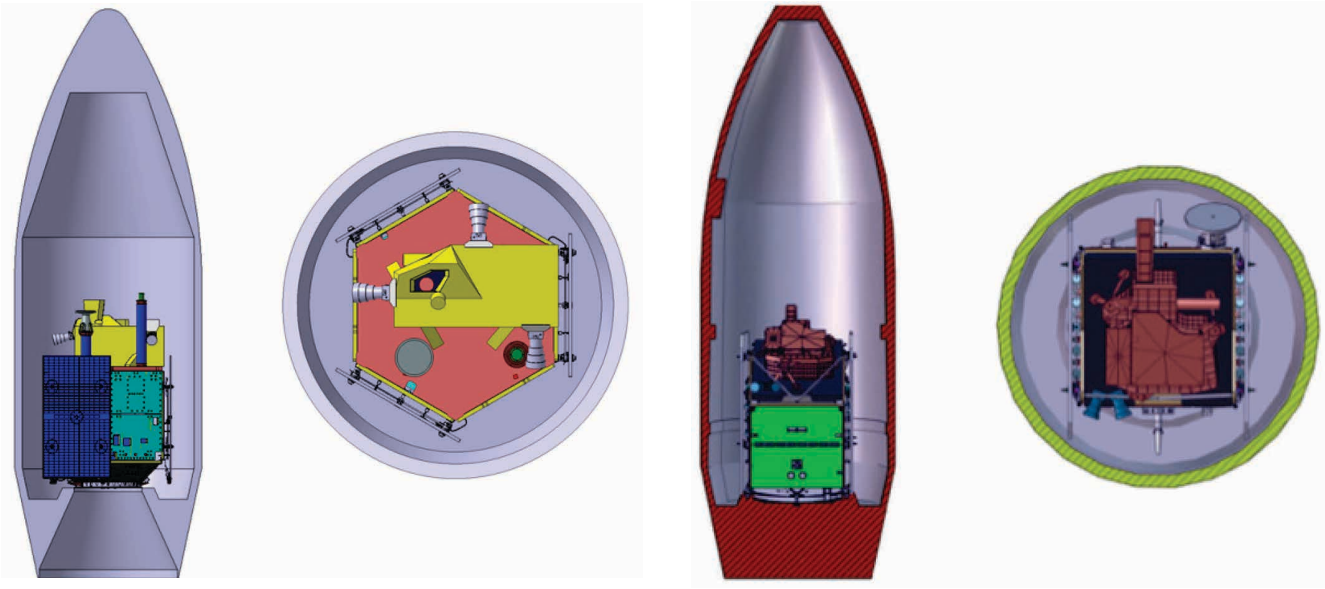

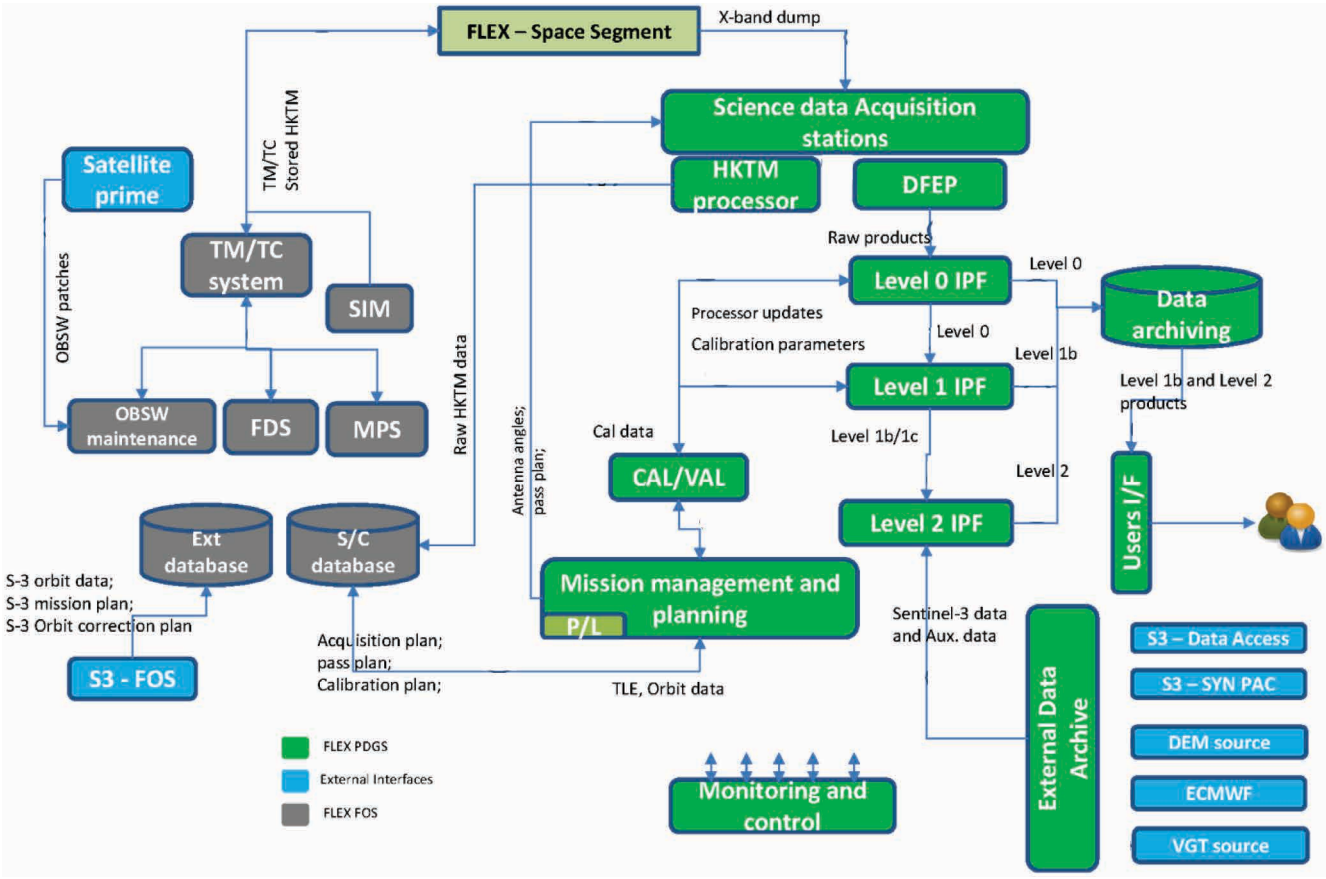

Figure 5.31. FLEX ground segment architecture. (Airbus Defence and Space)

— satellite monitoring and control
— flight dynamics and manoeuvre planning
— TT&C ground station network control
— overall satellite operations planning
— onboard software maintenance
— mission simulation
— FOS supervision
— spacecraft system data distribution, and
— interface with the launch site for LEOP

The PDGS is responsible primarily for receiving the science data from the satellite, applying the appropriate processing algorithms and delivering the data products to the users. It comprises the following functions:

— payload data acquisition and ingestion function for downlink of science data telemetry
— processing
— archiving
— dissemination
— mission planning
— quality control and calibration/validation (cal/val)
— monitoring and control
— user segment/services

The FOS and PDGS are kept as independent as possible. In particular, payload data are not processed by or transmitted through the FOS. Data exchanged between FOS and PDGS include mission planning requests and results, orbit

data, recorded HKTM from PDGS to FOS, and processed HKTM from FOS to PDGS. Existing interface formats and specifications supported by the ESA infrastructure software are used wherever applicable.

5.5.2 Flight Operations Segment

The FOS is based on existing ESA hardware and software infrastructure, adapted where necessary for FLEX.

5.5.2.1 TT&C

The baseline TT&C ground station is in Kiruna, Sweden. Both telemetry and telecommand functions are transmitted in S-band. No modification to the Kiruna station equipment is required to support FLEX. The primary data source for orbit determination in the routine operations phase is the onboard GPS receiver. There is, therefore, no need for ground station tracking data in the routine phase.

The principal task for TT&C passes during routine operations is telecommand uplink. Realtime HKTM will be acquired during these passes, even if it is not a driver for taking passes. The TT&C ground station is not dedicated to FLEX, but shared between missions. Station allocation planning – both TT&C and PDGS – is performed by the Estrack Management and Scheduling system (EMS) in cooperation with the Mission Planning System (MPS). EMS also generates the detailed operation schedules executed by Estrack ground station monitoring and control systems.

5.5.2.2 Mission control system

The Mission Control System (MCS) is based on the Earth Explorer MCS (EEMCS), which is an extension of SCOS-2000. The EEMCS is continually upgraded with functionality needed for specific missions and expected to be more widely useful. A small degree of customisation of the system (including same functional modifications) is likely to be necessary according to satellite design, ground interface specifications, the final operations concept and the existing capabilities of the EEMCS at the start of implementation for FLEX. No specific functional adaptation has been identified as necessary.

5.5.2.3 Flight dynamics

Flight dynamics is a service provided to missions that delivers orbit information and event files to the various planning entities as well as orbital predictions used by the Estrack ground stations. It also generates command sequences that are transferred to the MCS directly or via the MPS. Flight dynamics receives measurements from ground stations as well as satellite data, including GPS tracking data, from the MCS.

The FLEX flight dynamics infrastructure foresees a data communication link with the Sentinel-3 FOS. In fact, in order to maintain the formation and to meet the temporal coregistration requirements, FLEX will have access not only to the Sentinel-3 manoeuvres plan, but also to Sentinel-3 orbital parameters as well as relevant parameters for the simulation of the trajectory.

5.5.2.4 MPS

The FOS MPS is based on the EEMCS mission planning kernel. It generates schedules for execution by the MCS as well as command sequences for uplink to the spacecraft. The MPS will require configuration of mission-specific rules and constraints. As with the MCS, minor functional modifications may be needed, but no specific functional adaptation has been identified as necessary at this stage. The Estrack Management and Scheduling is responsible for planning ground station allocation to missions supported by Estrack and generation of detailed ground station schedules.

5.5.2.5 FOS operational approach and implementation

The mission operations are automated, as far as possible, to minimise risk and to contain the size of the operations team. Operations support is restricted to normal working hours, i.e. five days per week. Out of hours, on-call engineers are alerted automatically should a serious anomaly be detected. A serious anomaly is one that threatens system availability, such as significant data loss or a danger to the health of the satellite. The latter is in principle excluded thanks to the spacecraft autonomy. Other anomalies are only investigated in working hours.

A single S-band TT&C ground station (Kiruna) with one contact per day is assumed for the downlink of the HKTM. In view of the low frequency of TT&C passes, regular spacecraft health monitoring is assured via recorded HKTM, downlinked in X-band and forwarded to the FOS from the PDGS. Frequency and latency are not critical, but nominally the recorded telemetry would be acquired at each pass as part of the X-band data dump and forwarded as a single file after reception. No near-realtime planning is required.

The only external inputs to the FLEX FOS mission planning, apart from the PDGS, are the Sentinel-3 manoeuvre notifications from the Sentinel-3 FOS at Eumetsat. These are required to properly plan the timing and sizing of FLEX orbit control manoeuvres to maintain the formation between the two satellites. Since there is 100 km between FLEX and Sentinel-3 and owing to the small difference in ballistic coefficients of the satellites, the formation is considered very safe.

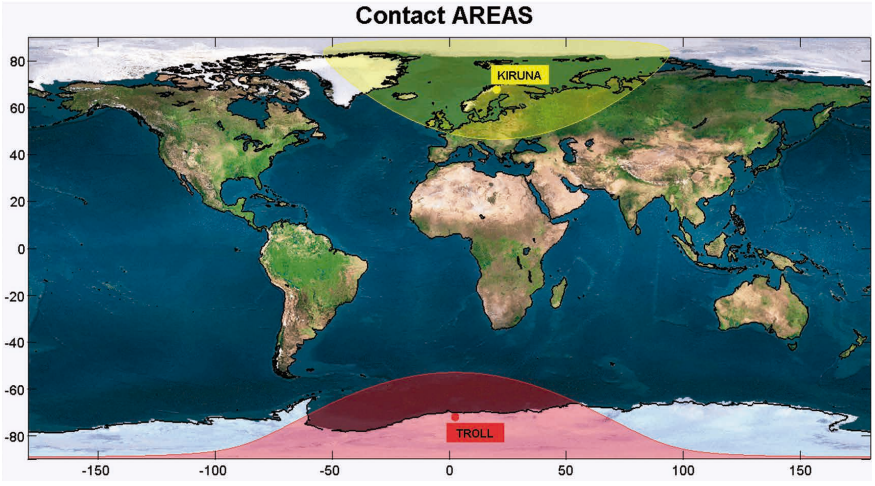

Figure 5.32. Location of X-band ground stations. (Airbus Defence and Space)

5.5.3 Payload Data Ground Segment

The current generation of Earth Explorer ground segments has been designed using generic components that are configured or adapted to each satellite, an approach used for the six current Earth Explorers. Thus, a standardised PDGS is planned, providing the following major functions:

— payload data acquisition and ingestion for downlink of science data telemetry
— processing
— archiving
— dissemination
— mission planning
— user services

Other infrastructure is also needed at the interfaces, such as computers and communication infrastructure, external calibration and validation services, and auxiliary data providers. The data delivery to the end users from the time of sensing is required to occur within 24 hours (five-hour goal). Although this data latency requirement has an impact on the maximum processing times of each Level-1b product, it can be fulfilled without any special provision.

5.5.3.1 Ground stations

The downlink of the science data and the recorded satellite telemetry will be performed in X-band. The choice of the acquisition stations is mainly driven by the overall contact time of downlink passes, the need to avoid filling the onboard memory and the need to avoid interference with Sentinel-3 during downlink of science data. A single ground station located at latitude beyond 61°N (or 61°S) and at a distance of >1000 km from Svalbard (as is Kiruna) is sufficient to support the mission, assuming a distance of at least 100 km between FLEX and Sentinel-3.

5.5.3.2 Processing

The PDGS will process the raw science data up to Level-1b and distribute them to the user segment using a data-driven architecture. Processing starts as soon as the science data are available and generates data products to be archived and distributed simultaneously to FLEX users. Level-1 auxiliary data (e.g. DEM, instrument calibration data) is static and the requirements on processing algorithms are not demanding.

5.5.3.3 Archiving

The Level-0, Level-1a and Level-1b products will be systematically generated and archived by the PDGS archiving function. Over the duration of the mission, the total amount of data resulting from the Level-0 and Level-1b products generated has been estimated and is quite modest, as stated in Table 5.14. The archiving function also interfaces with the user services to provide access to products and auxiliary data to users.

Table 5.14. Volumes of Level-0 and Level-1b data for archiving.

Product type	Volume (TB for 5 years)
Level-0	303–312.6
Level-1b	303–414

Besides the reprocessing of limited reference datasets usually handled by the main processing facility, systematic bulk reprocessing following e.g. upgrades of the data generation processors on ground is supported by a separate infrastructure. In view of the computing resources required over a limited time by bulk reprocessing campaigns, the current trend is to procure reprocessing as a service relying on shared resources.

5.5.3.4 Dissemination

The PDGS will routinely deliver the Level-1b data products to the FLEX users. As for all ESA Earth observation Level-1b data, access will be free and open. Systematic Level-0, Level-1a and calibration products will also be available for particular users (e.g. calibration and validation teams, instrument specialists etc.). All the data will be made available on an FTP server that can be directly accessed by users.

5.5.3.5 User services

The multimission infrastructure for the distribution of data products to end users will handle FLEX data products and end users. The user services will support data product browsing, access and visualisation, as well as provide general information on the mission status and help desk.

5.5.3.6 Calibration/validation

The main functions of the cal/val facility are:

— processing of inflight calibration measurements and update of onboard instrument settings or calibration parameters used by the ground processors, as required

— identification and characterisation of deviation based on the processing of inflight calibrations or vicarious measurements that may trigger payload planning requests (e.g. additional inflight calibrations) or possibly processor evolutions

— validation of coregistration between FLEX and Sentinel-3 data

— support to cal/val users (provision of special calibration products)

— configuration control of the instrument calibration databases

5.5.3.7 Instrument performance and monitoring

Monitoring of the payload performance allows identification of changes, failures or trends at payload level requiring corrective actions on board and on-ground instrument characterisation update. The quality control function is responsible for the continuous assessment of the quality of the FLEX products as well as ensuring that the products meet a minimum level of quality prior to distribution. The function is generally split into several sub-functions:

— a service in charge of systematic control of all generated products prior to their distribution to users

— offline tools allowing specific analyses on products, triggered by feedback from users

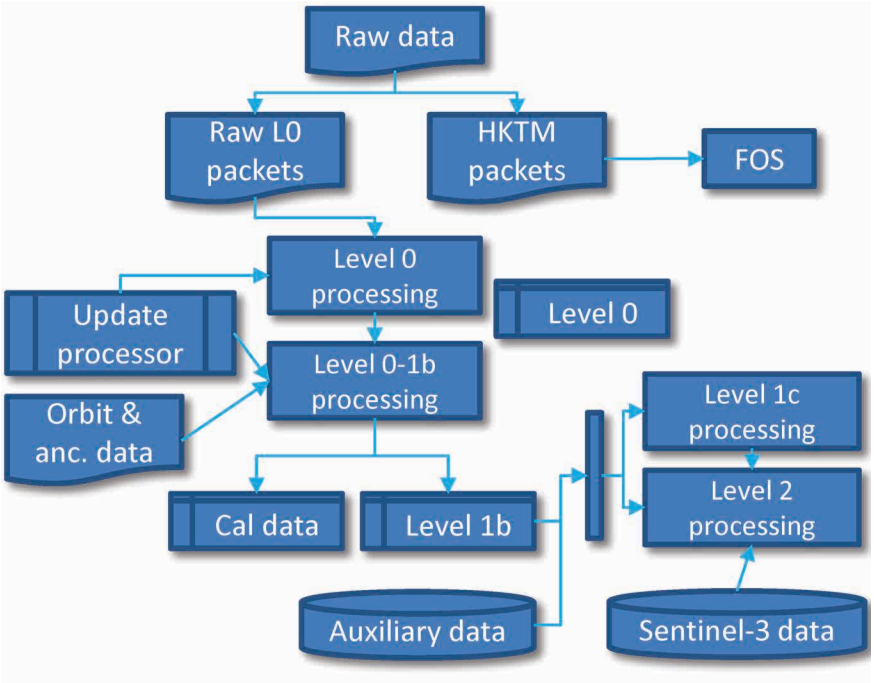

Figure 5.33. Main on-ground processing steps. (Airbus Defence and Space)

5.5.3.8 Monitoring and control

The main objective of the monitoring and control function is to ensure that the PDGS fulfils its objectives, in particular, in terms of performance and availability so that the mission requirements are met.

5.5.4 Level-0 to Level-1b Data Processing

A mission-specific ground processor is required to provide the FLEX end users with Level-1b data for higher level processing up to Level-2 and above. Figure 5.33 shows the main steps of the on-ground chain, which break down as follows.

From raw downlink data to Level-0:

— decoding
— removal of communication headers
— reordering of packets into chronological order
— repackaging of data (e.g. into files)
— appending any supplementary data (orbit data, time data, etc.)
— reporting on data quality (e.g. missing data)

From Level-0 to Level-1b:

— identification and tagging of saturated samples and neighbouring pixels

— dark signal removal, calculated via a simple extrapolation of the calibration results from the previous orbit, for each detector (e.g. given dark signal value, read expected temperature from a calibration look up table (LUT), calculate offset from observed value, calculate new dark signal from observed temperature, subtract this from observed signal)

— application of a calibrated gain for each sample (derived from on-ground calibration plus in-orbit calibrations)

— adjustment for non-linearity of gain (derived from on-ground calibration)

— straylight correction

— smearing signal correction

— geolocation (intersection with the WGS84 ellipsoid is calculated and a DEM is used to calculate location and altitude of acquired samples more precisely)

— sample classification

Starting from Level-1c, the FLEX data products require various Sentinel-3 products, either for coregistration, as in the case of the Level-1c FLEX products, or for the purpose of deriving higher-level physical parameters, as in the case of Level-2 FLEX products. A preliminary analysis has been conducted to estimate the expected data volume for FLEX over one day, resulting in the following file sizes: Level-0 ~180 GB and Level-1b ~180/230 GB, depending on the concept. The final selection of the PDGS facilities and hosting centres is performed through open competition at the beginning of Phase-C/D. As a consequence, a list of PDGS centres and their locations cannot be provided at this stage.

5.6 Operations, Utilisation and Disposal Concept

5.6.1 Overview

During the 3.5–5 years of nominal operations, the FLEX observations occur systematically over all land areas between 56°S and 75°N. Because of the solar illumination constraints, the acquisitions only occur during the descending part of the orbit. The FLEX operations concept is standard for a mission flying in a Sun-synchronous orbit, the need to maintain the formation with Sentinel-3 is the only operational constraint for the mission.

To fulfil the FLEX scientific objectives, the following mission phases are planned:

— LEOP and commissioning
— nominal operations
— contingency operations
— disposal

5.6.2 LEOP and Commissioning

Nominally, FLEX will be launched from Kourou, with Kiruna as the principal LEOP ground station, supported by the Estrack ground stations, e.g. Troll and Svalbard, as needed. LEOP constraints are standard and the operational approach proposed is in line with previous Earth Explorer missions.

The early orbit operations of the ground and space segment include:

— satellite separation from the launch vehicle
— angular rate damping
— deployment of solar arrays
— orientation into Sun-pointing mode to ensure battery charging capability
— acquisition of satellite by LEOP ground station network
— download of telemetry generated and stored on board prior to orbit acquisition
— platform subsystem checkout and health check
— formation acquisition

The first part of the LEOP sequence is carried out autonomously by the satellite, only requiring ground intervention if deployment fails. Upon completion of the sequence, S-band communication is initiated and an initial satellite checkout is completed to confirm success of the sequence and start the formation acquisition sequence.

In order to avoid any risk of collision, FLEX is launched into the same orbital plane as Sentinel-3, but at a slightly lower altitude. After completion of the launch dispersion correction manoeuvres, the formation acquisition sequence starts. An in-plane manoeuvre is performed to place FLEX in a parking orbit where the difference in altitude with respect to Sentinel-3 causes a drift between the relative positions of the two satellites. As soon as separation is reached, a final manoeuvre is executed to bring FLEX into its nominal orbit.

Commissioning operations prepare the nominal phase. The first part of the commissioning phase will be used to perform in-orbit functional and performance tests of all platform subsystems, including the payload data-handling subsystem. The payload is then commissioned and initial calibrations are performed. The whole end-to-end data chain is then verified (including ground processors) before nominal operations are cleared to start.

5.6.3 Nominal Operations

Nominal phase operations are considered routine and focused towards the regular production of Level-1b data products as the main output of the system (Fig. 5.34). The main tasks performed during routine operations are the mission planning of observation and data transfer to the ground, the maintenance of the orbit through regular orbit control manoeuvres, and the calibration operations.

Because of the repeat orbit and the nature of the observables, the mission operations are deterministic and repeatable every 27 days. A predefined multi-repeat-cycle plan is used over its applicability period with updates expected every two weeks. Calibrations are performed periodically and must be taken into account in the mission planning.

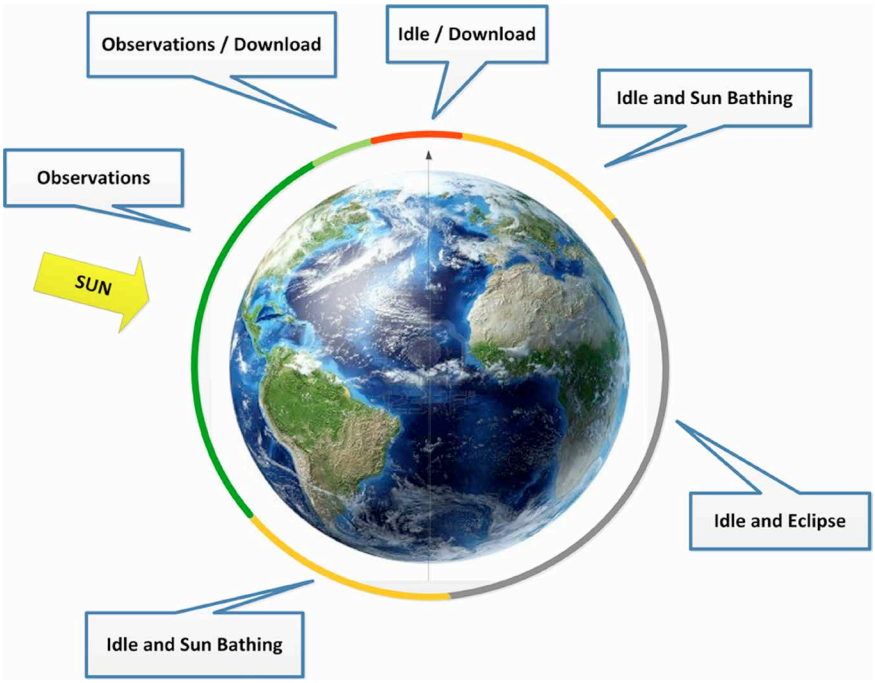

Figure 5.34. Example of FLEX nominal operations sequence. (Airbus Defence and Space)

Regular orbit control manoeuvres are performed to maintain the formation with Sentinel-3 and so fulfil the temporal coregistration requirement. The FOS predicts the relative trajectory between the two satellites, triggering an orbit control manoeuvre whenever the temporal coregistration requirement is violated. However, owing to the similarity of the ballistic coefficient of FLEX and Sentinel-3 (see subsection 5.2.2) this takes a very long time to happen and therefore FLEX orbit control manoeuvres follow strictly those of Sentinel-3.

Finally, the other regular routine operation is the calibration of the payload. As shown in the payload and performance sections (Subsection 5.3.2. and Chapter 7) the payload calibration activities are performed either at the South Pole (radiometric calibration) or over the eclipse part of the orbit (dark signal calibration) and so do not have a direct impact on the science observations.

5.6.4 Contingency Operations

The FLEX satellite is designed to survive for up to 72 hours if a single failure occurs. A hierarchical FDIR concept is employed, which will only fall back to safe mode for serious failures. The mission will not continue operations in case of a major failure. The FDIR design follows the common concept tailored in five failure levels, based on the degree of intervention:

— Level-0 failures are those associated with an internal single failure in one equipment unit, which can be automatically recovered by the unit itself without any impact on the rest of the whole system hardware devices or software applications. This level of functionality is fully autonomous and may be transparent to the FDIR system

— Level-1 failures happen when the unit itself cannot autonomously recover. The surveillance is performed by the Onboard Software (OBSW) through simple health checks on acquired parameters, and recovery actions are ordered. The failures might also require ground intervention

— Level-2 failures are identical to those in Level-1 as they are recovered completely by the OBSW. However, they are not confined to a single subsystem and may require recovery actions reaching across several subsystems. The detection of those failures is based on the monitoring of subsystem health and status information and cross-correlated checks of acquired parameters

— Level-3 failures are OBC internal and cannot be recovered autonomously by the OBSW, and as such are distinctly more severe than Level-0 failures. The recovery is done by hardware via the On Board Data Handling (OBDH) reconfiguration module

— Level-4 failures are those that have not been detected and recovered at lower levels and managed completely by hardware through proper independent system alarms hard-wired to the relevant reconfiguration module. These failures are considered as global satellite malfunctions

A fundamental aspect of an FDIR approach is that survival of the satellite and formation safety has absolute priority during all phases of the mission life. To ensure satellite safety, the transponder is completely managed in hot redundancy. All FDIR functions implemented in the OBSW are triggered by parameter values stored in the satellite. These functions can be enabled or disabled via telecommand from the ground and may be adapted and set according to the operational needs. Any FDIR data are stored in a log for investigation on the ground. The ground station has the final overall

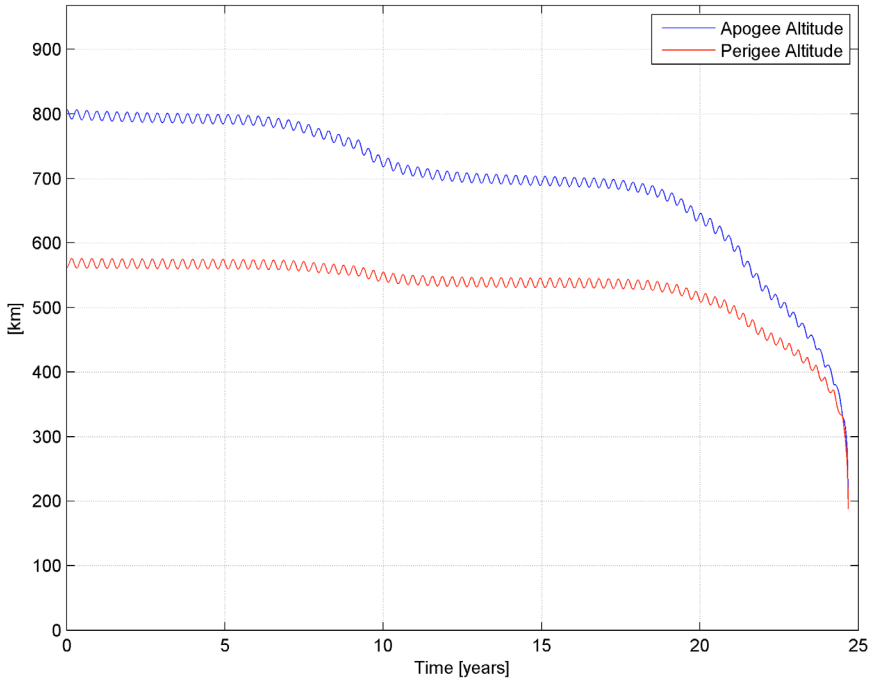

Figure 5.35. Perigee and apogee altitude evolution during EOL disposal. (Thales Alenia Space)

control over all failure recovery activities, even when they are performed autonomously by the satellite.

5.6.5 Disposal

FLEX meets the European Code of Conduct for Space Debris Mitigation. At the end of the mission life, the orbit altitude perigee is reduced so that the satellite re-enters the atmosphere in less than 25 years. This is performed through a series of orbit control manoeuvres using the total amount of remaining propellant. After the last manoeuvre, electric and fluid passivation is performed and all satellite units are switched off, except the OBC. The satellite then remains uncontrolled and enters the off mode when the battery is fully discharged. Figure 5.35 shows the evolution of the apogee and perigee altitude for FLEX once the disposal manoeuvre has been performed.

Compliance with the requirement on casualty risks, which must not exceed 1 in 10 000, has been assessed through dedicated reentry casualty risk analyses, which at this stage are still coarse. These analyses have shown that for the baseline Astrobus-250 and Proteus MKII platforms, the resulting risk is within or very close to the requirement. The analyses performed considering the use of a Myriade Evolution platform show that both concepts meet the requirement with comfortable margins.

→ SCIENTIFIC DATA PROCESSING AND VALIDATION CONCEPT

6. Scientific Data Processing and Validation Concept

This chapter outlines the main principles of the data processing, the vegetation fluorescence retrieval and the validation concept to be used for the FLEX mission. Retrieving the weak chlorophyll fluorescence spectrum from top-of-atmosphere (TOA) spectral radiance is a challenging task and adequate processing steps are required to derive the desired information from the data.

The first step involves the atmospheric correction process, which will produce 'apparent reflectance' at the top-of-canopy (TOC) level. The second step decouples the TOC apparent reflectance into true reflectance and TOC fluorescence emission. This is the core of the fluorescence retrieval algorithm. The FLEX mission will not only provide the full fluorescence spectrum, but also other Level-2 and higher-level products strongly related to vegetation status and photosynthetic activity.

6.1 Fluorescence Retrieval

The FLEX mission has been designed to fly in tandem with the Copernicus Sentinel-3 satellite. Sentinel-3 is equipped with the Ocean and Land Colour Instrument (OLCI) spectrometer, which covers 400 nm to 1020 nm, and the Sea and Land Surface Temperature Radiometer (SLSTR), which covers the 550 nm to 12 µm spectral range with two different viewing angles thanks to its conical scanning technique. On the one hand, this tandem concept is intended essentially to fully characterise atmospheric properties and also to better determine vegetation properties and photosynthetic status. On the other hand, the tandem concept implies a preprocessing task to merge information from the instruments on the different satellites. The main processing steps involving FLEX's Fluorescence Imaging Spectrometer (FLORIS), OLCI and SLSTR data are highlighted in Fig. 6.1.

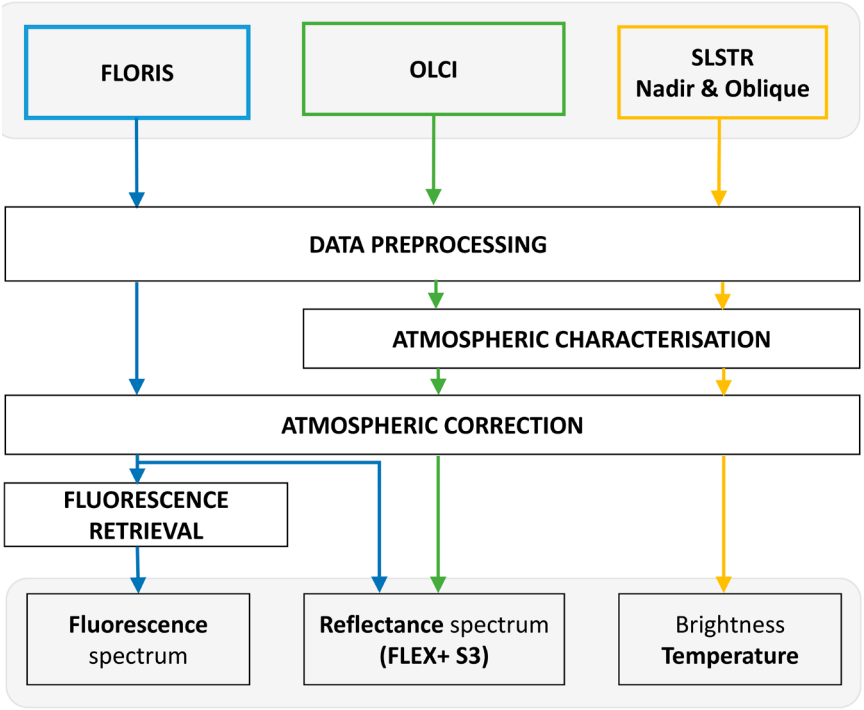

Figure 6.1. Schematic view of the processing chain for the FLEX mission to retrieve surface reflectance and fluorescence from measurements from FLORIS, OLCI and SLSTR. (University of Valencia)

6.1.1 Data Preprocessing

To mitigate error propagation in the retrieved fluorescence, a data preprocessing step prior to the scientific retrieval is essential. The starting point is Level-1c data, which consists of the geometric coregistration of Level-1b data from SLSTR, OLCI and FLORIS into a single geographical grid. This is needed because in the tandem concept the acquired images originate from different sensors and present different geometries. Accordingly, all images from OLCI, SLSTR and the low-resolution FLORIS spectrometer are coregistered to the FLORIS high-spectral-resolution spectrometer geometry in the Level-1c product.

In addition, it is necessary to perform a cross-radiometric calibration between the sensors. Sentinel-3 data radiometric levels must be consistent with FLORIS instrument radiometric levels. Thanks to the high resolution provided by FLORIS, it is possible to reproduce several OLCI and SLSTR bands and to establish radiometric consistency among the different signals.

6.1.2 Atmospheric Correction Algorithm

Radiation is perturbed by atmospheric components when it passes through the atmosphere. An accurate atmospheric correction procedure enabling reliable TOC reflectance/fluorescence retrievals is therefore mandatory. Out of all the atmospheric components, the main absorptions by gaseous compounds that affect the TOA radiance signal are molecular oxygen, ozone and water vapour.

The FLEX mission will measure the sun-induced chlorophyll fluorescence emission in the O_2-A and O_2-B absorption bands, where reflected solar irradiance is reduced while fluorescence is still high (Fig. 6.2).

The retrieval of fluorescence using water vapour absorption bands in the range of a high fluorescence signal was discarded owing to the highly variable spatial (horizontal and vertical) distribution and temporal variability of water vapour in the atmosphere at 300×300 m^2 resolution. Turbulent fluxes change the water vapour distribution even at local scales.

Spatial variability of oxygen is driven by surface pressure, well described by current Digital Elevation Models (DEMs) and meteorological data, thus accounting for the reference spatial variability in the atmospheric radiative transfer model and taking the spatial and temporal location into account.

Conversely, aerosol scattering affects the signal from 400 nm to nearly 2500 nm and therefore needs to be characterised. Characterisation of aerosols is done by means of their optical properties, which change according to the aerosol composition, shape and size.

Therefore, the atmospheric correction process to provide TOC data essentially consists of characterising the presence of aerosols and the total atmospheric columnar water vapour (CWV). Furthermore, before starting

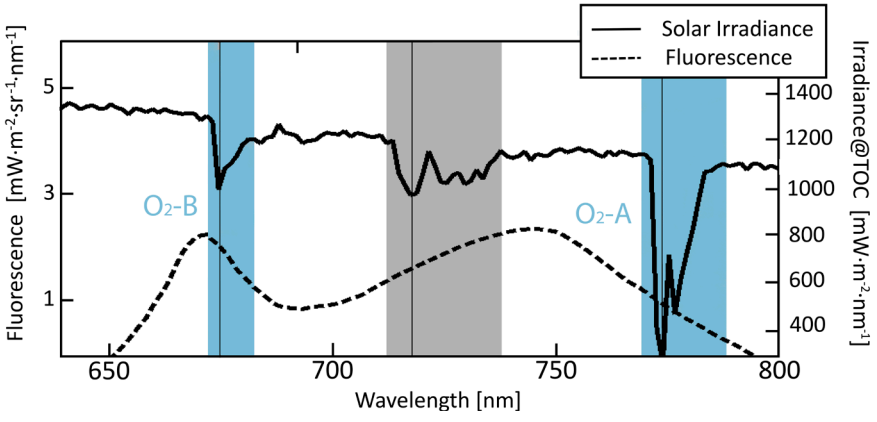

Figure 6.2. Fluorescence emission and solar irradiance at TOC (University of Valencia).

to characterise aerosols and water vapour, it is necessary to mask out clouds present in the image. The following subsections outline the details of the atmospheric characterisation method, and the decoupling of fluorescence from surface reflectance, as illustrated in Fig. 6.3.

6.1.2.1 Aerosol characterisation

The proposed aerosol retrieval algorithm is based on exploitation of the synergies between SLSTR and OLCI datasets. The algorithm makes use of the dual-view capabilities from SLSTR and the spectral coverage provided by OLCI. The synergy between these two instruments is achieved by means of an iterative process that merges the data provided by OLCI and SLSTR through a cost function (see eq. 6.1) and subsequently performs a model inversion for the retrieval of aerosol optical properties.

Aerosol type and content are characterised by a low spatial variability, which implies that no abrupt changes between pixels are to be expected. Here, the 300×300 m^2 resolution of FLORIS/OLCI data is exploited.

The determination of aerosol properties is performed on cloud-free aerosols and homogenous areas by using a MODTRAN Look-Up Table (LUT) inversion algorithm that exploits the spectral information from OLCI and SLSTR (dual-view). The aerosol retrieval algorithm determines the aerosol content and type through parameterisation of the aerosol optical properties. The properties used to describe the nature of the aerosols are:

— Aerosol Optical Thickness (AOT), the magnitude of which is related to the quantity of aerosols

— The Angstrom parameter α, which takes into account the wavelength dependency of AOT that defines aerosol type

— Anisotropy parameter of the scattering phase function g, also used to characterise aerosol type

The aerosol optical properties retrieval is subsequently based on an iterative process that minimises the following cost function:

$$\delta_{\lambda} = \sum_{pix}\left(\frac{1}{N}\sum_{\Omega}\sum_{\lambda}^{N}\varphi\left(L_{sen}^{SLSTR}-L_{sim}^{SLSTR}\right)^{2}+\frac{1}{M}\sum_{\lambda}^{M}\omega\left(L_{sen}^{OLCI}-L_{sim}^{OLCI}\right)^{2}\right) \quad (6.1)$$

where N and M are the number of bands in SLSTR (not including thermal bands) and OLCI sensors respectively, Ω refers to the dual-viewing angle of SLSTR, φ and ω are weighting functions defined as $\sim\lambda^{-2}$ according to each sensor configuration band, L_{sen} are OLCI and SLSTR nadir and oblique viewing angle TOA radiances, and L_{sim} are the corresponding simulated TOA radiances for each sensor.

In addition, the summation over pixels in eq. 6.1 exploits the discrimination of the surface and atmospheric contributions to the TOA radiance by selecting a set of pixels that represents the surface heterogeneity.

Spectral channels within gaseous absorption bands are not taken into account in eq. 6.1 to minimise the impact of uncertainties in gas content (e.g. CWV). The simulated at-sensor (i.e. TOA), radiance is subsequently obtained by approximating the expression as:

$$L_{sim} = \int_{\lambda_i}^{\lambda_f} (L_0 \bullet f) d\lambda + \int_{\lambda_i}^{\lambda_f} \frac{1}{\pi} (T \cdot E_{TOC} \cdot \rho \bullet f) d\lambda + \int_{\lambda_i}^{\lambda_f} \frac{1}{\pi} (T \cdot E_{TOC} \cdot S \cdot \rho^2 \bullet f) d\lambda \quad (6.2)$$

where L_0 is the path radiance, T is the upward total transmittance, E_{TOC} is the total irradiance at canopy level, S is the spherical albedo and ρ is surface reflectance.

On the one hand, the unknown surface reflectance is modelled using a predefined database where a wide range of spectra is stored at high resolution. On the other hand, surface bidirectional reflectance distribution function (BRDF) effects cannot be neglected when data from the dual-view angle of SLSTR is considered. The algorithm explores different spectra from nadir and oblique viewing angles independently.

6.1.2.2 Water vapour retrieval

The water vapour content is derived through a differential absorption technique using OLCI water absorption channels. In essence, differential absorption techniques calculate the ratio $R = L_{out}/L_{in}$ between the radiances L_{in} inside and L_{out} outside the water vapour absorption band. In OLCI this ratio is calculated at 940 nm. While L_{in} is TOA radiance acquired directly inside the absorption band, L_{out} is obtained by linear regression from the reference channels, i.e. channels close to the absorption band without being affected by it.

The CWV is retrieved by an LUT inversion, using numerical methods to minimise the cost function between the sensed and simulated ratios $\chi = R_{sim} - R_{sen}$. The simulated ratio uses the previously derived aerosol properties and approximates the surface reflectance in the measurement spectral channel as a linear interpolation between the reference channels. The retrieval is executed on a pixel basis owing to the high spatial variability of CWV.

6.1.2.3 Apparent reflectance retrieval

Once the atmospheric state has been characterised, it is possible to derive the FLORIS TOC apparent reflectance spectrum from the TOA spectral radiance. In eq. 6.3, fluorescence emission is coupled by means of the definition of a physical quantity, the apparent reflectance, i.e. true reflectance modified by fluorescence emission:

$$\rho_{app} = \rho + \frac{\pi F}{E_{TOC}} \quad (6.3)$$

where ρ_{app} and ρ are apparent and true reflectance respectively, F is emitted fluorescence radiance and E_{TOC} is total irradiance at TOC. Then, considering the Taylor expansion to the first degree of TOA radiance expression eq. 6.2 and the definition of apparent reflectance of eq. 6.3, the apparent reflectance term can be expressed as:

$$\rho_{app} = \frac{-T \cdot E_{TOC} + \sqrt{(T \cdot E_{TOC})^2 - 4T \cdot E_{TOC} \cdot S\pi(L_0 - L_{TOA})}}{2T \cdot E_{TOC} \cdot S} \quad (6.4)$$

where each of the products, that is $T{\cdot}E_{TOC}$,$T{\cdot}E_{TOC}{\cdot}S$ and L_0 have been previously calculated at very fine spectral resolution and subsequently convolved according to the FLORIS instrument spectral response function (ISRF).

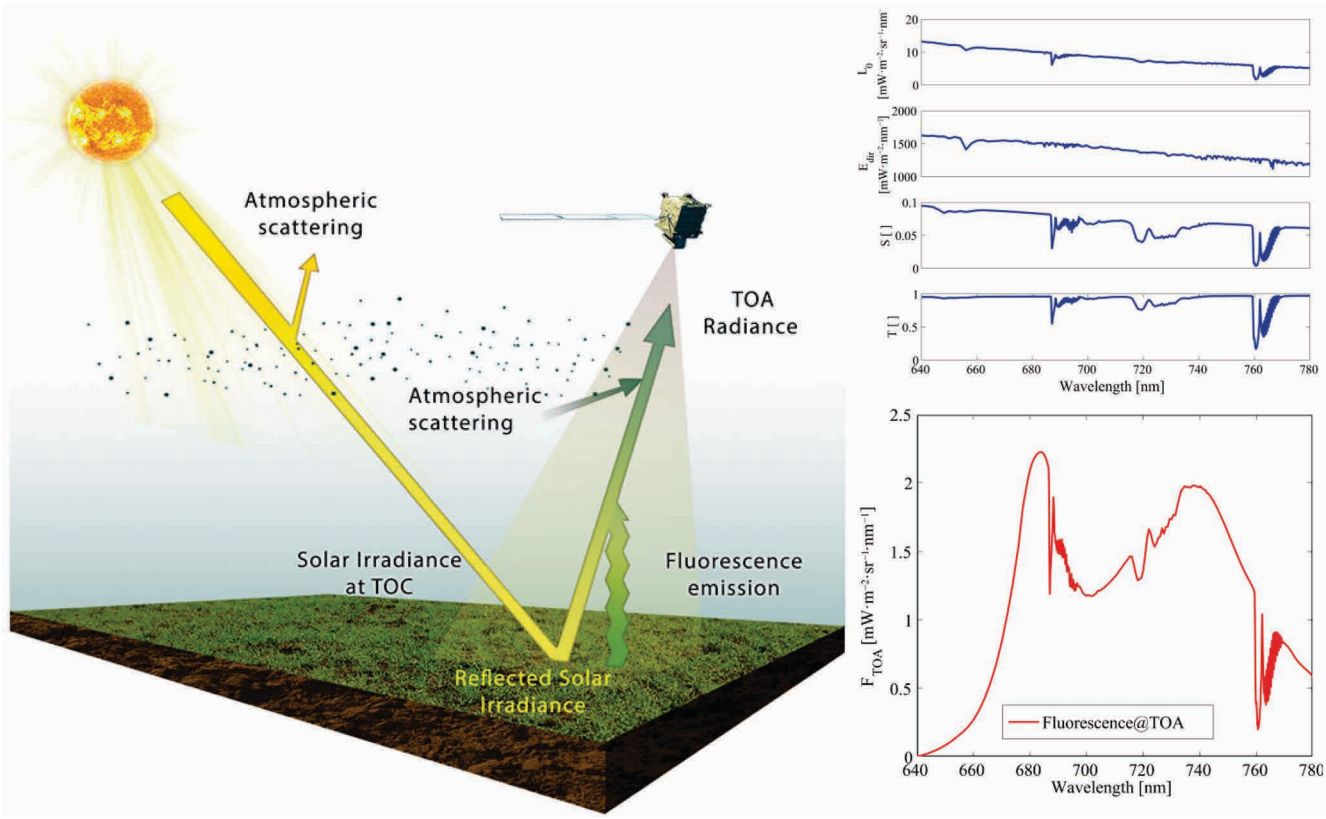

Figure 6.3. Left: Qualitative figure showing atmospheric and surface solar irradiance interactions before being acquired by the sensor. Top right: Atmospheric functions, from top down, atmospheric scattering (L_0), solar direct irradiance at TOC (E_{dir}), spherical albedo (S) and upward atmospheric transmittance (T). Bottom right: Fluorescence signal at the TOA showing atmospheric absorption features. (University of Valencia)

6.1.3 Fluorescence Retrieval

The fluorescence retrieval algorithm is based on an iterative Spectral Fitting Method (SFM) using full spectral information in the spectral range of fluorescence emission and the SpecFit algorithm. To start the iterative process, the SFM uses a preliminary estimation of the fluorescence values inside the O_2 absorption bands for a faster convergence, and delivers as output the full fluorescence spectrum.

6.1.3.1 First fluorescence estimation in O_2 absorption bands

For the first estimation of fluorescence data F, an algorithm is used that is based on the height of the peaks at the apparent reflectance with respect to baseline, which corresponds to a hypothetical elimination of absorption features in the solar irradiance. TOC radiance L_{TOC} can be described in terms of incoming total irradiance E_{TOC}, target directional true reflectance ρ and emitted F as:

$$L_{TOC} = \rho \frac{E_{TOC}}{\pi} + F \tag{6.5}$$

The apparent reflectance term obtained from the previous atmospheric correction process is then related to F as the combination of the true directional reflectance of the target and the emitted fluorescence divided by the total irradiance (eq. 6.3). Figure 6.4 shows the solar irradiance at surface level with and without O_2 and water vapour presence, and the apparent reflectance and the apparent reflectance baseline used to the first fluorescence estimation.

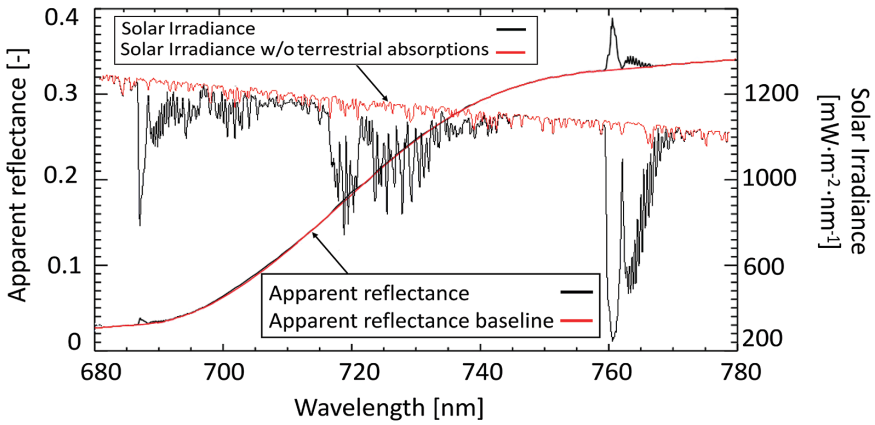

Figure 6.4. First estimation of fluorescence retrieval concept based on the estimation of the apparent reflectance and the baseline of the apparent reflectance and the solar irradiance for an atmosphere both without atmospheric absorptions (O_2 and water vapour) and with O_2/water vapour at top of canopy. (University of Valencia)

Apparent reflectance presents some peak features at wavelengths where the irradiance presents absorption features. The most prominent ones are caused by fluorescence infilling in the O_2 absorption lines. In particular, if TOC total irradiance free of O_2 absorptions (O_2 free atmosphere) is simulated, the resulting apparent reflectance ($\tilde{\rho}_0$) is smooth, without the O_2 peaks (note that the small Fraunhofer absorptions also produce peaks). Then, the difference between both cases can be expressed as:

$$\rho'_0 - \tilde{\rho}'_0 = \rho_0 + \frac{\pi F}{E_{TOC}} - \left(\rho_0 + \frac{\pi F}{\tilde{E}_{TOC}}\right) = F\pi\left(\frac{1}{E_{TOC}} - \frac{1}{\tilde{E}_{TOC}}\right) \quad (6.6)$$

Then:

$$F = (\rho'_0 - \tilde{\rho}'_0)\frac{\tilde{E}_{TOC} \cdot E_{TOC}}{(\tilde{E}_{TOC} - E_{TOC})\pi} \quad (6.7)$$

with the advantage that the real reflectance is no longer involved in the retrieval process. The estimation of this has always posed a challenge and is the largest error source in other retrieval strategies (Stancik and Brauns, 2008).

6.1.3.2 SFM applied to obtain full fluorescence spectrum

As detailed in the previous section, after the TOA radiance from FLORIS is converted to TOC radiance by the atmospheric correction process, the bottom of atmosphere radiance spectra is decomposed into contributions of fluorescence and the reflected light fluxes. On one hand, surface reflectance is modelled by means of a piecewise cubic-spline interpolation. The two red and far-red fluorescence emission peaks are modelled using different combinations of Gaussian, Lorentzian and Voigt functions. By means of an iterative process that minimises the cost function in eq. 6.8 it is possible to find the parameters of the mathematical functions representing reflectance and fluorescence. The

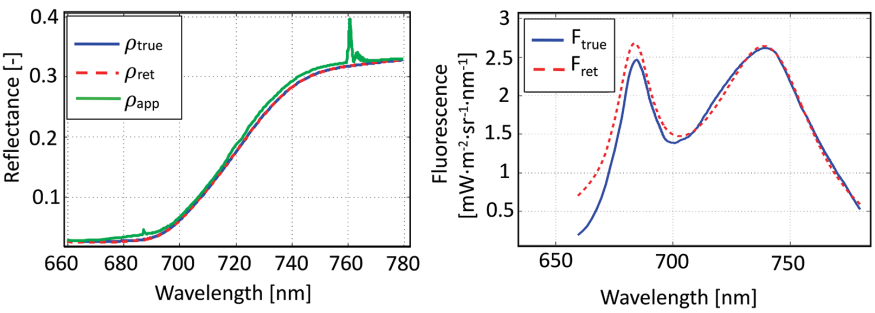

Figure 6.5: Reflectance (left) and fluorescence (right) spectra retrieved in the 670–780 nm region using the SFM based algorithm SpecFit. True (blue) and retrieved (red) values are shown. (University of Valencia)

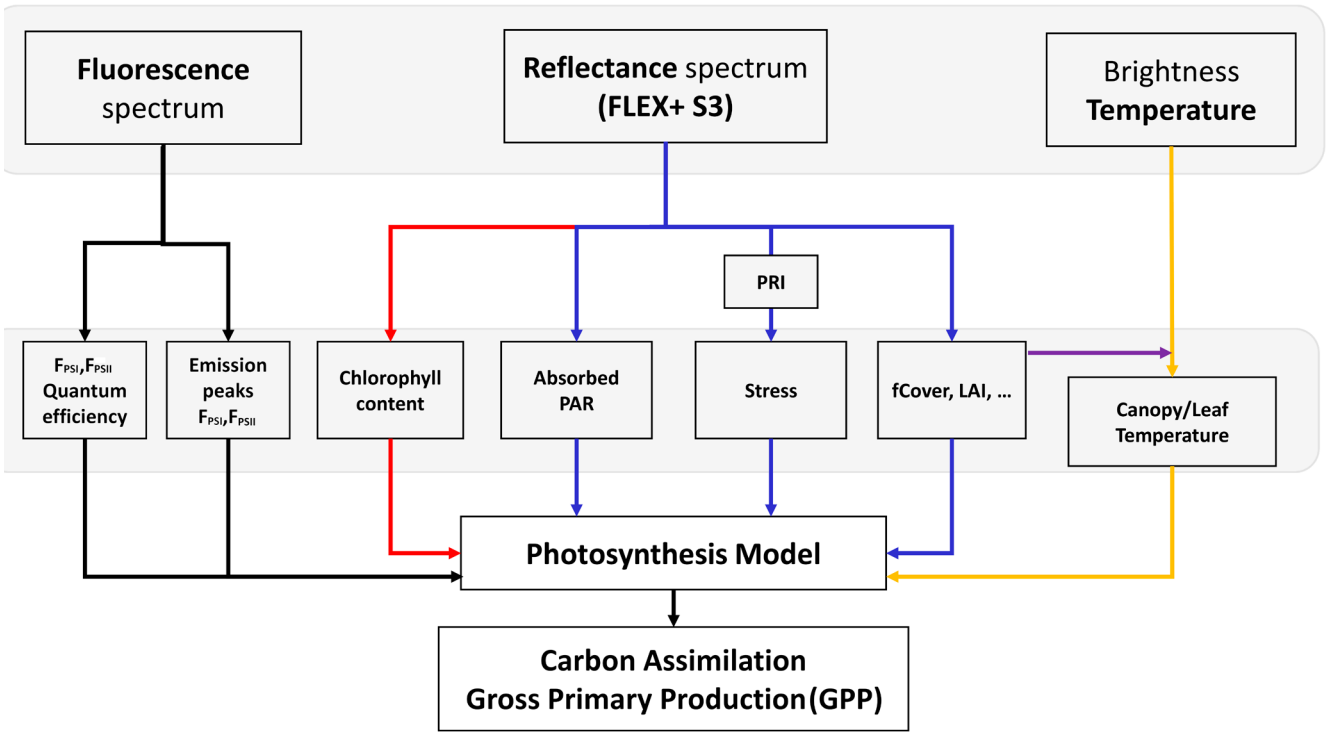

Figure 6.6. Advanced photosynthetic and carbon assimilation products that can be derived from the fluorescence spectra, the surface reflectance spectra and the brightness temperature Level-2 products. (University of Valencia)

minimisation process is performed through least squares nonlinear curve-fitting optimisation that minimises the sum of squared differences.

$$min \sum_{\lambda} \left(L_{TOC} - F - \rho \frac{E_{TOC}}{\pi} \right)^2 \tag{6.8}$$

An example showing the modelled ρ and F in such a broader spectral range and the retrieved fluorescence and reflectance spectrum in the red/far-red is shown in Fig. 6.5.

6.1.4 Products

As was shown in Figure 6.1, the FLEX mission will provide data products related to the following three primary categories: (1) fluorescence spectrum, (2) reflectance spectrum and (3) brightness temperatures observed in the thermal infrared (Fig. 6.1). For fluorescence, the key outputs from the retrieval described above are:

— fluorescence radiance emission at both red and far-red peaks, 687 nm and 740 nm, respectively

— total fluorescence radiance emission, i.e. integrated fluorescence over the whole spectral range (from 650 nm to 850 nm)

Figure 6.6 shows the FLEX advanced mission outputs derived from Level-2 products, covering vegetation photosynthesis, plant physiological status and carbon assimilation products.

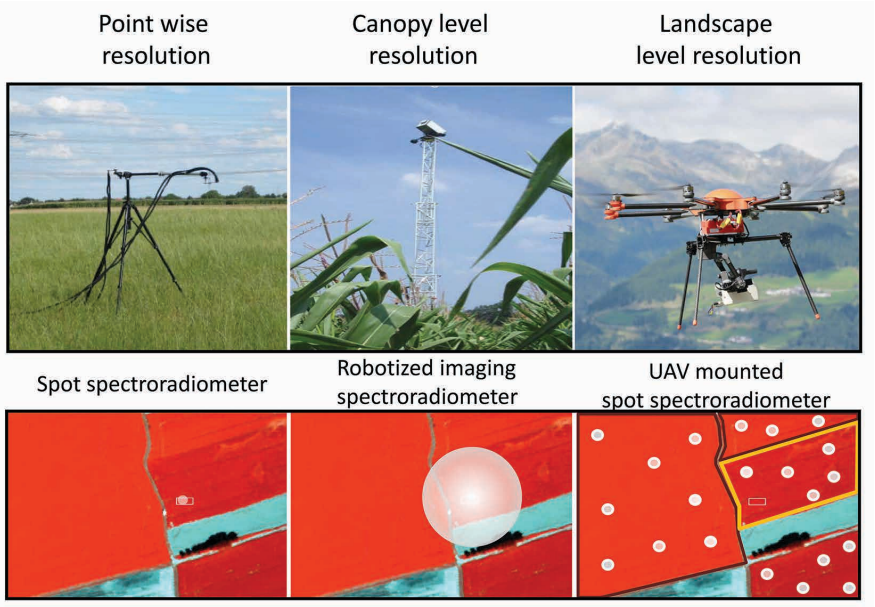

Figure 6.7. Different instruments used to perform the bottom-up validation strategy (top panel). Footprints covered by the different instruments are indicated as white circles (bottom panel). (University of Valencia)

6.2 Validation

This section presents a validation plan for the FLEX fluorescence products. Product validation is a mandatory step prior to the data release and ensures a proper characterisation of the uncertainties associated with a product. The proposed validation plan for the FLEX fluorescence products is based on the recommendations made by the Committee on Earth Observation Satellites (CEOS) (Morisette, 2006). It follows a 'bottom-up' strategy where ground-truth fluorescence TOC measurements are up-scaled to FLEX spatial resolution using aerial or satellite imagery from FLEX.

6.2.1 Bottom-up Scheme

To achieve such a bottom-up validation scheme, various activities will be planned in detail during the pre-launch phase to address issues such as site selection for validation, instrument deployment for continuous monitoring, database setup and management and organisation of dedicated validation campaigns.

When applying the bottom-up approach to the fluorescence validation scheme, three consecutive steps take place. It starts from point-wise TOC measurements, then moves up to canopy level at local coverage, and then extends to coarser spatial resolution at the regional level by means of an intermediate high-resolution data source (Fig. 6.7).

6.2.1.1 Point and canopy level

Tower-based TOC fluorescence measurements are fundamental to the validation of FLEX products. There are already hyperspectral radiometers with an even finer spatial or spectral resolution than FLORIS (e.g. Small Fluorescence Box system, S-FluorBOX, and Multiplexer Radiometer/Irradiometer, MRI) that are capable of the autonomous continuous monitoring of TOC fluorescence. With datasets collected by these sensors, it is possible to apply the same technique of spectral fitting as that defined for FLEX to retrieve fluorescence in a comparable manner. However, all the current systems are limited to spot measurements over a reduced area of a few square metres. In order to fully represent the spatial variability found in

natural vegetation at 300×300 m^2 resolution they will need to be extended to a larger area.

State-of-the-art instruments are being developed (e.g. within the framework of the OPTIMISE COST Action) that will be able to extend the sampling area to a level comparable to the FLORIS spectral range and resolution. These efforts cover:

— robotic systems situated on top of masts that scan the surroundings (e.g. Fully Ultraportable System for Imaging Objects in Nature, FUSION)

— miniaturisation of high-performance spectrometers for use in Unmanned Aerial Vehicles (UAVs)

— improvement in UAV flight autonomy and unsupervised operation (Fig. 6.7)

These improvements together with increasingly popular airborne systems capable of fluorescence measurement will change the capabilities for ground sampling. Moreover, spectroscopy technology is expected to evolve significantly in the next 10 years.

6.2.1.2 Landscape level

The following step moves away from field level (single vegetation type) to a local study site at the landscape level. It is important to realise that a landscape typically covers not only different vegetation types, but also non-vegetated surfaces. Airborne high spatial resolution data can function as an intermediate link between field measurements and FLEX products. Two approaches are pursued to generate high spatial resolution maps of fluorescence at landscape level.

— Directly deriving fluorescence emission from airborne data. In this case, a high spectral resolution sensor capable of fluorescence measurement is required. Consequently, this approach only covers dedicated campaigns since the availability of such sensors is limited. Therefore, TOC field measurement will be used to validate the intermediate data.

— Indirectly deriving fluorescence by modelling from airborne remote sensing data or land reference maps. In this case, a canopy fluorescence model is fed with inputs that are derived from moderate spectral resolution sensors that are already available on several satellite platforms, simulating fluorescence maps at FLEX spatial resolution for validation purposes.

At the landscape scale, UAVs are foreseen to play an important role in the coming years. UAVs have the capability of filling the gap between TOC instruments and traditional airborne systems, thereby providing more frequent measurements at a lower cost. It is foreseen that UAVs will be able to provide indirect upscaling accurately and reliably in the next few years. For direct upscaling (direct measurement of fluorescence) it will still take some effort to miniaturise spectrometers to fit into UAVs, but this is likely to happen well before FLEX is launched.

Finally, the resulting fluorescence maps must be convolved to the spatial resolution of FLEX using the available geometry of acquisition and the sensors' point spread function (PSF) to project each pixel field of view (FOV) onto the fluorescence map overlaid on a DEM (Amorós-López, 2011). The up-scaled map of each product will then be compared against the corresponding retrieved FLEX map. The resulting relative and absolute error maps will be analysed globally and locally within each of the classes present in the scene, with

particular attention to those locations where TOC measurement take place. At this point, it is also important to evaluate non-fluorescent targets such as bare soil. These targets can determine whether FLEX-based fluorescence retrievals provide the expected near-zero value. If this is not the case, then these surfaces will be used to recalibrate the spectral and radiometric characterisation of FLORIS or the retrieval process.

An additional validation check will be to analyse seasonal and yearly trends in retrieved fluorescence over selected targets and compare them with the temporal evolution of *in situ* measurements.

6.2.1.3 Ancillary parameters

Ancillary observations can also contribute to validation. It is important to obtain information on the weather conditions around the field while *in situ* measurements are collected. The AOT and water vapour in the atmosphere can affect the radiance measurements taken by the sensor. While these atmospheric conditions are unlikely to impact the *in situ* measurements using field spectrometers, they will, however, affect airborne and satellite acquisitions. Therefore, the collection of meteorological data can be used to validate the applied atmospheric correction to airborne and satellite data, and to allow *in situ* measurements to be upscaled to sensor values.

6.2.2 Validation Network

In order to ensure the global validity of FLEX fluorescence products and to assess the confidence level, it is necessary to cover the largest possible number of cases of ranges of photosynthetically active radiation (PAR), vegetation types, structures and phenology. Hence, a balanced representation of global vegetation types is required.

Incoming PAR depends on the season and latitude. Vegetation types can be characteristic of particular biomes or ecosystems, that is, regions with similar climatic conditions creating a typical ecosystem over a large area. Therefore, it is necessary to distribute a network of permanent validation sites throughout all latitudes. The different sites in the network will be classified as 'core', 'support' and 'auxiliary' sites, depending on the completeness of their instrumentation, thus the degree of precision attainable for the validation process. Core sites refer to established research sites (e.g. Forschungs Zentrum Jülich's TRansregio 32, CzechGlobe's Bily Kriz, and Laboratoire de Meteorologie Dynamique's Avignon-Montfavet site) that are dedicated to the continuous monitoring of fluorescence emissions. There are currently only few such sites and probably most of them will have already been linked to FLEX. Support sites extend the coverage of validation sites by setting up collaboration with an existing network of measuring sites, where most of the required infrastructure (premises, structures, maintenance and data collection) is available. They will require only the deployment and installation of the specific instrumentation for fluorescence measurements. Contact has already been established with FLUXNET (Baldocchi, 2001).

The selection criteria for candidate sites must require that the area being tested is sufficiently large and spatially homogeneous to provide at least one uniform pixel in FLORIS. It will be necessary to characterise reflectance and chlorophyll content at the same time in order to discriminate the fluorescence signal from other parameters that also evolve seasonally.

6.2.3 Dedicated Validation Campaigns

Whenever possible, airborne instruments will be used to extend the validation over large regions. These activities should be supported with extensive ground sampling that ideally should measure every parameter relevant to the retrieval and interpretation of the fluorescence signal. These datasets will be used to test all aspects of the process applied at permanent validation sites. Dedicated campaigns will provide the highest validation accuracy. Due to the complexity and cost of dedicated field campaigns, they may take place only sporadically and will be linked to selected sites. As part of the FLEX mission it is planned that dedicated campaigns take place primarily during the commissioning and early operation phases of the mission, and to a lesser extent during the remaining mission lifetime, since the validation process at permanent sites will be sufficiently refined by then. Note that these types of campaigns are already being performed using Hyplant, and they will further evolve in accuracy and reliability in the coming years with improved technology, protocols and processing.

To facilitate the dissemination of measurements and production of compatible and consistent results from all validation sites, the collected databases will be harmonised, particularly for datasets acquired at (existing) supporting and auxiliary validation sites, where there is already an established database protocol and infrastructure.

→ PERFORMANCE EVALUATION

7. Performance Estimation

In this chapter, the performance of the proposed mission implementation concepts is assessed against the mission requirements presented in Chapter 4. The performance is expressed first for the system-level parameters described in Chapter 5 including coverage, data latency, and availability. The performance for the system and Level-1 products is presented in Section 7.2. Performance assessments based on the FLEX-End-to-End simulator (FLEX-E) for Level-2 products are then outlined in Section 7.3. Furthermore, a precursor airborne fluorescence sensor has been developed and deployed in several dedicated campaigns to demonstrate the new observing capabilities of the FLEX mission. Results from the HyFlex and FLEX–US campaigns in 2012–14 (Rascher et al., 2015) are included in Sections 7.3.2 and 7.3.3.

7.1 FLEX-End-to-End Mission Performance Simulator

The FLEX-E mission performance simulator represents all relevant elements of the tandem mission concept including the platform, instruments, and payload data processing. Mission requirements and objectives can be consolidated and verified using thorough analyses of the computed performances.

The end-to-end simulation capabilities developed for the FLEX mission include a realistic scene generation tool, which can reproduce complex 3D scenes at a spatial resolution well below the instrument's supporting scale of 300×300 m^2. This is mandatory to test effects due to topography, atmospheric changes with altitude and surface variable illumination conditions, together with different environmental factors and subgrid scale heterogeneity (Fig. 7.1). The simulations also reproduce all the details of the instrument and geometry of observations. Several retrieval schemes have been tested and a final data processing scheme has been fully implemented to test the performance of the mission.

It is important to emphasise that the end-to-end simulation capabilities allow analysis of all geometric registration and colocation uncertainties, including detailed orbital geometry, sensor/detector configuration, and geometric and radiometric noises and artefacts introduced in the data

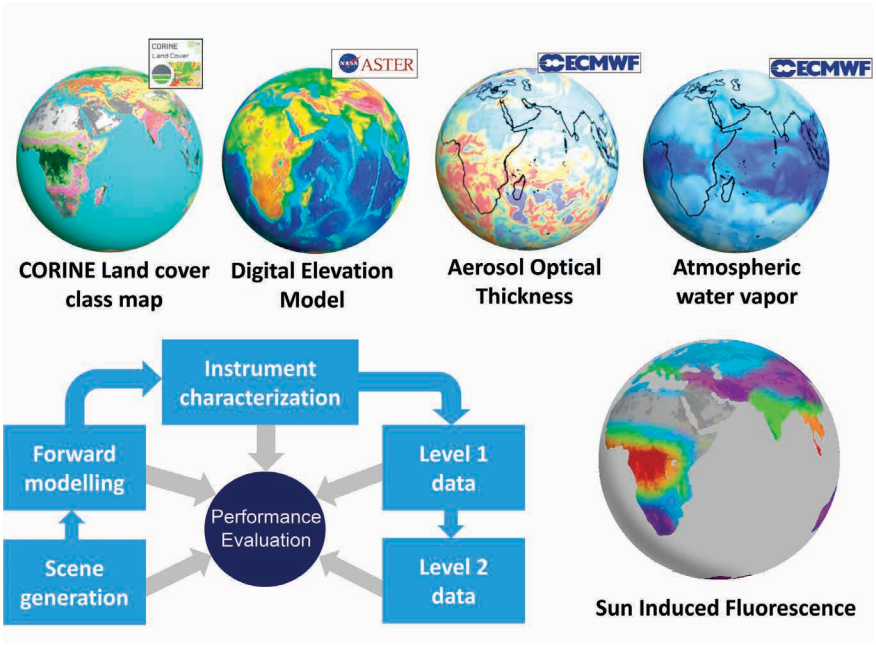

Figure 7.1. End-to-end mission simulation capabilities for global vegetation fluorescence. (University of Valencia)

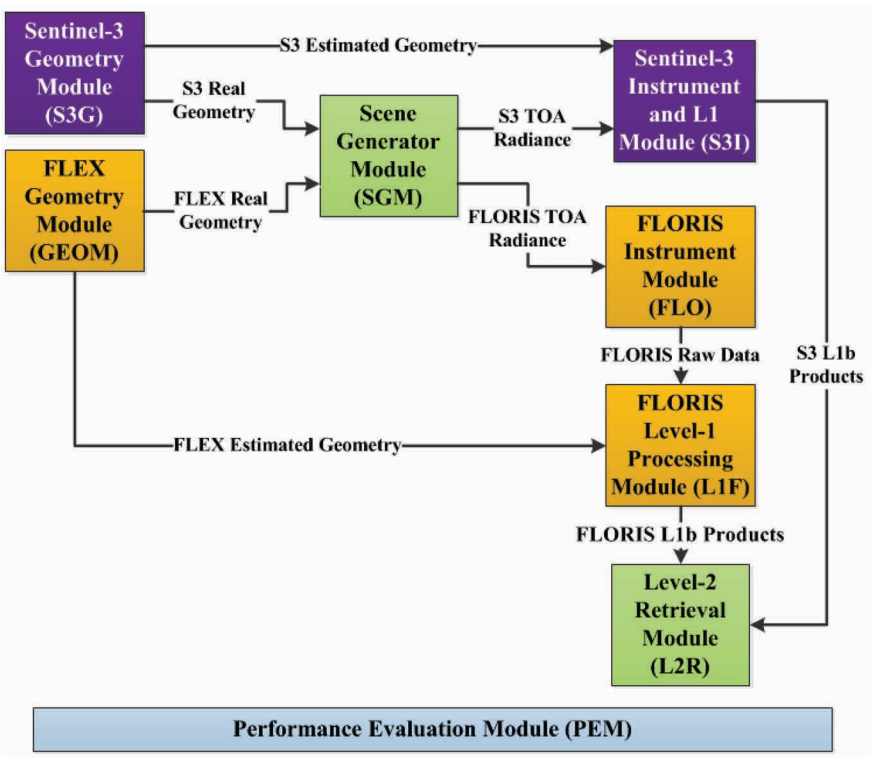

Figure 7.2. Architecture of FLEX-E end-to-end mission performance simulator. (University of Valencia)

processing scheme. Here FLEX-E is used to assess the mission performance at Level-1 and Level-2.

Figure 7.2 shows the FLEX-E high-level modular architecture, which includes the Observing System Simulator (OSS) modules in orange; the custom-made Sentinel-3 modules in purple; the Scene Generator (SGM) and Level-2 Retrieval (L2R) in green; and the Performance Evaluation Module (PEM) in blue. The OSS modules are developed in parallel for both Concept A and Concept B industrial studies and include a geometry module (GEOM), a FLORIS instrument module (FLO) and a FLORIS Level-1 Processing module (L1F). Similarly, the custom-made Sentinel-3 (S3) modules include its own geometry module (S3G) and the instrument+Level-1 processing (S3I) module. All modules were developed by different industrial and scientific partners independently and have been integrated within the generic simulation framework OpenSF to ease the configuration and execution of a simulation chain.

The interfaces between modules are performed through transfer of the files (in netCDF format) produced by each module. The setup of a simulation scenario is achieved by filling the configuration parameters within .xml files. These files are divided into 'global' and 'local' configuration files. In the global configuration file, the parameters that define the configuration of two or more modules (e.g. target location and acquisition epoch) are set. In the local configuration files (one per module) the specific configuration for each module is defined.

In terms of the operability of FLEX-E, all the modules are executed sequentially as shown in Fig. 7.2. The geometry modules (GEOM and S3G) are executed first, providing the observation geometry of each sensor over the defined target. The observation geometry is then used by the SGM, together with the scene configuration parameters, to generate the high spatial/spectral resolution scenes for each sensor involved in the FLEX/Sentinel-3 mission. These scenes are then acquired and processed up to Level-1b by two parallel instrument + Level-1b chains (one for FLEX and another one for Sentinel-3). Finally, the L2R module performs the fluorescence retrievals using the full combined FLEX and Sentinel-3 Level-1b data set. The PEM is executed at the end of the simulation chain and compares the Level-1b and Level-2 products

(outputs from L1F, S3I and L2R) against the reference data from the geometry and scene (GEOM, S3G and SGM).

From a functional point of view, the different modules implemented in FLEX-E perform the calculations described in the following subsections.

7.1.1 Geometry Modules

The FLEX Geometry Module is the first module to be executed. GEOM is in charge of simulating the relevant FLEX spacecraft orbit and attitude as well as generating the individual pixels' fields of view.

A custom-made S3G simulates the relevant spacecraft orbit and attitude as well as the instrument observation geometry for both the Ocean and Land Colour Instrument (OLCI) and Sea and Land Surface Temperature Radiometer (SLSTR) (nadir and oblique) instruments. The S3G module was developed for the FLEX-E project based on a tailored version of ESA's Sentinel-3 SPS.

To properly describe the geometry and illumination/observation angles for the FLEX/Sentinel-3 tandem mission concept, the GEOM uses the full orbital model of Sentinel-3 (actual detailed orbits for the 27-day repeat cycle, provided by ESA's European Space Operations Centre, ESOC) and computes the orbit of FLEX to be fully compatible with the actual orbit of Sentinel-3. Therefore, GEOM and S3G account for satellite separation and actual observation geometry individually for FLEX and Sentinel-3 at each point along the orbit.

To start each simulation, the user provides the geographical coordinates of the ground target area to be observed and the time window when the observation is required. Then, using the full orbital model, the geometry modules compute when Sentinel-3 and FLEX can overpass the area at the closest time to the user-selected acquisition epoch. GEOM and S3G calculate the viewing angles using the actual orbit and instrument pointing capabilities for each satellite. The platform attitude error and attitude variability due to platform vibrations and orbital instabilities are explicitly taken into account.

The line of sight from the satellite focal plane to the 3D ground surface is computed for each pixel in the image. The intersection of the line-of-sight with the 3D digital elevation model of the surface provides the ground observed area for each one of the focal plane pixels. This allows geometrical distortions and colocation issues to be taken into account using actual geometry for each pixel of each one of the instruments (OLCI, SLSTR, FLEX–FLORIS (two different spectrometers)). The dual conical scanning of SLSTR is explicitly modelled as a function of satellite motion and scan geometry, and the point spread function (PSF) for individual pixels is used to compute the area of the ground to be assumed to reproduce the radiance coming from each surface area.

The usage of the full 3D geometry along all the processing chain guarantees consistent geometrical treatment and allows explicit accounting for all topographic effects (varying illumination with terrain slopes, atmospheric effects associated with varying altitude, etc.) in a fully consistent manner.

7.1.2 Scene Generator Module

The Scene Generator Module (SGM) is one of the two scientific modules and is used to generate the scene to be observed by the different instruments. Using the outputs of the geometry model, the geographical area for each one of the individual pixels of FLORIS, OLCI, and SLSTR can be determined. This is achieved by projecting over the ground area the focal plane geometry using the actual satellite position and attitude angles for each individual pixel, the full 3D geometry of the surface (Digital Elevation Model, DEM) and the PSF for each pixel of each instrument. Given such realistic simulation, the ground observed area for individual FLORIS, OLCI and SLSTR pixels do not correspond

one-to-one, but rather different pixel sizes and observation geometries produce a pattern of ground areas for different pixels that correspond to what will actually happen in practice. Surface heterogeneity can explicitly be taken into account when analysing the fact that each pixel of each instrument is simultaneously observing a slightly different ground area.

The whole scene generation is performed in high spatial and spectral resolution. Typically a factor 10 of oversampling is used in the spatial and spectral domains to guarantee a proper implementation of PSF and Instrument Spectral Response Function (ISRF) at the instrumental module. That is, to simulate a 300×300 m^2 pixel, the input scene uses initial pixels of 30×30 m^2, so that one single FLEX pixel is simulated from about 100 initial high-resolution pixels. In the spectral domain, initial data are simulated with 0.01 nm sampling in order later to provide 0.1 nm outputs in the high-spectral-resolution mode. The Scene Generator allows generation of full FLEX scenes (150×150 km^2) or smaller areas (down to 10×10 km^2) to optimise memory and computation time for each different aspect to be tested in the mission analysis.

The scenes are built into a top-of-atmosphere (TOA) radiance hypercube map given at fine spectral and spatial resolutions. Each scene is intrinsic to each instrument on FLEX or S3, as it depends on the observation geometry. The generation of these synthetic scenes is based on the following steps:

— The SGM firstly distributes the bio/geophysical parameters (e.g. leaf area index (LAI), Chlorophyll-a) over the scene at the high spatial resolution of 30×30 m^2. The distribution of these parameters is based on an input land-cover class map such as the global Corine dataset or a user-defined product. In FLEX-E, each land-cover class is associated with a database that defines the spatial distribution (e.g. radial, linear, and random) and statistical distribution (e.g. Gaussian, Poisson) of each parameter. Alternatively, each class can be associated with a surface reflectance spectral database for the simulation of non-fluorescence targets

— The SGM secondly sets the values of the atmospheric parameters over the high-spatial-resolution scene grid. The values from the European Centre for Medium-Range Weather Forecasts (ECMWF) Monitoring Atmospheric Composition and Climate (MACC) reanalysis data are used to have global distribution maps with a temporal dynamic. The atmosphere is defined by the following parameters: columnar water vapour, aerosol optical thickness, aerosol type, and atmosphere type. These parameters are updated per pixel taking into account the surface topography, which is derived from a global DEM (ASTER) resampled at 30×30 m^2 resolution. In addition, the SGM obtains the wind fields to simulate cloud motion, to include the variation in the scene as observed by the FLEX and Sentinel-3 instruments

— Given the input biophysical/atmospheric parameters, the illumination/observation geometry and the surface topography, the SGM propagates the incoming Sun irradiance through the leaf-canopy and atmosphere by coupling the two radiative transfer models (RTMs) SCOPE and MODTRAN5. The propagation of the radiance signal takes the Bidirectional Reflectance Distribution Function (BRDF) effects of the leaf/canopy and the atmospheric adjacency effects into account. Generation of the synthetic scenes using RTMs allows the noise to be uncoupled from the use of external images (such as airborne data) and allows the surface reflectance, fluorescence and TOA radiance maps to be generated with the particular instrument observation geometry

The scene generator is able to simulate cloudy scenes, using cloud databases and high-resolution satellite imagery to simulate actual cloud geometry for each type, and actual cloud radiometric properties for radiative transfer

calculations. Individual clouds and cloud fields with realistic spatial patterns are modelled and located at a given height over the 3D surface geometry. In this way, topographic shadows and cloud shadows are both modelled.

7.1.3 Instrument and Level-1b Processing Modules

The FLORIS Instrument Module (FLO) belongs to the OSS industrial module and models the FLORIS sensor behaviour, processing the high-resolution input scene in both the spatial and spectral domains. It includes all the sensor electronics and onboard processing for production of Level-0 raw data in digital counts, including all instrument noise (both systematic and random). The implemented features within the FLO module are:

— simulation of the sensor PSF for the spatial convolution of the high-resolution input scene

— simulation of the ISRF for the spectral convolution of the high-resolution input scene and onboard band binning

— spectral stability effects of the instrument, such as the smile effect

— spectral and spatial radiometric noises, such as vertical pattern noise (i.e. vertical striping)

— detector and video-chain noises, including analogue-to-digital conversion

— intraband, spatial and temporal coregistration between FLORIS spectrometers and within each spectrometer

— straylight due to spurious light on the sensor

Since input TOA radiance maps are provided to the instrument module with high spatial and spectral resolutions (i.e. 30 m/0.01 nm), the instrument module uses the PSF and ISRF models to perform the spatial and spectral convolution when computing the response for each FLORIS pixel.

A very detailed and realistic straylight model is used in the instrument module, so that straylight effects are explicitly simulated. The fact that the Scene Generator allows the simulation of cloudy scenes, with individual bright clouds and cloud shadows over vegetation scenes, means the simulator allows testing of straylight issues under realistic scenarios that are relevant for the FLEX mission.

The FLORIS Level-1 Processing Module (L1F) is the third module within the OSS. It is in charge of simulating the ground processing for generating FLORIS Level-1b products, and includes different sources of spectral and radiometric calibration errors such as:

— spectral shifts through knowledge of the wavelength barycentre of the instruments

— errors in the absolute and relative radiometric accuracy (e.g. determination of gain/bias calibration factors, accuracy of the Sun spectrum)

The actual 3D surface geometry (DEM with 30 m resolution) is explicitly used to account for geometrical distortions and topographic effects, in a manner consistent with the approach used in the Scene Generator.

In parallel with the simulation of the FLORIS Level-1b products, a custom-made S3 L1 Module (S3I) was developed within FLEX-E for the simulation of the

OLCI and SLSTR Level-1b products. The S3I processes the high-resolution input scene in both the spatial and spectral domains by implementing the real PSF and ISRF of the instruments. The custom-made S3I simulates the instrument noises and calibration errors by a random number generator based on the official signal-to-noise (SNR) requirements for each instrument and spectral channel.

7.1.4 Level-2 Retrieval Module

The Level-2 Retrieval Module (L2R) is the second scientific module implemented in FLEX-E. It implements the algorithms for the retrieval of Sun-induced vegetation fluorescence based on the synergy between FLEX and S3 Level-1b products as described in Chapter 6. Given the complexity and realism of the instrumental effects included in the OSS modules, the L2R implements the full processing chain nearly as in the real ground processing. The L2R includes the following functions:

— The Level-1b data from the FLORIS, OLCI and SLSTR (nadir and oblique) sensors are coregistered into a common grid so that their data can be further exploited in synergy. This process makes use of the Level-1b geolocation coordinates and it is performed without the use of ground control points

— In order to reduce the incompatibilities between FLORIS and OLCI radiometric calibrations, these two sensors are radiometrically cross-calibrated. The radiometric cross-calibration between the coregistered Level-1b data is performed by the simulation of OLCI equivalent radiance data from those FLORIS spectral bands overlapping the OLCI bands within the 500–780 nm spectral range

— The Level-1b spectral calibration of FLORIS data is refined within the Level-2 retrieval scheme so that atmospheric correction and fluorescence retrieval algorithms match the reference absorption features from the atmospheric RTM used

— OLCI and SLSTR (nadir and oblique) coregistered Level-1b data are used in synergy in the atmospheric characterisation and correction algorithm. This algorithm derives the aerosol optical properties and atmospheric water vapour content through an atmospheric look-up table inversion method. The atmospheric parameters are used to simulate the atmospheric transfer functions (i.e. transmittance, irradiance, path radiance and spherical albedo) in order to retrieve the surface irradiance and apparent reflectance for FLORIS, OLCI and SLSTR

— The atmospherically corrected data from FLORIS is input into the Spectral Fitting Method technique to retrieve the fluorescence emission. The synergy between FLORIS and OLCI uses their surface reflectance measurements to retrieve additional biophysical parameters for a complete evaluation of the photosynthesis process

7.1.5 Performance Evaluation Module

The final module to be run within the simulation chain is the PEM. The PEM has been developed independently of the industrial and scientific modules and it assesses the quality of the entire processing chain by comparing each pair of reference and retrieved data. The reference data from the SGM (i.e. reflectance, fluorescence, TOA radiance and biophysical/atmospheric parameters) are

compared with the generated Level-1b and retrieved Level-2 products. The high-spectral/-spatial resolution data from the SGM are resampled so that they can be compared with the lower-resolution retrieved Level-1b and Level-2 data. The PEM implements error metrics to evaluate the spatial and spectral distribution of the errors, allowing tracking of the error propagation of the instrument noises and calibration errors into the retrieval process (e.g. atmospheric correction) and the final fluorescence products.

7.1.6 FLEX-E Test Scenario Description

The FLEX simulator has been designed with a level of realism that enables evaluation of the mission performance at Level-1b and Level-2 under synthetic and realistic scenes and with all the instrument effects included in the simulation.

The capabilities of the FLEX simulator are shown in Fig. 7.3 for a synthetic 20×20 km^2 scenario. The scene contains four homogeneous land cover classes of 20×5 km^2: one non-fluorescent bare soil and three different vegetation types with low to high fluorescence levels based on the combination of input LAI and Chlorophyll-a (Chl) parameters. A DEM divides the scene into two vertical strips of 10×20 km^2, with altitudes of 0 km and 2 km. The scenario also simulates the effects of cumulus cloud cover in order to include the instrument straylight effect in the analysis of the mission products. Both the terrain topography and the cloud cover will cast shadows over the surface given the illumination geometry. The atmospheric condition under which the scene is simulated is a standard mid-latitude summer atmosphere with a medium continental aerosol load.

This simulation scenario includes all the realistic instrument noise, non-uniformity effects and Level-1b calibration errors itemised in Table 7.1. Simulation of all these noises and errors allows a complete analysis to be performed with the nominal and realistic FLEX/FLORIS configuration.

This synthetic scenario will allow assessment of the mission performance on a realistic case ranging different fluorescence and non-fluorescence targets on a non-flat surface with standard atmospheric conditions. Including all the expected FLEX instrument noises and calibration errors adds realism for the estimation of the mission performance with the current state-of-the-art Level-2 retrieval algorithms.

7.1.7 Airborne Facilities/Campaigns

In 2012–14, several field campaigns were performed (see Section 7.3.2) covering agricultural fields, grasslands, and various forest types in Finland, Germany,

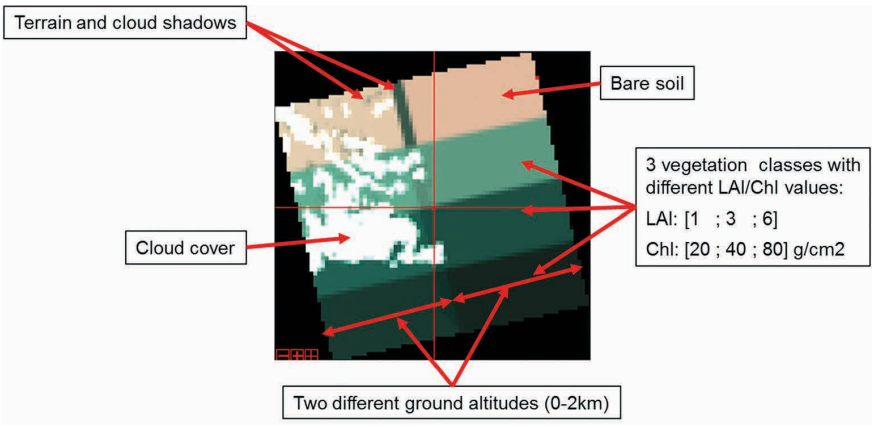

Figure 7.3 Reference scene generated by the FLEX simulator. (University of Valencia)

Table 7.1. Activated noises and calibration errors for the simulation of the test scenario.

Instrument noises and effects	
Sensor PSF	Yes
Sensor ISRF	Yes
On-board band binning	Yes
Spectral stability (e.g. smile)	Yes
Spectral and spatial radiometric noises (e.g. vertical stripping, read-out noise, relative gain non-uniformity, non-linear response, smearing)	Yes
Detector and video-chain noises	Yes
Analogue-to-digital conversion	Yes
Intraband, spatial and temporal coregistration between FLORIS spectrometers and within each spectrometer	Yes
Straylight	Yes
Level-1b calibration errors and effects	
Errors on the characterisation of FLORIS on the FLEX platform	Yes
Orbit and attitude estimation errors	Yes
Absolute and relative radiometric calibration errors	Yes
Dark signal non-uniformity knowledge	Yes
Spectral calibration errors (i.e. shifts on the knowledge of the wavelength barycentre)	Yes

France, Italy, Czech Republic and the US (in cooperation with NASA). During these campaigns the 'HyPlant' airborne imaging spectrometer was used (Fig. 7.4).

This high-performance imaging spectrometer was built by the Finnish company Specim under contract to the Forschungszentrum Jülich (Germany). It is a FLORIS airborne demonstrator that delivers high-spatial-resolution flight lines with a spectral resolution similar to that of FLEX. The device consists of two modules, one measuring surface reflectance with high spectral resolution in the range of 380–2500 nm (3 nm resolution in the VIS/NIR and 10 m resolution in the SWIR), and the second measuring surface reflectance in the range of 670–780 nm with a spectral resolution of 0.25 nm and a spectral sampling interval of 0.11 nm.

Extensive technical testing of the instrument was performed between delivery (autumn 2012) and today. The sensor was proven to provide stable results that are comparable with the proposed FLEX–FLORIS data. However, the signal-to-noise level is a factor of five lower than the proposed satellite instrument. Radiometric characterisation of this airborne instrument was done in close contact with ESA, and knowledge of the influence of spectral characteristics, such as the effects of the PSF or the effect of straylight, has greatly helped to improve the design of the airborne instrument. A detailed characterisation of the instrument is available in the HyFLEX campaign reports and in Rascher et al. (2015).

HyPlant was flown at altitudes of 600 and 1800 metres, delivering maps of 1 m and 3 m pixel resolution, respectively.

Based on these real-world measurement data, algorithms to quantify the two peaks of fluorescence were developed and tested. The proposed retrieval schemes of the FLEX mission were evaluated using data from the HyPlant sensor. Several maps of fluorescence were presented to the scientific community, resulting in various scientific papers that demonstrate the added value of fluorescence for vegetation monitoring. Such papers include a demonstration that fluorescence gives a better estimate of light absorption in dense canopies (Rascher et al., 2015) and a demonstration that the two peak

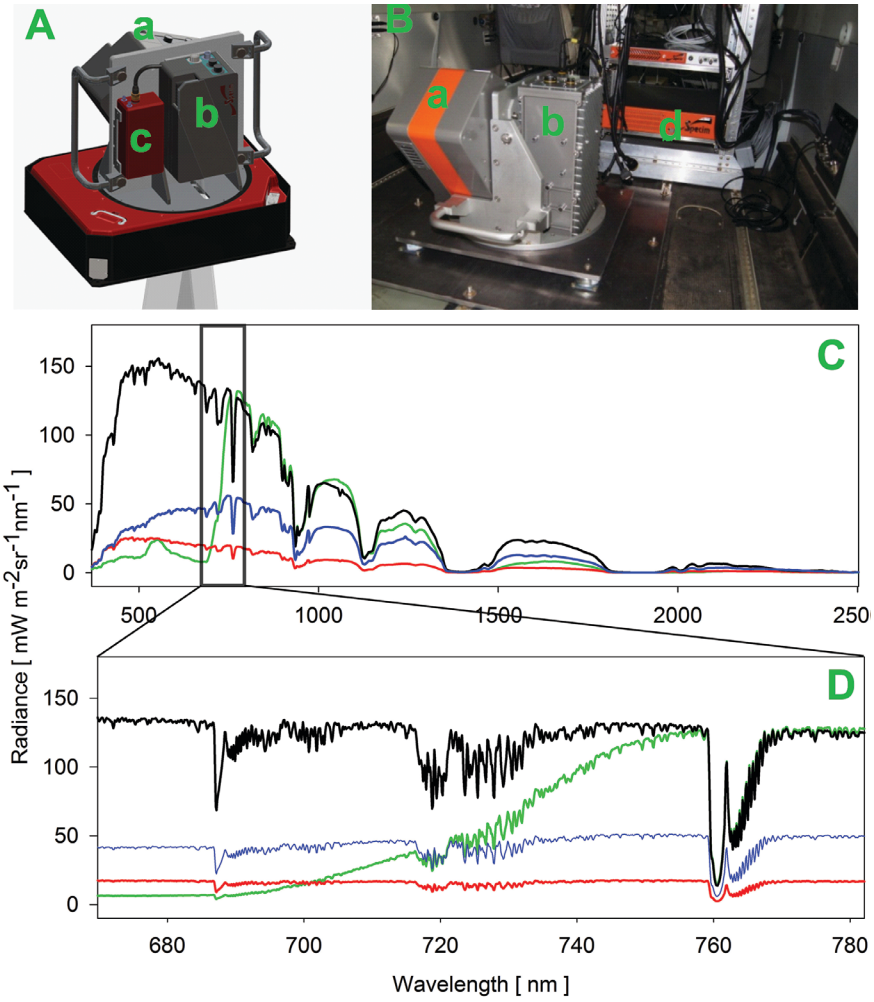

Figure 7.4. Airborne imaging spectrometer HyPlant. A: schematic drawing of the HyPlant sensor consisting of the broadband dual-module (a) and the high-resolution fluorescence module (b). The GPS/IMU positioning unit attached to the rack is shown (c). B: Installation of HyPlant on a Cessna aircraft during a campaign in 2012. The data acquisition unit is visible (d). C & D: representative radiance measurements from a bright target (black), dark target (blue), vegetation (green), and bare soil (red) from the dual and the fluorescence module, respectively. The spectrally high-resolution fluorescence module resolves the two oxygen absorption lines O_2-A and O_2-B at 760 nm and 687 nm, respectively. Water vapour absorption bands between 705 and 735 nm are also visible. Even very narrow Fraunhofer lines owing to absorption features in the solar atmosphere are visible at 750 nm. (Forschungszentrum Jülich)

feature of fluorescence can track fast changes in stress-induced limitations of photosynthesis (Rossini et al., 2015).

7.2 Level-1b Performance

7.2.1 Design Performance

This section presents the system and instrument Level-1b performance achieved by the two mission concepts described in Chapter 5. It compares the requirements against the performances and provides, whenever relevant, justification or further explanation on key performance parameters. This section starts with coverage, availability, data latency and geolocation and pointing, followed by the FLORIS instrument performance. The Level-1b performances are also presented in Section 7.2.3 by using the FLEX simulator tool.

7.2.1.1 Data latency

The data latency, defined as the time interval from the acquisition of data by the instrument to the delivery of the product at the user interface, is driven by various factors, e.g. data volume, number and location of downlink ground stations, space-to-ground downlink speed, transfer time to PDGS, and processing. Both concepts foresee the use of a single high-latitude ground station, which could be in either the northern or the southern hemisphere, so that the 24 h requirement

Table 7.2. Summary of the main observation requirements and achieved performances.

Observational requirement	Specification	Concept A	Concept B
Mission lifetime	3.5 years (T)/5 years (G)	5-year design	5-year design
Data latency	5 h (G)/24 h (T)	18 h	8 h
Coverage	All latitudes from 56° South to 75° North	Compliant through orbit choice	Compliant through orbit choice
Pointing	Nadir	Nadir pointing as baseline	Nadir pointing as baseline
Dynamic range	Covering L_{min} up to L_{max}	L_{min} up to L_{cloud}	L_{min} up to L_{cloud}
Swath width	100 km (T)/150 km (G)	150 km	150 km
Spatial Sampling Distance	<300 m	300 m ALT/300 m ACT	300 m ALT/280 m ACT
System Integrated Energy	>70% over an area of 1.2/1.1 SSD	78.7%	74%
	>90% over an area of 1.6/1.5 SSD	94.5%	90%
Spectral band coverage	See Table 5.2	Compliant	Compliant
		FLORIS-HR: 677–697 nm, 740–780 nm	FLORIS-HR: 677– 697 nm, 740 –780 nm
		FLORIS-LR: 500–780 nm	FLORIS-LR: 500 –740 nm
Spectral Resolution (and Sampling)	See Table 5.2	FLORIS-HR: 0.303 nm (~3 SSI)*	FLORIS-HR: <0.3 nm (3 SSI)
		FLORIS-LR: 2.03 nm (3 SSI)*	FLORIS-LR: < 2 nm (3 SSI)
Signal-to-noise ratio	See Table 5.2	Compliant	Compliant
Spectral stability over lifetime	1 nm	<0.1 nm	<0.1 nm
Spectral stability over operational orbit	0.1 SSI	~0.05 SSI	~0.05 SSI
Knowledge of ISRF	Better than 1% (TBC)	FWHM knowledge <0.5% expected (ISRF characterisation accuracy subject to OM pre-developments)	
Spectral coregistration	<0.1 SSI	FLORIS-HR: 0.07–0.15 SSI	FLORIS-HR: <0.018 SSI
		FLORIS-LR: 10 SSI** (L0 – w/o correction, compliant at L1b after resampling)	FLORIS-LR: <0.15 SSI (L0 – w/o correction, compliant at L1b)
Spatial coregistration (intra/interband)	<0.15/0.3 SSD	<0.1 SSD/<0.3 SSD	<0.1 SSD/<0.35 SSD***
Temporal coregistration with S3	6s (G) / 15s (T)	<15 s	<15 s
Inter-channel temporal coregistration	<2s	0 s	2 s
Absolute radiometric accuracy	5% including polarisation and straylight errors	3% on uniform scenes	3% on uniform scenes
		<1% polarisation (FLORIS-HR)	1% polarisation (FLORIS-HR)
		<1% straylight **** (For a step function with contrast L_{cloud} to L_{ref})	< 1% straylight **** (For a step function with contrast L_{cloud} to L_{ref})
Relative radiometric accuracy	1%	0.55% spatial	1% spatial and spectral together
		0.54% spectral	
Polarisation sensitivity (LR)	2%	1.2%	1.7%
Polarisation sensitivity (HR)	1%	0.35%	1.0%
Geolocation accuracy	0.4 SSD	<0.3 SSD	<0.4 SSD

G=goal, T=threshold; SSI: spectral sampling interval, SSD: spatial sampling distance
L_{min} and L_{max}: minimum (darkest soil/veg surface) and maximum (brightest soil/veg surface) spectral radiance levels; L_{cloud}: brightest cloud/snow spectral radiance level
* minor non-compliance considered recoverable in next design iteration
** alternatively to resampling, a corrective prism can be introduced similarly to the HR spectrometer, as planned in the optical model
*** action to recover the non-compliance currently under investigation
**** allocation after straylight correction

can be met comfortably. Estimated values from the two concepts range from 8 to 18 hours. Employing two downlink ground stations would allow the latency goal requirement of 5 hours to be met. However, this solution, while technically feasible, would increase mission implementation cost.

7.2.1.2 Mean operational availability

The mean operational availability is defined as the percentage of time during which the entire system (space and ground segment) acquires and delivers L1b data. The mean operational availability include scheduled outages (e.g. calibration, orbit control, formation flying manoeuvres) and unscheduled outages (e.g. Safe Mode events, hardware recoverable anomalies). The predicted mean operational availability over the lifetime is about 95% for both concepts.

7.2.1.3 Coverage

As explained in Chapter 5, FLEX will fly ahead of Sentinel-3 in the same orbital plane. For this orbit, the required coverage can be achieved with a swath of 105 km. The instrument has nevertheless been designed for the goal swath of 150 km, to achieve a shorter revisit time at high latitudes. Acquisition over land, coastal areas and major islands will be achieved via onboard implementation of an acquisition mask, triggered by orbit position tagged commands. The achieved coverage and revisit time are shown in Fig. 7.5.

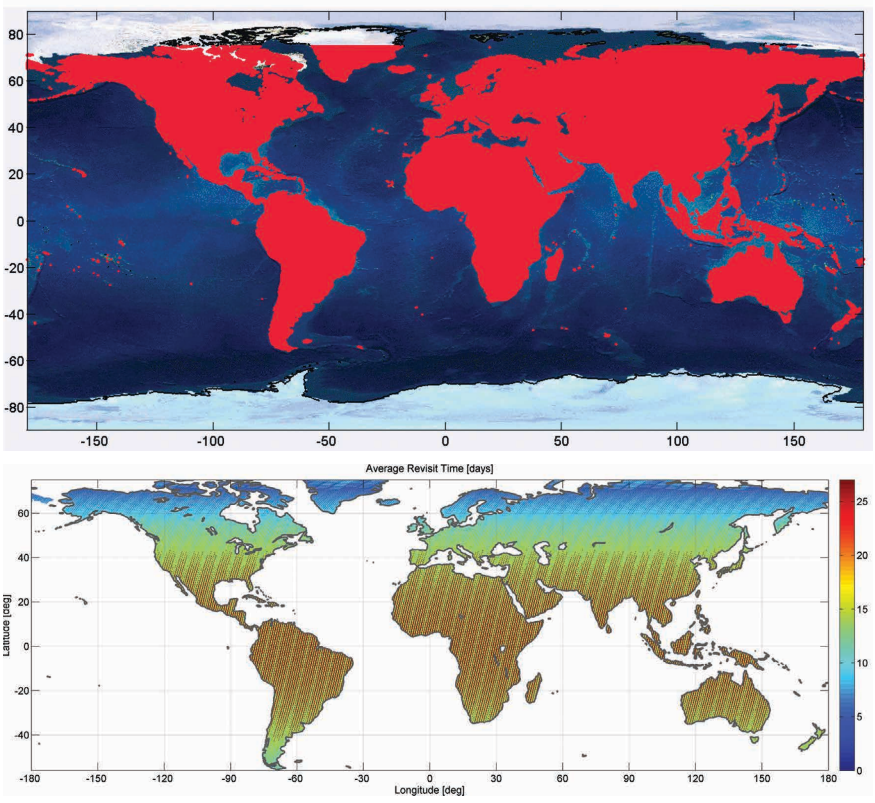

Figure 7.5. Top: FLEX coverage. (Airbus Defence and Space). Bottom: Revisit time. (Thales Alenia Space)

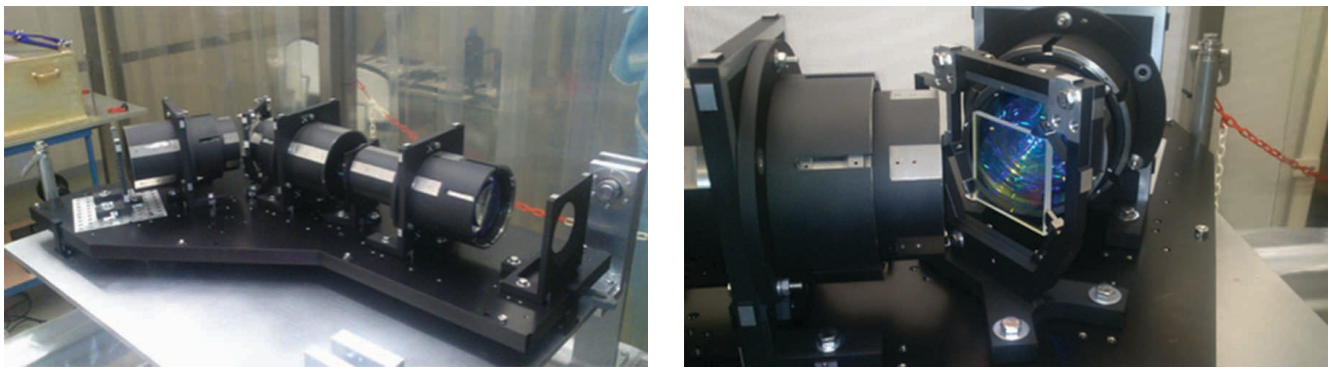

Figure 7.6. FLORIS EBB (Concept A); right: closer view of the grating assembly. (Airbus Defence and Space)

7.2.1.4 Geolocation and pointing

For both Concept A and B the geolocation requirement can be met with ample margins at Level-1b, even without the use of ground control points, by use of recurring avionics. The performance obtained is about 90 m, against a specification of 120 m. The pointing requirement of 1 km, derived from the FLORIS swath inclusion in the OLCI camera-4 swath, and temporal coregistration between FLEX and Sentinel-3 observations, can also be met with margins.

7.2.2 FLORIS Performance

In the frame of the industrial Phase-A/B1 studies, the realisation of two FLORIS Elegant Breadboards (EBBs) as representative as possible of the high-resolution channel has been initiated. One of these EBBs has been completed and tested (Fig. 7.6), and some of the measurements of the related performance will be reported in the following paragraphs. The other EBB is still under development. The breadboard activities were performed with the objective of reaching TRL 5, including for the HR grating, which has been identified as the most critical technology in the development of FLORIS. The breadboard also aims to demonstrate the manufacturability of flight-representative optical elements and the assembly compliance with tolerance analysis and contamination budgets, and to measure spectral and imaging performance.

7.2.2.1 Geometric performance

7.2.2.1.1 Swath width and spatial sampling

The FLORIS instrument has been designed for a field of view (FOV) of ±5.3° and achieves thereby the goal swath requirement of 150 km at the intended altitude. The requirements on SSD and SSI are also met by adapting the detector pixel configuration according to the requirements. Since the field of view is relatively small, there is also little variation with respect to the change of the sampling properties as a function of the swath position or the spectral channel locations (the wavelengths).

7.2.2.1.2 Spatial resolution and point spread function

As already pointed out in Chapter 5, the imaging performance of the FLORIS instrument is expressed as the System Integrated Energy (SIE), which includes,

Channel	SIE (Concept A)		SIE (Concept B)	
	1.2 SSD ALT x 1.1 SSD ACT	1.6 SSD ALT x 1.5 SSD ACT	1.2 SSD ALT x 1.1 SSD ACT	1.6 SSD ALT x 1.5 SSD ACT
HR	78.7%	94.7%	74%	90%
LR	77.1%	93.2%	74%	90%
Requirement	70%	90%	70%	90%

Table 7.3 SIE predicted performances for Concept A and B, showing compliance with the requirements.

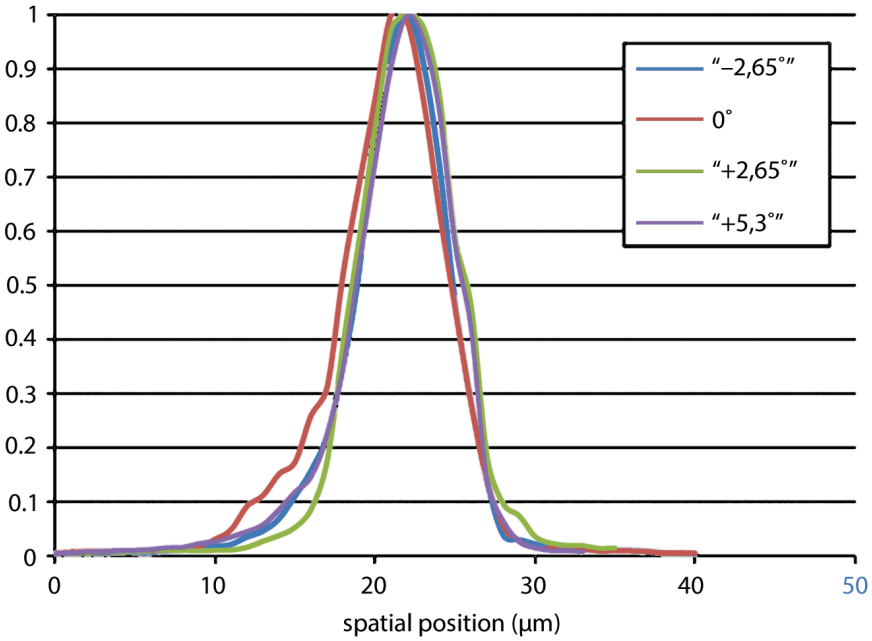

Figure 7.7. Optical PSF across-track measured on the EBB at four positions in the FOV. Abscissa axis denotes distance in µm in the (telescope) focal plane. The FWHM of the telescope PSF is equivalent to ~7 µm, corresponding to about 25 m. (Airbus Defence and Space)

besides the satellite movement as biggest contributor, the optical PSF and several other contributors such as the satellite pointing jitter, the separation of the point sources by the scrambler and some smaller contributors such as detector crosstalk and alignment changes. The predicted performance for Concept A and Concept B are shown in Table 7.3.

One uncertainty on optical performance is that the optical PSF depends on the errors that are introduced during the integration of all optical elements. The measurements performed during the Concept A EBB activity demonstrated that the optical integration was better than expected. The PSF Full Width at Half Maximum (FWHM) corresponds to ~25 m, which is a relatively small contribution compared to the pixel size of 300 m (Fig. 7.7). It is therefore expected that the SIE will meet or exceed the requirements. The realisations through the Concept B instrument breadboard and the planned Optical Module activities should provide further confidence.

7.2.2.1.3 Spatial coregistration

Since FLORIS is composed of two different spectrometers in both Concepts A and B, a distinction is made between spatial intraband (within the same spectrometer) and interband (between two spectrometers) coregistration. The interband coregistration of the spectral channels is affected by the initial design match of the spectrometers, the alignment accuracies, and possible changes originating from the ground to space transport, and by thermal changes occurring during the flight conditions.

Coregistration budget		ALT (µm)	ACT (µm)
Design realisation		6.83	14.09
Long term stability (mission lifetime)	HR and LR registrations	0.12	1.81
	LR versus HR lines of sight	3.47	6.34
Total long term in µm		10.42	22.24
Total long term as SSD fraction		0.13	0.27
Requirement (fraction of SSD)		0.3	0.3

Table 7.4. Long term coregistration budget between HR and LR channels for a typical alignment scheme of Concept A. Performance is expressed as distance at focal plane level in µm (1 SSD = 84 µm).

A thermo-mechanical analysis has therefore been performed considering extreme hot and cold cases. Interband coregistration differences are then derived by determination of the maximum location differences between optical spots (corresponding to the same ground samples) of FLORIS-HR and -LR. The results are presented in Table 7.4 for Concept A, showing that the requirement can be met. Concept B is slightly non-compliant, owing to the slit image curvature in FLORIS-LR. Further refinements of the optical design will address this aspect.

The intraband coregistration concerns the difference of the registration of each spectral channel within a single spectrometer. This performance is directly related to the keystone imaging performance of the optics and possible detector alignment imperfections. Measurements performed on the breadboard of Concept A are shown in Fig. 7.8. The maximum keystone (after a rotation correction of the detector is applied) is about 4 µm in the focal plane and corresponds to 0.05 SSD, showing that the contribution of the optical design to the coregistration is inherently very low. Detailed analyses considering additional error contributors such as detector alignment, gravity and moisture release have shown that the requirement of 0.15 SSD is met with reasonable margins.

The expected keystone values for the FLORIS-HR Concept B optical design are shown in Fig. 7.9. It can be seen that the keystone is far less than 1 µm (e.g. < 0.01 SSD) and therefore can be considered as negligible. The performance is therefore only constrained by the optics and detector alignment accuracy, and is expected to be met.

Figure 7.8. Keystone measurement results on FLORIS breadboard at three positions in the FOV. X- and Y-axes indicate the measured positions in the focal plane in µm. The slope of the curves originates from an imperfect detector alignment. The keystone corresponds to the deviation of the measured curves from linear behaviour. (Airbus Defence and Space)

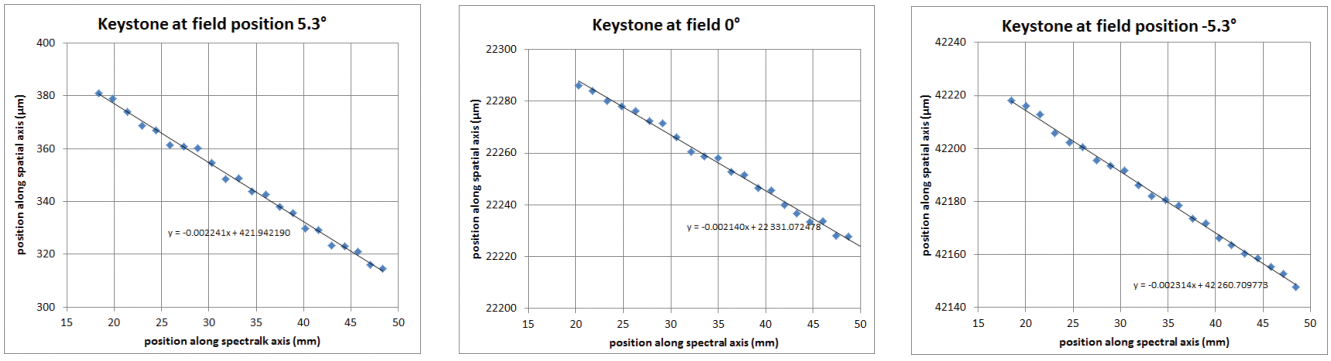

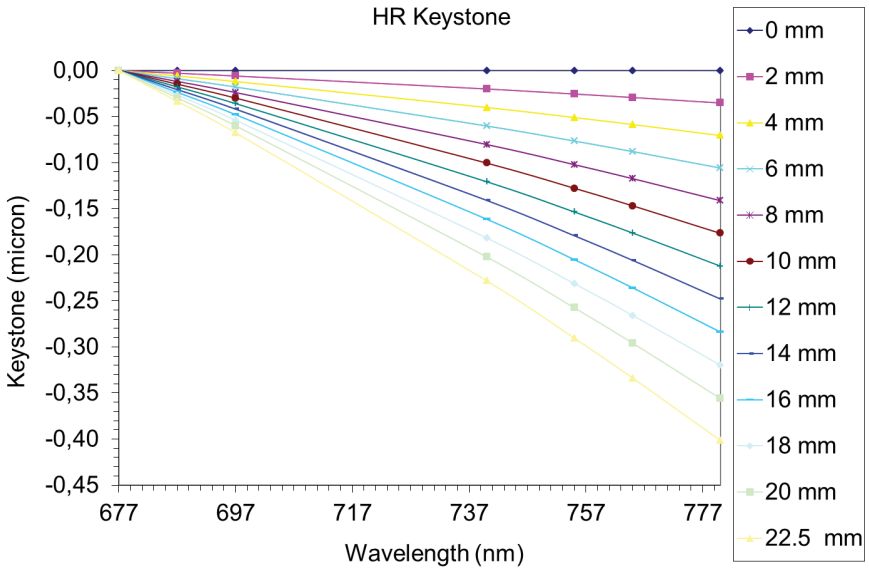

Figure 7.9. FLEX HR keystone of Concept B as a function of wavelength for different points in the FOV (given in mm along FOV starting from the FOV centre, with maximum FOV of 22.5 mm corresponding to 75 km on the ground). Keystone performance is expressed as distance at focal plane level in µm (1 SSD = 84 µm). It shows that the keystone is at submicron level (i.e. negligible) for Concept B. (Thales Alenia Space)

7.2.2.2 Spectral performance

7.2.2.2.1 Spectral sampling and spectral resolution

The realisation of the required spectral resolution is achieved by matching the optical performance (e.g. spot size and magnification), the grating dispersion and the detector pixel size. The slit size of the instrument is tuned such that the requirements of 0.3 nm for FLORIS-HR and ~2 nm for FLORIS-LR are fulfilled. The grating, besides providing the required spectral dispersion, has influence on the throughput and the scattering behaviour of the instrument. The predicted performances of the ISRF for FLORIS-HR and FLORIS-LR are shown in Fig. 7.10 for one of the optical designs, the other being almost equivalent. As indicated in Table 7.2, the predicted FWHM of the ISRF, e.g. the spectral resolution, meets the requirements for one concept and shows a slight deviation for the other, which will be recovered in the next design iteration.

The ISRF predicted performance is supported by the measurement result on the EBB for Concept A, which is shown in Fig. 7.11. For the FLORIS EBB the ISRF shape is approximately rectangular because the root mean square (RMS) spot size is very small. The convolution with the detector was applied using a

Figure 7.10. Predicted ISRF performance for the FLORIS-HR (left) and FLORIS-LR (right). (Airbus Defence and Space)

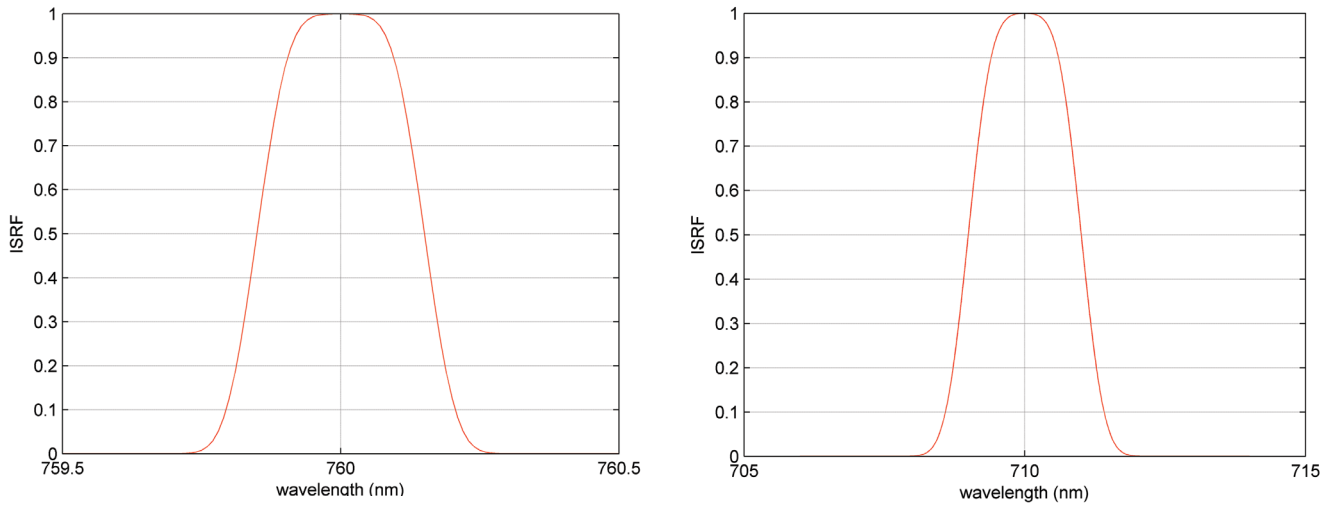

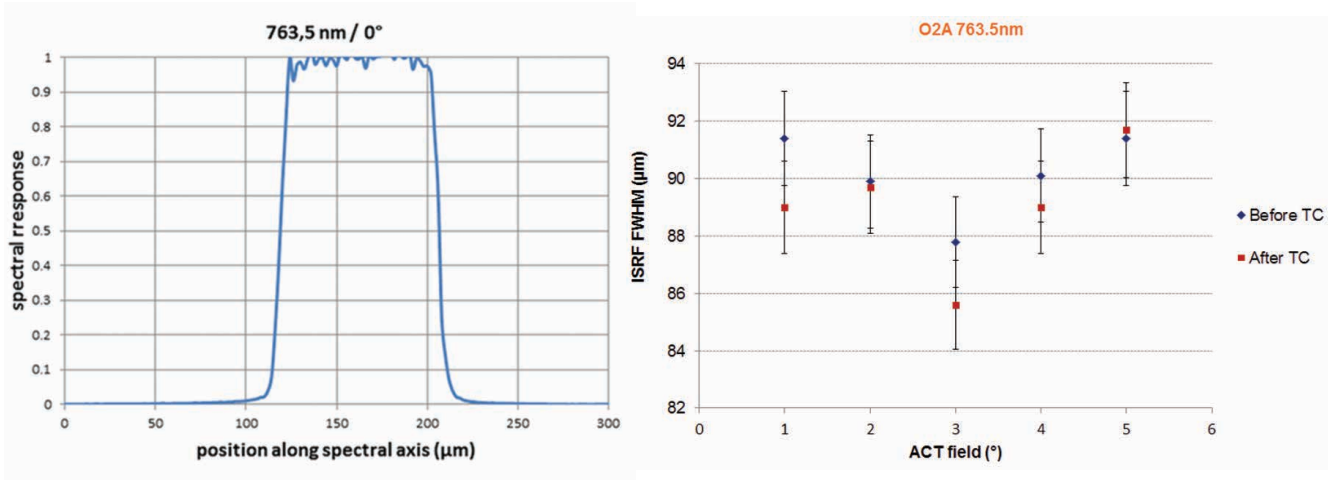

Figure 7.11. Left: FLORIS-HR ISRF measurement of the EBB of Concept A at the centre of the FOV and for the 763.5 nm channel, obtained by scanning in the across-slit direction the image of monochromatic light with a small detector (normalised). X-axis indicates the measured positions in the focal plane in µm (spectral dispersion of 0.1 nm / 28 µm). The FWHM is about 0.3 nm and is compliant with the requirement. Right: the FWHM of the ISRF for different FOVs before and after thermal cycling. (Airbus Defence and Space)

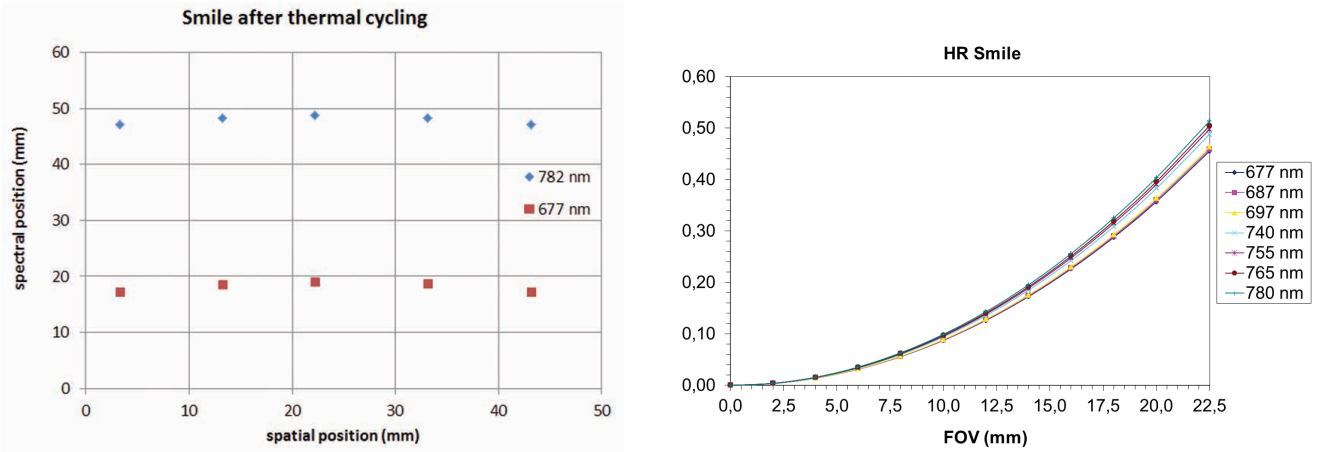

Figure 7.12. Spectral coregistration (smile). Concept A (left): Measurement on EBB. X-axis corresponds to spatial dimension across-track (in µm at focal plane), while Y-axis indicates wavelength direction (in µm at focal plane). Measurements confirm the design prediction (e.g. 1.62 mm measured versus 1.7 mm predicted at 782 nm). A large smile is measured since a correction prism was not yet implemented in the optical chain. (Airbus Defence and Space) Concept B (right): simulated performance showing the smile on the Y-axis (in µm) as a function of the FOV for various wavelengths. The maximum smile is 0.5 µm, which corresponds to 0.02 SSI, and gives confidence that the requirement can be met. (Thales Defence and Space)

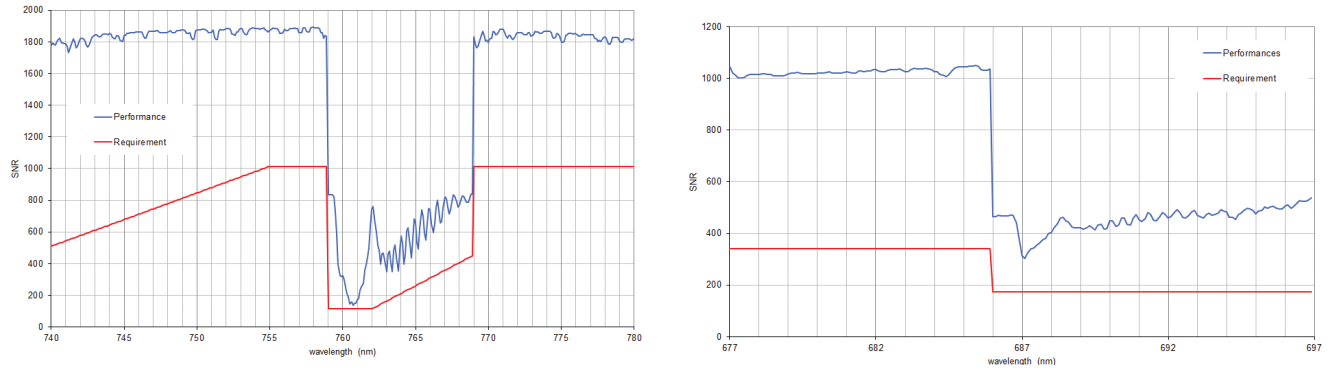

Figure 7.13. Predicted SNR values of FLORIS-HR for the FLEX reference scene. (Airbus Defence and Space)

detector with a small pixel size, and no scrambler was used in the EBB. The FWHM is about 0.3 nm and is compliant with the requirement.

7.2.2.2.2 Spectral coregistration

The spectral coregistration, or smile, of the spectrometer generates in the focal plane a change of the spectral sampling position of the spectral channels across the swath. Though this effect could in principle be corrected by post-processing of raw data, the chosen implementation is to reduce the signal variation along one charge coupled device (CCD) column (along the swath), to avoid electrical cross-coupling in the detector and to minimise the number of columns of the CCD. Concept B has no significant smile by design, while Concept A had to introduce a prism within the collimated part of the spectrometer for smile correction. Figure 7.12 shows experimental results of the EBB of Concept A and the theoretical expectation for Concept B.

7.2.2.3 Radiometric performance

7.2.2.3.1 Signal-to-noise ratio

The requested signal-to-noise ratio for the FLORIS instrument is relatively high and is most critical in the O_2-A absorption feature around 761 nm. Even at this wavelength the dominating noise contributor is photon noise, so that the performance depends mainly on the throughput of the instrument. Contributors are the transmission of the optical glass, the anti-reflection coating performance, filter transmissions, the grating efficiency and the spectral detection efficiency of the detector. Flat gratings as employed in Concept A can provide efficiencies better than 95%, whereas curved gratings such as in Concept B can reach efficiencies of up to 75%, meaning that both concepts become less challenging in terms of instrument aperture size. With the current configuration, it is expected that the SNR will be met with margins as can be seen in Fig. 7.13 for FLORIS-HR and in Fig. 7.14 for FLORIS-LR. The calculations assume an integration time of 45 ms, which corresponds to the equivalent time of a spacecraft movement of 300 m on the ground. Worth mentioning is that the charge-handling capacity of the detector will be tuned to match the full dynamic range requirements. In this case, FLORIS would be able to measure cloud radiance levels without saturation to apply straylight corrections.

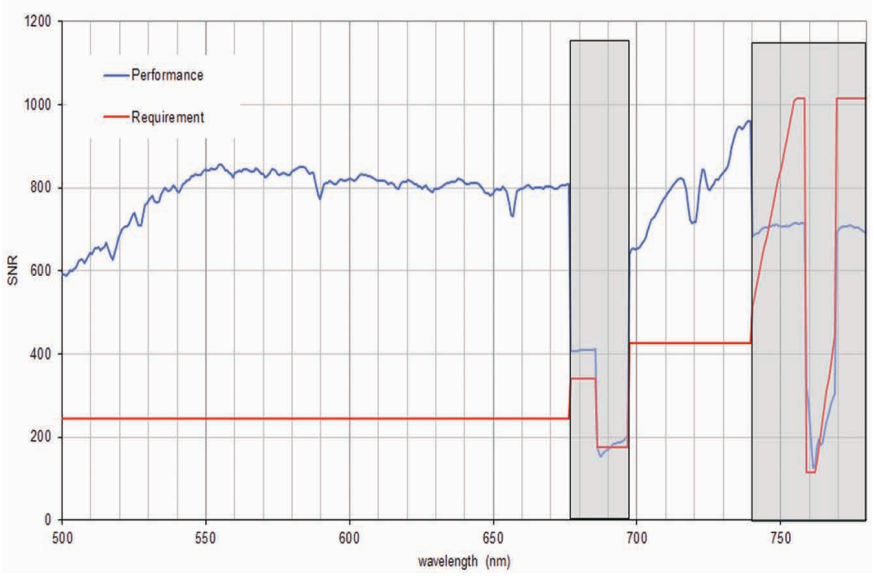

Figure 7.14. Predicted SNR values of FLORIS-LR for the FLEX reference scene. (Airbus Defence and Space)

Contributor	Type	Error (% of L_{ref})
Diffuser BRDF characterisation accuracy	bias	0.5
Diffuser ageing	bias	0.35
Spectral features / speckle	random	0.1
Angular knowledge – impact on BRDF knowledge	random	0.1
Angular knowledge – impact on Sun irradiance knowledge	random	0.4
FLORIS noise in calibration	random	0.05
Dark signal knowledge in calibration	random	0.1
Straylight in calibration	bias	0.3
Instrument stability between calibrations	bias	0.1
Instrument stability – pixel-to-pixel relative part	random	0.1
Polarisation differential between calibration / imaging	random	0.3
Dark signal knowledge in imaging	random	0.2
Instrument non-linearity residual	random	1.0
Detection crosstalk	random	1.05
Straylight in imaging	random	0.7
Absolute radiometric accuracy (uniform scenes)	$\Sigma_i Bias_i$ + SQRT($\Sigma_i Random_i^2$)	2.9
Requirement		3%

Table 7.5. Budget for the absolute radiometric accuracy (typical allocations)

7.2.2.3.2 Absolute radiometric accuracy

The required 5% absolute radiometric accuracy entails the use of an onboard calibration facility consisting of a mechanism deploying a Sun-illuminated diffuser in front of the entrance pupil of the instrument. The calibration will be performed close to the South Pole, where the instrument thermal environment is very representative of the observation phase. The uncertainty of this measurement can be established by determining the magnitude of individual contributors. The contributors and the corresponding budgets are shown in Table 7.5.

The table shows the radiometric accuracy of Earth radiance measurements assuming a perfect knowledge of the Sun. The Sun uncertainty therefore has to be added to Earth absolute radiance measurement uncertainty. Since the approach is based on knowledge of the Sun radiance, it is not necessary to radiometrically calibrate the system on the ground, or at least not with high accuracy. Disentangling spatially- and spectrally-varying contributions allows estimation and optimisation of the allocations of these errors. Current predictions match the relative spatial and spectral radiometric accuracy requirements and amount to about 0.5%.

7.2.2.3.3 Polarisation sensitivity

As discussed in Chapter 5, the degree of polarisation of the radiance can be very high in the vicinity of the absorption lines of the atmosphere. In order to reduce the instrument sensitivity to polarisation, both FLORIS designs implement a polarisation scrambler as the first element of the optical chain in both the HR and LR spectrometers. During the study, models of the scrambler have been developed by a leading manufacturer in order to meet the required residual polarisation. The result is presented in Fig. 7.15, which shows that the

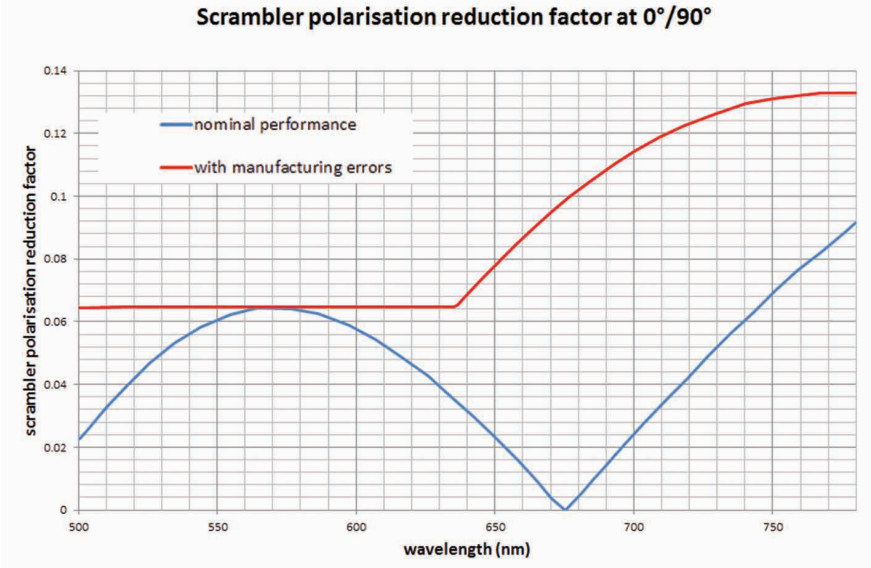

Figure 7.15. Predicted residual polarisation sensitivity after the polarisation scrambler. (Airbus Defence and Space)

residual spectrally-dependent polarisation sensitivity after the scrambler is compliant with the 1% requirement.

7.2.2.3.4 Straylight sensitivity

In order to investigate the radiometric error generated by the instrument, straylight calculations of the FLORIS optics have been made. The objective was to understand and identify important contributors to the in-field scattering and to have guidelines for the optics quality to establish requirements for the surface roughness, contamination and scattering from the grating. The scattering properties are then linked to the requirement by analysing the radiometric error generated by the instrument, by modelling its response to a reference scene. The reference scene selected for these computations is in line with that defined in Section 7.1.6 (Fig. 7.3), in which the illumination of the spectrometer slit is a step function across the FOV with contrast L_{cloud} to L_{ref}. The image in the focal plane as seen during a single acquisition is illustrated in Fig. 7.16 (left).

Figure 7.16. Left: visualisation of the spectral content of the reference scene, which is used to determine the radiometric errors caused by straylight. The radiance on one half of the FOV is set at a level of L_{cloud}, and the on other half at L_{ref}. Right: the corresponding errors generated by spectrometer contamination (the biggest contributor). Errors are reported as a percentage of the scene radiance (L_{ref}). (Airbus Defence and Space)

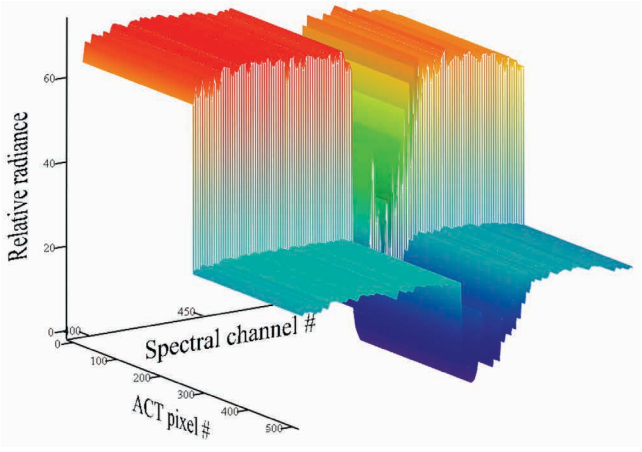

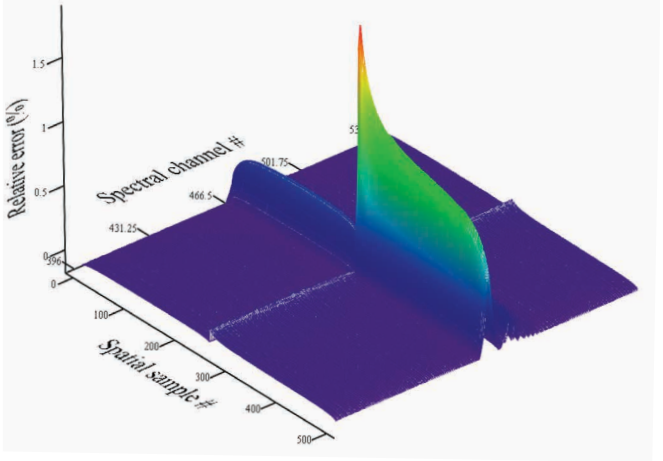

The calculation makes use of a Kernel function, which itself is calculated either analytically or with an optical design program. After convolution with the Kernel function (FLORIS response including the scattering function), the error can be estimated by comparing the nominal radiance to the radiance including the straylight contribution. A typical example is shown in Fig. 7.16 (right). For the reference scene (Fig. 7.16 left), the straylight is most critical in the oxygen A-band where it amounts to 2.38% at 761 nm and at a distance of 20 SSD from the edge of the illumination step function, exceeding the allocation for straylight error, which will therefore need to be corrected by a factor two to achieve compliance at Level-1b. Table 7.6 shows that the main contributors are contaminations and double reflections in the spectrometer and the grating, while contributions from the telescope are comparatively small. Diffraction from the slit and from the aperture is considered as a minor contribution (since FLORIS has relatively large apertures). The models allow further tuning of the performance of individual optical elements, eventually enabling minimisation of the straylight sensitivity of the instrument.

If the spectrometer is well sealed and if the sources of contamination are well controlled, then there will be no major change of the scattered light during the mission lifetime, so that the instrument response function, as established by characterisation on the ground and by modelling, can be used if necessary for the straylight correction scheme. The presented performance is only achieved with a relatively low surface roughness of about 1 nm RMS, and contamination levels which are (depending on the concept) between 30 ppm and 100 ppm inside the lens barrels and 150 ppm to 250 ppm for exterior optical surfaces. If such levels of contamination were exceeded, or doubled in the worst case, the correction factor for straylight would be around 4. This level of correction is not considered very demanding, since higher levels have been demonstrated by other spectrometers that have flown or are about to fly (e.g. MERIS, OLCI, TROPOMI) by pre-flight characterisation of the instrument scattering function. However, it will be necessary to follow a dedicated contamination control plan during all phases of on-ground instrument

	O_2-A (761 nm)	O_2-B (687 nm)
Total error relative to reference radiance at 20 SSD from cloud edge	2.38%	0.75%
Straylight contributor	**Relative contribution to the total straylight budget error**	
Double reflections (ghost)		
Telescope	0.3%	
Spectrometer	10.4%	
Surface roughness scatter		
Telescope	0.9%	
Spectrometer	12.0%	
Grating	12.6%	
Particulate contamination scatter		
Telescope	3.6%	
Spectrometer	55.7%	
Structure scatter		
Spectrometer	0.5%	
Diffraction		
Telescope	4%	

Table 7.6. Top: Overview of the radiometric errors generated by in-field straylight of the FLORIS instrument in Concept A. Bottom: Major straylight contributors in Concept A. Concept B analysis shows a similar overall budget, though with different relative contributions owing to the different design of the instrument.

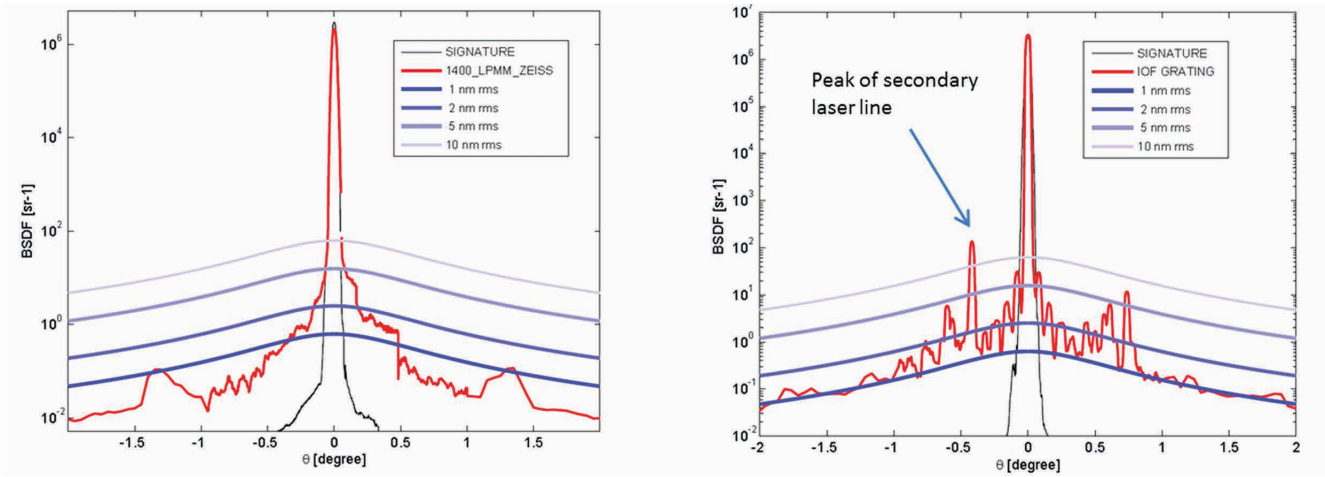

Figure 7.17. The BSDF of two different gratings from ZEISS (reflective grating on the left) and from IOF (transmission grating on the right). The corresponding BSDF functions of mirrors with different roughness are shown for comparison. (ESA)

activities. These requirements were also applied to the FLORIS EBB activities, and the first study has shown that they require very careful control throughout the entire on-ground characterisation of the instrument, as they are crucial for straylight performance. FLORIS is also equipped with dedicated band-pass filters (as mentioned in Chapter 5) such that out-of-band sensitivity remains below 1%.

In order to demonstrate and to establish the scattering properties of the gratings, several manufacturing runs were carried out during the pre-development phase. The corresponding scattering properties were characterised by establishing the Bidirectional Scattering Distribution Function (BSDF). The BSDFs of several gratings have been measured in ESA's European Space Research and Technology Centre (ESTEC) laboratories and some of the results are shown in Fig. 7.17 for gratings from potential suppliers such as ZEISS and Fraunhofer IOF, both in Germany. It was confirmed that the corresponding roughness of the grating is mostly close to 1 nm (as assumed in the above calculations) and therefore acceptable.

7.2.2.3.5 Out-of-field straylight

Out-of-field straylight is a concern mostly for the telescope. The expected errors generated by out-of-field cloud radiance are less than 0.1%. The baffle length has been investigated preliminarily for two cases (250 mm and 500 mm) for Concept A, showing error differences of about 0.05% for scenes at reference radiance. Presently, both Concepts A and B designs foresee a 500 mm length baffle as a comfortable allocation. However, it may be appropriate to consider shorter baffle lengths up to 250 mm in order to reduce the instrument envelope for accommodation on the Myriade Evolution platform. More detailed analyses of out-of-field straylight are currently planned within the development of the FLORIS optical models.

7.2.3 FLEX-End-to-End Mission Simulator Level-1b Performance

7.2.3.1 Geometric performance

7.2.3.1.1 Spatial sampling

The FLORIS SSD can be studied by using the synthetic Level-1b geolocated data provided by FLEX-E on a full-swath (i.e. 150 km) simulation. The simulation includes all the geolocation errors and effects indicated in Table 7.1 (Section 7.1.6). By transforming the geolocation data from latitude/longitude coordinates into UTM coordinates, the distance between two consecutive FLORIS pixels across-track (ACT) and along-track (ALT) can be calculated. The mean and standard deviation of these distances provides an estimate of the SSD in the simulated data of 297.3±0.9 m (ACT) and 304±1 m (ALT) which are compatible with the 300×300 m^2 mission requirement.

7.2.3.1.2 Geolocation accuracy

The geolocation accuracy performance at Level-1b can also be studied with FLEX-E by determining the absolute errors from the reference and estimated (i.e. after Level-1b geolocation) pixel coordinates. An absolute error of 12±4 m is obtained, fulfilling the specification of 0.4 SSD (120 m). The simulation includes the errors in the geolocation accuracy due to the typical temporal simulations of the estimated attitude and orbit. An error of 100 µm in the knowledge of the FLORIS mounting Euler angles reduces the geolocation to ~90 m, which is still within the specifications.

For both Concepts A and B the geolocation requirement can be met with ample margins at Level-1b, even without the use of ground control points, by use of recurring avionics. The performance obtained is about 90 m, against a specification of 120 m. The pointing requirement of 1 km, derived from the FLORIS swath inclusion in the OLCI camera-4 swath and temporal coregistration between FLEX and Sentinel-3 observations, can also be met with margins.

7.2.3.2 Spectral performance

7.2.3.2.1 Spectral sampling and spectral resolution

The realisation of the required spectral resolution (SR) and sampling (SSI) for FLORIS-HR and FLORIS-LR spectrometers can be checked from the simulated Level-1b data according to the scenario described in Section 7.1.6, which applies the expected FLORIS ISRF and performs the onboard binning of the spectral channels. The Level-1b data provided by FLEX-E includes the central wavelength position and FWHM of each spectral channel after the onboard binning. By calculating the differences of wavelength between consecutive channels, the SSI can be calculated.

The SSI and SR for both FLORIS spectrometers are given in Fig. 7.18 where it is shown that the instrument simulation in FLEX-E is compatible with the Phase-A/B1 performance analysis and fulfils the design requirements. The subplots Fig. 7.18 (left) show that FLORIS-HR has an intrinsic SSI of 0.1 nm and SR of 0.3 nm before the spectral channels are binned. After onboard binning, the SSI for FLORIS-HR increases to 0.5 nm with a resolution of ~0.5 nm. As with FLORIS-LR, the onboard binning reduces the sampling to 2 nm from an intrinsic sampling of 0.33 nm while keeping the resolution at 2 nm.

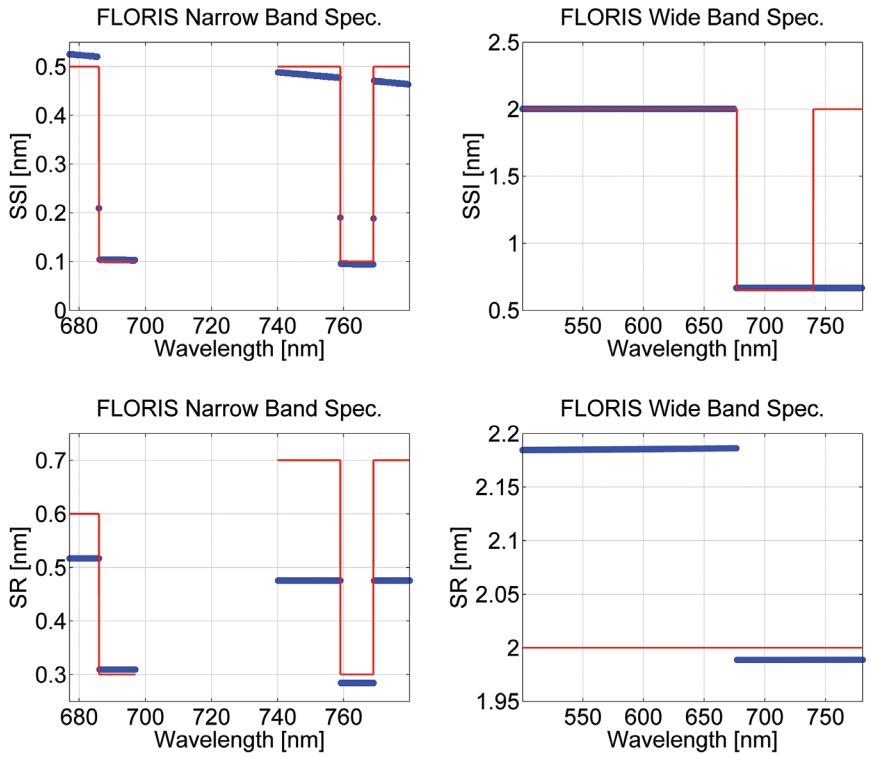

Figure 7.18. The blue lines show FLORIS SSI (top) and SR (bottom) evaluated for the HR and LR spectrometers (left and right, respectively) and compared against the requirement (red line). (ESA)

7.2.3.2.2 Spectral coregistration

The spectral smile can be seen by the change of the wavelength position of the spectral channels across the swath. Figure 7.19 analyses the spectral smile for the FLORIS-HR (left) and FLORIS–LR (right) spectrometers by running a full-swath simulation with the same OSS configuration as in the synthetic scenario explained in Section 7.1.6 (see Table 7.1), which includes the spectral stability effects.

The spectral smile shows parabolic behaviour (symmetrical with respect to the swath centre), and performance summarised in Table 7.7.

The spectral coregistration results obtained by FLEX-E are compatible with the Concept A results both by the quadratic shape of the spectral smile and the performance results. The current processing of the raw data includes the correction of the spectral smile for the HR and LR spectrometers.

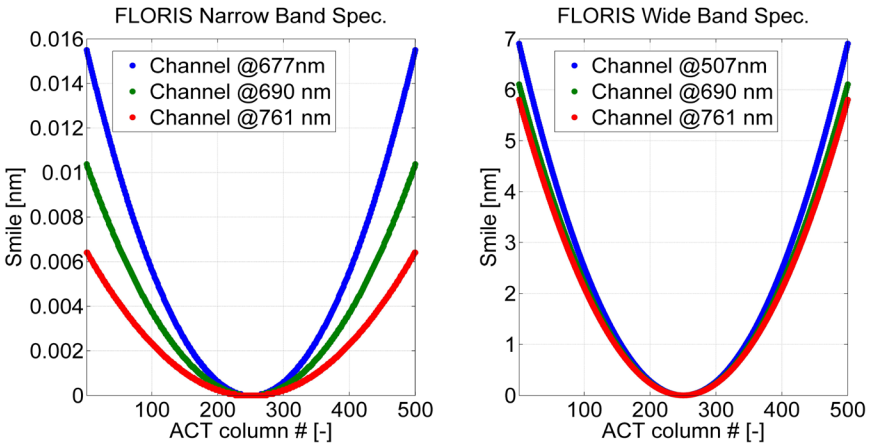

Figure 7.19. Spectral smile effect for FLORIS-HR (left) and FLORIS-LR (right) spectrometers evaluated at three spectral channels. (ESA)

Table 7.7. FLORIS spectral coregistration performance from the FLEX-E Level-1b synthetic data compared to the requirements.

	Smile performance	Requirement
FLORIS-HR	< 0.01 nm for non-binned channels (i.e. SSI=0.1 nm) < 0.015 nm for binned channels (i.e. SSI=0.5 nm)	< 0.1 SSI
FLORIS-LR	< 7 nm	Not applicable

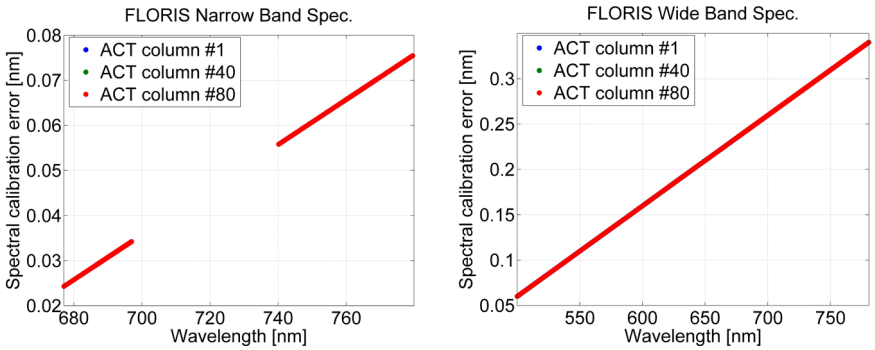

Figure 7.20. Level-1b spectral calibration errors for the FLORIS-HR (left) and the FLORIS-LR (right) spectrometers evaluated at three across-track columns of the detector (overlapped blue, green and red dots). (ESA)

7.2.3.2.3 Spectral calibration

The errors introduced by the spectral calibration for Level-1b data are shown in Fig. 7.20. In line with Table 7.1, these errors include the spectral stability effects.The knowledge of the barycentre wavelength at each spectral channel is obtained by calculating the absolute difference between the reference wavelength position (i.e. that used for the convolution of the high-spectral-resolution scene within the FLO module) and the estimated wavelength position obtained after spectral calibration in the L1F module. The absolute difference is calculated for all the spectral channels and for a set of three columns across-track to see the influence of the spectral smile.

The results indicate that the spectral calibration errors are linear, which is typical of imaging spectrometers. The errors are below 0.08 nm and 0.35 nm for the FLORIS-HR and FLORIS-LR spectrometers, respectively. Both are within the requirements (0.325 nm and 0.5 nm, respectively). The plots show that the calibration error linear curves for the three selected across-track pixels are overlapped, indicating that the spectral smile effect is well characterised at Level-1b.

7.2.3.2.4 Radiometric performance

The FLEX simulator can study the radiometric performance by analysing the SNR figures and the radiometric calibration error. The radiometric performance analysis is based on the simulation results provided by the scenario configuration explained in Section 7.1.6. Figure 7.21 shows the instrument noise effect at the spatial domain for the FLORIS-HR spectrometer at the O_2-A and O_2-B spectral channels (top and bottom rows, respectively).

The relative error map shows the reality of the noise implemented in the simulator, composed of random contributions as well as systematic effects (e.g. the visible vertical fixed pattern noise). The absolute error maps show how, indeed, the instrument noise is higher at higher radiance levels. This is particularly clear for the bright cloud pixels.

Notice that the resulting error maps include both random and systematic errors, mostly driven by instrument effects. In addition to individual random errors for each pixel (modelled by using Monte Carlo methods), scene-level

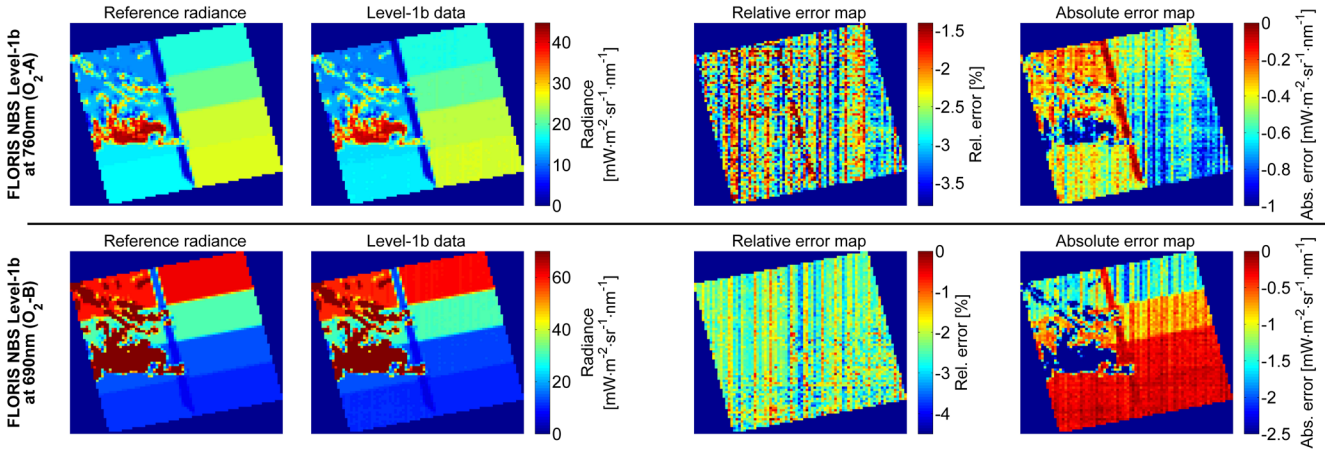

Figure 7.21. FLORIS Level-1b simulated performance at spatial domain for the high-resolution spectrometer at O_2-A (top) and O_2-B (bottom) spectral channels. From left to right: reference radiance after convolution of the scene by the ideal PSF and ISRF; Level-1b data after recalibration of the raw data; relative error map between reference and Level-1b radiance; and absolute error map between reference and Level-1b radiance. (University of Valencia)

effects such as straylight, smile and heterogeneity effects in individual detector pixels are explicitly modelled. The resulting error map reproduces the error level and spatial pattern expected for real FLEX images.

7.2.3.2.5 Signal-to-noise ratio

The high SNR requested for FLORIS is one of the critical aspects of the mission. To test if the implemented concept fulfils the requirements, a completely homogeneous scene was generated by FLEX-E. The scene consists of a 20×20 km^2 area where every grid element has the reference radiance spectrum. By introducing a homogeneous scene, the synthetic Level-1b data are only affected by the instrument noise, including all the systematic effects and spectral smile, as indicated in Table 7.1. The SNR (see Fig. 7.22) is derived from the Level-1b data at each column by dividing the mean radiance level by its standard deviation for the whole spectral channel. By averaging the resulting SNR for all the columns, the dispersion of the results are reduced, yielding a more precise characterisation of the instrument SNR.

Figure 7.22 shows how the SNR derived from simulated data for both FLORIS spectrometers matches the requirements for a fluorescence retrieval error of 10% at the reference radiance. The simulated results are as very compatible with the theoretical results given in Fig. 7.13 and Fig. 7.14.

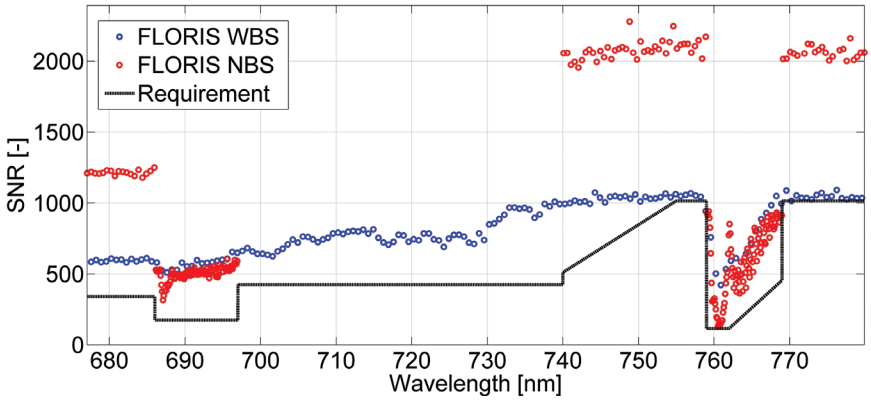

Figure 7.22. SNR for the FLORIS-HR (red) and FLORIS-LR (blue) spectrometers compared with the requirements (black-dashed line). (University of Valencia)

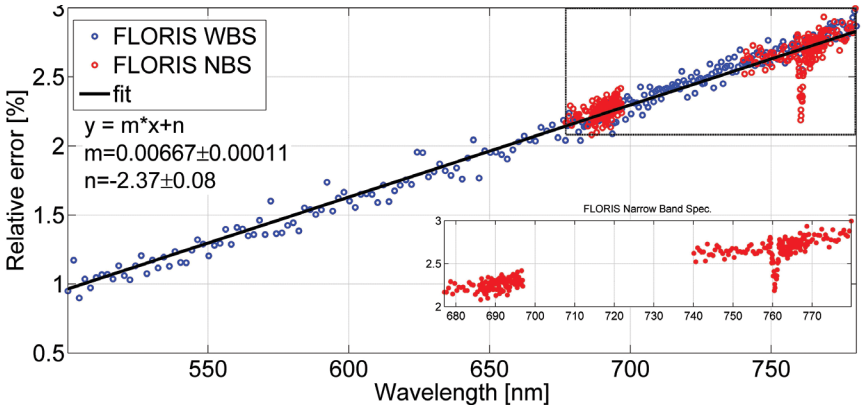

Figure 7.23. FLORIS Level -1b radiometric calibration errors for the FLORIS-HR (red) and FLORIS-LR (blue) spectrometers with the best linear fit (black line). (University of Valencia)

7.2.3.2.6 Absolute radiometric accuracy

The suitability of the implemented radiometric calibration errors within FLEX-E can be tested by comparing them with the required accuracy. The relative error between the reference data and the synthetic Level-1b data can be obtained for all the along-track pixels at all the spectral channels. By computing the mean of this relative error map, the absolute and relative radiometric accuracies can be determined (see Fig. 7.23). These calculations have been performed using the test scenario described in Section 7.1.1 as it includes all the random and systematic instrument noise, as well as all the radiometric and spectral calibration errors. The different instrument noise, non-uniformity effects and calibration errors lead to an absolute radiometric accuracy of 2.2±0.2% with a relative radiometric accuracy of 0.93±0.02%, i.e. a variation between 500 m and 780 nm from ~1% to ~3%. These error figures are compatible with the requirements for the absolute (3% goal, 5% threshold) and relative (1%) radiometric accuracies.

7.2.3.2.7 Level-1b performance summary

Altogether, the radiometric, spectral and geometric performance analysis by using the FLEX simulator indicates that the FLEX/FLORIS concept fulfils the requirements for a successful retrieval of sub-induced chlorophyll fluorescence retrieval. In addition, the results stated in the previous paragraphs stress the level of detail of the instrument noise, systematic effects and calibration errors implemented in the FLEX simulator. Having a simulator tool with full end-to-end capabilities, which is realistic enough to simulate the mission concept, allows an assessment study of the quality of the implemented Level-2 algorithms and retrieved fluorescence products to be performed.

7.3 Level-2 Retrieval Performance

The Level-2 retrieval performance assessment focuses on the quality of the following retrieved fluorescence products:

— total fluorescence integrated value
— first local maximum of the fluorescence curve (at ~690 nm)
— second local maximum of the fluorescence curve (at ~740 nm).

The Level-2 retrieval performance analysis is based on the use of the FLEX-E software tool (Section 7.3.1). The simulated performance results on the Level-2 products shown in this section are complemented with different field campaigns using the HyPlant airborne demonstrator data (see Section 7.3.2).

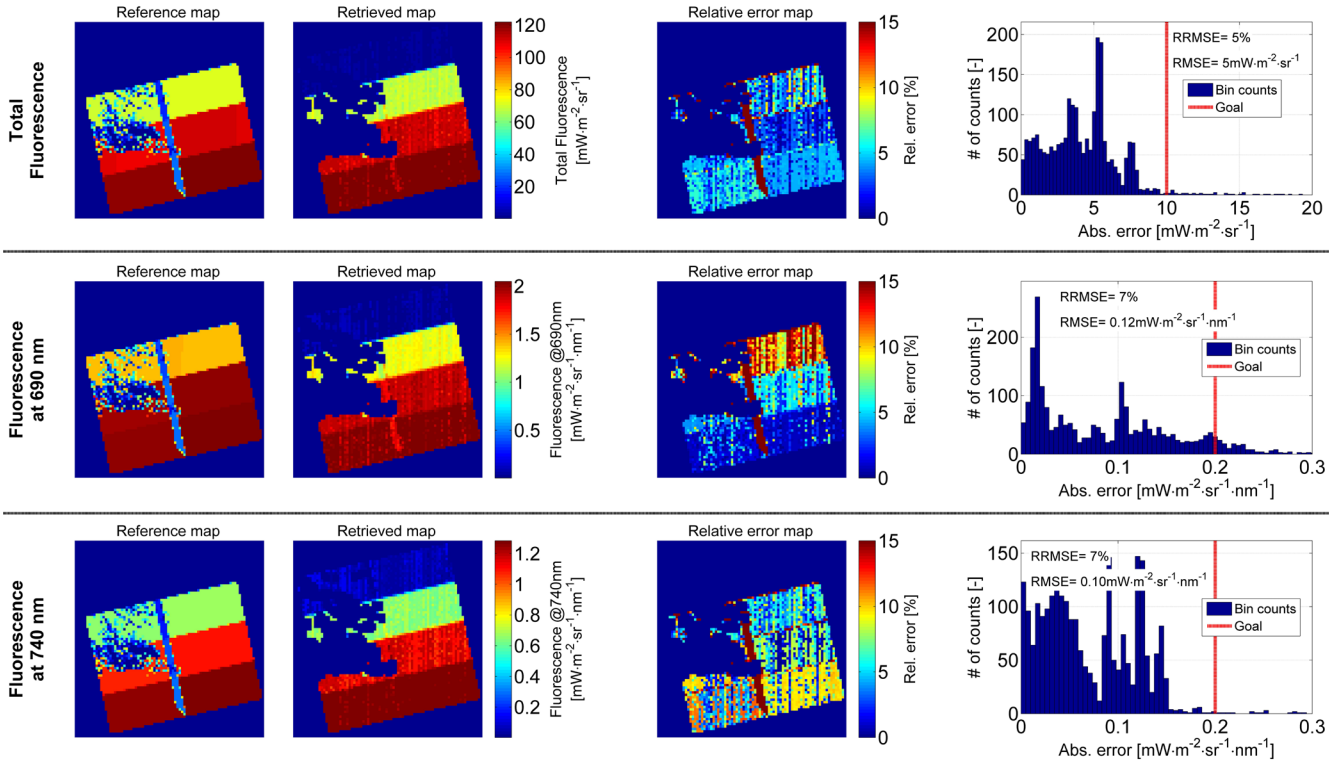

Figure 7.24. Level-2 performance on the total fluorescence (top row); fluorescence emission at 690 nm (mid-row); and fluorescence emission at 740 nm (bottom row). For each fluorescence product, each subplot shows: reference-retrieved fluorescence map (first-second columns); relative error map between reference and retrieved fluorescence (third column); and histogram of the absolute error map (fourth column). (University of Valencia)

7.3.1 FLEX-End-to-End Mission Simulator Level-2 Performance

The FLEX-E software tool can be used to determine the expected Level-2 performance for the FLEX mission. On one hand, this is due to the complexity of the simulated environmental effects such as the natural variability of the biophysical/atmospheric parameters, the use of state-of-the-art radiative transfer models or the consideration of the BRDF effect. On the other hand, the implemented instrument and Level-1b calibration effects reproduce, in detail, the actual instrument configuration as shown in Section 7.2.3. In addition, the Level-2 processing within FLEX-E is representative of the expected ground processing and deals with effects such as the ISRF knowledge errors, cross-calibration between OLCI and FLORIS, and the synergic Level-2 retrieval algorithm detailed in Chapter 6.

The performance of the fluorescence retrieval is first shown with the results obtained over the synthetic test scenario described in Section 7.1.6. A dataset consisting of a set of simulated images is then used for analysis of the fluorescence retrieval performance under different illumination and atmospheric conditions.

7.3.1.1 Synthetic test scenario results

Figure 7.24 shows the Level-2 simulated performance for the three fluorescence products at three typical fluorescence values (determined by each vegetation class) and two extreme surface height values.

A qualitative inspection of the results indicates that the instrument random noise and systematic bias do affect the retrieved fluorescence product maps. Nevertheless, the retrieved spatial distribution and values are compatible with the reference maps. The spatial distribution of the relative

	RMSE & Abs. error (mean/median/std)	RRMSE & Rel. error (mean/median/std) [%]
Total fluorescence emission	5 / 4 /4 /3 mW m^{-2} sr^{-1}	5 / 4 / 4 /3
Fluorescence emission at first peak	0.12 / 0.09 / 0.08 / 0.08 mW m^{-2} sr^{-1} nm^{-1}	7 / 5 / 4 /5
Fluorescence emission at second peak	0.10 / 0.08 / 0.06 / 0.06 mW m^{-2} sr^{-1} nm^{-1}	7 / 6 / 7 / 4

Table 7.8. Fluorescence product retrieval accuracy for the FLEX simulator performance analysis.

Case #	#1	#2	#3	#4	#5	#6
Aerosol type/aerosol optical thickness	Rural/ 0.05	Rural/ 0.05	Rural/ 0.05	Rural/ 0.25	Maritime/ 0.25	Urban/ 0.25
Illumination Solar Zenith Angle (SZA)[°]	Low (60)	Mid (45)	High (25)	Mid (45)	Mid (45)	Mid (45)

Table 7.9. Definitions of the cases run for the sensitivity analysis.

Vegetation class ID	#1	#2	#3	#3	#5	Bare soil
LAI [-] / Chl [g cm^{-2}]	5 / 20	1 / 80	5 / 80	3 / 40	1 / 20	N.A.
Fluorescent target (Yes/No)	Yes	Yes	Yes	Yes	Yes	No

Table 7.10. Land-cover class map configuration for the sensitivity analysis.

errors (third column) shows that the retrieval method performs better at the first peak on pixels with higher fluorescence emission, while there is no significant difference in the second peak as it is affected by higher noise. In addition, the longer atmospheric path within the O_2 absorption, caused by a lower surface altitude, increases the accuracy slightly (e.g. ~5% at 0 km and ~9% at 2 km for the second peak in the stripe with higher fluorescence). The areas with shadows show accuracy beyond the 20% threshold. The statistical analysis of the absolute errors (histogram in the fourth column) indicates that, overall, the retrieval is performed with accuracy better than the requirements (0.2 mW m^{-2} sr^{-1} nm^{-1} goal) for all three fluorescence products.

The performance of the Level-2 retrieval is summarised in Table 7.8 through the absolute and relative errors for each fluorescence product, indicating that the retrieval and mission concept fulfil the mission requirements.

7.3.1.2 Multiple image dataset results

Complementing the results on the synthetic test scenario given in the previous section, the FLEX-E tool is used for a performance analysis of the retrieval for a simulated image dataset consisting of six images with a varying configuration of the aerosol type and illumination conditions (Table 7.9). For each simulated image, all the instrument noise and Level-1b calibration errors as indicated in Table 7.1 (Section 7.1.6) have been included.

Each image consists of a cloud free scene at 0 km constant surface elevation and a land cover class map made of six different horizontal stripes defined as in Table 7.10. Among the different land cover classes, Vegetation classes #1–5 are vegetation targets with fluorescence emissions ranging from low to high. Cases Veg. #1 and #2 are considered as two extreme cases, given the combination of high-low LAI and Chlorophyll. A Bare Soil case is included in the analysis as a reference non-fluorescent target.

The combination of the six land cover classes with the various illumination and aerosol conditions makes a total of 36 different fluorescence levels. This

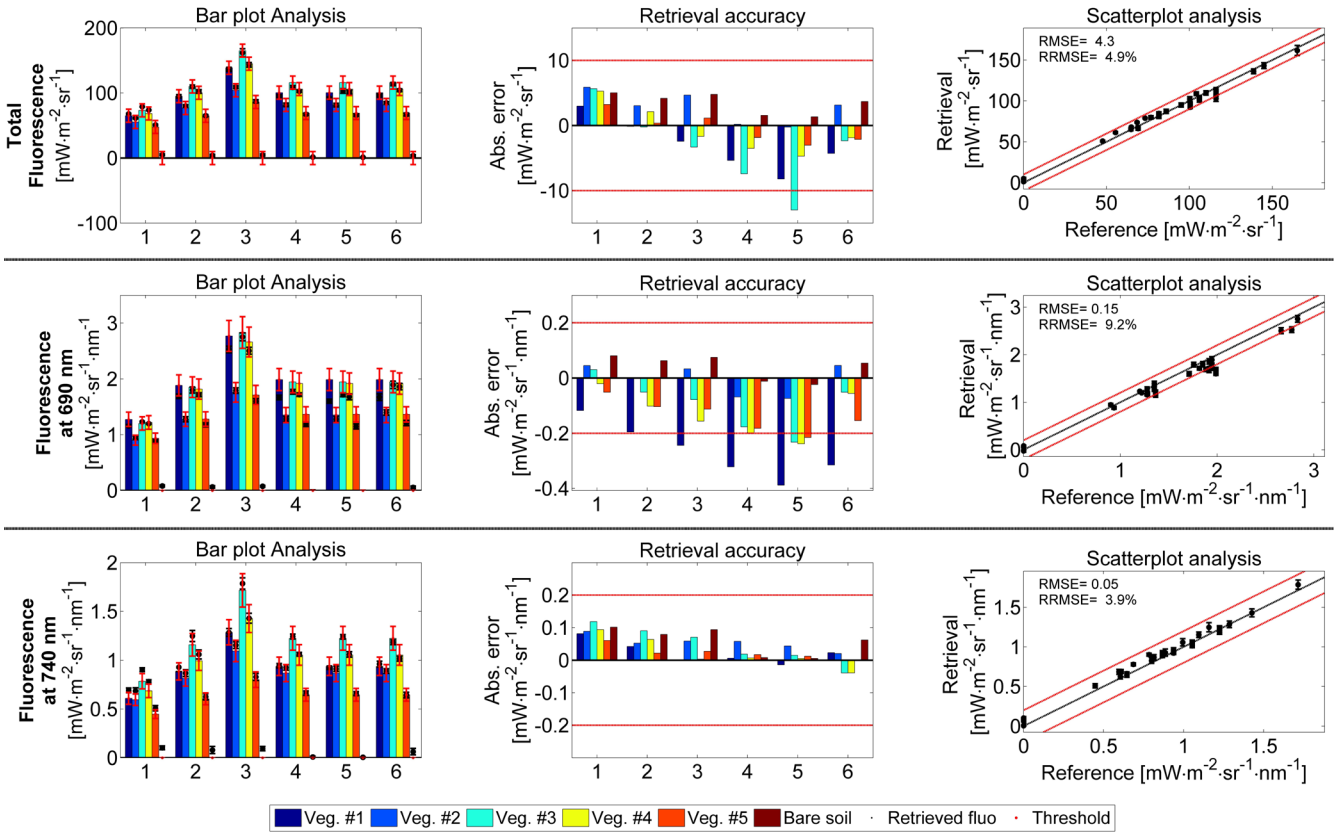

Figure 7.25. Sensitivity analysis for the total fluorescence emission (top row), fluorescence at 690 nm (mid-row) and fluorescence at 740 nm (bottom row). (University of Valencia)

allows the robustness of the fluorescence retrieval and suitability of the mission concept to be analysed under different ranges of fluorescence, illumination and atmospheric conditions for a realistic configuration of the actual FLEX platform and FLORIS instrument.

Figure 7.25 shows the results from the analysis of the image dataset by comparing (for each image) the average of the retrieved fluorescence at each land-cover class with its reference value. The products analysed are the total fluorescence (top row), fluorescence at the first peak (middle row) and fluorescence at the second peak (bottom row). From left to right, the following results are provided:

— Bar plot analysis: the retrieved values (black points) are compared with the reference values (bars) with the precision of the retrieval indicated with black error bars. The red error bars indicate the goal accuracy requirement

— Retrieval accuracy: presented as the absolute error between the reference and retrieved values with the red-dashed lines indicating the goal accuracy requirements

— Scatterplot of the retrieved values against the reference fluorescence. The lines indicate the ideal retrieval (black) and the required goal accuracies (red)

The results shown in Fig. 7.25 indicate that the retrieval is within the 0.2 mW m^{-2} sr^{-1} nm^{-1} goal accuracy in most cases for the various illumination and atmospheric conditions. The overall results are summarised in Table 7.11.

Table 7.11. Sensitivity analysis results for the fluorescence products retrieval accuracy.

	RMSE [mW m^{-2} sr^{-1}]	RRMSE [%]
Total fluorescence emission	4	5
Fluorescence emission at first peak	0.15	9
Fluorescence emission at second peak	0.05	4

Some conclusions can be derived from the analysis of the results:

— The comparison of the three first cases ranging from low to high illumination shows that the retrieval performs slightly lower for the lower illumination level. A lower SZA implies a lower fluorescence signal. This is particularly relevant within the second peak of the fluorescence emission curve

— Evaluation of the test cases #4 to #6 indicates that the atmospheric correction is performing successfully under different aerosol conditions. The performance is, nevertheless, lower when compared with case #2 (same illumination but lower aerosol content), mostly for the first fluorescence peak, owing to the higher impact of the aerosol characterisation in the red wavelength range

— For the non-fluorescent bare soil target, the retrieved fluorescence is <0.1 mW m^{-2} sr^{-1} nm^{-1}, which is better than the threshold requirements

— The retrieval of the first fluorescence peak on the target Veg. #1 appears to be underperforming systematically. This is due to the poor fitting of the polynomial modelling of the reflectance around the red spectral range

In addition to the analysis of the fluorescence products, the generated image set has been used to study the retrieval of the Photochemical Reflectance Index (PRI) (see Fig. 7.26). The results show that the PRI is retrieved with a mean absolute error of 0.013 owing to the error propagation of the atmospheric correction. The scatterplot, nevertheless, shows good linear agreement for the different range of values except for three points with a reference PRI value of 0.15–0.17. The bar-plot analysis shows that these three points correspond to the image generated with urban aerosols, for which the atmospheric correction is obtained with lower accuracy.

Overall, the use of FLEX-E demonstrated that the implemented Level-2 algorithms satisfy the required accuracies for the retrieval of fluorescence products simulating a realistic instrument configuration with the expected noise and calibration errors.

7.3.2 Complementary Level-2 Performance: Airborne Field Campaigns

7.3.2.1 Field campaign results

The synthetic results on the Level-2 performance using the FLEX-E software tool were complemented with a set of dedicated field campaigns where the Hyplant airborne demonstrator was employed. Several maps of fluorescence were calculated from HyPlant data (Fig. 7.25). Flight data were acquired from an altitude of 600 metres and fluorescence retrieval was based on an optimised atmospheric correction (Rascher et al., 2015). Fluorescence maps were produced for different ecosystems ranging from agricultural areas to natural and managed broadleaf and needle-leaf forests. In general, dense agricultural fields (Fig. 7.27, left) show fluorescence values that are higher than broadleaf

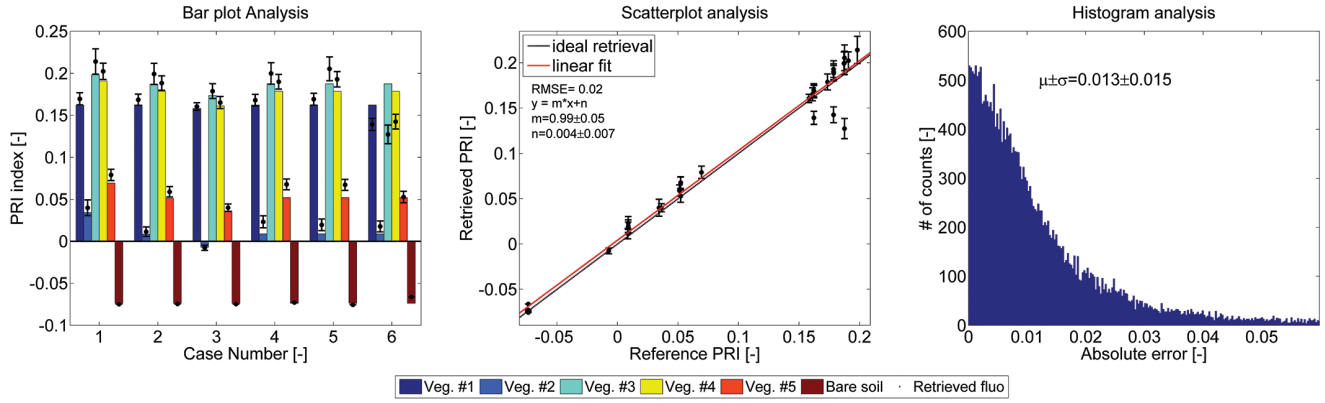

Figure 7.26. Sensitivity analysis for the PRI. (University of Valencia)

and needle-leaf forests, which were confirmed by ground-based top-of-canopy measurements.

HyPlant data were compared to ground measurements using the high-resolution measurement boxes (Cogliati et al., 2015). Readings at ground reference points were compared to simultaneous airborne measurements. Fluorescence at O_2-A bands was compared as this provides the best estimate of combined sensor and atmospheric variability. Ground and airborne data had negligible bias and the mean absolute error (RMSE) was 0.166 mW m^{-2} sr^{-1} nm^{-1}, thus below the specified threshold of 0.2 mW m^{-2} sr^{-1} nm^{-1} (Fig. 7.28). Further details can be found in Rascher et al., 2015.

In order to show the complementarity of information provided by reflectance and fluorescence, a HyPlant image over the agricultural area of Seelhausen was used. The image was collected at the end of August when the green crops were sugar beet with some corn and grassland. Figure 7.29 shows the fluorescence maps compared with supplementary reflectance indexes and vegetation products. There are two noteworthy features:

Figure 7.27. Fluorescence at 760 nm (F_{760}) from different ecosystems using HyPlant. High-performance reflectance data were obtained from 600 metres over Seelhausen, Germany, representing a typical agricultural area (left); over Duke forest, North Carolina, US, that is a mix of hardwood and loblolly pine (middle); over Parker Track, North Carolina, US, that represents an intensively managed pine forest. Fluorescence emission was quantified in the oxygen absorption band O_2-A, i.e. at 760 nm. Several flight lines were stitched for the agricultural map. These maps demonstrate the added value of HyPlant's high spatial resolution to resolve spatial heterogeneity of managed and natural ecosystems. The blue to red colour scale ranges from 0–2 mW m^{-2} sr–1 nm^{-1}. (Forschungszentrum Jülich)

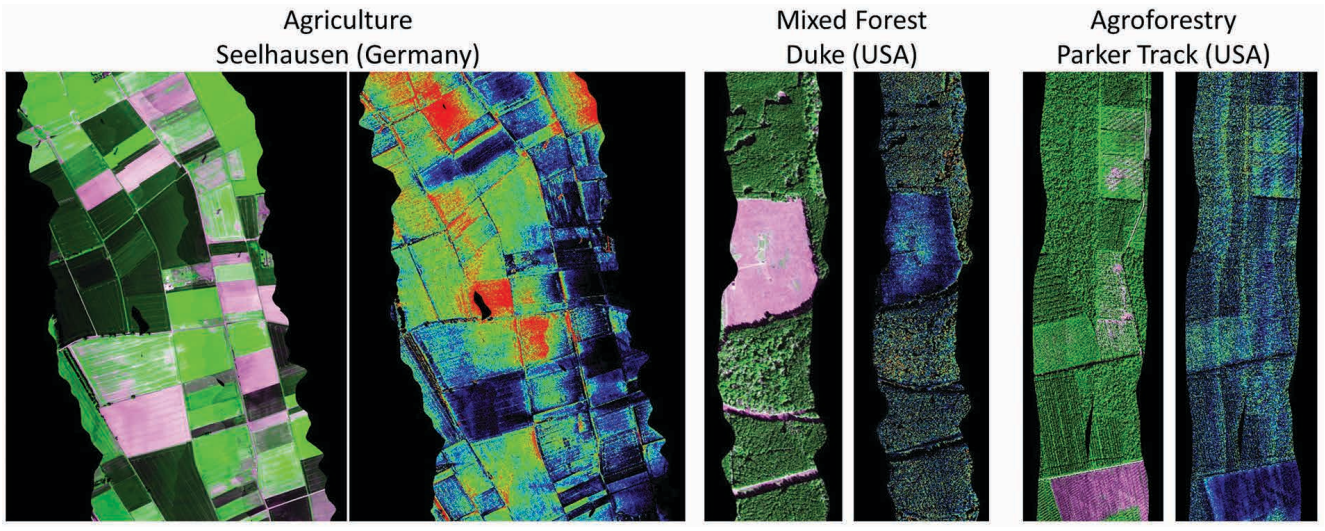

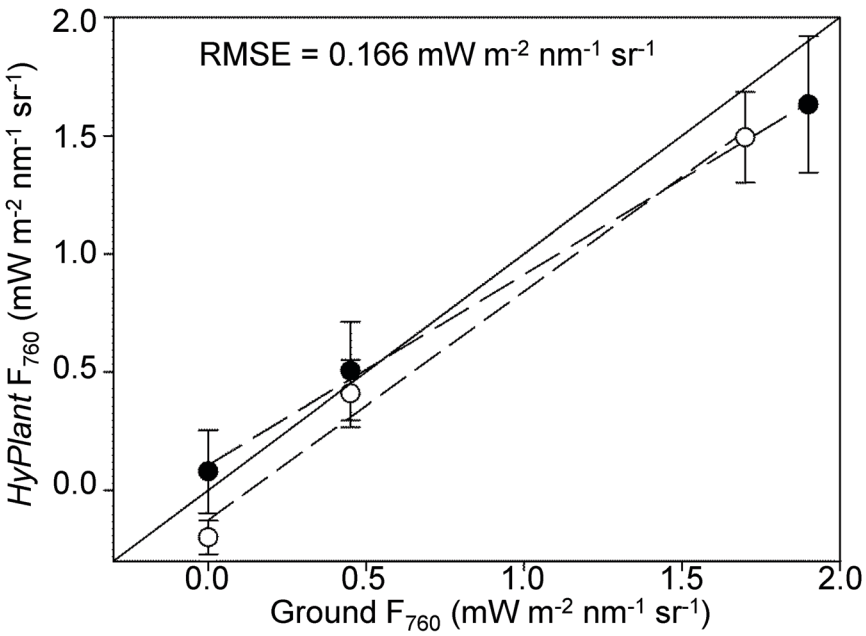

Figure 7.28. Comparison between ground and airborne measurements of fluorescence taken at flight altitudes of ~600 m (solid circles) and ~1800 m (open circles). Ground measurements from the high-resolution spectrometers were used as reference to estimate the error of airborne retrieval. Absolute error of the airborne retrievals of F_{760}, as estimated across different ecosystems, was 0.166 mW m^{-2} sr^{-1} nm^{-1} and therefore below the specified error of 0.2 mW m^{-2} sr^{-1} nm^{-1}. Based on Rascher et al., 2015.

— F_{760} values from non-vegetated fields are very close to zero. There is no fluorescence signal from soils or other surfaces. This underlines the selectiveness of fluorescence for photosynthetically active vegetation only.

— The classical vegetation products, such as PRI, leaf chlorophyll level, normalised difference vegetation index (NDVI) and PRI show rather similar pictures. They all represent the greenness of the vegetation and the amount of plant biomass. The fluorescence map clearly shows a different pattern. Only photosynthetically active fields have significant fluorescence emission.

From vegetation reflectance, different supplementary vegetation products will be derived as discussed in Chapters 3 and 4. Biophysical parameters such as LAI and leaf chlorophyll content (LCC) play two important roles within the framework of the FLEX mission concept. On the one hand, they can help in the interpretation of the information provided by fluorescence. On the other hand, these parameters might be used during the fluorescence retrieval process to constrain the fluorescence estimates.

7.3.2.2 Higher-level vegetation products

Higher-level vegetation products, such as vegetation stress detection, photosynthesis and GPP can be derived from FLEX measurements. These high-level products require fluorescence as the main input parameter, but they also rely on the availability of supplementary data that are either produced by the FLEX instrument, by Sentinel-3 or can be made available from other satellite missions.

To demonstrate the added value of the fluorescence products in combination with supplementary vegetation products, different approaches have been tested to derive and validate two representative high-level FLEX products. The following results are mainly based on outcomes of the FLEX photosynthesis study and the campaign results from the HyFLEX campaign in 2012 and 2014.

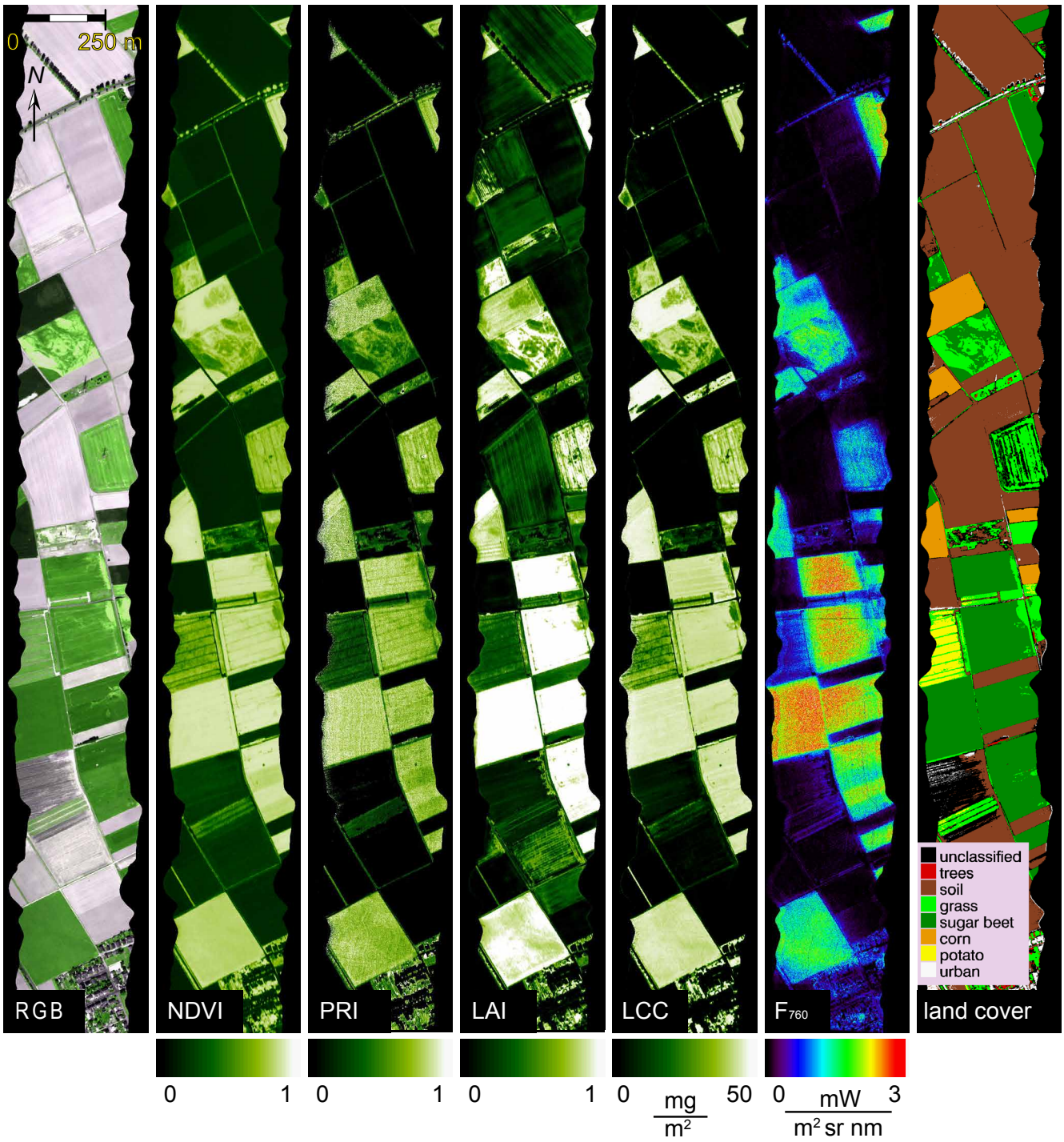

Figure 7.29. Spatial maps of established vegetation parameters and fluorescence at 760 nm (F_{760}) recorded in an agricultural area in Seelhausen, Germany, using the HyPlant airborne demonstrator. Maps were recorded from 600 metres elevation, and fluorescence was quantified as described by Rascher et al. (2015). (Based on Rascher et al., 2015)

7.3.2.3 Vegetation stress detection

Several studies investigated the performances of using F to detect vegetation stress conditions. For example, Meroni et al. (2008a, 2008b) focused on the capability of fluorescence and PRI to detect ozone stress under natural environmental conditions. Given the potential of fluorescence to quantitatively detect vegetation stress at leaf and potted canopy scale, a dedicated campaign (HyFlex) was organised in 2012 to prove that the two peaks of the

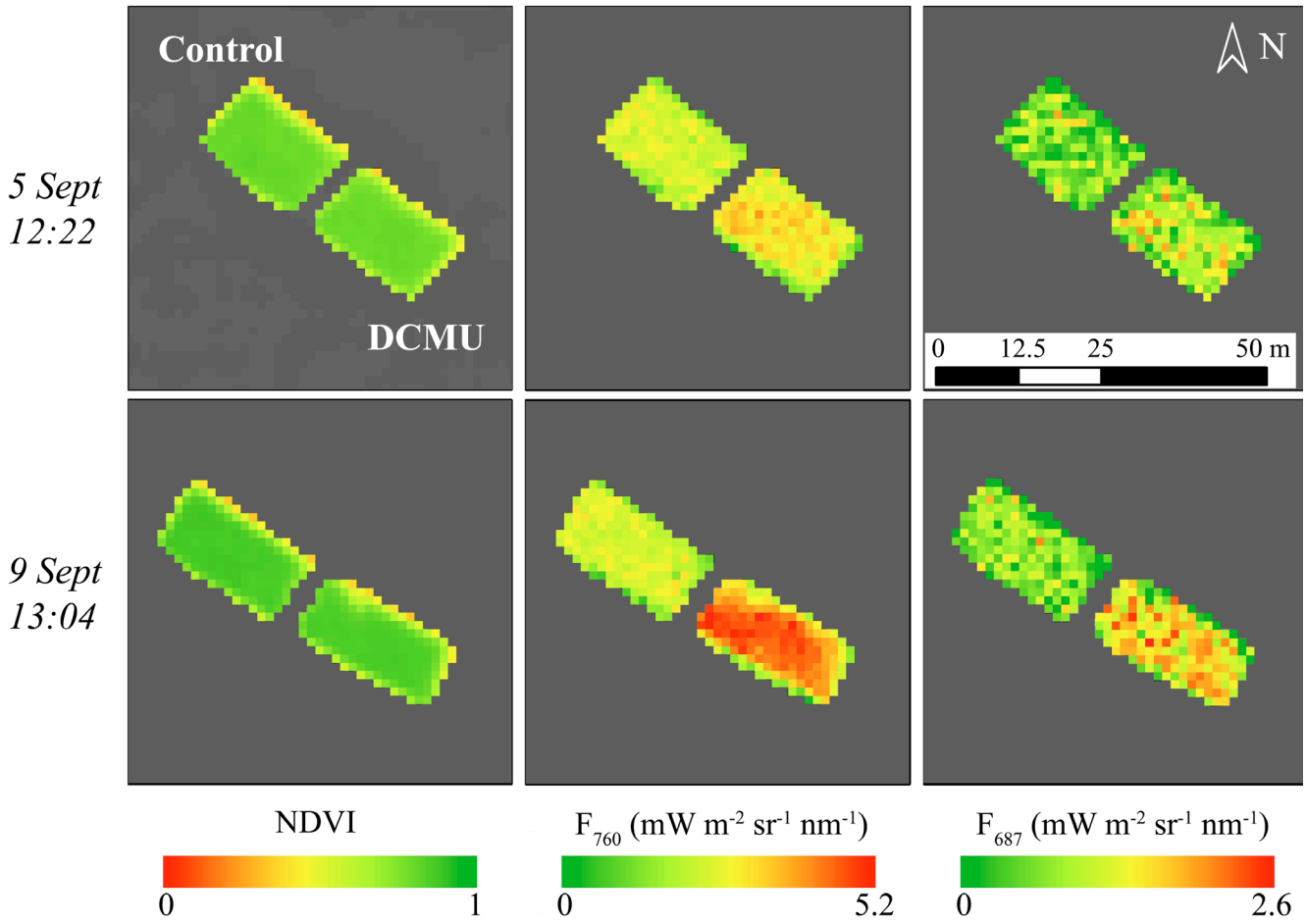

Figure 7.30. Control (left) and DCMU-treated (right) grass plots in airporne HyPlant images collected on two days. The NDVI, the far-red chlorophyll fluorescence (F_{760}) and the red chlorophyll fluorescence emission (F_{687}) are shown. The dates and time on the left indicate when the data were acquired. (modified from Rossini et al., 2015)

chlorophyll fluorescence spectrum can be accurately mapped from high-resolution radiance spectra and that the signal is linked to variations in actual photosynthetic efficiency due to the application of a stress factor. The HyPlant sensor was flown over two grass carpets, one of them treated with the herbicide 3-(3',4'-dichlorophenyl)-1,1-dimethylurea (DCMU), known to inhibit photosynthesis and enhance fluorescence emission. The herbicide application was performed twice: on 5 September 2012 (DCMU diluted to 10^{-5} M in 1% ethanol/water) and on 9 September with a herbicide concentration that was ten times higher. Airborne images were acquired on the same dates from an altitude of 600 m. F_{687} and F_{760} were significantly higher than the corresponding signal from an equivalent untreated grass carpet. The reflectance signal of the two grass carpets was indistinguishable, confirming that the fast dynamic changes in fluorescence emission were related to variations in the functional status of actual photosynthesis induced by the application of herbicide. With respect to the control, the magnitude of the F_{760} signal increased to 20% and 55% for the low- and high-concentration treatment, respectively, while it increased to 50% and 85% in the red region. This is due to the fact that F_{687} and a major portion of F_{760} originate from PS II at ambient temperatures and that only a small fraction of fluorescence from PS I contributes to F_{760}. Thus, it was confirmed that F_{687} is best suited to determine the photosynthetic efficiency modulated through e.g. optimised management or vegetation stress. The performances of the airborne demonstrator fulfil the research/observational objectives allowing the detection of differences in functioning of plants.

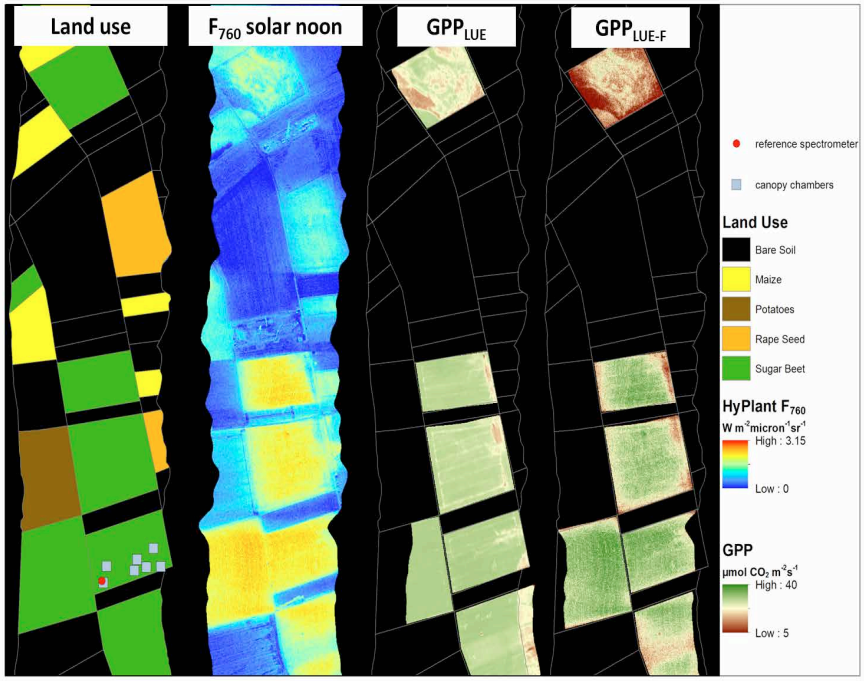

Figure 7.31. Comparison of GPP maps that are derived from LUE- and LUE-F model. The maps are from left to right: land cover classification, fluorescence at 760nm and estimated GPP using the classical Montheith approach and GPP using F. The locations of the canopy chambers that were used for validation are indicated by the blue squares. (Forschungszentrum Jülich)

7.3.2.4 Improvements of photosynthesis and GPP modelling

One of the most widely used methods to derive GPP from hyperspectral reflectance is the light use efficiency (LUE) model by Monteith (Monteith, 1972). Several studies have shown that it is possible to estimate GPP with the Monteith LUE approach, although this approach tends to overestimate carbon fluxes during low photosynthetic productivity and underestimate carbon fluxes during high photosynthetic productivity (Running et al., 2004; Turner et al., 2003; Xiao et al., 2008, 2004).

The possibility of estimating actual rates of photosynthesis (i.e. GPP) of sugar beet was evaluated by mapping chlorophyll fluorescence. First, GPP was calculated with the conventional LUE Monteith formula. The LUE model predicts GPP as a proportional relationship between the incident photosynthetically active radiation (PAR), the fraction of Absorbed Photosynthetically Active Radiation (fAPAR), estimated by NDVI, and a LUE value for this vegetation type (Running et al., 2004).

Secondly, the LUE model was modified to allow the use of fluorescence as a dynamic proxy for photosynthetic capacity in space and time (Wennberg et al., 2013). The adapted model is referred to as LUE-F model. Actual LUE was derived for both models from a reference canopy chamber. The LUE-F model additionally uses fluorescence maps as direct input parameters for the spatial distribution of plant status. The results of the two modelling approaches were compared and validated with independently recorded CO_2 uptake rate measurements derived from canopy chambers.

Using fluorescence to calculate GPP clearly provides different results from the traditional LUE model. GPP_{LUE-F} estimates show substantially greater variability between fields and patterns within single fields. GPP of bare soil or sparse vegetation is lower, and substantial between-field variability is detectable. In addition, field borders that are known to have lower GPP rates are also visible (Fig. 7.31).

The aircraft overpassed the study area three times (09:56, 11:50, 14:05 UTC). GPP derived from seven canopy chambers stationed within the flight line on a sugar beet field were compared with the estimated GPP from the two models. The results for the 21 samples are shown in Fig. 7.32. The coefficient of agreement of the LUE-F model (R^2) is, at 0.86, higher than the R^2 for the LUE

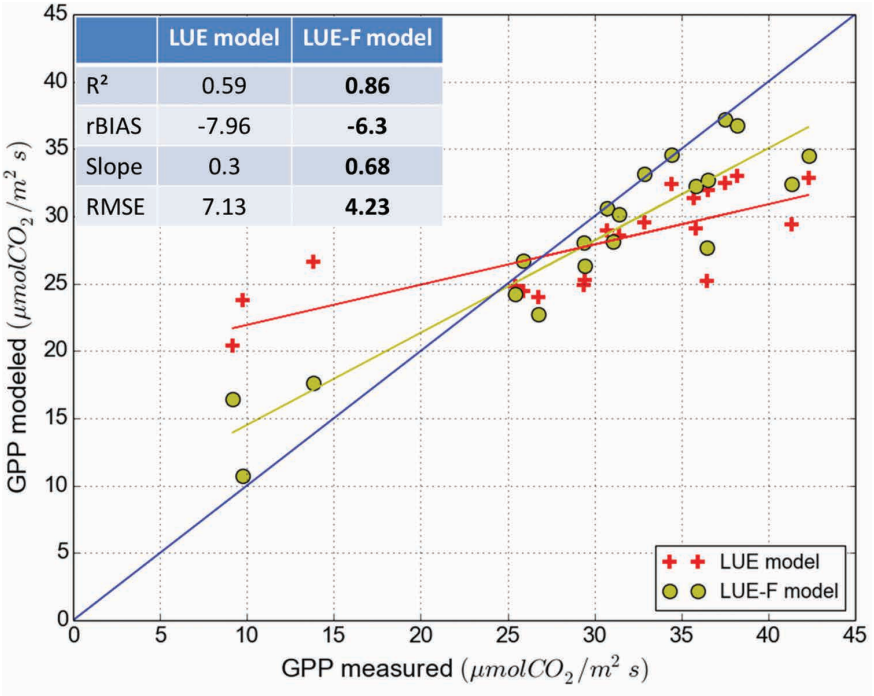

Figure 7.32. Relationship between the measured and estimated GPP for the LUE and LUE-F models with ground measurements of GPP. Ground reference measurements were derived from different canopy chamber measurements and airborne estimates of GPP were computed from HyPlant images. (Forschungszentrum Jülich)

model (0.72). Both methods underestimate GPP by around 6%, but the much higher slope of the LUE-F model (0.68 against 0.39) indicates that the F-based model captures much better high and low values of GPP. The root mean square error (RMSE) decreased from 6.23 µmol CO_2 m^{-2} s^{-1} for the LUE model to 4.23 µmol CO_2 m^{-2} s^{-1} for the LUE-F model.

These results demonstrate the potential for improving the prediction of actual rates of canopy photosynthesis and GPP. In particular, the spatio-temporal variability of green vegetation that adapts to the ever changing environmental conditions can be mapped. This will result in a fundamental new understanding of where and how vegetation reacts to the environment and will greatly improve our ability to predict how vegetation functions in times of global change.

→ MISSION CONTEXT

8. Mission Context

8.1 Global Context

8.1.1 Uniqueness of the FLEX Mission

FLEX is an advanced mission concept designed specifically for measuring vegetation chlorophyll fluorescence emission at spatial scales relevant to resource management requirements. The mission will be equipped to provide the most complete fluorescence retrievals of any current or planned satellite mission, along with all the critical auxiliary information needed for interpretation. In this regard, FLEX is unmatched by any other current or planned Earth observation mission (Fig. 8.1).

Preliminary space-based retrievals of far-red fluorescence have been reported from a few atmospheric missions operating at coarse spatial resolutions (≥30 km^2). These missions have included GOSAT (TANSO-FTS), MetOp (GOME-2) and Envisat (SCIAMACHY) (Garbulsky et al., 2014; Berry et al., 2013; Joiner et al., 2011, 2012, 2013, 2014; Frankenberg et al., 2011; Guanter et al., 2007, 2014b). Recently, NASA's OCO-2 mission was launched and will allow

Figure 8.1. Key characteristics and application potential of the FLEX mission concept compared to capabilities provided through other existing and future systems. (ESA/Forschungszentrum Jülich)

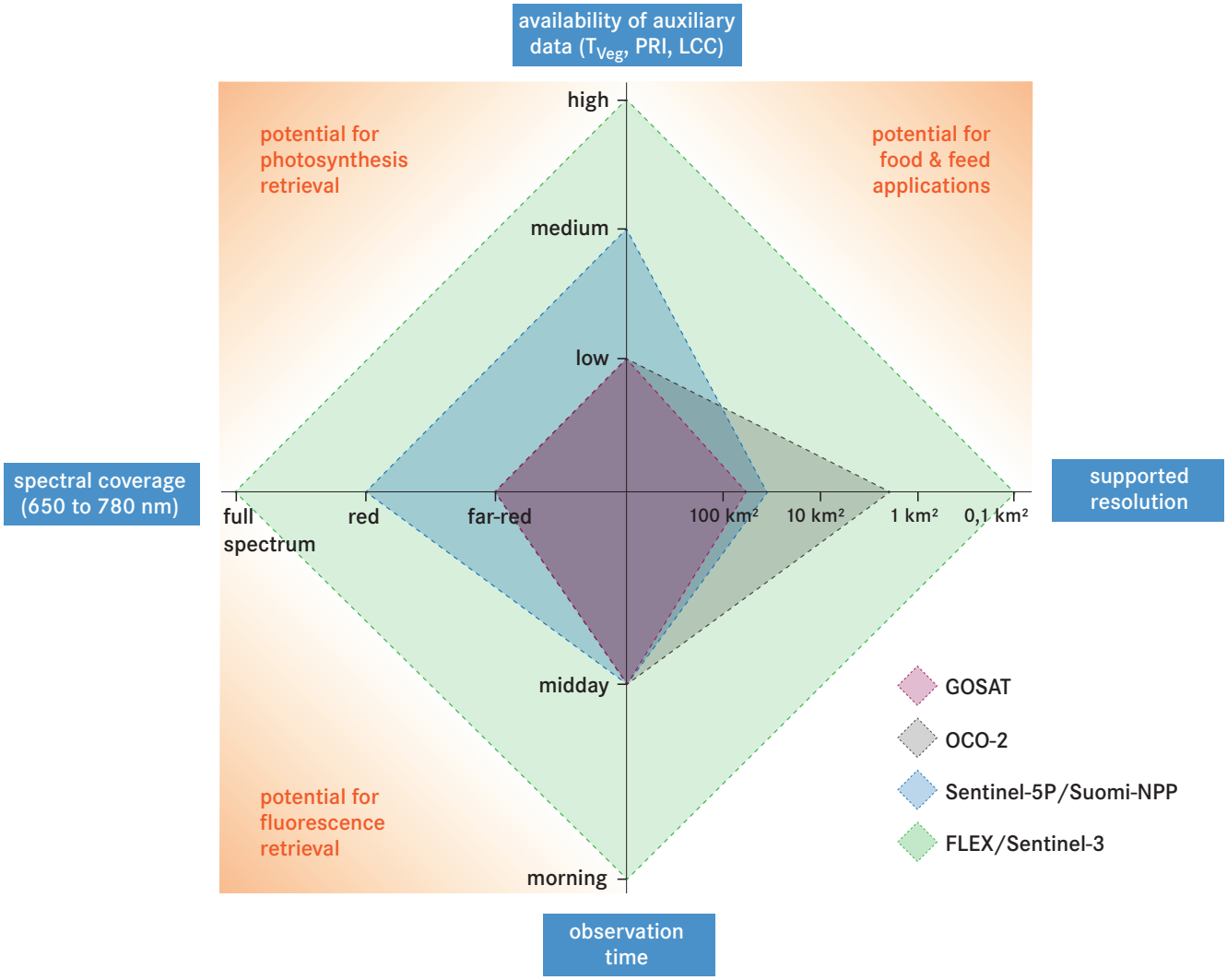

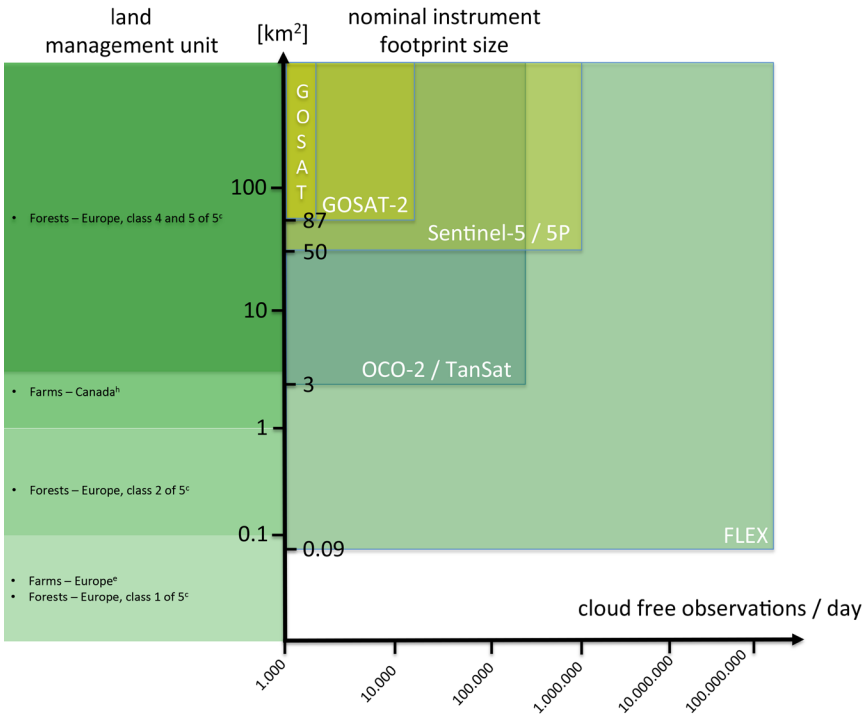

Figure 8.2. The FLEX mission concept provides measurements at a spatial resolution that will support the scale of individual management units with a sufficiently large number of cloud-free observations. No other current or planned mission concept addressing the retrieval of fluorescence can provide similar coverage. (ESA)

discontinuous (~3 km^2) spatial samples for fluorescence retrievals in the far-red spectrum only (Frankenberg et al., 2014) and without key ancillary vegetation information (surface temperature, Photochemical Reflectance Index (PRI), Leaf Area Index (LAI), etc.) to assist fluorescence interpretation for canopy photosynthesis and stress detection. This is significant because both red and far-red fluorescence, and ideally also the full fluorescence spectral emission and associated reflectance, are required to understand canopy carbon uptake and stress effects (Verrelst et al., 2015; and Chapter 2).

Out of the Copernicus Sentinel missions, the Sentinel-5 Precursor (TROPOMI) atmospheric mission is likely to be able to retrieve far-red fluorescence, but there are issues with discrimination of the trickier, but essential, red-peak emission (Guanter et al., 2014a). The green reflectance wavelengths are entirely missing and these are required to calculate PRI, which allows fluorescence changes and vegetation stress responses to be interpreted (Rascher et al., 2007; Gamon et al., 1992). Sentinel-5 (on MetOp Second Generation-A1/2/3 satellites) will provide higher resolution in the red band, but like Sentinel-5 Precursor they will not capture the green bands and unfortunately the data will not be sufficient for photosynthesis and stress detection because of a lack of other essential auxiliary data (such as surface temperature of the canopy and vegetation type). Both missions also have too low a spatial resolution (7×7 km^2) to allow ground-based interpretation and validation of the retrievals or to support management-level needs in forestry or agriculture. Large spatial footprints involve heterogeneous assemblages and it is difficult to obtain accurate ground-based information on species or vegetation types, micro-environmental factors, soil or topography over such large pixels. Large spatial footprints also imply greater contamination from clouds (Fig. 8.2), a problem that is reduced at the spatial resolution of FLEX.

None of these other missions were designed specifically for fluorescence retrieval, therefore efforts to use them for this purpose necessitate extensive data preprocessing, temporal averaging and strong assumptions to try to discriminate the fluorescence signal from background reflectance and atmospheric effects – not to mention tacit acceptance of other assumptions that can oversimplify fluorescence-photosynthesis relationships. Fluorescence emission is a subtle, but sophisticated, information-rich signature superimposed onto the reflectance spectrum. Discriminating it from the

background requires an optimised instrument, essential ancillary information, and exceptional mathematical algorithms – all of which have been carefully developed for the tandem Sentinel-3/FLEX mission, and which takes the full science into account. The mid-morning overpass time of FLEX also provides for sufficiently high incident light intensity to link fluorescence and photosynthetic patterns, and allows for stress detection (Mohammed et al., 2014).

The compact spatial footprint of FLEX is particularly advantageous as it allows for the capture of a wide assortment of land size classes, from small private woodlands and farm fields of <1 km^2 to areas of large national forests exceeding 100 km^2. In Canada, small privately owned forests, although occupying a modest proportion of total forest land area, contribute almost C$7 billion to the national GDP and provide most of the ecosystem goods and services in settled regions of the country – including watershed and water-quality conservation, biodiversity, wildlife habitat, and aesthetics (Canadian Association of Forest Owners, 2012). In Europe, about 97.5% of private and public forest holdings do not exceed 1 km^2 (100 ha) (Forest Europe, UNECE, FAO 2011). FLEX could assess many such forests, whereas other instruments with significantly larger spatial footprints would not be able to discriminate these important sizes. The FLEX/Sentinel-3 tandem mission is unique in that it is the only mission with strong and balanced competence for the assessment of all relevant features and land categories. This is essential to support a diverse global resource bioeconomy that benefits from efficiently and sustainably managed production units.

Considering FLEX's unprecedented combination of spectral and spatial resolution, the completeness of the fluorescence information, and the availability of auxiliary information by flying in tandem with Sentinel-3, it is clear that the mission is unparalleled in fulfilling its intended purpose. The benefits to societal and environmental applications of this innovative mission will be profound.

8.1.2 Synergies with Other Missions

As a mission optimised for its primary purpose, FLEX is well-suited to engage synergistically with missions that are likewise optimised for their primary purposes. During the lifetime of FLEX (~2020–25), there are many prospects for complementary interactions with other Earth observation missions. For instance, other satellite sensors can identify geographic regions where stressors may be emerging or intensifying as a result of natural events or anthropogenic factors. These at-risk areas – identified by atmospheric, land, or ocean missions such as MetOp, Sentinels-1, -2 & -4, Joint Polar Satellite System (JPSS-1/2), and the Meteosat Third Generation imaging satellites – can be prioritised for FLEX fluorescence data analysis and supporting ground-based validations to quantify early previsual impacts so that mitigation strategies could be put in place. Conversely, data from these other missions will be valuable for understanding environmental stress factors that trigger photosynthetic changes, e.g. land-use changes, drought, heatwaves, abiotic pressures, etc. Fluorescence can be a companion diagnostic tool for missions focused on quantifying stressors in the environment, affording them a way to train and validate their models with actual vegetation primary productivity, resilience, and recovery data. This capability can exponentially boost the scientific versatility, utility, and economic return from those missions. For FLEX, it signifies the full exploitation of fluorescence for tackling threats to the world's vegetation assets.

Satellite missions that characterise Earth's vegetation resources through high-resolution mapping of forests, agricultural areas, aquatic sites and sensitive ecosystems provide further complementarities. Such missions can supply value-added data to understand the degree and nature of canopy

compositional and structural heterogeneity within FLEX pixels. Even at FLEX's 300×300 m^2 resolution, which is already quite high, there can be complexities, which may be clarified with information from other missions. These missions would extend the spatial continuum to further refine information inputs on vegetation type, structure, and heterogeneity for calculation of stress indices, photosynthesis or Gross Primary Production (GPP). This could have almost immediate benefits for food production, where performances and stress resistance are needed for e.g. phenotyping and to improve management practices in field production systems.

Missions that could secondarily derive some information on fluorescence – e.g. Sentinel-5/5 Precursor and GOSAT-2 – will also benefit by, at last, having FLEX as a 'gold standard' to evaluate the accuracy and utility of their less-optimised fluorescence retrievals and to decipher the heterogeneity within their landscape-level and regional-scale data.

Synergistic activities or complementarities between the missions will be a powerful realisation of the efficacious use of Earth observation capabilities to address pressing environmental issues and to support the management of precious agricultural, forest, and aquatic resources. Satellites that work in concert to deliver greater benefits than are possible individually are the future, as recognised in the new Earth Observation Science Strategy for ESA (ESA 2015a, b).

8.1.3 Contribution to International Programmes

International institutions such as the Food & Agriculture Organization of the United Nations (FAO), the World Bank, the International Food Policy Research Institute, the International Water Management Institute, the International Energy Association, and the World Resources Institute predict impending regional and global crises as a result of natural and anthropogenic pressures on the world's resources and populations (see also Chapter 2). Concerns for food security, drinking and irrigation water sources, ecosystem health and function, forest resource sustainability, and human health have intensified. Consequently, there are now a number of national and international agencies and agreements that all require data and information to support decision-making. ESA's new Earth Observation Science Strategy (ESA 2015a) responds to this need by setting a high priority on responding to major global environmental trends, including climate change, pressures on food supplies and water quality, natural resources/energy issues, disasters, human health & pollution, and threats to biodiversity.

Earth observation can furnish information needed to make wise decisions. As a component of the Earth observation arsenal, assessment of vegetation health and productivity through the measurement of fluorescence will serve international efforts in pivotal ways.

8.1.3.1 Food Security

Assessment of food vegetation resources using fluorescence will provide a system of early warning and agricultural assessment of stress development and productivity in local, regional, and global food vegetation. This would be useful to programmes and initiatives such as ESA/EU's Global Monitoring for Food Security (GMFS) in Africa, FAO's Special Programme for Food Security (PESA) in Central America, CGIAR and the International Food Policy Research Institute's Agriculture for Nutrition and Health research programme, and the European Commission/Institute for Environment and Sustainability (IES)'s Monitoring Agricultural Resources (MARS) initiative.

8.1.3.2 Forest Health & Sustainability:

The capability to detect stress effects and perturbations in the cycling of carbon, water and energy using photosynthetic analysis is directly relevant to the activities of various organisations, such as the International Union of Forest Research Organization's (IUFRO) special programme on World Forests, Society and Environment; the World Resources Institute's Global Forest Watch, and its Global Restoration Initiative; the Center for International Forestry Research's various programmes in Forest Management, Food & Biodiversity, Forest Policy and Livelihoods; and the International Union for Conservation of Nature's programmes in Forest Conservation.

8.1.3.3 Earth System Understanding & Modelling

Measurement of actual photosynthesis, stress impacts and recovery serve multiple modelling applications in forecasting vegetation growth and productivity, global carbon/GPP modelling, predicting effects of climate change, biodiversity estimations, land-use planning, and designing management strategies. Such capabilities are linked to initiatives such as Future Earth and the World Climate Research Programme.

8.1.3.4 Integrated Observing Systems

Vegetation health indicators are priorities for the Global Terrestrial Observing System (GTOS), Global Climate Observing System (GCOS), Group on Earth Observations (GEO), and Global Ocean Observing System (GOOS). GOOS, for example, needs multidisciplinary data and information on ecosystem states, especially coastal zones.

8.1.3.5 Supporting Compliance Reporting

Tracking the health of ecosystems that provide important goods and services and that may be threatened by land degradation and species decline serves agreements such as the Convention on Biological Diversity, the United Nations Convention to Combat Desertification (UNCCD), and the Ramsar Convention on wetlands.

FLEX will interact with multidisciplinary cooperative initiatives such as the European Cooperation in Science & Technology (COST), which fosters synergy in fields of emerging research. FLEX preparatory activities already involve investigators in COST activities, and mission activities are directly relevant to certain COST initiatives: ES1309 (Innovative optical tools for proximal sensing of ecophysiological processes, OPTIMISE), ES1203 (Environmental changes in sensitive tree line ecosystems, SENSFOR), ES1104 (arid land restoration, assessment indicators), ES0903 (spectral sampling tools for vegetation biophysical parameters and flux, bridging of flux tower and remote sensing communities), FA1306 (phenotyping and stress tolerance in food varieties), and FP1304 (European forest data and multi-model predictions to decision makers, PROFOUND). Through such linkages, FLEX will be thoroughly integrated into international efforts.

8.2 User Community Readiness

Fluorescence scientists have envisaged a dedicated space-based fluorescence sensor for decades. In the meantime, a few researchers have been 'making

do' with data from atmospheric missions and other non-optimised satellites. However, such missions can compromise spectral and spatial fidelity, and applicability, complicating the signal retrieval. This can put obstacles in the way of researchers and application scientists who would otherwise be interested in fluorescence science. Fortunately, a window of opportunity now exists for space-based fluorescence measurement to be demonstrated comprehensively and convincingly through the FLEX/Sentinel-3 tandem mission. This breakthrough technology will provide a solid foundation to expand the research and applications communities and to truly welcome all interested parties.

Scientists are interested in the remote-sensing of fluorescence. This was evident at the 5th International Workshop on Remote Sensing of Vegetation Fluorescence (Paris, April 2014), which drew a capacity attendance of over 100 participants from the fluorescence, modelling, remote sensing, and sensor development communities. Chlorophyll fluorescence has also been featured at other international conferences and it has been reported in hundreds of publications on agriculture, forestry and aquatics since the 1990s (DeEll & Toivonen 2003; Papageorgiou & Govindjee 2004; Suggett et al., 2011). The technology, thus, benefits from a strong foundation in research and application.

Fluorescence users can now access a range of technologies: traditional laboratory and field sensors, near-remote instruments that can be operated from a few metres away from vegetation (e.g. Moya et al., 2004), and even a few airborne platforms (reviewed in Meroni et al., 2009b). A recent noteworthy invention is the HyPlant airborne sensor, which is a high-performance FLEX prototype with excellent imaging and mapping capabilities. HyPlant has been used in several international field campaigns to demonstrate and investigate FLEX-type fluorescence retrievals in stressed environments (Rossini et al., 2015; Rascher et al., 2015).

Advances in mechanistic modelling and stress-based research using chlorophyll fluorescence have supported and strengthened the user community by establishing links between fluorescence and photosynthesis, and between fluorescence and stress (Ač et al., 2015; Van der Tol et al., 2009). In addition, ESA preparatory activities in the last decade have yielded novel algorithms for fluorescence retrieval and interpretation at leaf and canopy scales (e.g. Mohammed et al., 2014; Moreno et al., 2014; Magnani et al., 2009; Miller et al., 2005). These advances are now ready for full implementation with the FLEX mission.

Several strategies will further enhance the successful entry and involvement of new users:

8.2.1 Communication

Fluorescence researchers currently participate in joint international research projects, fluorescence workshops, conferences, joint publications and media reports. These avenues maintain awareness and help to advance prospects for fluorescence applications. Additionally, integrating fluorescence communications into international Earth observation network activities (e.g. COST; Committee on Earth Observation, CEOS) will help to consolidate the communication of mission activities and results.

8.2.2 Addressing technical needs of users

Various levels of sophistication are required to incorporate fluorescence into applications. Users will benefit from having a full toolbox of fluorescence information with different capabilities, and from the development of more

powerful carbon-based biological models, appropriate calibration and validation methods, and the articulation of best practices for interpreting fluorescence information. These are examples where the user community will benefit greatly from the translational activities of knowledgeable FLEX scientists who have already devoted significant efforts over the past decade to advancing the basic understanding and use of fluorescence. The FLEX mission will provide important indications of further specific user support required in any future operational mission.

8.2.3 Ensuring data access

Digital technologies will facilitate data storage and delivery to a variety of users. Existing networks for measurement systems (e.g. FLUXNET), ecosystem monitoring (e.g. National Ecosystem Observatory Network, NEON), and scientific training (e.g. Integrated Carbon Observation System, ICOS) will also helpful for data dissemination.

8.2.4 Involving a wide range of participants

The FLEX mission is ideal for involvement of both specialised investigators and non-expert 'citizen scientists', the latter group being able to contribute information on species composition, seasonal progressions, and other aspects at local levels that may not otherwise be readily available. Involvement with a mission that measures the 'glow' emanating from vegetation evokes public curiosity, as does the availability of imagery and data to educators and students at all levels.

8.3 Applications

8.3.1 Land

The economic and environmental devastation caused by stress to vegetation health and productivity is immense and it is intensifying (see Chapter 2). Humanity suffers directly when food, fibre, fuel and feed sources are exhausted owing to sustained drought, pest invasion, temperature extremes, soil nutrient depletion, and other stressors. Because fluorescence is a direct indicator of the inner workings of the photosynthetic machinery, and since photosynthesis is the process that is most responsive to stress in plants, fluorescence serves as a reporter on photosynthetic stress dynamics. This translates into a mechanism to serve society's growing need for crop production, food security, safe drinking water and a sustained quality of life.

As an early warning that can precede the manifestation of visible symptoms of decline, e.g. leaf paling, browning, or branch dieback, fluorescence information from FLEX will support timely decisions for the implementation of remedial or salvage measures. In forests, this early detection tool with its excellent spatial resolution will be able to identify the effects of the early patchy encroachment of invasive alien insect pests before the wood becomes unusable. This will allow resource managers to salvage harvests before it is too late. Invasive alien pests cause billions of US dollars in losses to local, regional and national economies (Pimentel et al., 2005).

The combination of FLORIS and Sentinel-3's optical and thermal sensors allow for an integrated package of measurements to provide all the necessary auxiliary information to interpret data and feed photosynthesis productivity models. FLEX will provide measurements that have not been available before. Using this new Earth observation capability, the community will advance

science and have a positive impact on a large number of applications. Over land applications related to the following areas are foreseen:

8.3.1.1 Quantifying vegetation productivity

FLEX is optimised spectrally, spatially, temporally, and technically to capture the spatio-temporal dynamics of photosynthesis through the measurement of chlorophyll fluorescence. In conjunction with Sentinel-3, FLEX will interpret and model information in ways not feasible with any other current or planned Earth observation mission.

8.3.1.2 Probing ecosystem drivers

FLEX will deepen the understanding of global change stress drivers in canopies and ecosystems at local to large scales, including in under-studied wetlands, coastal and inland waters, and in agricultural lands and forests crucial to nutrient and water cycling, water quality, and human health. It will link land and aquatic vegetation science with trailblazing technology.

8.3.1.3 Planning for land use

FLEX will quantify photosynthetic performance in a wide array of land-use scenarios, including economically-vital small-land bases that are imperative for local and regional bioeconomies. It will enable management strategies and best practices to be devised for the sustained provision of products and services under changing environmental conditions.

8.3.1.4 Helping to solve issues and conflicts

FLEX will equip land managers and inform international programmes and compliance reporting with novel data on actual vegetation performance in different scenarios to sharpen land-use strategies and meet future needs for food, energy, fibre, feed and all ecosystem services within applicable geographic boundaries.

8.3.1.5 Characterised limiting factors

FLEX introduces the first Earth observation system to detect the effects of photosynthetic stress, a transformative technology for relating environmental stressors to impacts on Earth's agricultural, forest and aquatic vegetation. It will provide greatly improved inputs to diagnostic and predictive models, and it will build synergies with other remote-sensing missions tracking air pollutants, water stresses, temperature extremes and other stresses.
Optimism regarding space-based fluorescence detection is high, as evidenced by a recent comment in the journal *Science* suggesting that, *"Chlorophyll fluorescence is the most innovative and revolutionary observation that satellites will make."* (Hand, 2014).

8.3.2 Coastal Zones

The tandem mission presents opportunities for aquatic applications related to health of vegetation in sensitive coastal areas and inland waters, and including

the world's many ecologically important wetlands. There is a need for satellite missions that can advance beyond the measurement of basic parameters to quantitative understanding of biophysical and biogeochemical processes in coastal and inland waters (Mouw et al. 2015). Most sensors are designed for open oceans (where optically active constituents have very different dynamics). Coastal and inland waters require more spatially explicit data of high spectral range and resolution, and an EO capability that is flexible and able to handle the sensitivity and the spectral, spatial, and temporal scales that are important in coastal and inland systems – including for instance, sensing capacity in high turbidity water (Mouw et al. 2015).

A vital application is to cyanobacteria blooms, the frequency and extent of which have been intensifying worldwide. These blooms are notorious disruptors of aquatic ecological equilibrium, and they harm the quality and safety of drinking and irrigation water, poison fish stocks, contaminate terrestrial food production, and pose risks to human health (Matthews 2014). Notably, a large spectral region between 555 and 670 nm is not well sampled by existing sensors (except for MERIS 620 nm and MODIS 645 nm bands), but it is an informative range for the cyanobacterial pigment phycocyanin which absorbs light strongly around 620 nm, and which could be quantified by suitable RS data (Mouw et al. 2015).

Sentinel-3's Ocean and Land Colour Instrument (OLCI) has relevant wavebands for such detection and is anticipated by scientists (Matthews & Odermatt 2015). FLEX will augment OLCI's advantages with even finer spectral resolution in the necessary bands while also being able to report on algal photosynthesis, to identify successful control strategies against these damaging blooms over the course of progressive seasons. Additionally, various beneficial phytoplankton groups may be distinguished by spectral features, and here too FLEX can work strategically with OLCI to support identification and assessment of the photosynthetic vigour and productivity of vegetation communities that are so vital to the health of fisheries and whole ecosystem functioning.

The spatial resolution recommended for sampling in coastal and inland waters is about 100 m and not exceeding 500 m (Mouw et al. 2015), meaning the tandem mission is strategically placed. FLEX is considered to have high value for discrimination of cyanobacteria and algae in water, and for improved retrieval of chlorophyll-a and derivative products in water through improved red-edge characteristics in the range 680-750 nm (Matthews, 2014).

8.3.3 Atmosphere

In the original FLEX proposal, aerosols in the atmosphere were introduced as perturbations whose influence on the measurements needs to be corrected in the Level-2 fluorescence retrieval algorithm. However, during the mission proposal evaluation it was stated that the FLEX and Sentinel-3 tandem mission concept offers the potential to provide additional information on the aerosol content and its vertical distribution. It was therefore suggested to "Explore the scientific and technical feasibility of the aerosol vertical profile objective with a spectral resolution between 0.1 and 0.3nm." This is critical information required for the assimilation of aerosol data in Numerical Weather Prediction (NWP) models at the correct height, increasing thereby the accuracy of the prediction of the aerosols' transportation by air masses (Lindstrot et al., 2013).

Following this recommendation from the expert review panel, the potential of retrieving aerosol vertical distribution was evaluated. Although limited in scope it was concluded that spectrally highly resolved top-of-atmosphere radiance measurements in the oxygen absorption bands could be a viable tool for the remote sensing of aerosol vertical distribution. The high spatial resolution of FLEX measurements has major benefits: the effects from surface

inhomogeneity are reduced, contamination from sub-pixel clouds is easier to avoid, and binning several pixels can increase SNR. Retrievals for scenes characterised by bimodal aerosol vertical distribution cases led to promising results.

8.3.4 Benefits from a Future Operational Mission

The Earth Observation Science Strategy for ESA (ESA 2015a,b) emphasises cutting-edge technologies to address societal issues. FLEX is a unique mission that embodies and demonstrates the new mandate by meeting an acute need for indicators that serve food security and natural resource sustainability. As an Earth Explorer mission, FLEX would serve as a vanguard for a future operational mission based on measuring actual vegetation photosynthetic functioning. A brand new sector in global assessment services would be created, with opportunities in the provision of measurement and analytical services, training, and the industrial manufacture of remote and ground instrumentation. The spinoff prospects for providers of technical and ecosystem services are manifold, such as the following areas:

- forest health monitoring for vegetation management
- early detection and warning of stress-induced strain in perennial food crops and forest stands
- detection of environmental crime affecting forests or food crops
- evaluation of land-use management strategies on terrestrial and coastal vegetation
- productivity forecasting in managed, private, and public lands
- ongoing monitoring of pollution effects on urban green areas
- tracking of toxic algal/cyanobacteria blooms in populated coastal zones
- planning of salvage harvests in forests threatened by encroaching pest infestations
- phenotyping assessments of food and feed crops, e.g. stress-resistant crops
- inputs to national and regional reporting on the health status of important ecosystems

These spinoff benefits emphasise stress-induced impacts on vegetation health and productivity. They would use the full suite of fluorescence products pioneered by FLEX; fluorescence emission in both red and far-red peaks, Photosystem II and I contributions, integrated fluorescence over the whole spectral range, and fluorescence quantum yield to quantify stress effects on photosynthetic activity and vegetation health, and to make recommendations to resource managers. Fluorescence data and derived information would be used directly as stress reporters and as inputs to photosynthesis models supporting productivity forecasting. Such models would be operable at the vegetation canopy level and beyond, for example Dynamic Global Vegetation Models such as ORCHIDEE (Organizing Carbon and Hydrology in Dynamic Ecosystems) (Krinner et al. 2005).

Auxiliary data required to support these downstream activities would include chlorophyll concentration for land vegetation, operational meteorology data, fire occurrence, high-resolution land observations and vegetation-type identification, land cover, land-surface temperature, LAI, geohazard and risk assessment data, soil-type information, fraction of vegetated land, Photosynthetic Active Radiation (PAR), and fraction of Absorbed Photosynthetically Active Radiation (fAPAR). In aquatic applications such as algal bloom tracking, the Sentinel-3/FLEX tandem will carve out innovative pathways of synergy between ocean-colour sensors (e.g. OLCI), which can identify the presence of a toxic bloom, and fluorescence evaluations of bloom and associated aquatic vegetation dynamics.

→ PROGRAMMATICS

9. Programmatics

9.1 Introduction

This chapter presents the technical maturity, heritage and risks associated with both the mission-level scientific concepts and the system-level technical concepts as developed in the frame of the scientific and industrial Phase-A/B1 studies and described in Sections 9.2 and 9.3, respectively. The corresponding development approach and schedule are presented and discussed in Section 9.4 with respect to the compatibility of a target launch for the eighth Earth Explorer mission by 2022.

9.2 Scientific Maturity, Critical Areas and Risks

The Earth Explorer 8 FLEX candidate mission follows a recommendation from ESA's Earth Science Advisory Committee (ESAC) formulated as part of the Earth Explorer 7 mission selection process. Sentinel-3 has been identified as the optimal partner for the tandem concept since the measurements from its Ocean and Land Colour Instrument (OLCI) and Sea and Land Surface Temperature Radiometer (SLSTR) will enable a successful atmospheric correction for the fluorescence retrieval and the additional information needed for the derivation of photosynthetic activity.

The mission objectives and key observational requirements are consolidated and were not relaxed or changed during Phase-A/B1 compared to the Earth Explorer 7 concept and the original proposal for Earth Explorer 8 that was submitted to ESA in 2010. Total fluorescence emission will be retrieved with an accuracy of 10%. The scientific objectives were extended from an improved understanding of photosynthetic processes and Gross Primary Production (GPP) to vegetation stress detection and plant health analyses, following successful theoretical and experimental study activities as outlined in the previous chapters. Potential application areas, therefore, now include food security, and forest health and sustainability.

In the assessment of scientific maturity, the definitions of the Scientific Readiness Levels (SRLs) as described in ESA (2015c) have been considered. At the end of Phase-A/B1 an SRL of 5 is targeted, for which the qualification criteria are related to the scientific objectives, mission objectives, and requirements specified in the original proposal and/or the Mission Requirements Document at the time of selection for Phase-A. To achieve this readiness level the expected performance of the mission concept is assessed with respect to the initial scientific and mission objectives. Three elements are addressed in the following sections to evaluate the mission's scientific readiness for its objectives: the level of theoretical understanding, an experimental proof of concept, and user readiness.

In summary, the FLEX mission concept is judged to have fulfilled each of the steps necessary to attain the targeted scientific maturity and readiness. This judgment is based on the Report for Mission Selection, the Final Study Reports, the deliverables of the various activities performed during Phase-A/B1, and the preceding studies performed in the framework of Earth Explorer 7.

9.2.1 Theoretical Understanding and Status of Retrieval Algorithm Development

The two-step retrieval algorithm is consolidated and fully integrated in the end-to-end simulator. Draft documents on the theoretical basis of the algorithm have also been prepared. The first retrieval component addresses atmospheric

correction and generates top-of-canopy radiances from the Fluorescence Imaging Spectrometer (FLORIS), OLCI and SLSTR measurements. No first guess is used. However, it is assumed that the atmosphere is homogeneous over a 300×300 m^2 footprint for the performance calculations. In a second step, the reflected and emitted contributions are derived using the spectral fitting method.

With the current end-to-end simulator, the effects of clouds, cloud shadows, topography, and sub-pixel heterogeneity on the 30×30 m^2 scale can be evaluated using global input datasets for the scene generator and the instrument spectral response functions. The retrieval algorithm does not yet use additional information, e.g. land-cover type, on sub-pixel heterogeneity that could come from Sentinel-2 or Landsat observations. It is expected that the fluorescence retrieval accuracy can be improved over heterogeneous scenes once auxiliary data are integrated.

The results presented show realistic scenes that were generated to confirm the required fluorescence retrieval accuracy under a range of environmental conditions covering the expected dynamic ranges of the most significant geophysical variables. Exploiting the full (global) capabilities of the end-to-end simulator will still take some time owing to the computational effort required.

9.2.2 Experimental Proof of Concept and Campaigns

The HyPlant instrument was acquired by the Forschungszentrum Jülich, Germany, and built in partnership with Specim, Finland. It is a specific airborne demonstrator for the FLORIS instrument, in that it provides imaging capabilities over the entire spectral range at a spectral resolution similar to that envisaged for FLORIS. Obviously, the radiometric quality of the instrument is lower than expected for FLORIS. However, the most critical scientific questions have been addressed and the performance estimations based on the end-to-end simulations are complemented by experimental results. The campaign results support the validity of the mission concept with respect to the mission and science objectives.

Several campaigns have been carried out in Spain, France, Germany, Italy, Czech Republic, Finland and the US. A wide range of vegetation types including forests and agricultural areas were observed, fluorescence was retrieved and the results verified against independent *in situ* measurements. In addition, the campaigns were used to confirm the potential of fluorescence measurements for detecting pre-visual vegetation stress. Several herbicides that block the photosynthetic machinery at different stages were applied at various concentration levels to observe the response in the fluorescence signals.

During the US campaign, HyPlant was operated along with an infrared sensor to provide proxy measurements over forested areas that represent the full tandem mission concept. These data are being processed by NASA and will be presented during the User Consultation Meeting.

Because of the large volume of data, the full exploitation of the campaign data is still ongoing. An automated processor for the airborne data that will allow for faster processing of the images acquired is under development. Following its success in the campaigns, the HyPlant instrument is now available commercially.

The integration of campaign data into the end-to-end simulator is foreseen as a future activity during implementation to address requirements for achieving a higher SRL. Draft calibration and validation strategies are available; a consolidated cal/val plan will become available for the later phases and is also required for reaching the next, higher, SRL.

9.2.3 User Readiness

Interest in fluorescence measurements has been growing constantly over the past years, as confirmed by participation in dedicated workshops as well as by the variety of application areas covered in the corresponding presentations. The importance of fluorescence has been widely covered by leading scientific journals as well as by economy-oriented journals addressing the societal benefits of having information on fluorescence. Contacts with industry associated with the food and feed sector (e.g. Bayer Crop Science) have been established.

First evaluations of fluorescence measurements were performed and specific experiments related to vegetation health were carried out. Modellers have started to integrate measurements into numerical model systems (as reported in Chapter 7), approaching higher-level products.

Initial fluorescence test datasets have been provided to the user community. A larger and more systematic temporal and spatial coverage for the demonstration database is envisaged in order to reach the next SRL. This can be achieved through the end-to-end simulation capabilities and the automated processor for the airborne measurements described above.

FLEX is a true Earth Explorer in that the novel observations can also serve different communities and application areas. This versatility, however, neither drives the mission design nor does it relate to the scientific readiness. Nevertheless, versatility will be considered when finally assessing its success as an Earth Explorer mission. Much work remains to be done to analyse the application potential over coastal zones, related to aerosols in the atmosphere, and the potential benefits for the Sentinel-3 mission, e.g. through cross-calibration of the OLCI sensor with FLORIS. During the coming phases, collaboration with the oceanographic and atmospheric communities will be increased through dedicated study activities and combined campaigns.

9.2.4 Critical Areas and Risks

The retrieval of fluorescence is now well advanced and, using GOSAT and OCO-2 measurements, it has been demonstrated that vegetation fluorescence emission retrieval from space is feasible, closing a long debate about the feasibility of the required atmospheric correction. Over the past three years, the science related to atmospheric correction and fluorescence retrieval has been consolidated, resulting in a fully-fledged end-to-end simulator that demonstrates the scientific validity of the FLEX mission concept.

The next SRL aims at consolidating the science and products, which will be achieved during Phase-B2/C/D. The remaining scientific risks associated with progression to this level are low and no critical elements have been identified.

Progression to demonstrated science during or after the commissioning phase involves minor scientific risks. These are related to the data processing and retrieval, i.e. calibration and validation results in a first data product uncertainty analysis. As for any land mission, validation of the Level-2 products is challenging. During the next phases, a validation network, ideally linked to existing CO_2 flux sites, needs to be established. It must be noted that demonstration fluorescence datasets have been generated from missions such as GOSAT and OCO-2, but have not been validated systematically, although *in situ* measurement techniques are well established and readily available.

In terms of user readiness, it is expected that applications related to global carbon modelling at coarse spatial and temporal resolutions will benefit from existing fluorescence datasets in that model physics and data assimilation systems can be revised. For the integration of fluorescence measurements into regional- to point-scale soil–vegetation–atmosphere coupled model systems,

more dedicated work is needed using the existing parameterisations included in leaf and canopy models.

9.3 Technical Maturity, Critical Areas and Risks

As shown in Chapter 5, the system design is well consolidated thanks also to activities on fluorescence observing missions and technology that preceded the Phase-A/B1 studies, and the FLEX mission is considered technically feasible. Pursuing recurring solutions for the space segment as an essential condition for implementing Earth Explorer 8 led to the choice of existing platforms with subsystems based on flight-proven designs. Although some units require reconfiguration, the FLEX payload does not place any accommodation requirements on the platform that cannot be met by existing hardware. The FLORIS instrument is considered to pose some challenges, but is feasible thanks to extensive experimental preparatory activities and to the large technological heritage.

The overall system design is well consolidated with regard to the platform solutions developed as the baseline in the Phase-A/B1 system studies, with some optimisation supporting further payload–platform decoupling still possible in later phases. With respect to system solutions adopting smaller platforms, particularly those of the Myriade Evolution family investigated by the industrial consortia in the last part of the Phase-A/B1, the level of detail reached is typical of end of Phase-A with the results indicating overall compliance with the mission requirements and compatibility with a dual launch on a Vega, or its next implementation, Vega-C.

9.3.1 Platform

For the recurring platform proposed by the two consortia, namely the Astrobus-250 (also known as Astrobus-M) and the Proteus MKII, most of the subsystems have already reached a Technology Readiness Level (TRL) of 8–9, based on missions that have already launched (SPOT-6/7, KazEOSat-1) or are about to be launched (Sentinel-5 Precursor, SEOSAT/Ingenio and NATO satellites). For the Payload Data Handling Unit (PDHU) the TRL is 6 or higher, but it requires minor adaptations to fulfil the specific needs of the FLEX mission. For the option of using the recently developed Myriade Evolution platform, the various subsystems are being qualified in the frame of running activities (led by CNES), while first launch will be in 2019 with the CNES–DLR methane remote-sensing lidar mission MERLIN. Other comparable small platforms, e.g. the Astrobus-S under development for the ESA Space Science mission CHEOPS, are also considered promising alternatives for FLEX. Embarking FLORIS on such a smaller platform would open the possibility for a dual launch. On the other hand, initial studies indicate that the reduced system resources and capabilities fulfil the FLEX mission needs with limited margins.

9.3.2 FLORIS Instrument

The FLORIS instrument is a high-resolution imaging spectrometer that benefits from the heritage of similar instruments such as MERIS, OLCI, GAIA and VIRTIS. Though both designs presently reach TRL 5 or greater for most subsystems, two elements needed specific developments: the detector and the high-resolution (HR) grating. The low-resolution (LR) grating was considered less critical, but was nevertheless addressed through a specific development activity.

As mentioned in Chapter 5, both FLEX concepts employ the same detector for high- and low-resolution channels, so that only one detector type needs to be procured. The detector development benefits from very similar activities carried out for the Sentinel-4 and Sentinel-5 Precursor spectrometers, for example, and will use the same building blocks with minor differences in terms of detector format and charge-handling capacity. The development activities are well underway with an established manufacturer. The FLORIS-specific detector is expected to reach TRL 5 by the middle of 2016. The detector's technical feasibility is not in doubt, but the risk linked to its production schedule needs to be managed.

Two Elegant Breadboards (EBB) of the entire FLORIS-HR channel have been completed and tested or are being completed, with the objective of demonstrating TRL 5 for the HR grating and specifically to demonstrate manufacturability of flight representative optical elements, assembly compliance with tolerance analysis and the contamination budget, and critical performances such as imaging and spectral performance.

On the basis of the results obtained by the measurements on EBB and to further mitigate straylight issues related to scattering of the grating, additional activities have been performed to improve the manufacturing process of the HR grating. The results show that the optimised design yields a marked improvement in the scattering properties compared to that used in the breadboard. In addition, similar activities have been performed also for the LR grating. LR grating samples have been manufactured and they show that the required spectral dispersion and low scattering characteristics can be achieved. Both activities have produced solid and valuable results that will be taken into account in further breadboard activities.

In order to further mitigate risks and anticipate the instrument development phase, parallel activities on a FLORIS preliminary Optical Model (FLORIS pre-OM) have also started. The goal of these activities is to refurbish the FLORIS EBB, complete it by adding the LR channel, and measure the system performance. The FLORIS pre-OM will also allow debugging and optimisation of alignment procedures.

Though the spectrometer design is not novel, FLORIS will still face the challenges of similar past and future instruments that are related to the control of straylight, such as the cleanliness level of the optical surfaces, which will have to be maintained at the required values throughout the entire assembly, integration and on-ground characterisation phases. Based on the results of the analyses, correction factors for straylight between 2 and 4, depending on the achievable contamination levels, are assumed to reach compliance at Level-1b, which is well within current experience.

9.4 Development Approach and Schedule

9.4.1 Overall Design and Development Approach

FLEX will follow a phased development process (Phases-B2/C/D/E1) with system reviews (System Requirements Review (SRR), Preliminary Design Review (PDR), Critical Design Review (CDR), etc.) to verify the status of the system design, development, procurement and integration of the flight models. In order to establish a robust development schedule, the instrument and platform developments can be decoupled. As reference planning to minimise project cost and schedule, both industrial consortia have proposed parallel development activities on the instrument, platform and satellite levels, with integration performed during the Assembly, Integration and Testing (AIT) phase.

Since both concepts have been developed to maximise the reuse of existing hardware for the payload and platform, the development, integration, testing

and verification can be carried out as independently as is practical. This will minimise the risk of any schedule impacts propagating into other areas. Hence, the platform-related activities and procurements will start after instrument-related procurements have begun.

At satellite level, a 'hybrid approach' according to ECSS-E10-03A has been chosen. It comprises the following models:

— Proto-Flight Model (PFM) for full qualification and acceptance testing in terms of mechanical, thermal, Electromagnetic Compatibility (EMC) and functional/operational requirements.

— Structural Model (SM) for qualification of the structure against launch loads, for verification of structural stability, strength and stiffness, for verification of the finite element model and for validation of the interface loads for platform equipment and instruments.

— Electrical and Functional Model (EFM) for command, control and electrical interface verification of the platform avionics, for onboard software/hardware interaction verification, for Attitude and Orbit Control System (AOCS) performance verification by closed loop testing, for development and debugging of checkout software, and for initial validation of onboard flight procedures.

Figure 9.1. FLEX satellite development schedule.

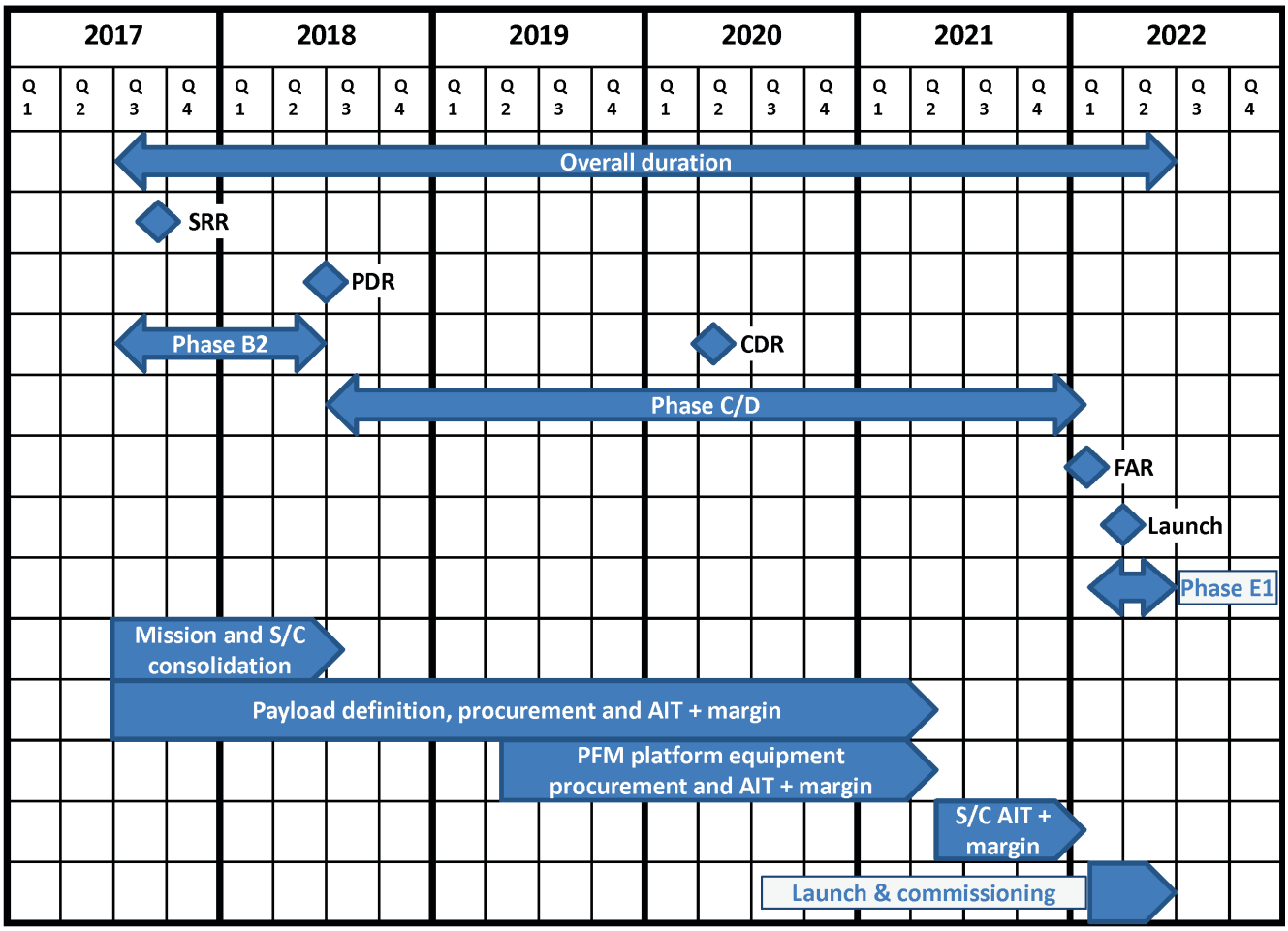

For the platform and related avionics, the development approach is based either on a strict PFM approach (as for Sentinel-5 Precursor, for the consortium led by Airbus Defence and Space); or on a PFM approach complemented by an SM for the platform and Payload Interface Module (PIM) (the case of Proteus MKII, for the consortium led by Thales Alenia Space). The development approach for the use of a Myriade Evolution-type platform, under elaboration, is expected to be similar. One concept proposes a PFM development approach thanks to the development and qualification that is being done for MERLIN, and does not envisage an SM or a Structural Thermal Model (STM).

For the instrument, the approach of both industrial consortia includes:

— an Optical Engineering Model (OEM) consisting of the current HR channel breadboard (refurbished e.g. by adding a polarisation scrambler, a filter in front of the detector and use of upgraded optical bench) and the LR channel. The objective of the OEM is to optimise the test procedures and optics alignment procedures, in particular the high/low-resolution channel co-alignment, and to check the overall optical performance. The OEM will undergo functional and performance tests, as well as some vacuum tests

— an instrument STM, for Concept B only

— an Engineering Model (EM) of the complete video chain: detectors, front-end electronics, Instrument Control Unit (ICU)

— the instrument PFM

9.4.2 Schedule

The schedule for the satellite development shown in Fig. 9.1 assumes Phase-B2/C/D/E1 kickoff in mid-2017 to allow six months at the start of the next cycle of the Earth Observation Envelope Programme for issuing the Phase-B2/C/D/E1 Invitation to Tender, for proposal submission and evaluation, and for contract negotiations. The overall schedule is driven by the instrument development and, therefore, it allows for later procurement of the platform without influencing the total development duration, provided the latter procurement is initiated early enough. The schedule also assumes a three-month margin between satellite delivery and start of the launch campaign and then a three-month launch campaign.

Early in Phase-B2, an SRR will be held to consolidate the satellite design and to set the system and subsystem requirements for the full development. The schedule includes a Phase-B2 of 12 months from the Kickoff Meeting to PDR, a Phase-C/D of 43 months, a Flight Acceptance Review (FAR) of the satellite after 55 months, a Phase-E1 of five months, including the launch campaign (two months) and in-orbit commissioning (three months). The schedule includes about three months of contingency on the delivery of the instrument to the satellite.

9.5 Conclusion

Assuming successful outcomes for the ongoing pre-developments, as expected, the maturity of critical technologies will reach the required level prior to the start of the implementation phases. The development schedule is compatible with a launch by 2022.

→ REFERENCES

References

Ač, A., et al. (2015). Meta-analysis assessing potential of steady-state chlorophyll fluorescence for remote sensing detection of plant water, temperature and nitrogen stress. *Remote Sensing of Environment* (submitted).

Alonso, L., et al. (2008). Improved Fraunhofer Line Discrimination Method for Vegetation Fluorescence Quantification. *IEEE Geoscience and Remote Sensing Letters*, 5(4), 620-624, doi:10.1109/LGRS.2008.2001180.

Amorós-López, J., et al. (2011). Multitemporal fusion of Landsat and MERIS images. Published in: *6th International Workshop on the Analysis of Multi-temporal Remote Sensing Images* (Multi-Temp), 2011 IEEE, 81–84, doi:10.1109/Multi-Temp.2011.6005053.

Baldocchi, D., et al. (2001). FLUXNET: A new tool to study the temporal and spatial variability of ecosystem-scale carbon dioxide, water vapor, and energy flux densities. *Bulletin of the American Meteorological Society*, **82**(11), 2415–2434.

Baret, F., et al. (2007). LAI, fAPAR and fCover CYCLOPES global products derived from VEGETATION. Part 1: Principles of the algorithm. *Remote Sensing of Environment*, **110**(3), 275–286.

Barnosky, A. D., et al. (2012). Approaching a state shift in Earth's biosphere. *Nature*, **486**(7401), 52–58.

Berry, J.A., Frankenberg, C. & Wennberg, P. (2013). Proc. New Methods for Measurements of Photosynthesis from Space, 26–31, August 2012, Keck Institute for Space Studies, Pasadena, CA. *http://www.kiss.caltech.edu/study/photosynthesis/2013KISS_fluorescence_final_report.pdf* .

Brienen, R. J. W., et al. (2015). Long-term decline of the Amazon carbon sink. *Nature*, **519**(7543), 344–348.

Buschmann, C. (2007). Variability and application of the chlorophyll fluorescence emission ratio red/far-red of leaves. *Photosynthesis Research*, **92**, 261-271.

Canadian Association of Forest Owners (2012). Privately owned forest land in Canada. CAFO/ACPF Info/Tech #1. *http://www.cafo-acpf.ca/wp-content/uploads/2012/04/CAFO-Info-Brochure.pdf*.

Committee on Earth Observation Satellites. 2014. Earth Observation Handbook. *http://www.ceos.org*.

Ciais, P., et al. (2005). Europe-wide reduction in primary productivity caused by the heat and drought in 2003. *Nature*, **437**(7058), 529–533.

Cogliati, S., et al. (2015). Continuous and long-term measurements of reflectance and Sun-induced chlorophyll fluorescence by using novel automated field spectroscopy systems. R*emote Sensing of Environment, in press, http://dx.doi.org/10.1016/j.rse.2015.03.027.*

Collar, C. (2014). Barley, Maize, Sorghum, Millet, and Other Cereal Grains. Chapter 6 in book: *Bakery Products Science and Technology*, second edition, 107-126. doi: 10.1002/9781118792001.

DeEll, J.R. & Toivonen, P.M.A. (2003). Use of chlorophyll fluorescence in postharvest quality assessments of fruits and vegetables. In: *DeEll JR, Toivonen PMA (eds.) Practical Applications of Chlorophyll Fluorescence in Plant Biology, Kluwer, 203–242*.

Demmig-Adams, B. & Adams W.W. (1996). The role of xanthophyll cycle carotenoids in the protection of photosynthesis. *Trends in Plant Science*, **1**(1), 21–26.

Demmig-Adams, B. & Adams W.W. (2000). Photosynthesis: Harvesting sunlight safely. *Nature*, **403**, 371–374, doi:10.1038/35000315.

ESA (2014a). Earth Observation Portal, Satellite Missions. *https://eoportal.org*.

ESA (2015a). Earth Observation Science Strategy for ESA: A New Era for Scientific Advances and for Societal Benefits. ESA SP-1329/1 (2 volumes), European Space Agency, Noordwijk, the Netherlands.

ESA (2015b). ESA's Living Planet Programme: Scientific Achievements and Future Challenges – Scientific Context of the Earth Observation Science Strategy for ESA, ESA SP-1329/2 (2 volumes), European Space Agency, Noordwijk, the Netherlands.

ESA (2015c). Scientific Readiness Levels Handbook. Mission Science Division (EOP-SM), EOP-SM/2776, V1.1.

European Commission, Agriculture and Rural Development, (2013). *http://ec.europa.eu/agriculture/statistics/rural-development/2013/index_en.htm*.

FOREST EUROPE, UNECE and FAO 2011: State of Europe's Forests 2011. Status and Trends in Sustainable Forest Management in Europe. Ministerial Conference on the Protection of Forests in Europe, 2011. ISBN 978-82-92980-05-7.

Frankenberg, C., Butz, A. & Toon, G.C. (2011). Disentangling chlorophyll fluorescence from atmospheric scattering effects in O2 A band spectra of reflected sunlight. *Geophysical Research Letters*, **38**, doi:10.1029/2010GL045896.

Frankenberg, C., et al. (2014). Prospects for chlorophyll fluorescence remote sensing from the Orbiting Carbon Observatory-2. *Remote Sensing of Environment*, **147**, 1–12.

Gamon, J.A., Peñuelas, J. & Field, C.B. (1992). A narrow-waveband spectral index that tracks diurnal changes in photosynthetic efficiency. *Remote Sensing of Environment*, **41**, 35–44.

Garbulsky, M.F., et al. (2014). Photosynthetic light use efficiency from satellite sensors: from global to Mediterranean vegetation. *Environmental and Experimental Botany*, **103**, 3–11.

Gerland, P., et al. (2014). World population stabilization unlikely this century. *Science*, **346** (6206), 234–237.

Goetz, S. J. & Prince, S.D. (1999). Modeling terrestrial carbon exchange and storage: Evidence and implications of functional convergence in light use efficiency. *Adv. Ecol. Res.*, **28**, 57-92.

Guanter, L., et al. (2007). Estimation of solar-induced vegetation fluorescence from space measurements. *Geophysical Research Letters*, **34**, doi:10.1029/2007GL029289.

Guanter, L., et al. (2014a). Potential of the TROPOspheric Monitoring Instrument (TROPOMI) onboard the Sentinel-5 Precursor for the monitoring of terrestrial chlorophyll fluorescence. *Atmospheric Measurement Techniques Discussions*, **7**, 12545–12588.

Guanter, L., et al. (2014b). Global and time-resolved monitoring of crop photosynthesis with chlorophyll fluorescence. Proceedings of the *National Academy of Sciences of the USA*, **111**, E1327–E1333, doi: 10.1073/pnas.1320008111.

Hand, E. (2014) Carbon-mapping satellite will monitor plants' faint glow. *Science*, **344**, 1211–1212.

IEA (2015), International Energy Agency, *www.iea.org*

IFPRI (2015). 2014–2015 *Global Food Policy Report*. Washington, DC: International Food Policy Research Institute.

IWMI (2011). International Water Management Institute, IWMI. An Ecosystem Services Approach to Water and Food Security, ISBN 978-92-807-3152-1. UNEP 2011

Joiner, J., et al. (2011). First observations of global and seasonal terrestrial chlorophyll fluorescence from space. *Biogeosciences*, **8**, 637–651.

Joiner, J., et al. (2012). Filling in of near infrared solar lines by terrestrial fluorescence and other geophysical effects: simulations and space based observations from SCIAMACHY and GOSAT. *Atmospheric Measurement Techniques*, **5**, 809–829.

Joiner, J., et al. (2013). Global monitoring of terrestrial chlorophyll fluorescence from moderate spectral resolution near infrared satellite measurements: methodology, simulations, and application to GOME 2. *Atmospheric Measurement Techniques*, **6**, 2803–2823.

Joiner, J., et al. (2014). The seasonal cycle of satellite chlorophyll fluorescence observations and its relationship to vegetation phenology and ecosystem atmosphere carbon exchange. *Remote Sensing of Environment*, **152**, 375–391.

Kastner, T., Erb, K. H., & Haberl, H. (2015). Global Human Appropriation of Net Primary Production for Biomass Consumption in the European Union, 1986–2007. *Journal of Industrial Ecology*, doi: 10.1111/jiec.12238.

Krinner, G. et al., 2005. A dynamic global vegetation model for studies of the coupled atmosphere-biosphere system. *Global Biogeochemical Cycles*, **19**, doi:10.1029/2003GB002199

Le Quéré, et al. 2009. Trends in the sources and sinks of carbon dioxide. *Nature Geoscience*, **2**, 831–836.

Leprince, S., et al. (2007). Automatic and precise orthorectification, coregistration, and subpixel correlation of satellite images, application to ground deformation measurements. *IEEE Transactions on Geoscience and Remote Sensing*, **45**(6), 1529–1558.

Lichtenthaler, H. K. & Rinderle, U. (1988). The role of chlorophyll fluorescence in the detection of stress conditions in plants. *CRC Critical Reviews in Analytical Chemistry*, **19**, Suppl. I, 29–85.

Lindstrot, R., et al. (2013). FLUSS – Atmospheric corrections for fluorescence signal and surface pressure retrieval over land. Final Report, ESA ESTEC Contract 4000102733, V1.1, 204 pp

Lobell, D. B., et al. (2014). Greater sensitivity to drought accompanies maize yield increase in the US Midwest. *Science*, **344**(6183), 516–519.

Magnani, F., et al. (2009). Assessment of Vegetation Photosynthesis Through Observation of Solar Induced Fluorescence from Space. ESA Contract No 20678/07/NL/HE, Study final report.

Matthews, M.W., 09 December 2014, personal communication.

Matthews, M.W. & Odermatt, D. (2015). Improved algorithm for routine monitoring of cyanobacteria and eutrophication in inland and near coastal waters. *Remote Sensing of Environment*, **156**, 374–382.

Mauser, W., Bach, H. & Klepper, G. (2015): Earth Observation Needs and Opportunities to Support Food Security and Sustainable Agriculture – EO4Food. ESA Contract No 4000109800, Study Final Report v0.9.

Meroni, M., et al. (2008a). Leaf level early assessment of ozone injuries by passive fluorescence and PRI. *International Journal of Remote Sensing*, **29**, 17, 5409–5422.

Meroni, M., et al. (2008b). Assessing Steady-state Fluorescence and PRI from Hyperspectral Proximal Sensing as Early Indicators of Plant Stress: The Case of Ozone Exposure. *Sensors*, **8**, 1740–1754.

Meroni, M., et al. (2009a). Using optical remote sensing techniques to track the development of ozone-induced stress. *Environmental Pollution*, **157**, 5, 1413–1420.

Meroni, M., et al. (2009b). Remote sensing of solar-induced chlorophyll fluorescence: Review of methods and applications. *Remote Sensing of Environment*, **113**, 2037–2051.

Miller, J.R., et al. (2005) Development of a Vegetation Fluorescence Canopy Model, ESA Contract No 16365/02/NL/FF, Study Final Report.

Mohammed, G.H., et al. (2014). 2012 FLEX/Sentinel-3 Tandem Mission Photosynthesis Study, ESA Contract No 4000106396/12/NL/AF, Study final report.

Moreno, J., et al. (2014). FLEX/S3 Tandem Mission Performance Analysis and Requirements Consolidation Study (PARCS), ESA Contract No 4000105078/11/NL/AF, Study final report.

Morisette, J.T., et al. (2006). Validation of global moderate-resolution LAI Products: a framework proposed within the CEOS Land Product Validation subgroup. *IEEE Transactions on Geoscience and Remote Sensing*, **44**(7),1804–1817.

Morison, J.I.L. & Morecroft, M.D. (Eds.) (2006). Plant Growth and Climate Change. Blackwell Publishing. ISBN 13: 978 14051 3192 6. 213 pages.

Mouw, C.B., et al. (2015). Aquatic color radiometry remote sensing of coastal and inland waters: Challenges and recommendations for future satellite missions. *Remote Sensing of Environment*, **160**, 15–30.

Moya, I., et al. (2004). A new instrument for passive remote sensing. 1. Measurements of sunlight induced chlorophyll fluorescence. *Remote Sensing of Environment*, **91**, 186-197.

Natural Resources Canada (2013): National research forests. *http://www.nrcan.gc.ca/forests/research-centres/afc/13171*.

Papageorgiou, G.C., & Govindjee (Eds.) (2004). Chlorophyll a Fluorescence: A Signature of Photosynthesis. Series: *Advances in Photosynthesis and Respiration*, *Vol. 19*. Springer. ISBN 978-1-4020-3218-9.

Parazoo, N. C., et al. (2014). Terrestrial gross primary production inferred from satellite fluorescence and vegetation models. *Global Change Biology*, **20**(10), 3103-3121. doi:10.1111/gcb.12652.

Penuelas, J., et al. (2013). Human-induced nitrogen–phosphorus imbalances alter natural and managed ecosystems across the globe. *Nature Communications*, **4**(2934), doi:10.1038/ncomms3934.

Pimentel D., Zuniga, R. & Morrison, D. (2005). Update on the environmental and economic costs associated with alien-invasive species in the United States. *Ecological Economics*, **52**, 273–288.

Quillet A., Peng C. & Garneau M. (2010). Toward dynamic global vegetation models for simulating vegetation-climate interactions and feedbacks: recent developments, limitations, and future challenges. *Environmental Reviews*, **18**, 333–353

Rascher, U., et al. (2007). Monitoring spatio-temporal dynamics of photosynthesis with a portable hyperspectral imaging system. *Photogrammetric Engineering & Remote Sensing*, **73**, 45–56.

Rascher, U., et al. (2015) Sun-induced fluorescence – a new probe of photosynthesis: First maps from the imaging spectrometer HyPlant. *Global Change Biology* (accepted for publication).

Rossini, M., et al. (2010). High resolution field spectroscopy measurements for estimating gross ecosystem production in a rice field. *Agr. Forest Meteorol.*, **150**, 1283–1296

Rossini, M., et al. (2015). Red and far-red sun-induced chlorophyll fluorescence as a measure of plant photosynthesis. *Geophysical Research Letters*, **42** (6), 1632–1639, doi: 10.1002/2014GL062943.

Sherwood, S. & Fu, Q. (2014). A Drier Future? *Science*, **343** (6172), 737-739. doi: 10.1126/science.1247620.

Smith, M. D., et al. (2015). Global environmental change and the nature of aboveground net primary productivity responses: insights from long-term experiments. *Oecologia*, **177**(4), 935–947.

Stancik, A.L. & Brauns, E.B (2008). A simple asymmetric lineshape for fitting infrared absorption spectra. *Vib. Spectrosc.*, **47**(1), 66–69.

Statistics Canada (2011). Census of Agriculture. *http://www.statcan.gc.ca/ca-ra2011/index-eng.htm*.

Suggett, D.J., Prášil, O. & Borowitzka, M.A. (Eds.) (2010). Chlorophyll a Fluorescence in Aquatic Sciences. Methods and Applications. *Developments in Applied Phycology*, **4**, Springer. ISBN 978-90-481-9267-0.

Tian, Y., et al. (2002). Multiscale analysis and validation of the MODIS LAI Product II: Sampling Strategy. *Remote Sensing of Environment*, **83**, 431–441.

Tripathi, A.K., & Gautam, M. (2007). Biochemical parameters of plants as indicators of air pollution. *Journal of Environmental Biology*, **28**, 127–132.

Van der Tol, C.,et al. (2009). An integrated model of soil-canopy spectral radiances, photosynthesis, fluorescence, temperature and energy balance. *Biogeosciences*, **6**, 3109–3129.

Van Wittenberghe, S. et al. (2013). Upward and downward solar-induced chlorophyll fluorescence yield indices of four tree species as indicators of traffic pollution in Valencia. *Environmental Pollution*, **173**, 29–37.

Van Wittenberghe, S., et al. (2014). A field study on solar-induced chlorophyll fluorescence and pigment parameters along a vertical canopy gradient of four tree species in an urban environment. *Science of the Total Environment*, 466–467C, 185–194. doi: 10.1016/j.scitotenv.2013.07.024

Verrelst J., et al. (2015). Global sensitivity analysis of SCOPE v1.53 model: what drives canopy-leaving sun-induced fluorescence? *Remote Sensing of Environment* (accepted).

Xia, J., et al. (2015). Joint control of terrestrial gross primary productivity by plant phenology and physiology. *Proceedings of the National Academy of Sciences,* **112**(9), 2788–2793.

Zhu X.G., de Sturler, E. & Long, S.P. (2007). Optimizing the distribution of resources between enzymes of carbon metabolism can dramatically increase photosynthetic rate: a numerical simulation using an evolutionary algorithm. *Plant Physiol.*, **145**, 513–26

Zhu X.G., Long, S.P. & Ort, D.R. (2010) Improving Photosynthetic Efficiency for Greater Yield. *Annu. Rev. Plant Biol.*, **61**, 235–261.

→ GLOSSARY

Glossary

Acronyms

ACT	Across Track
AIT	Assembly Integration and Testing
ALT	Along Track
AOCS	Attitude Orbit Control System
AOT	Aerosol Optical Thickness
APAR	Absorbed Photosynthetically Active Radiation
ATP	Adenosine Triphosphate
BRDF	Bidirectional Reflectance Distribution Function
BSDF	Bidirectional Scattering Distribution Function
CCD	Charge Couple Device
CDR	Critical Design Review
CEOS	Committee on Earth Observation Satellites
CFRP	Carbon Fibre Reinforced Plastic
COST	Cooperation in Science and Technology
CWV	Columnar Water Vapour
DCMU	Dimethylurea
DEM	Digital Elevation Model
DGVM	Dynamic Global Vegetation Models
EBB	Elegant Breadboard
ECMWF	European Centre for Medium-Range Weather Forecasts
EEMCS	Earth Explorer Mission Control System
EFM	Electrical and Functional Model
EM	Engineering Model
EMC	Electromagnetic Compatibility
EMS	Estrack Management and Scheduling System
EOL	End of Life
ESAC	Earth Science Advisory Committee
ESOC	European Space Operations Centre
ESTEC	European Space Research and Technology Centre
FAO	Food and Agriculture Organization of the United Nations
fAPAR	fraction of Absorbed Photosynthetically Active Radiation
FAR	Flight Acceptance Review
FDIR	Failure Detection Isolation and Recovery
FEE	Front End Electronics
FEM	Finite Element Model
FLEX	Fluorescence Explorer
FLEX-E	FLEX End-to-End
FLO	FLORIS Instrument Model
FLORIS	Fluorescence Imaging Spectrometer
FLORIS-HR	High spectral Resolution (FLORIS)
FLORIS-LR	Low spectral Resolution (FLORIS)
FOCC	Flight Operations Control Centre
FOS	Flight Operations Segment
FOV	Field of View
FPGA	Field-Programmable Gate Array
FWHM	Full Width at Half Maximum
GCOS	Global Climate Observing System
GEO	Group on Earth Observations
GEOM	Geometry Model
GIZ	Gesellschaft für Internationale Zusammenarbeit
GMFS	Global Monitoring for Food Security
GOOS	Global Ocean Observing System
GPP	Gross Primary Production
GPS	Global Positioning System
GTOS	Global Terrestrial Observing System
HKTM	Housekeeping Telemetry
HR	High Resolution
ICOS	Integrated Carbon Observation System
ICU	Instrument Control Unit
IEA	International Energy Association
IES	Institute for Environment and Sustainability
IFPRI	International Food Policy Research Institute
ISRF	Instrument Spectral Response Function
ISRO	Indian Space Research Organisation
IUFRO	International Union of Forest Research Organizations
JPSS	Joint Polar Satellite System
L1F	Level-1 Processing Module
L2R	Level-2 Retrieval
LAI	Leaf Area Index
LCC	Leaf Chlorophyll Content
LEOP	Launch and Early Orbit Phase
LOS	Line of Sight
LR	Low Resolution
LSF	Line Spread Function
LTDN	Local Time of Descending Node
LUE	Light-Use Efficiency
LUT	Look Up Table
MACC	Monitoring Atmospheric Composition and Climate
MARS	Monitoring Agricultural Resources
MERIS	Medium Resolution Imaging Spectrometer

MCS	Mission Control System
ME	Main Electronics
MLI	Multi-Layer Insulation
MMU	Mass Memory Unit
MPS	Mission Planning System
MSI	Multispectral Instrument
NADPH	Nicotinamide Adenine Dinucleotide
NAND	Not + AND
NDVI	Normalised Difference Vegetation Index
NEON	National Ecosystem Observatory Network
NPQ	Non-Photochemical Quenching
OBC	Onboard Computer
OBDH	On Board Data Handling
OBSW	Onboard Software
OEM	Optical Engineering Model
OLCI	Ocean and Land Colour Instrument
OM	Optical Model
OPTIMISE	Innovative Optical Tools for Proximal Sensing of Ecophysiological Processes
OQPSK	Offset Quadrature Phase Shift Keying
ORCHIDEE	Organizing Carbon and Hydrology in Dynamic Ecosystems
OSS	Observing System Simulator
PAR	Photosynthetic Active Radiation
PCDU	Power Conditioning and Distribution Unit
PDGS	Payload Data Ground Segment
PDHT	Payload Data Handling and Transmission
PDHU	Payload Data Handling Unit
PDR	Preliminary Design Review
PEM	Proximity Electronics Module
PESA	Special Programme for Food Security
PFM	Proto-Flight Model
PIM	Payload Interface Module
PIP	Payload Interface Panel
PQ	Photochemical Quenching
PRI	Photochemical Reflectance Index
PROFOUND	European forest data and multimodel predictions to decision makers
PSF	Point Spread Function
PSLV	Polar Satellite Launch Vehicle
PS I	Photosystem One
PS II	Photosystem Two
QPSK	Quadrature Phase Shift Keying
RF	Radio Frequency
RIU	Remote Interface Unit
RMS	Root Mean Square
RMSE	Root mean square error
RTM	Radiative Transfer Model
RVS	Radial Velocity Spectrometer
S3	Sentinel-3
S3G	Sentinel-3 Geometry Model
S3I	Sentinel-3 Instrument and Level-1 Processing Module
SDRAM	Synchronous Dynamic Random Access Memory
SENSFOR	Environmental changes in sensitive tree line ecosystems
SEDF	Spatial Energy Distribution Function
SFM	Spectral Fitting Method
SGM	Scene Generator Module
SIE	System Integrated Energy
SIF	Sun-Induced Florescence
SLSTR	Sea and Land Surface Temperature Radiometer
SM	Structural Model
SMU	Satellite Management Unit
SNR	Signal-to-Noise Ratio
SR	Spectral Resolution
SRL	Scientific Readiness Level
SRR	System Requirements Review
SSD	Spatial Sampling Distance
SSI	Spectral Sampling Interval
STM	Structural Thermal Model
SZA	Sun Zenith Angle
TM	Telemetry
TOA	Top of Atmosphere
TOC	Top of Canopy
TRL	Technology Readiness Level
TT&C	Telemetry, Tracking and Command
TWTA	Travelling Wave Tube Amplifiers
UAV	Unmanned Aerial Vehicles
UNCCD	United Nations Convention to Combat Desertification
UNECE	United Nations Economic Commission for Europe
VAU	Video Acquisition Units
VIRTIS	Visible and Infrared Thermal Imaging Spectrometer

Definitions

The following terms are used in the report and but are not defined in the text as they are only indirectly related to the key messages. For improved readability, the definitions are given in this annex.

— **C3 and C4** metabolic pathways describe the two major photosynthetic (or carbon fixation) pathways in terrestrial plants. In C3 photosynthesis, CO_2 is first incorporated into a three-carbon compound. This type of photosynthesis is the most typical pathway used by many species of plant. C4 photosynthesis is an adaptation to hotter and dryer environmental conditions. In C4 plants, the CO_2 is prefixed in specialised cells within the leaf as a four-carbon compound and shuttled to the 'normal' photosynthetic cells. This additional step, however, requires extra energy. The ecological advantage is that in dry habitats, C4 plants lose less water and so have a high water-use efficiency that favours this metabolic pathway in more arid environments. Agriculture is often based on the biochemical properties of C4 photosynthesis, and many crops are C4 species, such as corn, sugar cane, millet and sorghum.

— **Ecosystem services** is a new term that was popularised by the millennium ecosystem assessment in the early 2000s. Humankind benefits in a multitude of ways from ecosystems. Ecosystem services are generally grouped into four broad categories: *provisioning*, such as the production of food and water; *regulating*, such as the control of climate and disease; *supporting*, such as nutrient cycles and crop pollination; and *cultural*, such as spiritual and recreational benefits. Many ecosystem services are being assigned economic values to aid decision-making.

— **Bio-based economy** or **bio-economy** refers to the sustainable use of biological resources such as plants, animals and microorganisms. It involves a large number of industries including agriculture and forestry, horticulture, fishery and aquacultures, plant breeding, the food and drink industry, in addition to the wood, paper, leather, textile, chemical, and pharmaceuticals industries, and even parts of the energy industry. Many European governments have explicitly adopted this term in their strategies to facilitate a structural transition to bio-based industries. At the same time, research and innovation will be the basis for taking on international responsibility for global nutrition and the supply of commodities and energy from biomass, as well as for climate and environmental protection.

ESA Member States

Austria
Belgium
Czech Republic
Denmark
Estonia
Finland
France
Germany
Greece
Hungary
Ireland
Italy
Luxembourg
Netherlands
Norway
Poland
Portugal
Romania
Spain
Sweden
Switzerland
United Kingdom

An ESA Communications Production